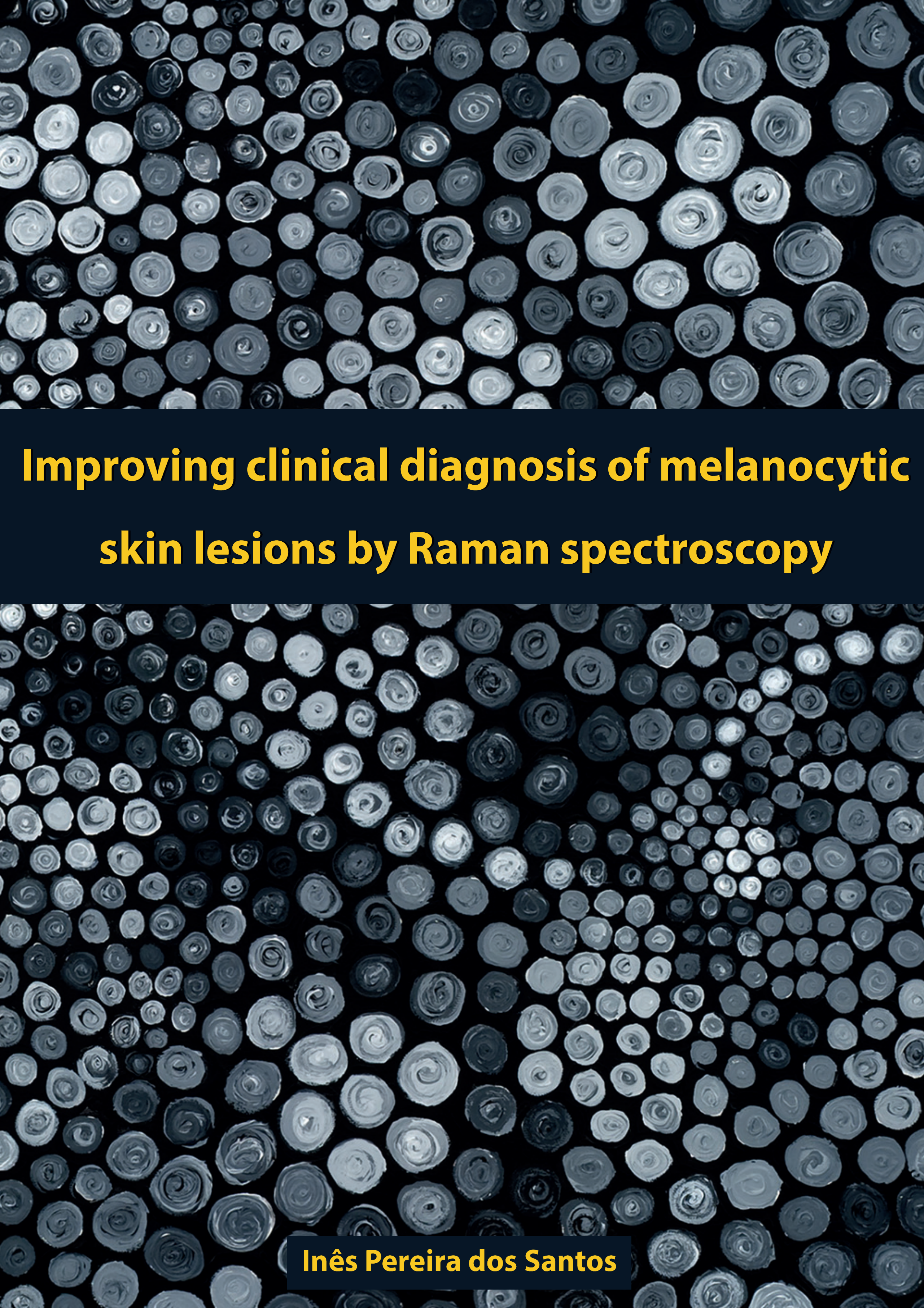

Improving clinical diagnosis of melanocytic skin lesions by Raman spectroscopy

Inês Pereira dos Santos

Improving Clinical Diagnosis of Melanocytic Skin Lesions by Raman Spectroscopy

Inês Pereira dos Santos

ISBN: 978-94-6299-958-9

Author: Inês Pereira dos Santos

Lay-out: Inês Pereira dos Santos

Cover design: Uma Rani Iyli (*Cellular Pattern-Greyscale*, 2009 | www.umaraniiyli.com), printed with permission of the artist, and Inês Pereira dos Santos

Print and publishing by: Ridderprint | www.ridderprint.nl

Copyright © 2018 Inês Pereira dos Santos.

All rights reserved. No part of the material protected by this copyright may be reproduced, stored in a retrieval system, or transmitted in any form or by any means without prior written permission from the author, or when appropriate, from the publisher of the publication.

The work described in this thesis was performed at the Department of Dermatology of the Erasmus Medical Center Rotterdam, the Netherlands and was funded by the *Innovatiegerichte Onderzoeksprogramma* (IOP) Photonic Devices and managed by AgentschapNL, Ministry of the Economic Affairs from The Netherlands.

Improving Clinical Diagnosis of Melanocytic Skin Lesions by Raman Spectroscopy

Het verbeteren van de klinische diagnose van melanocytaire

huidlaesies met behulp van Raman spectroscopie

Thesis

to obtain the degree of Doctor from the

Erasmus University Rotterdam

by command of the rector magnificus

Prof. dr. H. A. P. Pols

And in accordance with the decision of the Doctorate Board.

The public defense shall be held on

Wednesday, 27th June 2018 at 11:30

by

Inês Pereira dos Santos

born in Fundão, Portugal

Erasmus University Rotterdam

Doctoral Committee

Promotor	Prof. dr. T. Nijsten
Other members	Prof. dr. C. Verhoef
	Prof. dr. A. M. M. Eggermont
	Prof. dr. I. Notingher
Co-promoters	dr. S. Koljenović
	dr. P. J. Caspers

Contents

CHAPTER 1

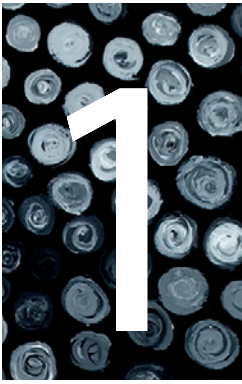

General introduction

Anatomy and physiology of the human skin

The skin is the largest organ of the human body. It has many functions beyond the primary vital function of being a protective barrier between the internal body and the external environment. The skin also has important roles in temperature regulation, endocrine, immunological and sensory functions, and ultraviolet (UV) radiation protection. The composition of the skin is characterized by several distinctive structural layers. The outer layer, the epidermis, is a stratified epithelium. The epidermis is supported by a layer of connective tissue, the dermis. Underneath the dermis is a layer of subcutaneous fat, also called hypodermis. The interface between the dermis and the epidermis shows dermal projections into the epidermis, forming dermal *papillae* and epidermal rete ridges (Figure 1). The total thickness of the epidermis varies between 50 and 150 µm, depending on the anatomical location, whereas the dermal thickness varies between 1.5 mm and 4 mm.

The dermis is mainly composed of collagen. In addition, this supporting matrix of the epidermis contains elastic fibers (elastin) and glycoproteins and glycosaminoglycan/proteoglycan macromolecules. Collagen represents approximately 80–85% of the dry weight of the dermis and is responsible for the great tensile strength of the skin. Collagen type I is the most abundant type of collagen in the dermis, whereas collagen type IV is essentially located in the basement membrane of dermis-epidermis junction.[2,3] Glycosaminoglycan and proteoglycan macromolecules in the dermis are responsible for the significant ability of this layer to retain water.[2] The dermis has

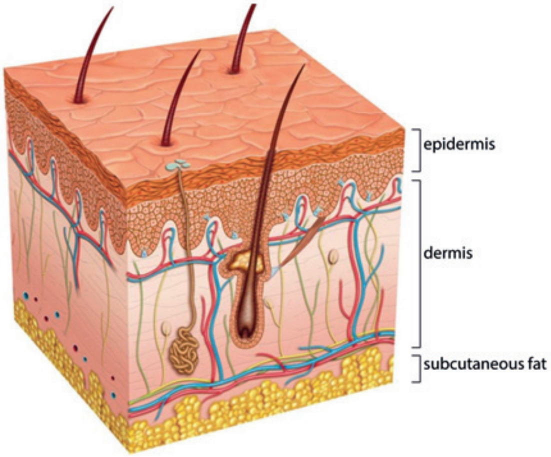

Figure 1. Schematic cross section of skin. Adapted from [1].

a very rich blood supply, presenting a superficial and a deep vascular plexus and a rich network of lymphatic vessels. The two vascular plexus are interconnected by vertical vessels and have branches to vascularize the dermal *papillae*.[4]

The epidermis contains different types of cells: (1) keratinocytes, the generic cell type of the epidermis that are dynamically regenerative; (2) melanocytes, which are responsible for the production of melanin, the natural pigment of the skin; (3) Langerhans' cells, which are antigen-presenting cells and have a role in immune response in the skin; and (4) Merkel cells, which act as sensory mechanoreceptors.[5,6]

The epidermis is not vascularized. This layer is under constant renewal, with a cycle time of approximately 30 days. Renewal of the epidermis involves a continuous process of generation, terminal differentiation and desquamation of keratinocytes. These are the generic cell type of the epidermis. Keratinocytes produce keratin and the major cellular constituent of the epidermis. The epidermis has morphologically different sub-layers reflecting the state of differentiation, as shown in Figure 2. Keratinocytes originate from stem cells located in the lowermost cell layer of the epidermis, the basal layer (*stratum basale*). In a process of maturation, keratinocytes migrate upward from the *stratum basale*, where keratinocytes are cuboid cells that have large, dense nuclei and an high mitotic rate. It usually constitutes a single cell layer. As the keratinocytes progress upward in their differentiation process, they show an increasing number of bundles of keratin filaments. Those filaments are extended, forming desmosomes, to bound to surrounding keratinocytes, what confers the spiny aspect of these cells in the *stratum spinosum* layer.[2,4] Upward, there is the *stratum granulosum* that is characterized by few layers of flattened polygonal cells filled with keratohyalin granules, a precursor of insoluble keratin.[4,7] The outermost layer of skin, the *stratum corneum*, is composed by many layers of corneocytes, flattened non-nucleated keratinized cells without cytoplasmatic organelles. In these cells, there is an increase of cellular compaction and crosslinking of keratin with transglutaminases to form an insoluble keratin matrix that, together with lipids (fatty acids, sterols, ceramides) and cornified-envelope proteins form the *stratum corneum*.[2,8] This cornified cells and its surrounding intracellular substances are responsible for the permeability characteristics of the skin.[2]

Melanocytes are mostly located in the basal layer. Apart from producing melanin, they use their dendrites to distribute this pigment to the surrounding keratinocytes.[2] Their dendrites extend to the upper layers of the epidermis, into the interstices, establishing contact with keratinocytes.[4,9] Each melanocyte is associated with approximately 30-36 keratinocytes, forming the epidermal melanin unit.[9,10] The production and storage of melanin occur in the melanosome, an intracellular lysosome-like structure.[11,12]

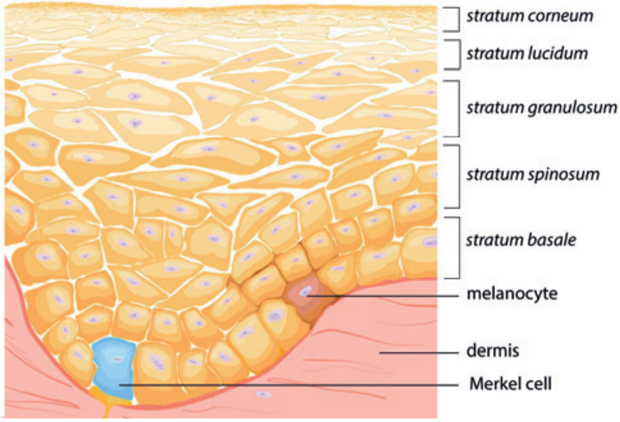

Figure 2. Schematic representation of the epidermal layers.

The process of melanin synthesis is regulated by tyrosinase, which is an enzyme that converts tyrosine firstly into 3,4-dihydroxyphenylalanine, then into dopaquinone, which is then converted into melanin after a series of transformations.[5] Once mature, the highly dense melanin granules migrate within the melanocytes dendrites to be transferred to nearby keratinocytes. Inside the keratinocyte, melanin accumulates in the supranuclear region of the cytoplasm, thereby protecting the DNA in the nucleus from the damaging effects of UV radiation.[4] One of the most important functions of the skin is to protect the body from the UV radiation. The hazard of UV radiation in human skin cells is due to the propensity of DNA to absorb UV radiation, which can result in DNA damage and lead to the formation of mutations in the highly mitotic active cells of the epidermis.[9,11] The synthesis of melanin by melanocytes is stimulated by UV radiation.[13] Melanin scatters and absorbs a wide spectrum of UV radiation and specifically protects the nucleus, which harbors the cell's DNA.

There are a multitude of lesions that can appear in the skin. Skin lesions can have several origins, in different types of cells. In this thesis, we confine on the pigmented skin lesions that have their origin in the melanocytes.

Melanocytic lesions

Melanocytic lesions are lesions with origin in the proliferation of melanocytes. They can vary between benign lesions, also termed melanocytic nevi, to malignant lesions, termed melanomas.[13]

Benign melanocytic lesions: nevi

Benign melanocytic nevi, commonly called moles, can be congenital or acquired.[14] Acquired nevi are the most common form of benign melanocytic lesions, which tend to appear during childhood or teenage years and appear more often in sun-exposed areas of the body.[13] It is known that sun protection measures can reduce their incidence, which implies that exposure to UV-radiation can be a pathogenic factor for melanocytic nevi formation.[13] Mutations in the BRAF gene (gene responsible for encoding the BRAF protein, from the RAF protein family, whose role is cell growth control), can be found frequently both in acquired benign and malignant melanocytic lesions. This mutation has an important role in the initial proliferation of melanocytes in melanocytic lesions.[15]

Dysplastic melanocytic nevi are melanocytic lesions that present clinically or histologically some degree of irregularity or architectural disorder at the cell level.[16-18] The term dysplastic is used as histological description whereas atypical nevus is a clinical description.[19] Sometimes the terms can be used interchangeably. In recent literature, dysplastic nevi are also termed as intermediate neoplasms.[13] A clinically atypical melanocytic nevus is a lesion larger than 5 mm showing irregular border and irregular pigmentation with a degree of inflammation. The histopathological description of a dysplastic nevus includes a description of an architectural disorder with individual or clustered melanocytes distributed at all levels within the epidermis and possibly from the papillary dermis into the lower dermis and elongation of epidermal rete ridges.[19,20] There is debate among the field about whether dysplastic nevi are biologically intermediate lesions between common nevi and unequivocal melanoma.[13]

Very often the clinical differentiation between benign melanocytic lesions and melanoma can be challenging, even for experienced dermatologists.

Malignant melanocytic lesions: melanoma

Epidemiology

Melanoma is the most fatal form of skin cancer. Yearly 232,000 new cases of melanoma are diagnosed worldwide and 55,488 deaths are reported.[21] The melanoma incidence has been steadily increasing in the last decades. The incidence varies significantly worldwide, with the Caucasian population affected most and the dark-skinned and Asian populations with the lowest incidence.[21] Although it is not the most common type of skin cancer, melanoma is the most aggressive and lethal form of skin malignancy. It is preferably diagnosed at an early stage because of the high risk of metastasis at a later stage. In more advanced stages melanoma is in almost all cases incurable.[22-24] Even though normal melanocytes can be found in non-cutaneous tissues (*e.g.*

in the eye) and in mucosal tissues (oral cavity, esophagus, nasal cavity and sinuses, genitals, and anus),[25] this thesis focuses on cutaneous melanoma only.

Melanomas may arise without having any pre-existing lesion (*de novo*) or can result from an evolution of an already existing lesion, usually from a melanocytic nevus (in approximately 25% of the cases).[26]

Melanomas can be categorized in: (1) those originated in skin that is chronically damaged by long-term exposure to UV radiation (chronic sun damage, CSD melanomas), or (2) those arising in intermittently sun-exposed skin but not chronically damaged by UV radiation (non-CSD melanomas).[13,27] CSD melanomas appear mainly in the head and neck region and on the dorsal side of distal extremities, and is more common in individuals >55 years.[13,27] On contrast, non-CSD melanomas commonly arise on the trunk of proximal extremities in younger individuals.[13,27] This is the most common subtype of melanoma in the Caucasian population.[27]

Risk factors

The risk of developing melanoma is determined by a combination of environmental risk factors, most importantly exposure to UV radiation, number of sunburns at a young age, and host risk factors.

Genetic predisposition is an important host risk factor and several specific mutations have been identified which significantly increase the risk of developing melanoma.[13,14,28] Most of the non-CSD melanomas are BRAF-mutant. Several studies on genetics of melanoma report that BRAF-mutant melanomas are more likely associated with the presence of multiple melanocytic lesions than non-BRAF-mutant melanomas, suggesting that this mutation is *per se* insufficient to contribute to melanoma development.[27,29-31] A family history of melanoma is also related to an increased risk of developing melanoma, especially in first-degree relatives. Several genes are associated with the higher predisposition in melanoma families.[32]

The number and type of nevi are another host risk factors. A meta-analysis performed by Gandini *et al.* on risk factors for cutaneous melanoma based on 46 studies, concluded that subjects that have more than 100 common nevi have up to seven times increased risk of melanoma compared with subjects with a lower number of common nevi (<15).[33] Individuals that present multiple atypical/dysplastic melanocytic nevi, usually more than 50, especially in conjunction with a family history of melanoma, are at an even greater risk of developing melanoma.[28] Although high-grade dysplastic nevi are associated with an increased risk of developing melanoma, [19,20,34] there is still debate whether dysplastic nevi are precursors of melanoma.[17,18] This is reflected in a lack of clinical management agreements about excision of dysplastic lesions. [35,36]

Melanoma stages

Melanoma typically develops in three histological stages. In an earlier stage, the neoplastic melanocytes are confined to the epidermis (melanoma *in situ*). In a melanoma *in situ*, the melanocytes can be distributed across the full thickness of the epidermis (pagetoid spread). Some malignant cells can start spreading horizontally within the epidermis (radial growth phase).[19] In an early stage, the melanoma cells still do not spread into the dermis (melanoma *in situ*). In a later stage, the spreading of malignant cells proliferates into the dermis (vertical growth phase), which is the start of the invasive stage in which tumor cells can invade vessels and metastasize.[19,23,24] Invasive melanoma can be potentially lethal.

Breslow thickness is the most important prognostic factor because it strongly correlates with the metastatic propensity. It is defined as the distance between the *stratum granulosum* of the epidermis and the deepest melanoma cell. The staging of melanoma relies on the Breslow thickness.[37-39]

According to the 8th edition of the American Joint Committee on Cancer, melanomas with a Breslow thickness < 0.8 mm can be treated surgically with a high cure rate and 5-year survival of 97-99%.[40] In contrast, the 5-year survival rate decreases rapidly to approximately 69% for melanomas with a Breslow thickness of 4 mm.[40] Patients with thicker melanomas and signs of distant metastasis have a 5-year survival rate < 30%.[40]

Classification of melanoma

The historical classification of melanoma is based on its clinical and histological characteristics,[22,23] comprising superficial spreading melanoma, lentigo maligna, acral lentiginous melanoma, nodular melanoma and other less common melanomas in mucosal sites.

Superficial spreading melanoma (SSM) is the most common type of cutaneous melanoma, especially among fair-skinned individuals. It is most often seen on the trunk of men and on the legs of women.[25,41] The main clinical features of the SSM consist of an irregularly pigmented macula with well-defined but irregular borders, and sometimes a raised plaque. Histologically, SSM is characterized by spreading of malignant melanocytes across the full depth of the epidermis, with an irregular distribution of either single malignant cells or nests of cells.[22,23]

Lentigo Maligna is a subtype of melanoma *in situ* and is seen most frequently on sun-exposed skin, especially in head and neck regions. Lentigo maligna is the precursor of a histological subtype of melanoma, the Lentigo Maligna Melanoma. In clinical evaluation, lentigo maligna is typically recognized by a varying brown macula with irregular borders and located on regions of severe sun damaged skin. The main histological characteristic of lentigo maligna is a spread of atypical melanocytes along the dermal-epidermal junction. When lentigo maligna is invasive it is called lentigo maligna melanoma.[23]

Acral Lentiginous Melanoma shows histological similarity to lentigo maligna melanoma, with the distinguishing difference that acral lentiginous melanoma is located on non-hair bearing regions such as palms, soles or subungual sites. The acral lentiginous melanoma can show both a radial and a vertical growth phase. The most common clinical features are very irregular borders of a pigmented macula, varying colors of the macula, and an elevated nodule with or without ulceration.[23] Histological features are characterized by large and atypical melanocytes with long dendrites and aberrant nuclei disposed along the basal layer. Not uncommon is the migration upwards of nests of malignant cells towards the *stratum corneum*.

The *Nodular Melanoma* is the only class of melanoma that has a minimal radial growth phase and an extensive vertical growth phase.[19,20,23] Clinically, this type of melanoma presents a rapid growing nodule, which is usually well-defined and symmetrical. It may present black or blue color. The histological features include a dense invasion into the dermis with the radial growth not being wider than the width of three dermal *papillae*.[23,42]

Figure 3 depicts the clinical presentation of the different classes of melanomas described above.

The problem: diagnosis of suspicious melanocytic lesions

The earliest possible clinical diagnosis of melanoma is of utmost importance for a good prognosis for the patient, to dramatically reduce the risk of dying from this disease. Nevertheless, discrimination of melanoma from benign melanocytic lesions can be challenging, even for experienced dermatologists. The first examination and clinical diagnosis of melanoma is based on visual inspection and recognition of its most common morphological characteristics, sometimes aided by dermoscopy. There are a variety of different algorithms that list and score the most common morphological characteristics of melanoma. Such algorithms and lists are used by dermatologists to recognize structures and help to establish a clinical diagnosis.

One of the most known algorithms is the ABCDE rule, which describes the following clinical characteristics of melanomas: (A) **A**symmetrical shape, (B) irregular **B**orders, (C) irregular pigmentation (**C**olour), (D) **D**iameter often > 5 mm, and (E) **E**volution of lesion over time. Other algorithms may include the presence of irregular dots, the possible presence of regression structures and atypical vascular pattern.[22-24,43,44] However, some melanomas lack common clinical features and therefore, are difficult to diagnose.[45]

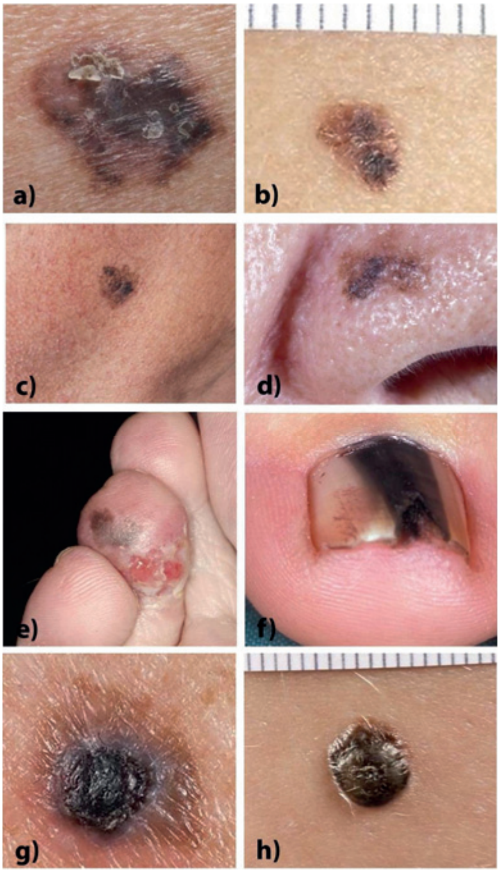

Figure 3. Examples of clinical presentation of melanomas. **a-b)** superficial spreading melanoma, **c-d)** lentigo maligna melanoma, **e-f)** acral lentiginous melanoma, **g-h)** nodular melanoma. (photographs kindly supplied by dr. R. van Doorn, LUMC, The Netherlands).

Because the clinical distinction between melanoma and benign pigmented lesions can be so difficult, and because of the severe consequences for the patient if an early melanoma is misdiagnosed, all suspicious lesions are excised for histopathological diagnosis to avoid the risk of missing a melanoma. The fact that most melanomas closely resemble benign melanocytic lesions and that clinical diagnosis is done by visual inspection of morphologic aspects results in a far-from-perfect diagnosing accuracy.[46]

The clinical accuracy depends on: (1) the detected true positive (TP) cases, (2) the missed true melanoma cases that were not identified during the clinical diagnosis (false-negatives, FN) and (3) the excised suspicious lesions that turn out benign after histopathological evaluation (false-positives, FP).

The number needed to treat (NNT) that is the number of benign pigmented lesions excised to detect one melanoma, varies between 4-15 for melanoma diagnosis by dermatologists and between 20-30 for general practitioners.[47-55] The NNT can be even higher in a population of young patients with less than 30 years (NNT = 75) or in high-risk populations (*e.g.* familial melanoma).[49-53,55] These numbers mean that out of all excised skin lesions suspected of melanoma, only 7-23% turns out to be a melanoma after histopathological diagnosis for dermatologists.[53] It is reported that for biopsy or referral accuracy, among general practitioners the sensitivity varies between 70-88%, and among dermatologists between 82-100%, and the specificity varies between 70% to 87% among general practitioners and between 70%-89% among dermatologists.[56] This implies that, according to those numbers a substantial number of early-stage melanomas goes unnoticed and will progress to the metastatic stage before being diagnosed. Obviously, the underdiagnosis of such fatal disease must be avoided. On the other hand, there is ample room to reduce the amount of (unnecessary) excisions because 77-93% of excised lesions did not have to be excised after all.[54]

Room for improvement

It is obvious that there is room for improvement in the clinical diagnosis of melanoma. By improving the accuracy of early melanoma diagnosis, not only the risk of lethal metastatic progression would be decreased, but it also would reduce the number of unnecessary surgical removals of benign skin lesions. In this way, new and accurate methods are needed to improve the specificity (probability of a clinical melanoma diagnosis, given that the patient has melanoma) and sensitivity (probability of a negative result, given that the patient does not have melanoma) of melanoma diagnosis.

Morphology-based techniques

Currently, the most used tool in the current practice by the clinicians worldwide for the examination of suspicious pigmented lesions and clinical recognition of melanoma is the epiluminescence microscopy, also known as dermoscopy. It consists of a magnifier and a polarized light source. It is used in combination with an oil medium, so that the light reflections on the skin surface can be reduced, which makes pigmented structures in the epidermis and dermal-epidermal junction visible.[43] Usually, the images are digitalized for further inspection and to check at a follow-up if the lesion has evolved.

Several studies report that the use of dermoscopy can improve the accuracy of detection of melanoma as compared to the unaided eye. However, this improvement is only seen when the dermoscopy is used by trained clinicians, implying that the learning curve for dermatologists to become experts in the interpretation of dermoscopic images is possibly lengthy.[57-59] The limitations of dermoscopy are confirmed by the relatively low clinical diagnostic accuracy (correct clinical diagnosis) for melanoma,[44] ranging between 56% and 80% for non-experienced and highly experienced dermatologists respectively.[60] As referred, these values depend on the training experience of the clinician, but not only. The high intra-observer variability among clinicians and the difficulty to an effective assessment are set by the fact that the dermoscopic images show many different structures with various different algorithms for interpretation. Besides, there are difficult cases where some lesions mimic melanoma morphologic features and vice-versa.

Other approaches are used to improve the diagnosis of early melanoma. Examples are total body photography, which enables assessment of changes in morphology of multiple pigmented skin lesions, and comparison of digital dermoscopy images taken at different time points (serial dermoscopy). These approaches aim at providing additional accuracy over unaided eye examination with dermoscopy, however, scientific evidence for the effectiveness of these more time-consuming methods is limited.[61]

Various methods have been investigated to objectively diagnose melanoma, almost all of which rely on image analysis and the detection of morphological differences. Examples of such methods are reflectance confocal microscopy,[62-64] confocal microscopy,[65,66] multispectral imaging [67,68] and automated dermoscopy image analysis.[69] Incremental improvements in diagnostic accuracy are feasible through optimization of these morphology-based methods. However, these technologies, the discrimination between melanoma and benign melanocytic lesions are again (as in the case of dermoscopy) based on morphological criteria that is subjective.

Even though electrical impedance spectroscopy is not an image-based technique, it evaluates morphological changes by measuring tissue impedance.[70,71] It can detect changes in cell shape, size and membrane composition.[72-74]

In the last years, automated image analysis based on deep learning algorithms has evolved largely. Applications for smartphones using these algorithms dedicated to dermatologists or to the public have flourished. Those algorithms can be fed with millions of images of lesions correlated to their clinical or histopathological diagnosis.[75-77] Although artificial intelligence algorithms have proved to help separate skin lesions classes, it is still necessary to evaluate its performance in clinical settings.[75] Besides, the diagnosis of skin lesions is also based in other contextual factors beyond visual inspection, like host factors. The interpretation of the visual inspection (digitally or not) by dermatologists can be complemented by objective methods with an insight over the biochemical composition of the lesions.

Biochemical composition-based techniques

A promising approach is the analysis based on biochemical and genetic differences. It is known that these differences are greater and more specific than those in morphological appearance.[78,79] Research in proteomics and genomics have revealed that melanoma and benign melanocytic lesions demonstrate marked differences with respect to their biomolecular composition.[80-84] On the DNA, RNA and protein level thousands of melanoma-specific alterations have been identified in tumor tissue and cultured cells.[85-88] Methodologies that aim to identify characteristics of the biomolecular composition of the pigmented skin lesions are more promising to provide a major step towards the improvement of melanoma diagnosis, since the molecular specificity enhances the specificity of the diagnosis. With molecular-based technologies, the discrimination of melanoma would not be dependent on the clinician's experience in recognizing morphological features, but on the molecular composition of the lesion itself. Besides enhanced sensitivities, specificities and positive predictive values of diagnosis, such methods would potentially enable diagnosis at an earlier stage of disease, which would enable improvement of treatment efficiency and survival rates.

Raman spectroscopy

Raman spectroscopy is an optical technique, based on the inelastic scattering of light. It enables the non-invasive analysis of tissue composition due to specific vibrations of the molecules comprising the tissue. This technique has been extensively used in many oncological applications, including in skin cancer diagnosis.[89-93]

The principle of Raman scattering

Raman scattering was discovered simultaneously and independently by L.I. Mandel’shtam and G.S. Landsberg in the USSR and by the Indian physicist Sir Chandrasekhara Venkata Raman in 1928. Raman was the person who was rewarded with the Nobel Prize of Physics in 1930 for this discovery and the person the phenomenon was named after.

Raman scattering is a process of inelastic scattering of light upon interaction with matter. When photons interact with molecules, they polarize the molecule’s electron cloud, raising the vibration energy of the molecule to a so-called ‘virtual energy state’ (Figure 4). After an extremely short time, commonly about 10^{-14} seconds, the molecule drops back to its vibrational ground state. In elastic scattering, also known as Rayleigh scattering, the molecule returns to the original ground state and thereby emits a photon in a random direction. This photon has the same energy as the incident photon, i.e. the wavelength of the emitted photon is the same as the wavelength of the incident photon (Figure 4).

It is also possible that an excited molecule falls back to an energy state different from the original state. This process is called inelastic scattering of light, also known as Raman scattering. The emitted photon has a slightly higher or lower energy than the original photon. This energy shift exactly matches the energy difference between the vibrational states. An observer can measure such energy shifts of scattered photons determine the vibrational energy levels of the molecules involved. When the molecule returns to an excited vibrational state, the energy of the emitted photon has decreased. This is called Stokes Raman scattering. When the molecule was in a vibrational state and returns to the ground state, the emitted photon has increased. This process is called anti-Stokes Raman scattering (Figures 4 and 5). The shift in energy between the incident and scattered photons can be observed as wavelength shifts. Stokes scattering results in a shift to a longer wavelength and anti-Stokes scattering results in a shift to a shorter wavelength. Rayleigh scattering is about 10^6 to 10^8 times more common than Raman Scattering, meaning that Raman signal is relatively weak when compared to the elastic scattering. At room temperature, the majority of molecules is in their ground state. As a result, elastic scattering is predominantly attributed to Stokes Raman scattering.

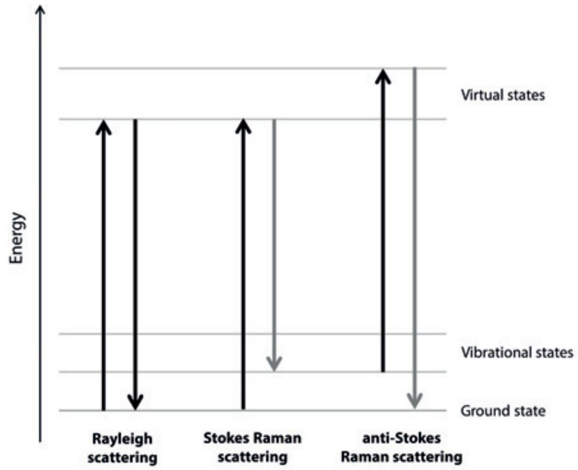

Figure 4. Diagram of energy states of a molecule in elastic scattering of light (Rayleigh) and in inelastic scattering of light (Raman). Adapted from [94].

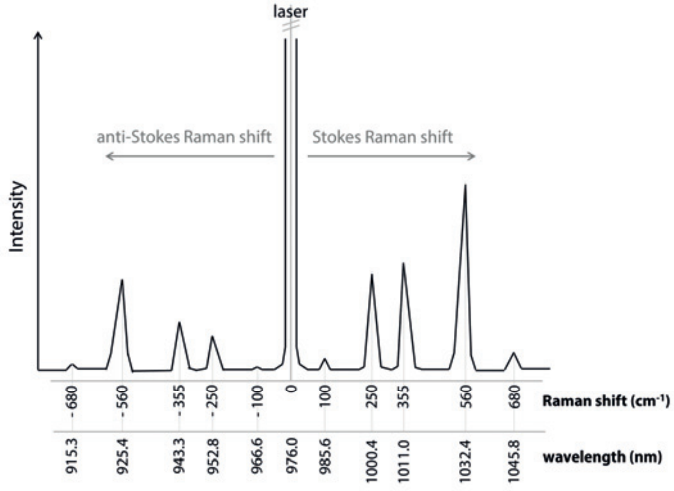

Figure 5. Schematic representation of a Raman spectrum with the respective Stokes and anti-Stokes shifts around the laser wavelength (in this example, 976 nm). Adapted from [95,96].

A Raman spectrum is a plot of the intensity of the elastically scattered light versus the Raman frequency shift. As illustrated in Figure 6, Stokes and anti-Stokes shifts are symmetrically positioned around the Rayleigh scattered light. At room temperature, Stokes-shifted Raman peaks are much more intense than the anti-Stokes-shifted Raman peaks. In the research described in this thesis, only Stokes-shifted Raman signal was investigated.

The position of a peak in the Raman spectrum corresponds to the energy required to excite a molecule to a certain energy level. Each peak in a Raman spectrum corresponds to a well-defined molecular vibration. Thus, a Raman spectrum provides specific information about the vibrational energy levels of a molecule, which are dependent on its molecular structure and which are a unique characteristic of that molecule. Raman shifts are commonly described in wavenumbers, which directly relate to energy. Conversion between wavelength and wavenumbers is done with the equation,

$$\Delta w = \left(\frac{1}{\lambda_0} - \frac{1}{\lambda_1}\right) \tag{1.1}$$

where Δw is the Raman shift expressed in wavenumbers (cm^{-1}), λ_0 is the initial wavelength of the excitation light (expressed in cm) and λ_1 is the wavelength of the Raman scattered photons (expressed in cm).

A Raman spectrum can be divided into two distinct spectral regions: the fingerprint region and the high-wavenumber (HWVN) region. The fingerprint region is typically defined as the range 400-1800 cm^{-1} and contains more spectral detail than the HWVN region, which ranges from 2500 to 4000 cm^{-1}. The HWVN Raman spectrum of tissue is dominated by the stretching vibrations of the chemical CH groups (Carbon- Hydrogen bond) and OH groups (Oxygen-Hydrogen bond).

Raman instrumentation

The functional components of a Raman instrument are simple. A Raman instrument contains a light source, delivery and collection optics, a spectrometer and a detector. However, because of the fundamentally extremely low intensities of Raman signals and the requirement to accurately measure wavelength shifts, an actual Raman instrument can be a rather complex device.

Lasers are the light sources of choice for Raman spectroscopy because they can provide intense monochromatic light of a stable and narrow wavelength. For applications involving Raman measurements on pigmented samples, as in the case of melanoma, intense laser light can induce tissue auto-fluorescence. The intensity of the fluorescence can be orders of magnitude stronger than the intensity of the weak Raman scattered light, and poses a major problem to obtain good quality Raman spectra. The use of lasers with longer wavelengths can diminish this problem to a level where good quality Raman spectra can be obtained from pigmented tissues (Chapter 2 of this thesis). The delivery of light from the laser unit to the sample can be done in various ways depending on the specific application. For instance, for *in vivo* medical applications, the most convenient solution is delivering light through a flexible fiber-optic probe, which enables Raman measurements on different parts of the patient's body.

The spectrometer, or spectrograph, is the element used to disperse the Raman photons into their different wavelengths.

The detector is the component that detects the Raman scattered photons. Because the intensity of Raman signals is extremely low, typically tens to hundreds of photons per second, the detector must be sensitive and produce extremely little noise. The choice of detector also depends on the wavelength range. For visible to near-infrared wavelengths (up to 785 nm) the state-of-the-art detector is a cooled silicon-based Charge Coupled Device (CCD) detector, which combines very low noise levels with high sensitivity for wavelengths up to 1100 nm. For longer wavelengths, detector types other than silicon-based should be used. Examples are germanium, indium-gallium, indium-gallium-arsenide detectors. Such detectors are characterized by their inherently high noise levels.

Raman spectroscopy for diagnosis of melanoma

Over 20 years Raman spectroscopy has been investigated as candidate technique for *in vivo* characterization of biological tissue and, more specifically for noninvasive diagnosis of non-melanoma skin cancer. Non-melanoma skin cancers do not have their origin in melanocytes and are therefore usually not pigmented. Examples of non-melanocytic skin cancers are basal cell carcinoma and squamous cell carcinoma. Many studies have reported good results of Raman spectroscopy in discriminating between non-melanoma skin cancer and benign lesions or healthy skin.[89-93] Specific characteristics that make Raman spectroscopy especially interesting for diagnostic applications in dermatology are the potentially high discriminating sensitivity and specificity and the ability to be used *in vivo*, directly on the skin of the patient. Such Raman spectroscopic measurements are painless, do not require tissue preparation and do not require (histochemical) staining or labeling or use of reagents. These are important characteristics to facilitate translation to the clinic.

Hurdle of applying Raman spectroscopy for diagnosis of pigmented lesions

However, the application of Raman spectroscopy for the analysis of pigmented biological samples, such as melanocytic lesions, presents a major hurdle. When using visible or near-infrared laser excitation wavelengths up to about 850 nm, the absorption of light by melanin in pigmented skin lesions results in strong laser-induced tissue fluorescence. This fluorescence signal is generally much more intense than the Raman signal from the tissue, to a point where the Raman spectral features are completely masked by the interfering fluorescence. This makes difficult, if not impossible, to obtain high-quality Raman spectra from pigmented tissues.

Several strategies have been developed to reduce the interference from fluorescence. However, these solutions have insufficiently resolved the problem for Raman spectroscopy of pigmented tissues. Frequent problems were insufficient reduction of interference from fluorescence, too complex measurement setups for use outside the laboratory environment and insufficient perspective for application *in vivo*. Many efforts to solve the fluorescence interference problem have focused on a correction of the detected signal for fluorescent backgrounds. These inevitably result in spectral artifacts, in particular with a Raman signal that is weak compared to the fluorescence background. Other strategies resulted in long acquisition times incompatible with the clinical application.

The solution, as described in this thesis, aimed at avoiding the generation of fluorescence at the source, by using a laser with a longer wavelength well into Short Wave Infrared range, in combination with the employment of a novel low noise multi-channel detector to enable recording of high quality Raman spectra in short signal collection times.

The research described in this thesis was performed in the framework of the RASKIN project, funded by *Innovatiegerichte Onderzoeksprogramma* (IOP) Photonic Devices and managed by AgentschapNL, Ministry of the Economic Affairs from The Netherlands. The RASKIN project was comprised by a consortium that involved expertise from research, clinical and company-oriented partners: (1) the Raman group at the Center for Optical Diagnostics and Therapy (CODT) of the Erasmus University Medical Center; (2) Leiden University Medical Center; (3) Philips Lighting B.V.; (4) RiverD B.V; (5) the Netherlands Organization for Applied Scientific Research (TNO); (6) Delft University of Technology, and (7) Avantes B.V.. This project had as final goal the development of a low-cost, easy-to-use Raman spectroscopic device for use by dermatologists and primary care physicians, for objective, rapid identification of suspicious pigmented skin lesions.

Aims of this thesis

High-quality Raman signals from melanocytic lesions compatible with a possible clinical application have not been demonstrated yet. The objectives of the work described in this thesis were:

I: The development of a Raman spectroscopic prototype for objective and fast assessment of melanocytic skin lesions clinically suspicious for melanoma;

II: Identification of the main spectroscopic features of melanoma and benign melanocytic lesions suspicious for melanoma;

III: Assessment of the feasibility of Raman spectroscopy as an adjunct technique to improve clinical diagnosis of melanocytic skin lesions.

Outline of this thesis

Chapter 2 describes the developed Raman instrument based on a low-noise InGaAs imaging camera. In this study, we demonstrate the application of a novel imaging camera as a spectroscopic detector in Raman spectroscopy. Results are presented of high-quality HWVN-Raman spectra with low fluorescence background of samples, which would not be possible with CCD-based instruments. The feasibility of using this detector for Raman spectroscopy was demonstrated by shot-noise limited multichannel Raman spectroscopic measurements of pigmented biological samples in the SWIR region.

Chapter 3 describes an alternative laser source developed within the RASKIN project. A 986-nm CW electrically pumped VECSEL is characterized and implementation in the SWIR multi-channel Raman spectroscopy instrument has been investigated. This study tests the suitability of the VECSEL for Raman spectroscopy applications. Vertical-external-cavity surface-emitting lasers (VECSELs) are an interesting

alternative laser source for Raman spectroscopy. VECSELs offer a narrow linewidth, high power stability, good power efficiency and circular beam profile characteristics, and their wavelength can be engineered over a broad range in the near-infrared. In addition, they offer the potential of low-cost mass production, and they are small in size. The VECSEL was characterized in relation to the requirements set by this biomedical application. For the first time, Raman spectra of pigmented skin lesions with a VECSEL in the SWIR region were demonstrated. The results show that the VECSEL fulfills the requirements of a laser source to be applied in Raman spectroscopy, opening the possibility of using VECSELs for low-cost compact hand-held Raman spectroscopy applications.

In Chapter 4, the developed instrument was employed to obtain Raman measurements of freshly excised skin lesions clinically suspected of melanoma in an out-patient clinic that follow high-risk patients with familial melanoma. These are medically important use cases, with clinical relevance. The main objective was to explore whether there is spectroscopic information in the HWVN range (2800–3050 cm^{-1}) to discriminate melanoma from benign melanocytic lesions. In total, 82 excised lesions were measured. The analysis was limited to include only histopathologically homogeneous lesions. This decision was based on the lack of point-to-point correlation between the Raman measurement location and the respective histopathology, which precluded a reliable gold standard for individual measurements on heterogeneous lesions. The results showed that the main spectral differences between melanoma and benign melanocytic lesions can be assigned to the symmetric CH stretching vibrations of lipids, with the Raman spectra of melanoma having an increased contribution from lipids compared to the other histopathological classes. In this study, a classification model was developed using PCA-LDA to investigate the discriminatory power of the CH region of HWVN Raman spectra. The model was optimized to discriminate melanoma from all the other lesion classes included in the analysis, with a leave-one sample-out cross-validation. Our preliminary classification model correctly classified all melanomas (sensitivity 100%) with a specificity of 45%.

Chapter 5 describes a development of a diagnostic model to discriminate melanoma from benign melanocytic lesions using multiple measurements within the lesion. This makes the method less sensitive to lesion heterogeneity. In order to have a representative Raman signal contribution, a filtering method of non-informative spectral contributions of keratin and collagen was developed.

Chapter 6 provides an overview of the current status of the Raman technology towards clinical translation, using Technology Readiness Levels (TRL) for each Raman clinical study. The TRL is an index used to measure the maturity and usability of an evolving technology. The problems that need to be solved in order to bring the technique successfully to the end-users in the hospital setting are discussed. The importance of defining the clinical needs and requirements, for different applications, is also explored in this review.

Chapter 7 presents the implementation of the simplest possible probe design, which is a single-fiber probe, in the SWIR multi-channel Raman spectroscopy instrument. The purpose of this study was to characterize its sampling depth to test its viability for (early) melanoma diagnosis and to test the feasibility of the implemented single-fiber probe for *in vivo* Raman spectroscopy measurements on pigmented skin lesions.

In Chapter 8 a general conclusion is drawn from the work developed and described in this thesis, as well as a discussion about the prospects of the implementation of Raman spectroscopy for improvement of clinical diagnosis of melanocytic skin lesions.

References

1. "Cytoplan blog," 2016. [Online]. Available: https://blog.cytoplan.co.uk/la-piel/. [Accessed: 10-Jan-2018].
2. J. A. McGrath and J. Uitto, "Anatomy and Organization of Human Skin," in *Rook's Textbook of Dermatology*, 8th ed., Eds. T. Burns, S. Breathnach, N. Cox, and C. Griffiths, Wiley-Blackwell, 2010, 3.1-3.53.
3. T. T. Nguyen, C. Gobinet, J. Feru, S. B. -Pasco, M. Manfait, and O. Piot, "Characterization of Type I and IV Collagens by Raman Microspectroscopy: Identification of Spectral Markers of the Dermo-Epidermal Junction," *Spectrosc. An Int. J.*, 2012, 27, 5–6, 421–427.
4. J. Malley, H. Lebowitz, and P. J. Boyle, Eds., "Skin," in *Basic Histology*, 11th ed., McGraw-Hill, 2005, pp. 360–372.
5. L. C. Junqueira and J. Carneiro, Eds., "Skin," in *Basic Histology*, 11th ed., McGraw-Hill, 2005, 360–372.
6. C. B. Archer, "Functions of the Skin," in *Rook's Textbook of Dermatology*, 8th ed., D. A. Burns, S. M. Breathnach, N. H. Cox, and C. E. M. Griffiths, Eds. Wiley-Blackwell, 2010, p. 4.1-4.11.
7. G. C. Priestley, "An Introduction to the Skin and its Diseases," in *Molecular Aspects of Dermatology*, Ed. G. C. Priestley, John Wiley & Sons, 1993, 1–17.
8. A. Sandilands, C. Sutherland, A. D. Irvine, and W. H. I. McLean, *J. Cell Sci.*, 2009, 122, 9, 1285–1294.
9. A. J. Thody, "Skin Pigmentation and its Regulation," in *Molecular Aspects of Dermatology*, Ed. G. C. Priestley, John Wiley & Sons, 1993, 55–73.
10. G. Li, K. Satyamoorthy, and M. Herlyn, *Crit. Rev. Oral Biol. Med.*, 2002, 13, 1, 62–70.
11. H. Ando, Y. Niki, M. Ito, K. Akiyama, M. S. Matsui, D. B. Yarosh, and M. Ichihashi, *J. Invest. Dermatol.*, 2011, 132, 4, 1222–1229.
12. J. Y. Lin and D. E. Fisher, *Nature*, 2007, 445, 7130, 843–850.
13. A. H. Shain and B. C. Bastian, *Nat. Publ. Gr.*, 2016, 16, 6, 345–358.
14. M. Rastrelli, S. Tropea, C. R. Rossi, and M. Alaibac, *In Vivo*, 2014, 28, 6, 1005–1011.
15. P. Uribe, I. I. Wistuba, and S. González, *Am. J. Dermatopathol.*, 2003, 25, 5, 365–370.
16. A. M. Goldstein and M. A. Tucker, *Cancer Epidemiol. Biomarkers Prev.*, 2013, 22, 4, 528–532.
17. K. Duffy and D. Grossman, *J. Am. Acad. Dermatol.*, 2012, 67, 1, 1–27.
18. K. Duffy and D. Grossman, *J. Am. Acad. Dermatol.*, 2012, 67, 1, 1-27.
19. J. A. Newton Bishop, "Lentigos, Melanocytic Naevi and Melanoma," in *Rook's Textbook of Dermatology*, 8th ed., Eds. T. Burns, S. Breathnach, N. Cox, and C. Griffiths, Wiley-Blackwell, 2010, 54.1-54.57.
20. D. J. Santa Cruz, "Tumors of the skin," in *Diagnostic Histopathology of Tumors*, 3th ed., Ed. C. D. M. Fletcher, Churchill Livingstone - Elsevier, 2007, 1423–1526.
21. World Health Organization, "GLOBOCAN 2012: Estimated Cancer Incidence, Mortality and Prevalence Worldwide in 2012," 2012. [Online]. Available: http://globocan.iarc.fr. [Accessed: 22-Mar-2017].
22. R. L. Barnhill, M. C. Mihm, and G. Elgart, "Malignant Melanoma," in *Skin Cancer*, Ed. K. Nouri, 2007, 140–166.
23. E. de Vries, F. Bray, J. W. Coebergh, L. Cerroni, D. J. Ruiter, D. E. Elder, J. F. Thompson, G. N. P. van Muijen, R. A. Scolyer, and P. E. LeBoit, "Malignant Melanoma: Introduction," in *World Health Organization Classification of Tumors. Pathology and Genetics of Skin Tumors.*, Eds. P. E. LeBoit, G. Burg, D. Weedon, and A. Sarasain, IARC Press, 2006, 52–61.
24. B. Bandarchi, L. Ma, R. Navab, A. Seth, and G. Rasty, *Dermatol. Res. Pract.*, 2010, 2010: 583748.
25. N. Kibbi, H. Kluger, and J. N. Choi, "Melanoma: Clinical Presentations," in *Melanoma*, Eds. H. L. Kaufman and J. M. Mehnert, Springer International Publishing Switzerland, 2016, 107–129.
26. C. Bevona, W. Goggins, T. Quinn, J. Fullerton, and H. Tsao, *Arch. Dermatol.*, 2003, 139, 12, 1620.
27. D. C. Whiteman, W. J. Pavan, and B. C. Bastian, *Pigment Cell Melanoma Res.*, 2011, 24, 5, 879–897.
28. M. Berwick, D. B. Buller, A. Cust, R. Gallagher, T. K. Lee, F. Meyskens, S. Pandey, N. E. Thomas, M. B. Veierod, and S. Ward, *Melanoma*, 167. Cham: Springer International Publishing, 2016.
29. N. E. Thomas, S. N. Edmiston, A.

Alexander, R. C. Millikan, P. A. Groben, H. Hao, D. Tolbert, M. Berwick, K. Busam, C. B. Begg, D. Mattingly, D. W. Ollila, K. T. Chiu, A. Hummer, J. Lee-Taylor, and K. Conway, *Cancer Epidemiol. Biomarkers Prev.*, 2007, 16, 5, 991–997.

30. J. N. Poynter, J. T. Elder, D. R. Fullen, R. P. Nair, M. S. Soengas, T. M. Johnson, B. Redman, N. E. Thomas, and S. B. Gruber, *Melanoma Res.*, 2006, 16, 4, 267–273.
31. J. L. Maldonado, J. Fridlyand, H. Patel, A. N. Jain, K. Busam, T. Kageshita, T. Ono, D. G. Albertson, D. Pinkel, and B. C. Bastian, *JNCI J. Natl. Cancer Inst.*, 2003, 95, 24, 1878–1890.
32. J. Read, K. A. W. Wadt, and N. K. Hayward, *J. Med. Genet.*, 2015, 53, 1, 1–14.
33. S. Gandini, F. Sera, M. S. Cattaruzza, P. Pasquini, D. Abeni, P. Boyle, and C. F. Melchi, *Eur. J. Cancer*, 2005, 41, 1, 28–44.
34. M. Arumi-Uria, N. S. McNutt, and B. Finnerty, *Mod. Pathol.*, 2003, 16, 1, 764–771.
35. L. Strazzula, P. Vedak, M. P. Hoang, A. Sober, H. Tsao, and D. Kroshinsky, *J. Am. Acad. Dermatol.*, 2014, 71, 6, 1071–1076.
36. C. C. Kim, S. M. Swetter, C. Curiel-Lewandrowski, J. M. Grichnik, D. Grossman, A. C. Halpern, J. M. Kirkwood, S. A. Leachman, A. A. Marghoob, M. E. Ming, K. C. Nelson, E. Veledar, S. S. Venna, and S. C. Chen, *JAMA dermatology*, 2015, 151, 2, 212–218.
37. R. Alteri, M. Kalidas, L. Gadd, and K. Stump-Sutliff, “Survival Rates for Melanoma Skin Cancer, by Stage,” *American Cancer Society*, 2016. [Online.. Available: https://www.cancer.org/cancer/melanoma-skin-cancer/detection-diagnosis-staging/survival-rates-for-melanoma-skin-cancer-by-stage.html. [Accessed: 19-Jan-2018].
38. R. Siegel, J. Ma, Z. Zou, and A. Jemal, “Cancer statistics, 2014,” *CA. Cancer J. Clin.*, 2014, 64, 1, 9–29.
39. C. M. Balch, J. E. Gershenwald, S. J. Soong, J. F. Thompson, M. B. Atkins, D. R. Byrd, A. C. Buzaid, A. J. Cochran, D. G. Coit, S. Ding, A. M. Eggermont, K. T. Flaherty, P. A. Gimotty, J. M. Kirkwood, K. M. McMasters, M. C. Mihm, D. L. Morton, M. I. Ross, A. J. Sober, and V. K. Sondak, *J. Clin. Oncol.*, 2009, 27, 36, 6199–6206.
40. J. E. Gershenwald, R. A. Scolyer, K. R. Hess, V. K. Sondak, G. V. Long, M. I. Ross, A. J. Lazar, M. B. Faries, J. M. Kirkwood, G. A. McArthur, L. E. Haydu, A. M. M. Eggermont, K. T. Flaherty, C. M. Balch, and J. F. Thompson, *CA. Cancer J. Clin.*, 2017, 67, 6.
41. C. Longo, A. Casari, and G. Pellacani, “Superfical Spreading Melanoma,” in *Reflectance Confocal Miscroscopy for Skin Diseases*, Eds. R. Hofmann-Wellenhof, J. Malvehy, G. Pellacani, and H. P. Soyer, Springer Verlag Berlin Heidelberg, 2012, 151–178.
42. C. Kuchelmeister, G. Schaumburg-Lever, and C. Garbe, *Br. J. Dermatol.*, 2000, 143, 2, 275–80.
43. N. H. Cox and I. H. Coulson, “Diagnosis of Skin Disease,” in *Rook’s Textbook of Dermatology*, 8th ed., Eds. T. Burns, S. Breathnach, N. Cox, and C. Griffiths, Wiley-Blackwell, 2010, 5.1-5.26.
44. M. E. Vestergaard, P. Macaskill, P. E. Holt, and S. W. Menzies, *Br. J. Dermatol.*, 2008, 159, 669–676.
45. H. Skvara, L. Teban, M. Fiebiger, M. Binder, and H. Kittler, *Arch. Dermatol.*, 2005, 141, 2, 155–60.
46. C. M. Grin, A. W. Kopf, B. Welkovich, R. S. Bart, and M. J. Levenstein, *Arch. Dermatol.*, 1990, 126, 6, 763–766.
47. S. Sidhu, O. Bodger, N. Williams, and D. L. Roberts, *Clin. Exp. Dermatol.*, 2012, 37, 1, 6–9.
48. L. Kofler, M. Egger, and H. Kofler, *Clin. Dermatology*, 2014, 2, 2, 73–76.
49. R. Marks, D. Jolley, C. McCormack, A. P. Dorevitch, *J. Am. Acad. Dermatol.*, 1997, 36, 5, 721–726.
50. J. K. Robinson and B. J. Nickoloff, *Arch. Dermatol.*, 2004, 140, 1, 49–56.
51. J. P. Banky, J. W. Kelly, D. R. English, J. M. Yeatman, and J. P. Dowling, *Arch. Dermatol.*, 2005, 141, 8, 998–1006.
52. N. Nathansohn, A. Orenstein, H. Trau, A. Liran, and J. Schachter, *Isr. Med. Assoc. J.*, 2007, 9, 10, 708–712.
53. C. Hansen, D. Wilkinson, M. Hansen, and G. Argenziano, *J. Am. Acad. Dermatol.*, 2009, 61, 4, 599–604.
54. P. Carli, F. Mannone, V. De Giorgi, P. Nardini, A. Chiarugi, and B. Giannotti, *Melanoma Res.*, 2003, 13, 2, 179–82.
55. G. Argenziano, L. Cerroni, I. Zalaudek, *et al.*, *J. Am. Acad. Dermatol.*, 2012, 67, 1, 54–60.
56. S. C. Chen, D. M. Bravata, E. Weil, and I. Olkin, *Arch. Dermatol.*, 2001, 137, 12, 1627–1634.
57. M. Binder, M. Schwarz, A. Winkler, A. Steiner, A. Kaider, K. Wolff, and H.

Pehamberger, *Arch Dermatol*, 1995, 131, 286–291.

58. M. Binder, M. Puespoeck-Schwarz, a Steiner, H. Kittler, M. Muellner, K. Wolff, and H. Pehamberger, *J. Am. Acad. Dermatol.*, 1997, 36, 2, 197–202.
59. J. I. van der Rhee, W. Bergman, and N. a Kukutsch, *Br. J. Dermatol.*, 2010, 162, 3, 563–567.
60. C. A. Morton and R. M. Mackie, *Br. J. Dermatol.*, 1998, 138, 2, 283–287.
61. G. Salerni, C. Carrera, L. Lovatto, J. A. Puig-Butille, C. Badenas, E. Plana, S. Puig, and J. Malvehy, *J. Am. Acad. Dermatol.*, 2012, 67, 1, e17–e27.
62. I. Alarcon, C. Carrera, J. Palou, L. Alos, J. Malvehy, and S. Puig, *Br. J. Dermatol.*, 2014, 170, 4, 802–808.
63. P. Guitera, S. W. Menzies, G. Argenziano, C. Longo, A. Losi, M. Drummond, R. A. Scolyer, and G. Pellacani, *Br. J. Dermatol.*, 2016, 175, 6, 1311–1319.
64. A. D. Stevenson, S. Mickan, S. Mallett, and M. Ayya, *Dermatol. Pract. Concept.*, 2013, 3, 4, 19–27.
65. C. Curiel-lewandrowski, C. M. Williams, K. J. Swindells, S. R. Tahan, S. Astner, R. A. Frankenthaler, and S. Gonza, *Arch Dermatol*, 2004, 140, 9, 1127-1132.
66. P. Guitera, S. W. Menzies, C. Longo, A. M. Cesinaro, R. A. Scolyer, and G. Pellacani, *J. Invest. Dermatol.*, 2012, 132, 10, 2386–2394.
67. R. R. Winkelmann, J. Yoo, N. Tucker, R. White, and D. S. Rigel, *J. Clin. Aesthet. Dermatol.*, 2014, 7, 12, 16–18.
68. X. Delpueyo, M. Vilaseca, S. Royo, M. Ares, L. Rey-Barroso, F. Sanabria, S. Puig, J. Malvehy, G. Pellacani, F. Noguero, G. Solomita, and T. Bosch, *J. Biomed. Opt.*, 2017, 22, 7, 79801.
69. L. Yu, H. Chen, Q. Dou, J. Qin, and P. A. Heng, *IEEE Trans. Med. Imaging*, 2017, 36, 4, 994–1004.
70. Y. Glickman, O. Filo, and M. David, *Ski. Res. Technol.*, 2003, 9, 3, 262–268.
71. D. A. Dean, T. Ramanathan, D. Machado, and R. Sundarajan, "Electrical impedance spectroscopy stydy of biological tissues," *J. Electrostat.*, 2008, 66, 3-4, 165–177.
72. L. Rocha, S. W. Menzies, S. Lo, M. Avramidis, R. Khoury, L. Jackett, and P. Guitera, *Br. J. Dermatol.*, 2017, 177, 5, 1432-1438.
73. P. Mohr, U. Birgersson, C. Berking, C. Henderson, U. Trefzer, L. Kemeny, C. Sunderkötter, T. Dirschka, R. Motley, M. Frohm-Nilsson, U. Reinhold, C. Loquai, R. Braun, F. Nyberg, and J. Paoli, *Ski. Res. Technol.*, 2013, 19, 2, 75–83.
74. R. P. Braun, J. Mangana, S. Goldinger, L. French, R. Dummer, and A. A. Marghoob, *Dermatol. Clin.*, 2017, 35, 4, 489–493.
75. A. Esteva, B. Kuprel, R. A. Novoa, J. Ko, S. M. Swetter, H. M. Blau, and S. Thrun, *Nature*, 2017, 542, 7639, 115–118.
76. X. Zhang, *Comput. Assist. Surg.*, 2017, 22(sup 1), 267–277.
77. Y. Li and L. Shen, *Sensors (Basel)*, 2018, 18, 2.
78. D. Leupold, M. Scholz, G. Stankovic, J. Reda, S. Buder, R. Eichhorn, G. Wessler, M. Stücker, K. Hoffmann, J. Bauer, and C. Garbe, *Pigment Cell Melanoma Res.*, 2011, 24, 3, 438–445.
79. T. E. Matthews, I. R. Piletic, M. A. Selim, M. J. Simpson, and W. S. Warren, *Sci Transl Med.*, 2011, 3, 71, 71ra15.
80. G. S. Inamdar, S. R. V. Madhunapantula, and G. P. Robertson, *Biochem. Pharmacol.*, 2010, 80, 5, 624–637.
81. D. Sengupta and A. J Tackett, *J. Proteomics Bioinform.*, 2016, 4, 9, 1–7.
82. J. A. Carlson, J. S. Ross, A. Slominski, G. Linette, J. Mysliborski, J. Hill, and M. Mihm, *J. Am. Acad. Dermatol.*, 2005, 52, 5, 743–775.
83. R. Akbani, K. C. Akdemir, B. A. Aksoy, M. Albert, A. Ally, S. B. Amin, *et al.*, *Cell*, 2015, 161, 7, 1681–1696.
84. G. Botti, L. Marra, A. Anniciello, G. Scognamiglio, V. Gigantino, and M. Cantile, *Int. J. Clin. Exp. Pathol.*, 2015, 8, 9, 9742–9751.
85. B. C. Bastian, A. B. Olshen, P. E. LeBoit, and D. Pinkel, *Am. J. Pathol.*, 2003, 163, 5, 1765–1770.
86. C. G. Lian, Y. Xu, C. Ceol, F. Wu, A. Larson, K. Dresser, W. Xu, L. Tan, Y. Hu, Q. Zhan, C. W. Lee, D. Hu, B. Q. Lian, S. Kleffel, Y. Yang, J. Neiswender, A. J. Khorasani, R. Fang, C. Lezcano, L. M. Duncan, R. A. Scolyer, J. F. Thompson, H. Kakavand, Y. Houvras, L. I. Zon, M. C. Mihm, U. B. Kaiser, T. Schatton, B. A. Woda, G. F. Murphy, and Y. G. Shi, *Cell*, 2012, 150, 6, 1135–1146.
87. J. A. Curtin, J. Fridlyand, T. Kageshita, H. N. Patel, K. J. Busam, H. Kutzner, K.-H. Cho, S. Aiba, E.-B. Bröcker, P. E. LeBoit, D. Pinkel, and B. C. Bastian, *N. Engl. J. Med.*, 2005, 353, 20, 2135–2147.

88. S. D. Byrum, S. K. Larson, N. L. Avaritt, L. E. Moreland, S. G. Mackintosh, W. L. Cheung, and A. J. Tackett, *J Proteomics Bioinform*, 2013, 6, 3, 43–50.
89. A. Nijssen, K. Maquelin, L. F. Santos, P. J. Caspers, T. C. Bakker Schut, J. C. Den Hollander, M. H. A. Neumann, and G. P. Puppels, *J. Biomed. Opt.*, 2007, 12, 3.
90. C. A. Lieber, S. K. Majumder, D. L. Ellis, D. D. Billheimer, and A. Mahadevan-Jansen, *Lasers Surg. Med.*, 2008, 40, 7, 461–467.
91. S. A. Fox, A. A. Shanblatt, H. Beckman, J. Strasswimmer, and A. C. Terentis, *Lasers Surg. Med.*, 2014, 46, 10, 757–772.
92. H. Lui, J. Zhao, D. McLean, and H. Zeng, *Cancer Res.*, 2012, 72, 10, 2491–500.
93. N. Kourkoumelis, I. Balatsoukas, V. Moulia, A. Elka, G. Gaitanis, and I. D. Bassukas, *Int. J. Mol. Sci.*, 2015, 16, 7, 14554–14570.
94. P. Coombe and K. Sandeman, “Raman spectroscopy,” *University of Cambridge*. [Online]. Available: https://www.doitpoms.ac.uk/tlplib/raman/printall.php. [Accessed: 10-Jan-2018].
95. K. Maquelin, “*Confocal Raman miscroscopy - a novel diagnostic tool in medical microbiology*,” Erasmus Universiteit Rotterdam, 2002.
96. S. Koljenović, “*Towards Clinico-Pathological Application of Raman Spectroscopy,”* Erasmus Universiteit Rotterdam, 2008.

CHAPTER

Implementation of a novel low-noise InGaAs detector enabling rapid near-infrared multichannel Raman spectroscopy of pigmented biological samples

Inês P. Santos, Peter J. Caspers, Tom C. Bakker Schut, Remco van Doorn,

Senada Koljenović and Gerwin J. Puppels,

Journal of Raman Spectroscopy, **2015**; 46 (7): 652-660.

Abstract

Pigmented tissues are inaccessible to Raman spectroscopy using visible laser light due to the high level of laser-induced tissue fluorescence. The fluorescence contribution to the acquired Raman signal can be reduced by using an excitation wavelength in the near infrared range around 1000 nm. This will shift the Raman spectrum above 1100 nm, which is the principal upper detection limit for silicon-based charge-coupled device (CCD) detectors. For wavelengths above 1100 nm Indium Gallium Arsenide (InGaAs) detectors can be used. However, InGaAs detectors have not yet demonstrated satisfactory noise level characteristics for demanding Raman applications.

We have tested and implemented for the first time a novel sensitive InGaAs imaging camera with extremely low readout noise for multichannel Raman spectroscopy in the Short-Wave Infrared (SWIR) region. The effective readout noise of 2 electrons is comparable to that of high quality CCDs and 2 orders of magnitude lower than that of other commercially available InGaAs detector arrays.

With an in-house built Raman system, we demonstrate detection of shot-noise limited high quality Raman spectra of pigmented samples in the high wavenumber region, whereas a more traditional excitation laser wavelength (671 nm) could not generate a useful Raman signal due to high fluorescence.

Our Raman instrument makes it possible to substantially decrease fluorescence background and to obtain high quality Raman spectra from pigmented biological samples in integration times well below 20 seconds.

Introduction

Raman spectroscopy is widely used to characterize biological tissues and to detect the molecular changes associated with pathological processes, *e.g.* distinguishing malignant from non-malignant tissue.[1,2] However, the application of Raman spectroscopy in the analysis of highly pigmented biological samples presents a problem. When using laser excitation wavelength up to about 850 nm intense laser-induced tissue fluorescence often makes it difficult or impossible to obtain high quality Raman spectra.

Several strategies to reduce the interference from fluorescence have been developed, such as time gated detection,[3,4] photobleaching, [5,6] a confocal signal detection scheme, [7]surface enhanced Raman spectroscopy (SERS) [8] and resonance Raman (RR) scattering. However, these solutions have insufficiently solved the problem for (*in vivo*) Raman spectroscopy of pigmented tissues because they are either not sufficiently effective, lead to complex measurement setups, and/or have not shown to be applicable *in vivo*.

Even though confocal Raman instruments can significantly reduce fluorescence background from out-of-focus regions, this reduction is insufficient for highly fluorescent samples. Also digital background subtraction techniques [9-12] are not an appropriate solution to the fluorescence problem because they may be able to subtract the background but not the shot noise that is generated by the fluorescence. Some studies have used 785 nm excitation to obtain spectra of several types of pigmented skin lesions in the so-called fingerprint region (500-1800 cm^{-1}); baseline removal algorithms have to be employed to remove the very strong fluorescence background. [13] This inevitably results in spectral artifacts, in particular when the Raman signal is weak compared to the fluorescence background. Moreover, background subtraction cannot remove the shot noise that is added by the background. Nevertheless, using a large measurement volume (200 μm core diameter single fiber that illuminates a 3.5 mm diameter skin area), Lui *et al.* obtained useable Raman signals from excised pigmented tissues.[13]

The most established approach to reduce sample fluorescence in Raman spectroscopy is the use of excitation wavelengths outside the visible range: either in the near infrared (NIR) region, far above 700 nm,[14] or in the ultraviolet (UV), below 250-300 nm.[15] For application on biological tissues *in vivo* UV laser excitation is not desirable, as it may cause cell and DNA damage.[16] In addition, the penetration depth of UV light in tissue is only in the order of a few microns.[16,17] Several studies have suggested that using an excitation wavelength with a photon energy far from the energies of electronic transitions is most promising in this respect.[14,16,18,19]

Fourier-Transform (FT) Raman has been successfully used to obtain spectra of pigmented skin lesions.[20,21] This proves that the problem of tissue fluorescence can be overcome by using a longer laser excitation wavelength (1064 nm in the case of FT-Raman). However, FT-Raman spectroscopy is a multiplexing single-channel technique for which signal integration times are typically several orders of magnitude longer than for multi-channel Raman spectroscopy. This is not compatible with *in vivo* medical applications. Patil *et al*. have reported dispersive Raman spectroscopy of tissues with strong auto-fluorescence using 1064 nm excitation in combination with an Indium-Gallium-Arsenide (InGaAs) detector array.[14] Laser-induced tissue fluorescence was significantly reduced as compared to laser in the visible wavelength range, but at the cost of much lower signal-to-noise ratio (SNR) due to the high detector noise of the traditional InGaAs detector technology.

The ideal solution would be to use a higher wavelength laser excitation to reduce fluorescence in combination with low noise multi-channel Raman spectroscopy to enable short signal collection times.

Further reduction in interference from tissue fluorescence is seen in the high wavenumber (HWVN) spectral range (ca. 2500-4000 cm^{-1}), which is the part of the Raman spectrum with the largest Stokes-shift from the laser line and thereby in most cases also away from the spectral region with the highest tissue fluorescence intensity.

Although the HWVN spectral region is not as rich in spectral features as the fingerprint region, it has been shown to provide clinical diagnostic information just like the more commonly used fingerprint region (400-1800 cm^{-1}), enabling the distinction of malignant and healthy tissue. Ample evidence supports the presence of sufficient spectral features required for demanding biomedical applications, such as a diagnostic tool for tissue malignancies.[1,2,22,23] In addition, in this spectral range the interfering Raman signal from fused silica in optical elements such as lenses and optical fibers is virtually absent, enabling very simple fiber optic probe construction.[24]

Until now the detection of Raman signals in the SWIR region (>1100 nm) was constrained by limitations of the detector technology. For visible to NIR excitation the state-of-the-art detector is the cooled Charge Coupled Device (CCD) detector, which combines very low readout noise and very low dark current with high quantum efficiency. However, light with wavelength above 1100 nm cannot be detected due to the band gap of silicon. An alternative in this spectral range are InGaAs detectors, which enable detection at wavelengths well above 1100 nm.

During the past years there has been an increasing demand for low-noise dispersive spectroscopy solutions in the SWIR wavelength range. Dispersive spectroscopy allows multichannel detection. This, in contrast to for instance FT-Raman, enables simultaneous detection of Raman signal over a range of wavelengths, reducing the total integration time. Several companies have recently moved towards the SWIR range and have introduced InGaAs-based Raman devices. However, as mentioned above, InGaAs detectors show a very high inherent readout noise in comparison with CCD detectors. Also, the dark current is orders of magnitude higher than in CCD's, even when cooled to 77 K with liquid nitrogen. As a result of the relatively poor noise characteristics of InGaAs detectors the SNR of the Raman signal is limited by the detector noise of the InGaAs detector and not by shot noise of the Raman signal, which is typical for CCD-based Raman spectroscopy. This is not ideal for demanding Raman applications such as Raman spectroscopy of biological tissues.

A new type of deep-cooled InGaAs detector for SWIR imaging applications has recently been introduced by Xenics (Leuven, Belgium). This detector exhibits extremely low noise characteristics, approaching those of high-end CCD detectors, combined with a high quantum efficiency (>90%) up to 1570 nm.

We have developed a Raman instrument based on this novel low-noise InGaAs imaging camera. We show how it can be used for Raman spectroscopy and provide examples of its performance in obtaining high quality HWVN-Raman spectra with low fluorescence background of samples that are difficult to obtain using CCD-based instruments. In this paper we test the feasibility of this detector for Raman spectroscopy and demonstrate shot-noise limited multichannel Raman spectroscopy of biological samples in the SWIR region.

Materials and Methods

SWIR multichannel Raman instrument. A SWIR multichannel Raman instrument was constructed in-house (Figure1). The excitation light source was a single-mode continuous wave diode laser with a wavelength of 976 nm and an output power of 150 mW (Model R-type, Innovative Photonic Solutions, Monmouth Junction, NJ, USA).

The collimated light from the diode laser was expanded to a beam of 7.8 mm in diameter using two achromatic lenses (f = 9 mm, Ø6 mm and f = 100 mm, Ø25 mm, Edmund Optics Barrington, NJ, USA) and focused in the sample to a Gaussian spot with a diameter of ~6 μm using an achromatic lens (f = 35 mm, NA 0.36, Edmund Optics Barrington, NJ, USA). The backscattered Raman signal is collected by the same lens and focused onto the entrance slit (25 μm) of the spectrometer using an identical achromatic lens (f = 35 mm, NA 0.36). The achromatic lenses used in this setup have an anti-reflection coating (<0.5% reflection in the SWIR region of 900-1700 nm). Two long pass edge filters (OD>6.0, cutoff at 1064 nm, Model Raman Edge Filter, Edmund Optics, Barrington, NJ, USA) were used for laser light suppression in the signal detection path in front of the spectrometer. The f/#2 spectrometer, has an entrance slit with a width of 25 μm and a 5 cm^{-1}

spectral resolution and was customized to cover the spectral range between 1300-1550 nm (BaySpec Inc., San Jose, CA, USA).

The detector for the Raman signal is a Cougar-640 InGaAs imaging camera (Xenics, Leuven, Belgium) with an InGaAs focal plane array sensor with 512 x 640 pixels, cooled with liquid nitrogen to 77 K. The Cougar-640 camera offers two distinct readout modes. In the classical Integrate-Then-Read mode, the photo-electrons are collected for a fixed exposure time after which the accumulated charge is probed and the buffering capacitors are reset. This scheme results in a relatively high capacitor-reset noise. The second scheme uses the Read-While-Integrate (RWI) mode. In this scheme the accumulating photo-electrons are probed non-destructively during the integration period without resetting the buffering capacitors. In combination with a noise level that is already low for a single readout, the non-destructive sampling option can be used to virtually eliminate the effective readout noise of the detector. This will be explained in more detail in the section *Data pre-processing*.The captured spectral range of 1340-1540 nm corresponds approximately to a Raman spectrum from 2780 to 3750 cm^{-1}. The Raman spectrum is imaged on 512 pixels. The direction of the pixel readout process of the InGaAs-chip is perpendicular to the spectral direction, which avoids possible cross-talk effects between adjacent pixels.

A custom-made sample cartridge was used to hold an excised skin sample between two fused silica windows (Figure 2). For Raman measurements the cartridge was inserted inside an anodized aluminum cartridge holder that was mounted perpendicularly to the laser beam (Figure 2). The skin sample was placed in the laser beam and the focus position optimized on the Raman signal.

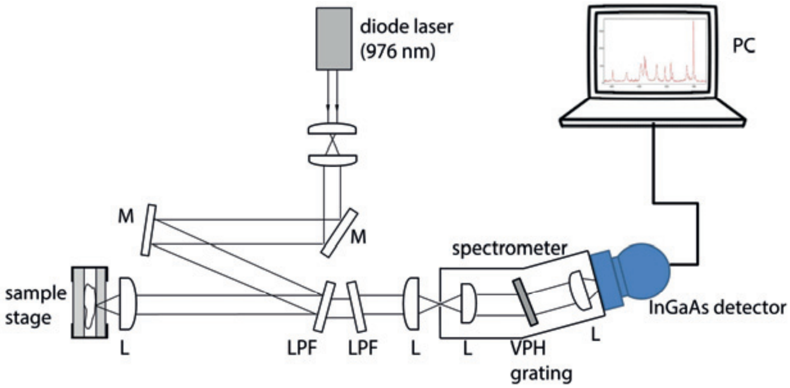

Figure 1. Scheme of the SWIR Raman spectroscopy setup. L: lens; M: mirror; LPF: long pass filter; VPH: volume phase holographic grating.

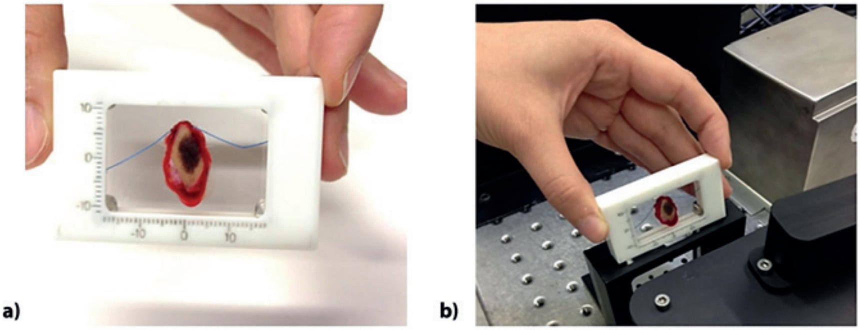

Figure 2. Skin sample holder. **a)** The skin sample is held between two fused silica windows; **b)** The sample cartridge is inserted in the cartridge holder.

State-of-the-art commercial Raman device. We used a commercial spectroscopic Raman device (Model 3510SCA Skin Analyzer, RiverD International B.V., The Netherlands), equipped with a 671 nm laser to record Raman spectra in the high wavenumber region, to compare the high wavenumber Raman spectra obtained with a CCD-based Raman multichannel system to the spectra obtained with the new SWIR-Raman setup. The CCD detector was an air-cooled back-illuminated CCD with 1024 x 128 pixels (Andor iDus type DU401A-BR-DD, Andor Technology Ltd., U.K.). The spectral range of this instrument is 2500 to 4000 cm^{-1}, with a spectral resolution better than 5 cm^{-1}.

Data pre-processing

The Cougar-640 InGaAs detector was originally designed for SWIR imaging. In order to use it for Raman spectroscopy software algorithms were developed and implemented to read and pre-process the raw data that are generated by the camera using the RWI scheme.

Non-destructive readout detection. The RWI mode has been described for low light level imaging in astronomy,[25-28] and is also known in the literature as the up-the-ramp readout scheme. During the course of a single integration the electrons generated in each pixel are buffered on a capacitor with a fixed pixel clock frequency. The voltage across the capacitor is then probed without resetting the capacitors, at regular time intervals that can be chosen by the user. The total integration time is thus divided into N equidistant intervals. RWI operation starts with a simultaneous global reset of the buffering capacitors of the entire array, followed by multiple non-destructive readouts which trace the evolution of the accumulating charge for each pixel (Figure 3). Because the noise in the successive non-destructive readouts is uncorrelated, the effective readout noise for the full signal integration time can be reduced by fitting a straight line through the successive readouts. To employ this readout scheme, the accumulating signal in each pixel was translated into a slope of a line fitted through all intermediate sampling points for that individual pixel. The counts in Analog-to-Digital converter Units (ADU) are then converted to the number of generated electrons, which equals the number of detected photons. The global conversion gain for the Cougar-640 camera is 0.168 photons per ADU. From the slope (number of detected photons per number of readouts) and the sampling rate (number of readouts per second), the signal intensity detected by each pixel was computed as the number of detected photons per second.

Using *N* uniformly spaced readouts, the readout noise in the total acquisition r_{out} is given by [26]:

$$r_{out} = \sigma_r / \sqrt{N} \tag{2.1}$$

where σ_r is the standard deviation of the residuals with respect the fitted line and defined by:

$$\sigma_r = \sqrt{\frac{\sum_{i=1}^{N}[(y(i) - p(x(i))]^2}{N}} \tag{2.2}$$

In this equation y(i) are the measured intermediate readouts and p(x(i)) are the values of the fitted line.

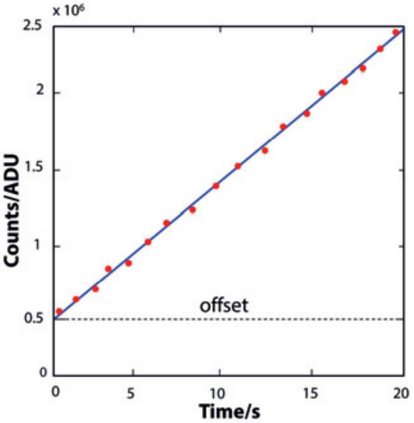

Figure 3. Representation of signal accumulation process for a single pixel. The red dots represent intermediate non-destructive readouts of the charge accumulated by the pixel, during accumulation. The slope of the linear regression represents the average signal intensity in counts per second.

Linearization of pixels response. During the characterization of the camera the response showed progressive non-linear behavior after the accumulated signal exceeded a certain threshold. We identified a cutoff threshold for the linear behavior. An algorithm was implemented to correct for this non-linear response of the pixels above the threshold value. A first order polynomial was fitted to the linear range during the first part of the integration period (Figure 4b). The ratio between the fitted line (in blue, Figure 3) and the intermediate pixel readouts (red dots, Figure 3) were stored in a lookup table together with the corresponding pixel readout values. The lookup table was created from the averaged result of 10 ratios. Thus for each pixel readout the lookup table provided a correction factor by linear interpolation. The response for each pixel was then linearized by multiplying the readout by the corresponding correction factor from the lookup table. For each pixel a first order polynomial was fitted to the linearized data to determine the slope (see Figure 4b) which represents the number of photons detected per second (Figure 4c).
Finally the slopes of the pixels in a region of interest of 12 pixels perpendicular to the spectral direction were co-added (Figure 4d) to result in a single detected intensity per super pixel for each spectral point.

Calibration of Raman spectra. Raman spectra were corrected for wavelength-dependent detection efficiency of the setup, using a NIST calibrated glass (NIST, Gaithersburg, Maryland, USA). Since no standard reference material (SRM) was available for 976 nm excitation wavelength, we used an SRM for 830 nm excitation (SRM 2246, NIST, USA) and compared the spectra acquired with an 830 nm laser to the spectrum acquired with the default 976 nm laser. The relative difference was smaller than 6%. We decided that this difference would be sufficient to use the SRM 2246 with an excitation wavelength of 976 nm to correct for the wavelength-dependent detection efficiency of the setup with satisfactory accuracy. The theoretical curve for 830 nm excitation and the curve obtained with the 976 nm laser were divided to determine a correction curve.
At the start of each measurement session a spectrum of the SRM 2246 was measured (with 976 nm excitation) to determine the wavelength dependent response of the instrument. All recorded Raman spectra in that session were corrected for this response.
The relative wavenumber calibration was determined using a calibration neon-argon lamp. The exact wavelength of the laser was determined using cyclohexane as a Raman standard spectrum, and the laser line position was computed from the Raman bands at 2852.9, 2923.8 and 2938.3cm^{-1}.
The Raman background that originates from the optics was subtracted from all spectra.

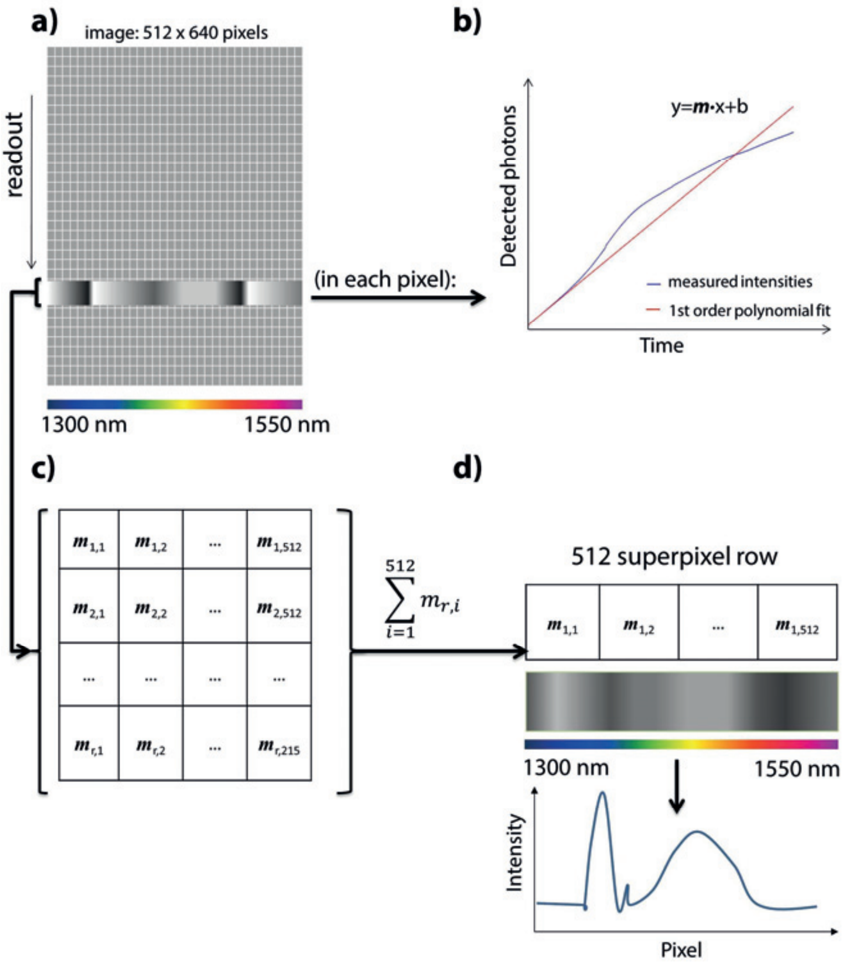

Figure 4. Schematic overview of the RWI processing algorithm. **a)** Only 12 rows of pixels are used to record the spectrum. The readout direction is indicated in the figure. **b)** For each pixel, the response as a function of time is linearized and the slope is determined; **c)** the slopes for different pixels are then co-added in the readout direction as indicated in a); **d)** the final Raman spectrum is obtained.

Sample preparation.

Ex vivo human skin. Pigmented human skin lesions suspected of melanoma were excised in the dermatology outpatient clinic of the Leiden University Medical Center (LUMC) as part of the standard patient care. Skin samples were obtained from one female and from one male subject. This study was approved by the medical-ethical committee at LUMC (C13.06). Informed consent was obtained from the patients.

The freshly excised skin samples were rinsed with NaCl 0.9% solution, gently flattened between two fused silica windows and measured within a maximum of 30 minutes after surgery with the in-house built SWIR Raman instrument. After measuring, the skin samples were put in a formaldehyde aqueous solution (4%) and sent to the pathology department for the routine diagnostic procedure. During this procedure it was also verified that no visual damage had occurred due to the measurements.

Human hair. A dark brown hair was clipped from one Caucasian female subject and measured immediately after collection. No hair treatment such as dying, waving, or other styling methods were used. Spectra were collected on the first third of the total length of the hair, close to the hair root.

Red wine. Dark red wine (grape type Aragonez, 13% alcohol) was obtained from a local store and measured in a fused silica cuvette of 1x1 cm diameter. The cuvette was placed in the sample holder and positioned in the laser focus.

Results

Readout noise and dark current

Table 1 shows the detector readout noise for a single readout and the dark current with the detector operating in a room at 23° C. The readout noise (per single readout) was determined according to equation 2.2, described in *Materials and Methods*.

Non-linearity in the detector response

The detector response was measured for different pixels until the saturation level of 3.5×10^6 detected photons was reached, using the Raman signal of cyclohexane (Figure 5a). Figure 5b shows the detector response of pixels exposed to different light intensities. The accumulated charge, expressed in number of detected photons, is shown as a function of time. With the time-axis normalized on the time to reach detector saturation the response of pixels exposed to different light intensities overlap (Figure 5c). This demonstrates that the non-linearity in the pixel

Table 1. Experimentally determined noise characteristics of InGaAs Cougar-640, Xenics®

Noise source	Electrons ± SD
Readout noise (e^- per single readout)	22.7 ± 5.9
Dark current (e^-/s/pixel) at room temperature	69.4 ± 4.5

response is a function of the total number of detected photons only and independent of the light intensity or rate at which photons are detected.

Figure 6 shows two HWVN-Raman spectra obtained *ex vivo* of a skin sample and illustrates the effect of non-destructive readout. Both spectra were obtained using a signal collection time of 10 seconds. The upper spectrum (spectrum a, Figure 6) was obtained using non-destructive readout at a sampling rate of 10 readouts/s (100 intermediate readouts in 10 seconds) and the bottom spectrum (spectrum b, Figure 6) was obtained with a sampling rate of 0.2 readouts/s (2 intermediate readouts in 10 seconds).

The readout noise given in Table 1 decreases significantly when more sampling readouts were performed during the integration time, in accordance with Equation. 1.1. Table 2 presents the

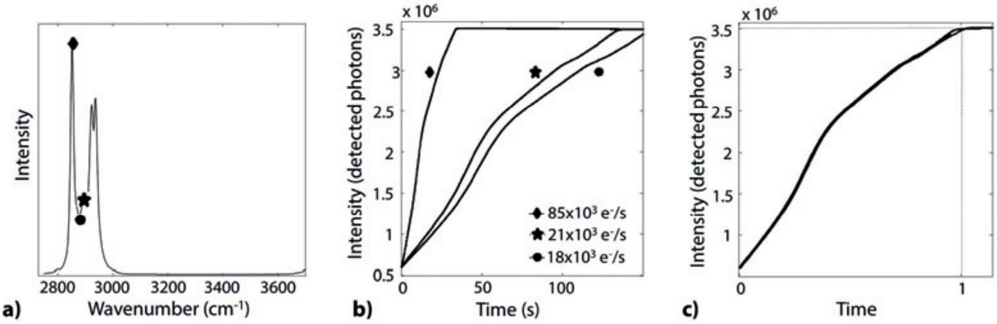

Figure 5. a) Raman spectra of cyclohexane; **b)** response curve of three different pixels (shown in **a**) exposed to different light intensities during the signal integration period; **c)** accumulation of charge as a function of normalized time, i.e. integration time divided by the time to reach the intensity threshold of saturation.

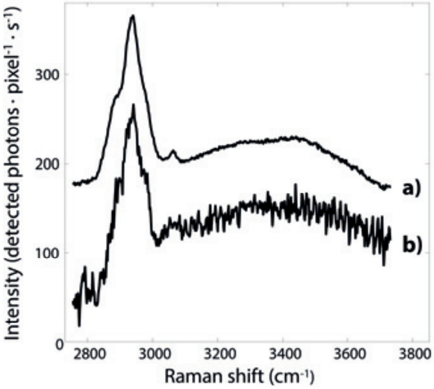

Figure 6. Raman spectra of *ex vivo* skin obtained with a signal integration time of 10s. The spectra are offset along the intensity axis for clarity. **a)** Spectrum obtained with a non-destructive readout rate of 10 readouts/s; **b)** Spectrum obtained with a nondestructive readout rate of 0.2 readouts/s.

readout noise (e^-/pixel) and the signal intensity in generated electrons of the spectra shown in Figure 6, which were measured with a different number of readouts. The signal intensity is the maximum intensity in the CH band at 2938.3 cm^{-1}. The readout noise was determined according to Equation. 1.1, (*Materials and Methods*).

Figure 7a shows how the spectral noise develops with increasing signal collection time. All spectra are acquired at the same non-destructive readout rate of 10 readouts/s. The HWVN-Raman spectra were obtained *ex vivo* of a pigmented skin lesion using different exposure times of 0.5 s, 1 s, 2 s, 4 s, 8 s and 16 s.

Table 2. The effective readout noise of the Cougar-640 detector

Number of intermediate readouts	Signal intensity (e-/pixel/s)	Effective readout noise (e-/pixel)	Dark current at room temperature (e-/s/pixel)
2	200	16.1	69.4
100	200	2.27	69.4

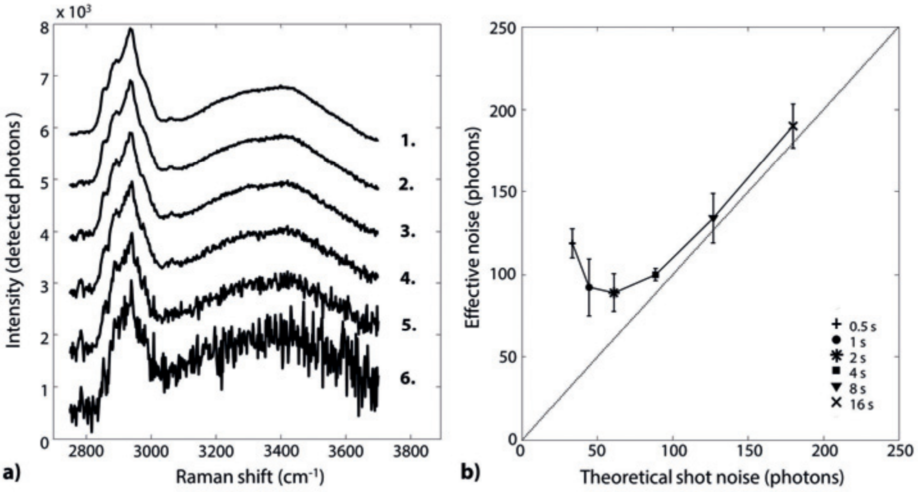

Figure 7. a) *Ex vivo* Raman spectra of pigmented human skin measured with different integration times with a non-destructive readout rate of 10 readouts/s. The spectra are offset along the intensity axis for clarity. 1) 16 s integration time; 2) 8 s integration time; 3) 4 s integration time; 4) 2 s integration time; 5) 1 s integration time; 6) 0.5 s integration time. **b)** Measured spectral noise of the spectra shown in a) versus the theoretical shot noise. The dashed line indicates the level at which the empirical noise equals the theoretical noise.

Figure 7b shows the measured spectral noise plotted against the calculated shot noise defined as square root of the signal.[29] The empirical noise in signal was determined after fitting a 2nd order polynomial to part of the OH-band (3360-3470 cm^{-1}) and then calculating the standard deviation of the residual.

To test the feasibility of acquiring Raman spectra of pigmented samples, we tested a number of samples which show high fluorescence when excited with visible light (red wine and dark brown human hair). This was done using 671 nm laser light and using 976 nm laser light (Figure 8).

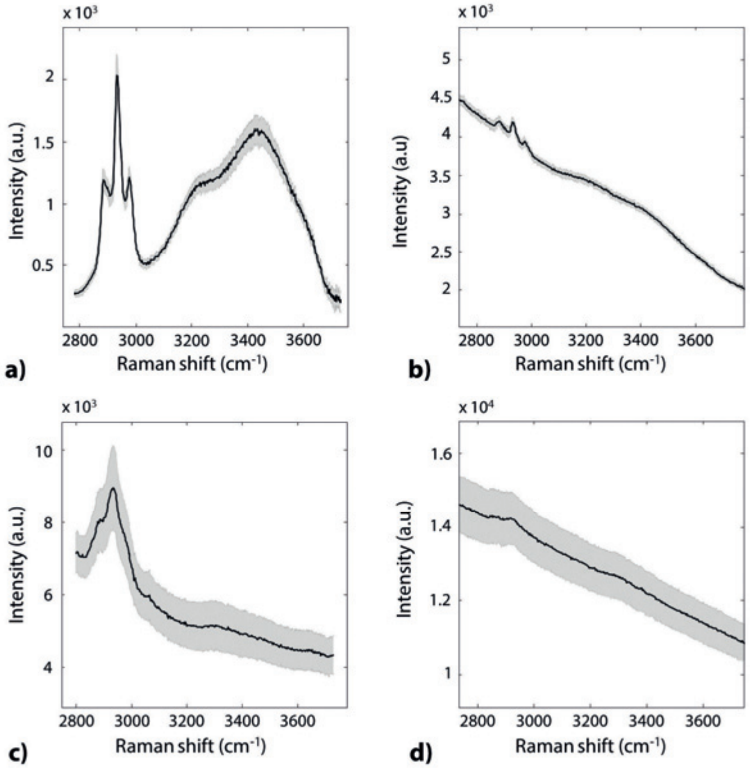

Figure 8. Raman spectra of pigmented biological samples. **a)** HWVN-Raman spectra of red wine obtained using 976-nm laser excitation and the SWIR Raman instrument built in-house. Signal collection time: 10 s; non-destructive readout rate: 10 readouts/s; **b)** HWVN-Raman spectra of red wine obtained using 671-nm laser excitation and a CCD-based Raman instrument (Model 3510 SCA, RiverD International B.V., the Netherlands). Mean spectrum and spectral variance are shown (25 spectra measured with a signal collection time of 1 s each); **c)** HWVN-Raman spectra of a human brown hair obtained using 976-nm laser excitation, a 10-s signal collection time, and non-destructive readout rate of 10 readouts/s; **d)** HWVN-Raman spectra of a human brown hair obtained using 671-nm laser excitation. Mean spectrum and spectral variance are shown (25 spectra measured with a signal collection time of 1 s each). In all figures the solid line represents the mean spectrum, and the shadow area represents the spectral variance (eight repeated measurements).

Figure 9 presents two examples of HWVN Raman spectra of highly pigmented excised human melanocytic nevi using the 976 nm SWIR Raman instrument. The spectra were acquired from eight different locations of the pigmented lesions shown in Figure 9a and 9c. The spectra presented were intensity-normalized and offset along the intensity axis for clarity.

Discussion

The purpose of this in-house built SWIR Raman instrument was to enable rapid acquisition of high quality Raman spectra of freshly excised pigmented human skin lesions. For detection of the Raman signals a novel SWIR InGaAs imaging camera was employed and adapted to Raman spectroscopy.

The choice of an excitation wavelength of 976 nm was guided by the requirement to collect signal in the 2780 - 3750 cm^{-1} spectral range with NIR excitation and by the 1570 nm sensitivity cut-off of the low-noise InGaAs detector. Using 976 nm excitation laser, the spectral range of 2780 - 3750cm^{-1} corresponds to signal detection in the 1340 nm - 1540 nm wavelength range. This spectral

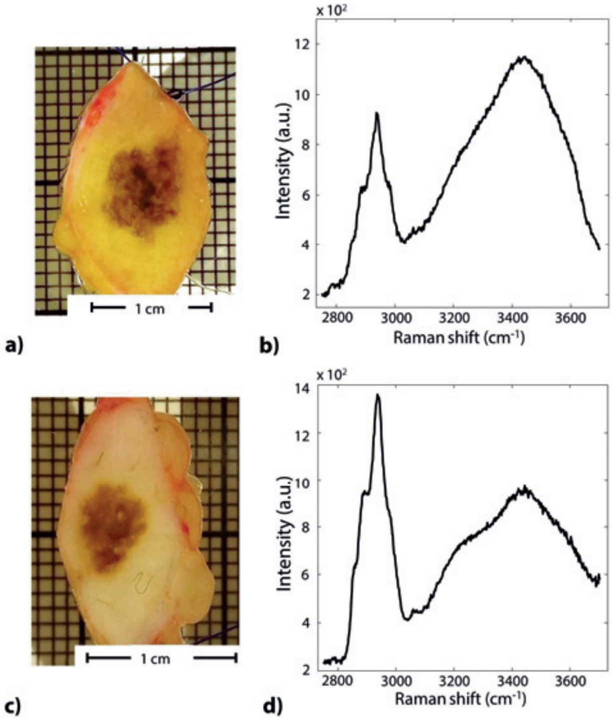

Figure 9. Photographs and corresponding Raman spectra of freshly excised human pigmented skin lesions using 976-nm laser excitation and the SWIR Raman instrument. Exposure time: 10 s. **a) and b)** Melanoma in situ; **c and d)** benign melanocytic nevus.

interval covers the CH-stretching, NH-stretching and OH-stretching regions, which enables the detection of protein, lipid, NH and OH vibration bands. We have shown earlier that this wavenumber range provides diagnostic information to differentiate malignant tissue from benign tissue.[1,2]

Noise characteristics SWIR InGaAs camera

The RWI readout scheme was specially designed for low light intensity applications, which also makes this camera of special interest for application in Raman spectroscopy. This readout scheme is a novelty for Raman spectroscopy and enables virtual elimination of readout noise. The detector noise characteristics were experimentally verified and approach those of high-quality CCD detectors, which is unprecedented for InGaAs detectors (Table 1). For instance, in a 10 second exposure time with a frame rate of 10Hz, the effective readout noise is reduced to 2.27 electrons (Table 2), which is comparable to the readout noise levels found in cooled slow-scan CCD detectors used in spectroscopy.

The experimentally determined dark current value (69.4 ± 4.5 e^-/s/pixel) is about seven times higher than specified by the manufacturer (< 10 e^-/s/pixel). In this manufacturer specification the dark current is measured in a cold room with an additional cold shield mounted in the detector housing, which significantly reduces the influence of thermal radiation from the environment. The dark current in this paper is determined under standard operational conditions without an internal cold shield and therefore reflects the effective dark current including collection of normal thermal radiation from the environment. The pixel reset of the InGaAs detectors introduce small variations in the pixel-capacitor values at the start of an integration. This results in a significant pixel-noise component, which could limit low-light applications. Using the RWI readout scheme, this reset noise component can be completely cancelled because the slope of the accumulated charge for each individual pixel is used, not the offset (Figures 3 and 4).

During integration cycles with a constant light source the detector showed a strong non-linear response of accumulated pixel charge versus time. The characteristic curve resembles an S-shape and is due to a fundamental feature of the type of capacitors used in this detector (Figure 5). This non-linearity is essentially caused by the bias leakage in the pixel circuitry of the readout chip that decreases during the integration period, which results in decreasing sensitivity. In order to obtain a linear response of the Raman spectral intensities, a non-linearity correction was performed on the individual pixels. This was possible because we could verify that the non-linear response was dependent on the accumulated charge of a pixel and not on the intensity or photon flux, and did not vary between pixels. This means that a single lookup table could be used to convert the non-linear scale of accumulated charge to the linear scale of number of detected photons for a given integration time. The practical implication is that linearization of the detector response can easily be implemented on-line in the acquisition software and does not require much processing power.

Shot noise or Poisson noise is associated with the particle nature of light and can be quantified by the square-root of the number of detected photons in a given time interval. For very strong signals the associated shot noise is generally the dominant noise factor but for weak signals, such as Raman signals from biological tissues, the detector noise can become a limiting factor. Ideally, the signal-to-noise ratio in a Raman spectrum is not limited by the detector noise but only by the unavoidable shot noise in the Raman signal. To test whether we could obtain quality shot-noise limited Raman spectra with the developed instrument we measured some biological samples that give low intensity Raman signals. Figure 6 illustrates that readout noise is drastically reduced by using the InGaAs detector in RWI mode with multiple non-destructive readouts during acquisition. Figure 7 shows how Raman signal evolves after 0.5, 1, 2, 4, 8, 16 s of acquisition. For shorter integration times the readout noise exceeds the signal shot noise. At high signal intensities the shot noise dominates other noise sources. The effective noise in the spectra approaches the theoretical shot noise values for exposures longer than 4 seconds, i.e., the noise in the spectra is determined by Poisson statistics and no longer by detector noise. The fact that the effective noise is slightly higher (about 9 photons) than the square root of the signal reflects the inaccuracy in the empirical determination of the effective noise in the spectra. It is clear from Figure 7 that, using the non-destructive readout scheme of this InGaAs detector (RWI), we were able to obtain shot-noise limited detection of weak HWVN-Raman signals from biological tissues with excitation and detection in the NIR and SWIR region.

We present some example spectra of naturally highly pigmented samples, of which it is extremely difficult to obtain high-quality and low-background Raman spectra with visible laser excitation. In the first example (Figures 8a and 8b) of red wine it is evident that the spectrum acquired with the 976 nm setup shows hardly any fluorescence background and a strong Raman signal is well visible, whereas the spectrum acquired with 671 nm excitation shows a very strong fluorescence background in comparison to the superimposed Raman signal. In the second example (Figures 8c and 8d), we could get a strong Raman spectrum from human brown hair, with the protein band and CH vibration features well perceptible on top a still noticeable fluorescence background. When measuring the same sample with 671 nm the background largely obscures the Raman signal, which that is only marginally noticeable on top of the strong background. The first measurements also show the feasibility of the in-house built instrument to obtain high-quality Raman spectra of biological pigmented samples in just few seconds of integration time. We also presented two examples of high quality Raman spectra of pigmented human skin lesions measured in only 10 s (Figure 9).

Now that technological limitation of multichannel detection above 1100 nm with extremely low noise levels is overcome, it is possible to use longer excitation wavelengths in Raman spectroscopy in order to decrease tissue fluorescence that would otherwise obscure the Raman signal. This detector enables low-fluorescence spectra from pigmented biological samples with a multichannel NIR detector.

Conclusions

In this paper, we describe a novel Raman instrument for obtaining high quality spectra from pigmented samples, using short signal integration times.

The key element in this setup is the low-noise InGaAs detector. It enables near shot-noise limited signal collection and opens a wide field of demanding applications, *e.g.* in medical diagnosis, food quality control, or other fields in which high quality Raman spectra of pigmented samples are required.

Acknowledgements

This project is funded by the IOP Photonic Devices managed by the Netherlands Enterprise Agency, Ministry of the Economic Affairs from The Netherlands (grant no. IPD12004).

References

1. A. Nijssen, K. Maquelin, L. F. Santos, P. J. Caspers, T. C. Bakker Schut, J. C. den Hollander, M. H. A. Neumann, G. P. Puppels, *J. Biomed. Opt*., 2007, 12, 3.
2. S. Koljenovic, T. C. Bakker Schut, R. Wolthuis, B. de Jong, L. Santos, P. J. Caspers, J. M. Kros, G. P. Puppels, *J. Biomed. Opt*., 2005, 3, 10.
3. D. V Martyshkin, R. C. Ahuja, A. Kudriavtsev, S. B. Mirov, *Rev. Sci. Instrum*., 2004; 75, 3.
4. P. Matousek, M. Towrie, C. Ma, W. M. Kwok, D. Phillips, W. T. Toner, A. W. Parker, *J. Raman Spectrosc*., 2001, 32, 12.
5. H. Wang, J. Zhao, A. M. D. Lee, H. Lui, H. Zeng, Photodiagnosis Photodyn. Ther. 2012; 9, 4.
6. A. M. Macdonald, P. Wyeth, *J. Raman Spectrosc*., 2006, 37, 8.
7. G. J. Puppels, W. Colier, J. H. F. Olminkhof, C. Otto, F. F. M. De Mu, J. Greve, *J. Raman Spectrosc*., 1991, 22.
8. M. R. Kagan, R. L. McCreery, *Anal. Chem*., 1994, 66, 23.
9. J. Zhao, H. Lui, D. I. McLean, H. Zeng, *Appl. Spectrosc*., 2007; 61,11.
10. Z.-M. Zhang, S. Chen, Y.-Z. Liang, Z.-X. Liu, Q.-M. Zhang, L.-X. Ding, F. Ye, H. Zhou, *J. Raman Spectrosc.,* 2009, 41, 6.
11. C. Lieber, A. Mahadevan-Jansen, *Appl. Spectrosc*., 2003; 57, 11.
12. C. M. Galloway, E. C. Le Ru, P. G. Etchegoin, *Appl. Spectrosc*., 2009, 63, 12.
13. H. Lui, J. Zhao, D. McLean, H. Zeng, *Cancer Res*., 2012, 72, 10.
14. C. Patil, I. J. Pence, C. Lieber, A. Mahadevan-Jansen, *Opt. Lett*., 2014; 39, 2.
15. N. Tarcea, M. Harz, P. Rösch, T. Frosch, M. Schmitt, H. Thiele, R. Hochleitner, J. Popp, *Spectrochim. Acta. A. Mol. Biomol. Spectrosc*., 2007, 68, 4.
16. E. B. Hanlon, R. Manoharan, T. W. Koo, K. E. Shafer, J. T. Motz, M. Fitzmaurice, J. R. Kramer, I. Itzkan, R. R. Dasari, M. S. Feld, *Phys. Med. Biol*., 2000, 45, 2.
17. R. Rox Anderson, J. A. Parrish, *J. Invest. Dermatol*., 1981, 77, 1.
18. B. Schrader, S. Keller, T. Lochte, S. Fendel, D. S. Moore, A. Simon, J. Sawatzki, *J. Mol. Sctructure*, 1995, 348.
19. B. Schrader, *Anal. Bioanal. Chem*., 1996, 355, 3.
20. M. Gniadecka, P. A. Philipsen, S. Sigurdsson, S. Wessel, O. F. Nielsen, D. H. Christensen, J. Hercogova, K. Rossen, H. K. Thomsen, R. Gniadecki, L. K. Hansen, H. C. Wulf, *J. Invest. Dermatol*., 2004, 122, 2.
21. P. A. Philipsen, L. Knudsen, M. Gniadecka, M. H. Ravnbak, H. C. Wulf, *Photochem. Photobiol. Sci*., 2013, 12, 5.
22. J. Mo, W. Zheng, J. J. H. Low, J. Ng, A. Ilancheran, Z. Huang, *Anal. Chem*., 2009, 81, 21.
23. K. Lin, D. L. P. Cheng, Z. Huang, *Biosens. Bioelectron*., 2012, 35, 1.
24. L. F. Santos, R. Wolthuis, S. Koljenović, R. M. Almeida, G. J. Puppels, *Anal. Chem*., 2005, 77, 20.
25. I. S. McLean, Electronic Imaging in *Astronomy: Detectors and Instrumentation*. 2008, Springer.
26. J. D. Offenberg, D. J. Fixsen, B. J. Rauscher, W. J. Forrest, R. J. Hanisch, J. C. Mather, M. E. McKelvey, R. E. McMurray Jr., M. A. Nieto-Santisteban, J. L. Pipher, R. Sengupta, H. S. Stockman, *Publ. Astron. Soc. Pacific*., 2001, 113, 780.
27. B. J. Rauscher, O. Fox, P. Ferruit, R. J. Hill, A. Waczynski, Y. Wen, W. X. Serafino, B. Mott, D. Alexander, C. K. Brambora, R. Derro, C. Engler, M. B. Garrison, T. Johnson, S. S. Manthripragada, J. M. Marsh, C. Marshall, R. J. Martineau, K. B. Shakoorzadeh, D. Wilson, W. D. Roher, M. Smith, C. Cabelli, J. Garnett, M. Loose, D. Lyon, W. Xia-Serafino, *Publ. Astron. Soc. Pacific*., 2007, 119, 857.
28. M. Robberto, *Instrument Science Report WFC 2007-12*. Space Telescope Science Institute, 2012.
29. A. Papoulis, S. U. Pillai, Probability, *Random Variables and Stochastic Processes*, 2nd Edition, 1984, McGraw-Hill, New York.

CHAPTER 3

Novel VECSEL for short-wave infrared Raman spectroscopy applications

Inês P. Santos, Alexander van der Lee, Xi Gu, Peter J. Caspers, Tom C. Bakker Schut,

Remco van Doorn, Vincent Noordhoek Hegt, Senada Koljenović, and Gerwin J. Puppels

Journal of Raman Spectroscopy, **2017**; 48 (6): 872–877.

Abstract

Raman spectroscopy of pigmented samples can be problematic due to strong laser-induced auto-fluorescence. Moving the laser excitation more into the near-infrared region (>900 nm) and detection to the short-wave infrared region (1200-1600 nm) significantly decreases laser-induced-fluorescence for many pigmented samples. However conventional near-infrared (NIR) diode-lasers suitable for Raman Spectroscopy are expensive. Vertical-external-cavity surface-emitting lasers (VECSELs) are an interesting alternative laser source for Raman spectroscopy. VECSELs offer a narrow linewidth, high power stability, good power efficiency and circular beam profile characteristics, and their wavelength can be engineered over a broad range in the NIR. In addition, they offer the potential of low-cost mass production and they are small in size. We developed a 986 nm VECSEL for a specific biomedical application (Raman measurements of pigmented skin lesions). We implemented and tested the feasibility of the novel 986 nm VECSEL in a short-wave infrared (SWIR) multi-channel Raman spectroscopy instrument. We have characterized the VECSEL in relation to the requirements set by this biomedical application and have demonstrated for the first time Raman spectra of pigmented skin lesion with a VECSEL in the SWIR region. Our results show that the VECSEL fulfils the requirements of a laser source to be applied in Raman spectroscopy. This opens the possibility of using VECSELs for low-cost compact hand-held Raman spectroscopy applications.

Introduction

Dispersive Raman spectroscopy has been mainly restricted to using visible excitation wavelengths due to the band gap of silicon, which does not enable the use of charge coupled device (CCD) detectors for wavelengths above 1100 nm. When using visible laser excitation wavelengths up to about 850 nm on pigmented samples, intense laser-induced tissue fluorescence is generated, which overwhelms the Raman signal. Because of that, pigmented biological tissues are traditionally inaccessible for dispersive Raman spectroscopy using a CCD detector and visible wavelength lasers. The short-wave infrared (SWIR) region (wavelengths from 0.9 to 1.7 μm) is an interesting region for Raman spectroscopy of pigmented tissues because the use of a longer laser excitation wavelength significantly reduces the tissue auto-fluorescence backgrounds.[1,2]

Laser diode sources in the 900-1000 nm range are not so much used in Raman spectroscopy and those with narrow and stable linewidth are expensive. Besides, edge-emitting laser diodes are characterized by their elliptical beam output and astigmatism.[3,4] There are several requirements that a laser light source needs to fulfil to be used in Raman spectroscopy. It is essential to have a narrow and highly stable linewidth (typically better than 1 cm^{-1}) to achieve high spectral resolution of the Raman spectrum and to avoid spectral shifts or spectral broadening.[5-7] The laser must have stable laser power to enable subtraction of background signals from the Raman spectra. Another requirement can be fundamental transverse mode operation to obtain a diffraction-limited beam quality, particularly important for confocal Raman (micro)spectroscopy.[5,7]

Recent developments in the vertical-external-cavity surface-emitting lasers (VECSEL) technology have brought their characteristics in the realm of Raman spectroscopy, with special interest for low-cost hand-held devices.[7-12] VECSELs are semiconductor lasers based on a vertical-cavity surface-emitting (VCSEL) chip. Therefore, in a VECSEL the light is emitted perpendicularly to the top surface of the chip. An additional mirror is used to create an external cavity, allowing control of the transverse mode properties while enlarging the area of gain in the semiconductor laser. This achieves a combination of high continuous-wave (CW) output power, due to a large gain area, and a low-divergence near-diffraction-limited beam, due to the transverse mode control of the extended cavity. The advantages of VECSELs over edge-emitting semiconductor lasers are: circular output beam, easy array fabrication, small size, and low cost at mass production.[4,13] Their cost advantages stem from their vertical nature, which allows on-wafer testing, easy extension to an extended cavity, and a better match with conventional semi-conductor equipment. However, a disadvantage of extended cavities is the presence of multiple longitudinal modes, which can potentially lead to mode-hopping. In order to avoid mode hops the temperature and current need to be tightly controlled or, alternatively, volume Bragg reflectors could be introduced as an external mirror.

In our previous work we tested the feasibility of an in-house built Raman spectroscopy device to acquire high-quality Raman spectra of pigmented skin lesions.[2,14] The instrument comprised a near-infrared (NIR) 976 nm edge-emitting diode laser. The Raman signal was detected in the SWIR region, using a sensitive indium-gallium-arsenide (InGaAs) detector with extremely low detector noise. With this prototype we demonstrated high-quality, shot-noise-limited high-wavenumber (HWVN) Raman spectra of pigmented skin lesions with acquisition times sufficiently short to be compatible with application in a clinical setting.[2]

In this study we have developed a 986 nm CW electrically pumped VECSEL and implemented this laser in the SWIR multi-channel Raman spectroscopy instrument to test the suitability of the VECSEL for Raman spectroscopy applications. We demonstrate that high quality Raman spectra from pigmented skin lesions in the SWIR region can be obtained.

Materials and Methods

VECSEL instrumentation. The developed CW electrically pumped VECSEL consists of a large oxide emission aperture (approximately 150 µm) semiconductor (GaAs/AlGaAs) cavity with a partial transmitting mirror on one side augmented with an external mirror for transverse mode control. A reduced reflectivity n-distributed Bragg reflector (DBR) structure was grown on a GaAs substrate. The active region consists of 3 quantum wells (QW) in one anti-node of the standing wave. The QWs contain indium and are separated by barriers containing phosphorus. Next to this active region was grown a thin layer with high aluminum content, which was oxidized to provide a current aperture. The growth was completed with a full reflectivity p-DBR structure. The device was processed with a full contact on the epitaxial side and therefore meant for flip-chip mounting i.e. substrate side emission. The backside of the substrate is anti-reflection coated. The external mirror with 90% reflectivity is a flat mirror as the lens developing in the substrate by temperature gradients (thermal-lens) is sufficient to define a stable resonator.

The VECSEL chip size is 1.7 by 1.7 mm. Current was supplied by a current source (model Keithley 2420, Tektronix, Beaverton, OR, USA). During operation the temperature of the VECSEL was kept stable within 21.05±0.05 ˚C using a thermal electric cooler with controller (model LDC 3744B, ILX Lightwave, Bozeman, MT, USA).

VECSEL beam profile and emission spectrum. The beam profile was measured with a beam profiling camera (Model WinCamD DataRay Inc., Redding, CA, USA) and corresponding stage. The ISO Standard 11146 describe test methods for laser beam widths, divergence and beam propagation ratios.[15] Following this standard the M^2 value of the beam was measured by focusing the laser with a lens (f= 19 mm focal length, Model C280-TMB, Thorlabs Inc., Newton, NJ, USA) and moving the camera through the focus region of the beam. The M^2 value was then calculated from the second order moment of the beam profile. To measure the emission spectrum of the VECSEL we used an optical spectrum analyzer (resolution of 10 pm at high resolution mode, resolution of 100 pm at low resolution mode, model Q8347, Advantest, Tokyo, Japan).

Current versus VECSEL optical output power curve. In order to measure the current versus optical output power curve we used a current supplier (model Keithley 2420, Tektronix, Beaverton, OR, USA) and the optical output power was measured with an integrating sphere power meter (model S145C, Thorlabs Inc, Newton, NJ, USA).

VECSEL wavelength stability. To determine the exact wavelength of the VECSEL we recorded the Raman spectrum of cyclohexane with well-defined Raman peaks at 2852.9, 2923.8 and 2938.3 cm^{-1}.[16] Possible variations in laser wavelength are reflected in variations in the peak positions of the Raman spectra of cyclohexane. From the accurate wavelength position of each peak of cyclohexane and their Raman shifts follows the corresponding laser wavelength. The laser wavelength was calculated from the average of those three peaks. Peak positions were accurately calculated from the zero-crossing of the first derivative of Raman spectra. We have tested the VECSEL wavelength stability over a short-term interval at a high spectrum-sampling rate (40 measurements within 30 minutes) for possible wavelength fluctuations and over an extended period of time, corresponding to a full-day of measurements at a low spectrum-sampling rate (one measurement every 20 minutes over approximately 5 hours) to identify possible wavelength drifts. The temperature of the VECSEL was kept constant to within 21.05±0.05˚C during all the experiments.

VECSEL power stability. The VECSEL power stability was tested over a short-period of time at an acquisition sampling rate of 10Hz over 16 minutes and over a longer period of time, corresponding to a full-day of measurements (approximately 5 hours). An optical power meter (Ge photodiode, Model S132C, Thorlabs Inc, Newton, NJ, USA) was mounted on the optical table, behind the sample position. During the experiments, the stabilized temperature of the VECSEL was monitored.

Raman spectroscopy instrumentation. A SWIR multichannel Raman instrument was constructed in-house and has been described elsewhere [2]. The collimated light from the VECSEL was focused in the sample to a Gaussian spot with a diameter of ~6 μm. The f/#2 spectrometer that was used (BaySpec Inc., San Jose, CA, USA), had an entrance slit with a width of 25 μm and had a 5 cm^{-1} spectral resolution. The spectrometer has been customized to cover the spectral range between 1300 and 1550 nm when using an excitation wavelength of 976 nm from the diode laser (IPS, Monmouth Junction, NJ, USA). The captured spectral range 1337.6-1532.4 nm corresponds to a Raman spectrum from 2659.0 cm^{-1} to 3609.7 cm^{-1} when using the 986 nm VECSEL.

Raman spectroscopy measurement protocol on pigmented skin lesion. Six excised pigmented skin lesions from an on-going study (approved by the Medical Ethics Committee of the Leiden University Medical Center, C13.06) were measured with the Raman spectroscopy instrument and the VECSEL laser in the Leiden University Medical Center (LUMC). Immediately after surgery, the freshly excised skin samples were rinsed with NaCl solution (0.9%), wiped with gauze soaked in ethanol (70%), pressed between two fused silica windows and inserted into the sample cartridge for Raman measurements.[2,14]

Pre-processing and calibration of Raman spectra. Raman spectra were corrected for the wavelength-dependent detection efficiency of the setup as described elsewhere, using an SRM2246 intensity standard (National Institute of Standards and Technology, Gaithersburg, Maryland, USA). The absolute wavenumber axis was calibrated using the spectral lines of a neon-argon lamp and the Raman spectrum of cyclohexane. The Raman background that originates from the optics was subtracted from all spectra.[2]

Results

VECSEL beam profile and emission spectrum. The developed VECSEL operates with a circular beam (ellipticity 0.95:1). The beam $1/e^2$ diameter output is approximately 100 μm. Figure 1a shows the beam profile measured with the beam profiling camera. The determined M^2 value is 1.5. Figure 1b shows the VECSEL spectrum with the central wavelength of emission at 986 nm and spectral linewidth of 5.75 pm (full width at -3dB) which spectrally corresponds approximately to 0.03 cm^{-1} in the detected Raman range (1350-1550 nm). The side mode suppression ratio is >30 dB. The temperature drift of the VECSEL is 0.03 nm/°C.

Current versus VECSEL wavelength and optical output power. Figure 2a shows the wavelength of the device versus current. As the current increases the device shows longitudinal mode hops, i.e., changes in the emitting central wavelength. The curve shows several ranges of 10 to 20 mA wide, on which the laser is stably operating in a single mode. For measurements on these stable plateaus the sensitivity of the wavelength with current is 0.01 nm/mA. However, when the current is set between 500 mA to 600 mA the laser operates in a higher order transverse mode regime and may be multimode. In this range the wavelength is no longer stable. Therefore, tight temperature control and current control are required to keep the VECSEL operating in a stable single mode with a constant wavelength. We have chosen to operate the VECSEL at 450 mA, which corresponds to an output power of approximately 100mW, for the Raman measurements in this study. The optical output power versus current (LI) characteristic curve in figure 2b shows the output power of the VECSEL at a temperature of 21.05 ±0.05°C. At currents below 200 mA there is no emission. Above 200 mA the optical output power increases roughly proportionally to slightly above 100 mW at a current of 500 mA.

VECSEL wavelength stability . Figure 3 shows the results for the wavelength stability tests. Figure 3a shows the measured Raman spectra of cyclohexane and the peaks used to calculate the laser wavelength. The three peaks of cyclohexane Raman spectrum were detected at 1373.63 nm, 1386.27 nm and 1389.20 nm, respectively. The results of the experiments carried out to detect possible laser wavelength changes in short and long-term are shown in figures 3b and 3c, respectively. The standard deviation of fluctuations in laser wavelength in the short-term measurement was ±0.01 nm. The maximum variation in the peak position was obtained during the long-term measurement (over period of 5 hours), corresponding to a SD of ±0.025 nm.

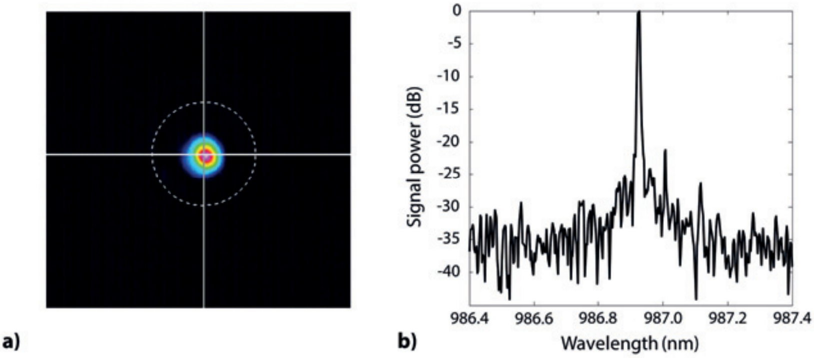

Figure 1. a) Beam profile(fundamental transverse TEM00 mode) recorded with a CCD camera. **b)** Measured VECSEL spectrum centred at the wavelength of 986 nm.

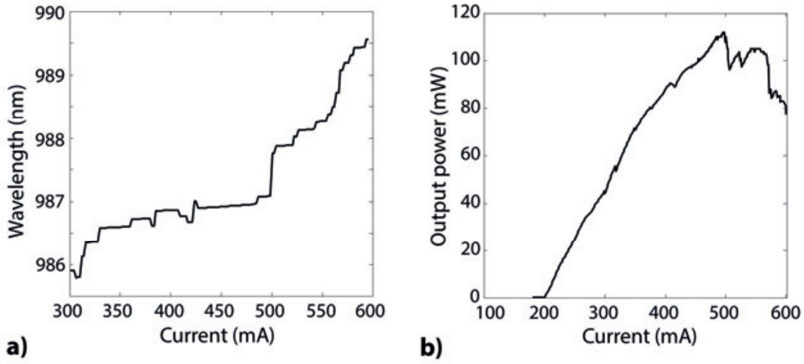

Figure 2. a) Wavelength-current curve of the 986-nm tested VECSEL; **b)** Optical output power -current (LI) curve of the 986-nm tested VECSEL (at 21.05 °C).

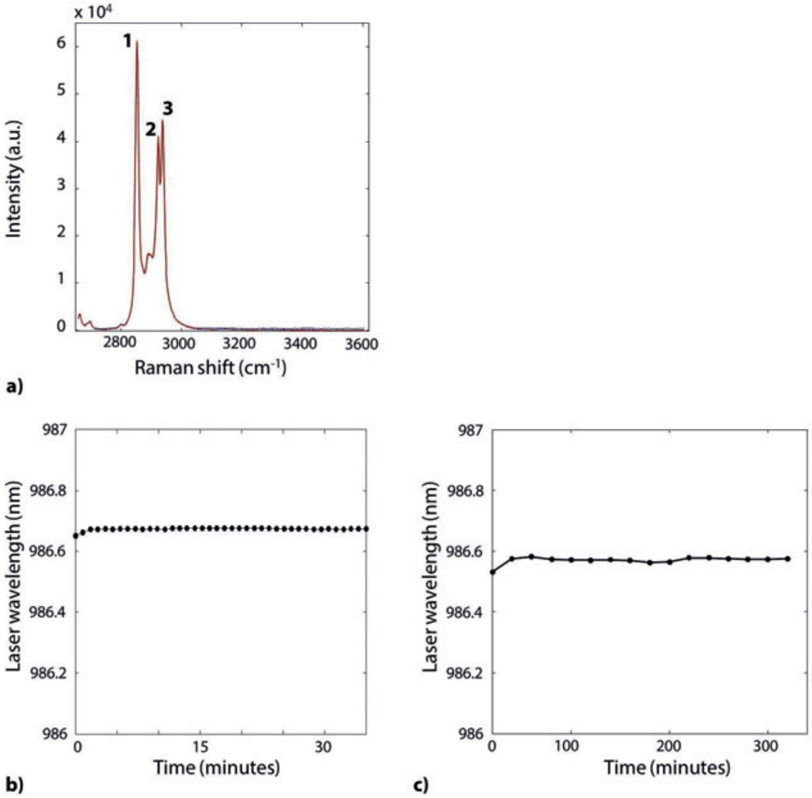

Figure 3. VECSEL wavelength stability. **a)** Cyclohexane was measured 40 times within 35 min for the short-term wavelength stability test. **b)** VECSEL wavelength stability over a period of 35 min (40 measurements, average wavelength: 986.6726 nm, SD = 0.01 nm); **c)** VECSEL wavelength stability over a period of 5 h (16 measurements, average wavelength: 986.5694 nm, SD = 0.025 nm).

VECSEL power stability The results for power stability tests of the VECSEL are presented in figure 4. Figure 4a shows the power variation during a single measurement of 16 minutes at an acquisition rate of 10Hz. The average value is 79.85±0.01 mW (SD). Figure 4b shows the power variation during a period of approximately 5 hours. During this time the power was measured 16 times, each time for 15 seconds at an acquisition rate of 10Hz. The average value is 79.95±0.01 mW (SD). The variation represents <0.02% of the average power. Raman spectra measured using the VECSEL showed laser light interference in the 1330-1530 nm spectral range (Figure 5). This interference could be sufficiently suppressed by insertion of an edge short-pass filter (OD>5.0, cutoff at 1000 nm, Model FESH1000, Thorlabs Inc., Newton, NJ, USA).

Demonstration of Raman measurement on pigmented skin tissue Figure 6 shows typical Raman spectra measured on two different excised pigmented skin lesions using the 986nm VECSEL (Figure 6a) and the 976 nm edge-emitting diode laser (Figure 6b). This figure illustrates a qualitative comparison of a Raman spectrum obtained with the developed VECSEL and the commercial edge-emitting diode laser. Each spectrum was obtained in an integration time of 30 seconds. Both spectra were intensity-normalized using the extended multiplicative scatter correction (EMSC) method.[17]

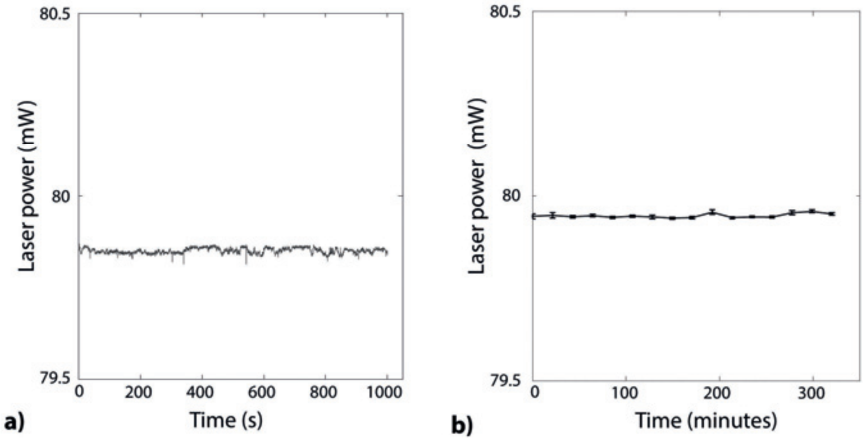

Figure 4. VECSELpower over **a)** 16 min; **b)** a period of approximately 5h.

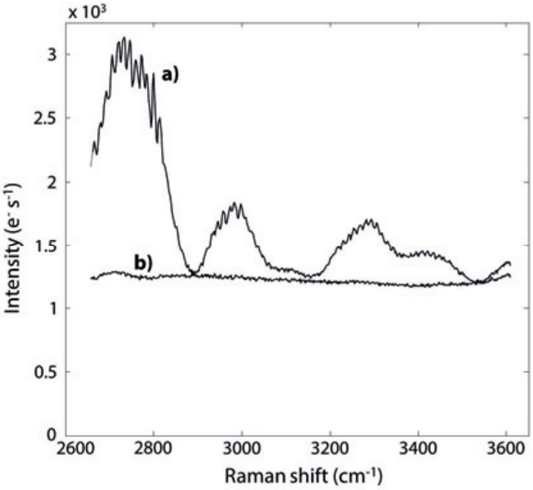

Figure 5. a) Background signal without additional filtering. **b)** After introduction of an edge short-pass filter (OD > 5.0, cutoff at 1000 nm) in the laser path this background signal was sufficiently suppressed.

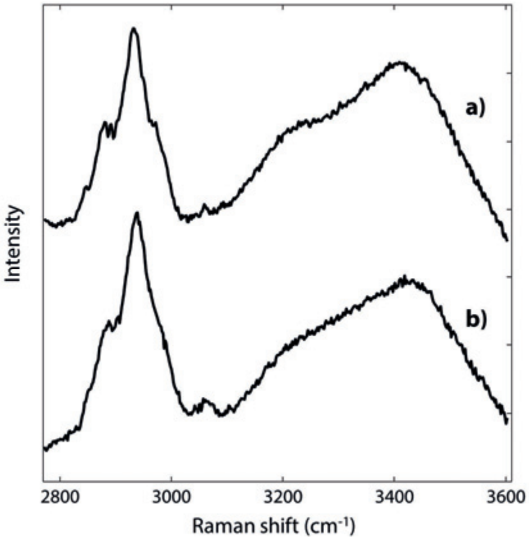

Figure 6. Examples of Raman spectra measured from two different excised pigmented skin lesions using the same in-house built Raman instrument. Acquisition time per spectrum: 30 s. The spectra are offset along the intensity axis for clarity. **a)** Using the developed 986-nm VECSEL (100 mW). **b)** Using a 976-nm edge-emitting diode laser (150 mW).

Discussion

The findings of this study show the feasibility of a novel developed VECSEL for Raman spectroscopy. The design wavelength of the VECSEL in this study was optimized to enable for Raman spectroscopy on pigmented tissues. However, the design wavelength can be changed to accommodate other applications as well. The design wavelength of the VECSEL can be tuned from approximately 800 - 1200 nm by changing the bandgap of the quantum well.

The tested VECSEL yields an excellent round beam profile with an ellipticity close to 1. In respect to beam spatial quality, the parameter M^2 indicates how much stronger a laser beam diverges angularly in the two transverse directions as compared with a single-transverse mode diffraction-limited beam, which is designated by M^2 value of 1.[4] In this tested VECSEL, the determined M^2 value was 1.5, which is close to a perfect Gaussian beam. This value is more than sufficient for the intended Raman application. In terms of spectral linewidth, the measured value is 5.75 pm (1.77 GHz), which was the operational resolution of the optical spectrum analyzer. This linewidth is very good for Raman spectroscopy. The possibility that the linewidth of the laser was more narrow could not be confirmed due to the limit of resolution of the optical spectrum analyzer used. The commercial 976 nm diode laser linewidth was specified at better than 18 pm (value limited by the resolution of the optical spectrum analyzer). In respect to spectral purity, the side mode suppression ratio is better than 30 dB, which corresponds to an OD3. This value is sufficient for many Raman spectroscopy applications. However, additional filtering with a short-pass filter in the laser path can remove unwanted light emission. In this study light emission from the laser source around 1300-1500 nm caused an enhanced background radiation which limited the sensitivity for the Raman signal (Figure 5a). This was solved by inserting a short-pass filter (OD>5) in the laser light emission path, blocking all light above 1000 m (Figure 5b).

The wavelength of the VECSEL is mainly dependent on the stabilization of its operating temperature and of the laser current. In figure 2a, we can see the effect on laser wavelength with increasing current. As the current increases the device shows longitudinal mode hops (in the order of 0.1 nm, which corresponds well with the expected mode spacing for a 4 mm extended cavity), in the region from 320 to 500 mA. In this range we can find plateaus of about 10 to 20 mA where the laser is operating in a single mode and the wavelength is stable. At higher currents (above 500 mA) the VECSEL operates in a high order transversal mode (M^2 value gets significantly higher) and multiple transverse modes can be lasing at the same time. Therefore, the drive current needs to be selected and kept constant to avoid longitudinal mode hops at currents in the fundamental mode region between 320 and 500 mA.

Temperature variations cause changes of the refractive index, and hence on the optical path length of the cavity. This induces changes in wavelength and output power. The temperature induced wavelength drift of the VECSEL semiconductor cavity is ~0.03 nm/°C. This means that the temperature needs to be stable at <0.1°C to limit wavelength changes to less than 3 pm. As mentioned before, to prevent mode-hopping the current should be chosen such, that the VECSEL operates in the middle of the single-mode stable plateaus of about 10 to 20 mA wide (Figure 2a). To limit the influence of current fluctuations on the wavelength of the VECSELs it is desired to make it 10 times smaller than the Raman sensitivity limit of 1 cm^{-1}, corresponding to 1 pm. This would result in a current stability of 0.1 mA. To ensure the overall wavelength stability, a requirement on current of 0.1 mA and temperature of 0.1°C is desired. The tested VECSEL was in contact with a Peltier element to ensure constant heatsink temperature during the measurement period. During these experiments the VECSEL temperature was kept stable within 0.1°C using the laser controller temperature driver. Temperature and current stabilization are easy to achieve, but additional hardware and power dissipation are needed for temperature stabilization. Temperature stabilization can be achieved using conventional package technologies with thermo-electric cooling and would fit in a TO-Can package.

A Raman spectrum provides a convenient and sensitive method to test laser wavelength stability by accurately monitoring small shifts in Raman peak positions. We did not observe noticeable fluctuations on a short time-scale of 30 minutes (SD=0.01 nm), nor did we see drifts over longer period of time of over 5 hours (SD=0.025 nm), which is a regular working period with the equipment. The short-term and long-term wavelength stability tests were performed on different days (Figures 3b and 3c, respectively). There is a slight wavelength difference ($d\lambda = 0.1032$ nm) between these days. The magnitude of this difference is comparable with mode hop differences shown in figure 2a, which suggests that the VECSEL was operating at a different longitudinal mode of the external cavity between those days. Nevertheless, long-term measurement within the same day, during which the VECSEL was not turned off, did not show these wavelength changes and the wavelength remained stable within ±0.025 nm. This is very good for most of Raman spectroscopy purposes.

The laser is required to have stable power because the background signal, which originates from optical elements in the laser path, must be subtracted from the Raman signal. However, the background signal from optical elements is typically low in the HWVN region and the influence of power fluctuations up to 10% is negligible. In the power stability tests we did not observe significant fluctuations on a short time-scale nor did we notice significant drifts over a 5-hours superior (maximum variation is less than 0.5 % of average power). The short-term power stability test and the long-term power test were performed on different days (Figures 4a and 4b, respectively), with power variations of 0.1 mW between these days. As before, this might be due to the VECSEL operating at a different mode of the external cavity between these days, which would be reflected to a slightly different output power. However, within the same day, the power is kept stable (SD= 0.01 mW). In summary, the results presented above show that the VECSEL fulfils the power and wavelength stability requirements of a laser source to be applied in Raman spectroscopy.

We presented typical example of Raman spectra of pigmented human skin lesions measured in 30 seconds (Figure 6). The presented spectra prove that high quality Raman signals can be obtained when using the tested VECSEL as the laser source.

With this work we demonstrate the feasibility of using VECSELs, which offer circular output beam, easy array fabrication, low cost at mass production, and compactness, for Raman spectroscopy applications.

Conclusion

In this paper, we tested the feasibility of a novel VECSEL source for Raman spectroscopy applications. Our results show that the VECSEL fulfils the requirements as a light source for Raman spectroscopy and has the characteristics to be employed in a low-cost compact hand-held Raman instrument device.

Acknowledgements

This project is funded by the IOP Photonic Devices managed by the Netherlands Enterprise Agency, Ministry of the Economic Affairs from The Netherlands (grant no. IPD12004). The authors acknowledge Stefan Gronenborn for stimulating discussions and Ben Wassink for fine mechanical support.

References

1. C. Patil, I. J. Pence, C. Lieber, A. Mahadevan-Jansen, *Opt. Lett.*, 2014; *39*, 2.
2. I. P. Santos, P. J. Caspers, T. Bakker Schut, R. van Doorn, S. Koljenović, G. J. Puppels, *J. Raman Spectrosc.*, 2015; *46*,7.
3. A. Mahadevan-Jansen, in *Biomedical Photonics Handbook*, Ed T. Vo-Dinh, CRC Press LLC, Boca Raton, 2003, 30.1-30.27.
4. M. Kuznetsov, in *Semiconductor Disk Lasers. Physics and Technology*, (Ed: O. G. Okhotnikov), Wiley-VCH, Weinheim, 2010, pp. 1-57.
5. A. van der Pol, P. J. Caspers, in *Handbook of Cosmetic Science and Technology*, (Eds: A. O. Barel, M. Paye, H. I. Maibach), Informa Healthcare, New York, 2010, 151–164.
6. R. L. McCreery, in *Raman Spectroscopy for Chemical Analysis*, (Ed: J. D. Winefordner), John Wiley & Sons, New York, 2000, 127–148.
7. W. Wang, A. Major, J. Paliwal, *Appl. Spectrosc. Rev.*, 2012, *47*, 2.
8. H. Moench, A. Andreadaki, S. Gronenborn, J. S. Kolb, P. Loosen, M. Miller, T. Schwarz, A. van der Lee, U. Weichmann, *Proc. SPIE*, 2014, 8966, 89660H1-10.
9. J. Hastie, S. Calvez, M. Dawson, T. Leinonen, A. Laakso, J. Lyytikäinen, M. Pessa, *Opt. Express*, 2005, *13*, 1.
10. A. Garnache, A. Laurain, M. Myara, J.-P. Perez, L. Cerutti, A. Michon, G. Beaudoin, I. Sagnes, P. Cermak, D. Romanini, *Proc. SPIE*, 2011, *7919*, 791914-1.
11. I. Kardosh, "Blue Light Emitting Electrically Pumped VECSELs with Optical Powers in the Milliwatt Range," *Annu. Rep. Inst. Optoelectron. Ulm Univ.*, 2007, 43-46.
12. J.-F. Seurin, G. Xu, Q. Wang, B. Guo, R. Van Leeuwen, A. Miglo, P. Pradhan, J. D. Wynn, V. Khalfin, C. Ghosh, *Proc. SPIE Vol. 7615*, 2010, *7615*, 609.
13. W. P. Pallmann, C. A. Zaugg, M. Mangold, V. J. Wittwer, H. Moench, S. Gronenborn, M. Miller, B. W. Tilma, T. Südmeyer, U. Keller, *Opt. Express*, 2012, *20*, 22.
14. I. P. Santos, P. J. Caspers, T. C. Bakker Schut, R. van Doorn, V. Noordhoek Hegt, S. Koljenović, G. J. Puppels, *Anal. Chem.*, 2016, 88, 15.
15. ISO 11146-1:2005 *Lasers and laser-related equipment – Test methods for laser beam parameters – Beam widths divergence angle and beam propagation factor*, 2005.
16. R. L. Mccreery, in *Handbook of Vibrational Spectroscopy. Volume 1: Theory and Instrumentation.*, (Eds: J. M. Chalmers, P. R. Griffiths), John Wiley & Sons, 2006, 920-932.
17. H. Martens, E. Stark, *J. Pharm. Biomed. Anal.*, 1991, *9*, 8.

CHAPTER 4

Raman spectroscopic characterization of melanoma and benign melanocytic lesions suspected of melanoma using high-wavenumber Raman spectroscopy

Inês P. Santos, Peter J. Caspers, Tom C. Bakker Schut, Remco van Doorn, Vincent Noordhoek Hegt, Senada Koljenović, and Gerwin J. Puppels,

Analytical Chemistry, **2016**; 88 (15): 7683-7688.

Abstract

Melanoma is a pigmented type of skin cancer, which has the highest mortality of all skin cancers. Because of the low clinical diagnostic accuracy for melanoma, an objective tool is needed to assist clinical assessment of skin lesions that are suspected of (early) melanoma. The aim of this study was to identify spectral differences in the CH region of HWVN (high-wavenumber) Raman spectra between melanoma and benign melanocytic lesions clinically suspected of melanoma. We used these spectral differences to explore preliminary classification models to distinguish melanoma from benign melanocytic lesions. Data from 82 freshly excised melanocytic lesions clinically suspected of melanoma were measured using an in-house built Raman spectrometer, which has been optimized for measurements on pigmented skin lesions (excitation wavelength 976 nm and a wavelength range of the Raman signal 1340–1540 nm). Clear spectral differences were observed between melanoma and benign melanocytic lesions. These differences can be assigned mainly to the symmetric CH_2 stretching vibrations of lipids. Our results show that the Raman bands between 2840 and 2930 cm^{-1} have increased intensity for melanoma when compared to benign melanocytic lesions, suggesting an increase in lipid content in melanoma. These results demonstrate that spectroscopic information in the CH-stretching region of HWVN Raman spectra can discriminate melanoma from benign melanocytic lesions that are often clinically misdiagnosed as melanoma and that Raman spectroscopy has the potential to provide an objective clinical tool to improve the clinical diagnostic accuracy of skin lesions suspected of melanoma.

Introduction

Melanoma is a form of skin cancer derived from melanocytes; the pigment-producing cells of the skin. Melanoma cells have a propensity to disseminate to distant organs and once metastasis has occurred the prognosis of patients is very poor. Metastasis and mortality from melanoma depend to a large extent on the stage of the disease and the thickness of the primary tumor on diagnosis. When diagnosed at an early stage, melanomas can be treated and cured by surgical resection in most cases.[1,2,3] When diagnosed at a later stage, melanomas have a considerable risk of progression to lethal metastatic disease. Improving the early diagnosis of melanoma therefore constitutes an important clinical objective.

Clinical differentiation between melanoma and benign melanocytic lesions can be challenging, even for experienced dermatologists. The clinical examination and diagnosis of melanoma is based upon visual inspection and recognition of morphologic characteristics, usually supported by tools such as a dermoscope. The use of a dermoscope can improve the accuracy of melanoma diagnosis but only when used by trained clinicians.[4,5,6,7] Even with the use of a dermoscope by an experienced clinician the sensitivity of diagnosing melanoma varies between only 68% and 96%.[8,9,10] Because the distinction between early-stage melanoma and benign pigmented lesions is difficult to make, many pigmented skin lesions are unnecessarily surgically removed. Literature reports clinical positive predictive values as low as 7% to 23% for melanoma diagnosis by dermatologists in a specialized pigmented lesion clinic.[11] Despite the over-diagnosis and subsequent unnecessary excisions, a substantial number of early-stage melanomas is still missed at the first clinical presentation with severe risk to progress to a metastatic stage.[7,12,13] It has been reported that there are up to 30% missed melanomas among general practitioners.[12] Objective methods are needed to improve the clinical diagnostic accuracy of melanoma in general and early melanoma specifically.

Various methods have been investigated to objectively diagnose melanoma, almost all of which rely on the detection of morphological differences between benign and malignant tumors. Examples of such methods are reflectance confocal microscopy,[14] electrical impedance spectroscopy,[15] confocal microscopy,[16] multispectral imaging,[17] and automated dermoscopy image analysis.[18] Incremental improvements in diagnostic accuracy are feasible through optimization of these morphology-based methods.

A promising approach is the analysis based on biochemical differences. Biochemical differences are potentially much more specific than morphological characteristics.[19,20] Besides the enhanced sensitivity, specificity and positive predictive value of diagnosis, these methods would have the advantage of facilitating accurate earlier diagnosis, which would enable improvement of treatment efficiency and survival rates.

Raman spectroscopy is an excellent candidate technique to characterize *in vivo* biological tissue and to detect non-invasively the molecular changes associated with pathological processes, i.e. to successfully distinguish tumor from healthy tissue.[21,22] Raman spectroscopy is an optical non-destructive technique that uses light scattering to characterize non-invasively tissue at a molecular level. It does not require any labelling, reagents or preparation of the tissue to be analyzed, which facilitates translation to the clinic.

Until now, the application of Raman spectroscopy in the analysis of highly pigmented biological samples presented a major hurdle. When using visible or near-infrared laser excitation wavelengths up to about 850 nm, the absorption of light by melanin in pigmented skin lesions leads to laser-induced tissue fluorescence. This is generally much more intense than the tissue Raman signal, to the point that it obscures the Raman spectral features.

In our previous work we tested the feasibility of an in-house built Raman spectroscopy device to acquire high-quality Raman spectra of pigmented biological samples.[23] We used infrared laser-excitation at 976 nm in order to decrease the laser-induced tissue fluorescence. The Raman signal was detected in the short-wave infrared (SWIR) region, using a sensitive indium-gallium-arsenide (InGaAs) detector with extremely low detector noise. With this prototype we demonstrated high-quality, shot-noise-limited high-wavenumber (HWVN) Raman spectra of pigmented skin lesions with acquisition times sufficiently short to be compatible with application in a clinical setting.[23]

In this paper we identify the main spectral differences between melanoma and benign melanocytic lesion classes and explore whether there is spectroscopic information in the CH-stretching region (2820-3040 cm^{-1}) to discriminate melanoma from benign melanocytic lesions.

Methods and materials

Excised skin lesions. This study was approved by the Medical Ethics Committee of the LUMC (C13.06). After clinical assessment performed by a dermatologist, pigmented skin lesions suspected of melanoma were excised and submitted for histopathological diagnosis in the dermatology outpatient clinic of the Leiden University Medical Center (LUMC). These excisions were performed according to the national melanoma guideline and standard protocol of the

LUMC department of dermatology. The standard excision protocol was followed; prior to surgery, the excision margins of the lesions were delineated with a permanent marker. The entire surgical area was wiped with a gauzed soaked in antiseptic chlorhexidine solution (0.5% in 70% ethanol). Local anesthesia (Lidocaine hydrochloride 2% epinephrine 1:100,000 solution) was administered via intradermal injection close to the excision margins, circumferential to the lesions.

Measurement protocol. Immediately after surgery, the excised skin samples were rinsed with NaCl solution (0.9%), wiped with a gauze soaked in ethanol (70%) to remove residual ink from pen marker, gently flattened between two fused silica windows and inserted into a custom-made sample cartridge for Raman measurements (Figure 1). The maximum time allowed for the experimental procedure described below was fixed at 30 minutes after surgery, to keep optimal tissue preservation and to avoid interference with the routine histopathological examination of the excised specimen. Multiple locations within the lesion were measured. Approximately 15 point measurements were performed per lesion. Each point measurement had an integration time of 30 seconds. After the Raman spectroscopy measurements, the skin samples were put in a formaldehyde solution (4%) and sent to pathology for the routine diagnostic procedure.

Histopathological diagnosis. All excised lesions suspected of melanoma that were measured with the Raman spectroscopy instrument were diagnosed by two dermopathologists. The final histopathological diagnosis, upon agreement, was used as the gold-standard reference for correlation with the Raman measurement.

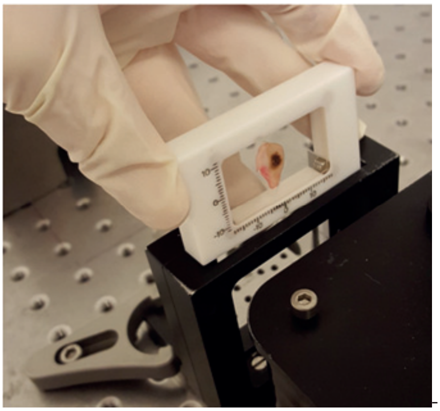

Figure 1. Excised skin lesion inserted into the sample cartridge.

Sample inclusion criteria. In total, 149 freshly excised pigmented lesions clinically suspected of melanoma were measured with the Raman spectroscopy instrument. Only histologically homogenous melanocytic lesions were included in the study. Lesions that were histopathologically heterogeneous, i.e., that did not have a consistent histologic appearance throughout the entire lesion, were excluded from data analysis after evaluation by two dermopathologists based on histopathological findings only (n=42) before data analysis. This group of 42 excluded lesions contained 13 melanomas. Non melanocytic lesions (n=11) and lesions that present strong spectral artefacts (due to presence of fixed pattern noise or equipment failure) were excluded (n=14).

Raman spectroscopy instrumentation. A SWIR multichannel Raman instrument was used to obtain Raman spectra.[23] The excitation light source was a single-mode continuous wave diode laser with a wavelength of 976 nm and an output power of 150 mW (Model R-type, Innovative Photonic Solutions, Monmouth Junction, NJ, USA). The captured spectral range 1340-1540 nm corresponds to a Raman spectrum from 2780 to 3750 cm^{-1}. The custom-made sample cartridge was used to hold the excised skin sample between two fused silica windows. For Raman measurements, the sample cartridge was inserted inside an anodized aluminium sample holder that was mounted perpendicular to the laser beam. The light was focused in the sample to a Gaussian spot with a diameter of ~6 µm. The sample holder was mounted on a 3-axis translation stage to enable measurements at a range of locations in the sample. The sample was placed in the laser beam with the focus position optimized on the Raman signal from the tissue.

Pre-processing and calibration of Raman spectra. Raman spectra were corrected for the wavelength-dependent detection efficiency of the setup, using an SRM2246 intensity standard (National Institute of Standards and Technology, Gaithersburg, Maryland, USA). The absolute wavenumber axis was calibrated using the spectral lines of a neon-argon lamp and the Raman spectrum of cyclohexane. The Raman background that originates from the optics was subtracted from all spectra. The spectra presented were scaled to the average of all individual spectra using extended multiplicative signal correction (EMSC) with a first order polynomial background.[24] Due to a presence of fixed interference in the Raman spectra generated by the detector response, we filtered the data with a 5th order spline function to remove the fixed interference. All spectra were cropped to the spectral range (2820-3040 cm^{-1}), which corresponds to the CH-stretching band region. This is the spectral region that includes the main information about protein and lipid vibrations.

Data Analysis. Average Raman spectrum per histopathological class. For each pigmented lesion included in this study, the Raman spectra from multiple measurements within the lesion were averaged. For interpretation of the spectral features per histopathological class, an average Raman spectrum was calculated for each histopathological class. A first derivative of these class-average Raman spectra was calculated to emphasize the spectral differences between the classes.

Spectral difference between melanoma and benign melanocytic nevus classes. Spectral differences between melanoma and the other histopathological classes were assessed by creating difference spectra. Difference spectra were calculated by sequentially (i) averaging all spectra within each histopathological class, (ii) normalizing intensity of each spectrum using extended multiplicative scatter correction (EMSC)[24] with a first order polynomial background, (iii) subtracting each of the average Raman spectra from the average spectrum of melanoma.

PCA-LDA model with averaged spectra per sample. Linear discriminant analysis (LDA) classification modelling was used to investigate the discriminatory power of Raman spectral information for distinguishing melanoma from common benign melanocytic nevi. LDA models were created using the averaged spectrum per lesion as input. Because some classes only contain few samples, histopathological classes represented by less than 5 different lesions were left out of the LDA classification model. Principal component analysis (PCA) was performed to reduce the dimensionality of the data prior to LDA modelling. The performance of LDA on lesion averaged spectra was assessed using leave-one-lesion-out cross validation. For each leave-one-lesion-out LDA model, the scores on the most significant principal components (determined by the highest confidence levels in a student t-test of group differences) were selected as input parameters. An ROC (Receiver Operator Characteristic) curve was made to assess the discriminative power and optimal discrimination thresholds. In this study, specificity was computed as the fraction of correctly predicted negatives (not melanoma) from the total number of benign melanocytic lesions in the analyzed sample set. Sensitivity was calculated as the fraction of correctly predicted positives (melanoma) from the total number of melanomas in the analyzed sample set.

The software used for all computations was Matlab R2015b (Mathworks Inc., Natick, Massachusetts, United States).

Results and discussion

The purpose of this study was to investigate whether there is diagnostic information in the CH-stretching region of HWVN Raman spectra and to identify the main spectral differences between melanoma and benign melanocytic lesions.

After application of the inclusion criteria, the final dataset contained Raman spectra from 82 lesions of which 24 were melanomas (including melanoma *in situ*, superficial spreading and nodular), 10 dysplastic/atypical nevi and 48 benign melanocytic nevi (including compound melanocytic nevus, dermal melanocytic nevus, junctional melanocytic nevus, combined melanocytic nevus, blue nevus, Spitz nevus and lentigo simplex) (Table 1).

For spectral analysis, we used the CH-stretching spectroscopic region (2820-3040 cm^{-1} range), which includes the main protein and lipid vibration information.

The Raman spectra averaged by histopathological class are shown in Figure 2. The first derivative of each average Raman spectrum is shown to accentuate spectral differences between the classes.

Figure 3 shows the spectral differences between melanoma and the other benign melanocytic classes. Each plot shows the residual of the spectrum of each of the classes indicated in the figure subtracted from spectrum of melanoma class.

Analyzing the spectral differences between Raman spectra of the melanoma group and the Raman spectra from benign melanocytic lesions (Figure 3), we found that the melanoma group shows increased Raman signal intensities between 2840 cm^{-1} and 2930 cm^{-1}.

The peak visible in the residual spectra at 2854 cm^{-1} is assigned to the symmetric CH_2 stretching vibrations of lipids,[25,26,27] and implies that the Raman spectra of melanoma exhibit an increased lipid contribution when compared to the other histopathological classes (dysplastic/atypical melanocytic nevus, dermal melanocytic nevus, junctional nevus and blue nevus). An exception is seen for the Spitz nevus. The negative peak of the difference spectrum between melanoma and Spitz nevus corresponds to the position 2848 cm^{-1} and suggests that melanoma has less lipids than Spitz nevus. Whether this observed difference for the Spitz nevus is coincidental or reflects a characteristic of Spitz nevus could not be established due to the low number of Spitz nevi (n=2) in this study.

Table 1. Summary of included homogenous melanocytic skin lesions clinically suspected of melanoma

Histopathological diagnosis		**n**
Melanoma (inc. i*n situ*)		24
Benign melanocytic lesions	dysplastic	10
	compound	23
	dermal	14
	junctional	4
	blue nevus	2
	lentigo simplex	2
	Spitz	2
	combined	1

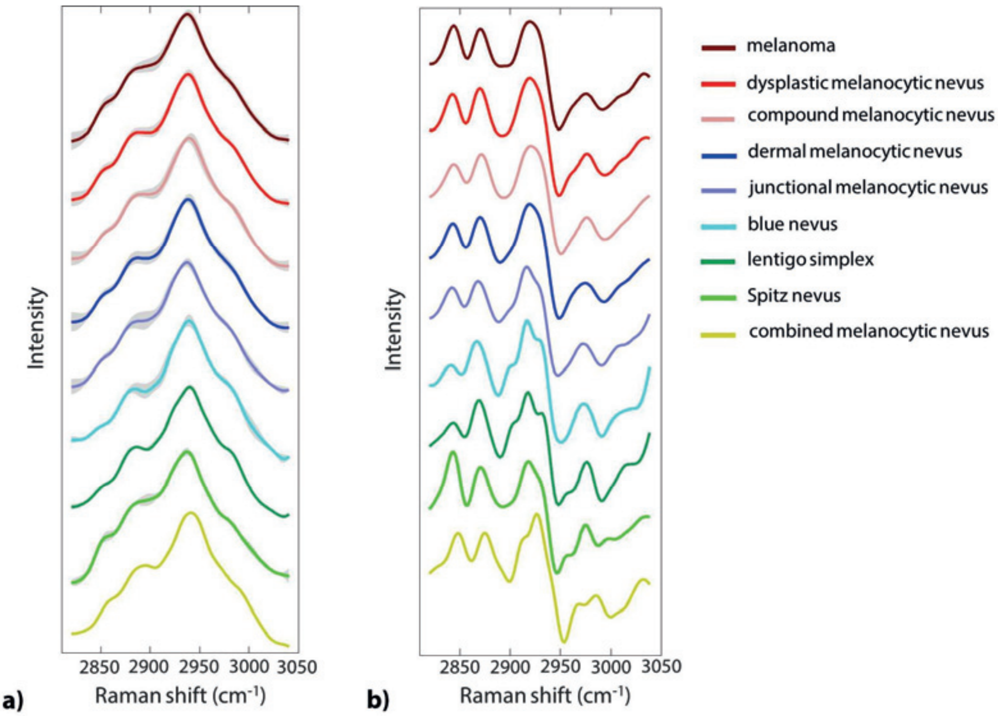

Figure 2. a) Average HVWN Raman spectra per histopathological class ± standard deviation (gray). **b)** First derivative of the spectra shown in A. In both figures the spectra are offset along the intensity axis for clarity.

In the same spectral region, we can identify another peak at 2896 cm^{-1} that is more intense in melanoma group compared to the other histopathological classes. This peak is assigned to asymmetric CH_2 stretching vibrations of lipids.[27,28] In the difference spectrum between melanoma and compound melanocytic nevi (figure 3), the peak is not as evident as in the other difference spectra, although it is still visible. Another peak, at 2876 cm^{-1}, is visible in both residuals between melanoma-combined melanocytic nevi and melanoma-compound melanocytic nevi. This peak is assigned to the asymmetric CH_2 stretching vibration of lipids.[27,28] An extra band at 2922 - 2930 cm^{-1} is visible at the residual spectrum between melanoma and combined melanocytic nevi. This band is assigned to the symmetric CH_3 stretching vibration of lipids and proteins.[27,29]

In contrast to lipid contributions, Raman spectra of melanoma show consistently lower intensity in the spectral range between 2930 and 3000 cm^{-1} compared to the other groups. The negative peak visible in the spectral residual at 2950 cm^{-1} is assigned to CH_3 stretching vibration of proteins.[30] As before, the Spitz nevus group is an exception.

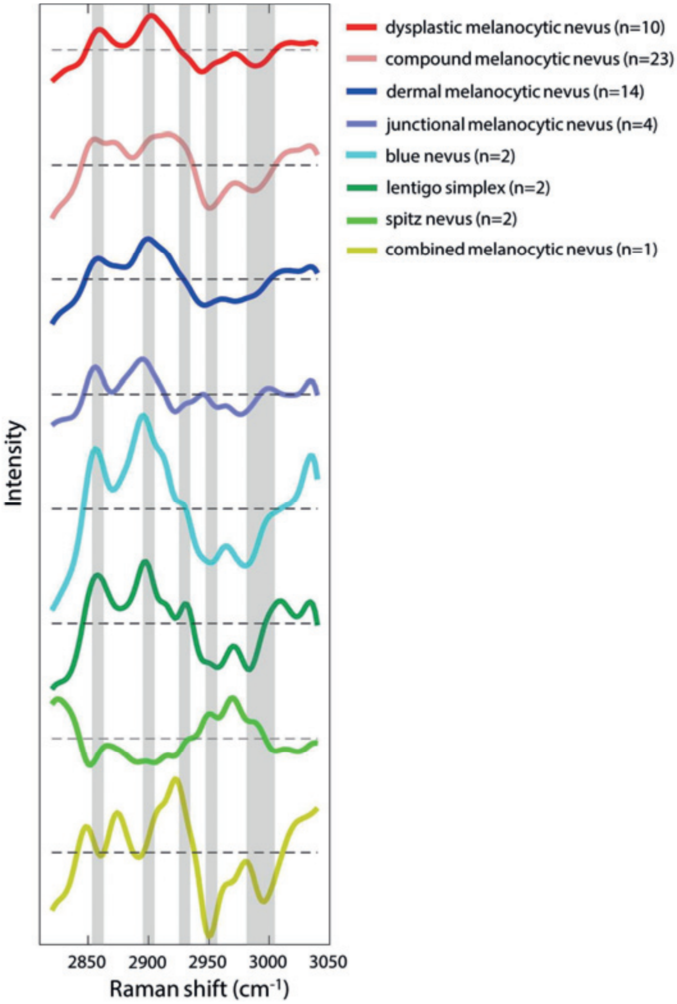

Figure 3. Difference spectra between the average Raman spectrum of melanoma and the average Raman spectra of each of the other histopathological classes. The spectra are offset along the intensity axis for clarity.

In summary, our results show that Raman spectra of melanoma have an increased contribution from lipids when compared to the other histopathological classes. The results presented above show that the most distinctive spectral feature between melanoma and the other classes in the spectral region assigned to CH_2 -CH_3 stretching vibrations is attributed to a higher lipid-protein ratio in melanoma. These findings are in agreement with the findings of Gniadecka *et al.* [31], in which the authors used Fourier-transform Raman spectroscopy and found that melanoma presents increased lipid-specific bands around 1310 cm^{-1} when compared to pigmented nevi (benign melanocytic lesions) and basal cell carcinomas and seborrheic keratoses (non-melanocytic lesions).

The authors also mentioned the fact that the range between 2840 - 3000 cm^{-1} was an important region for the differentiation between melanomas and pigmented nevi, basal cell carcinomas and seborrheic keratoses by neural network analysis.[31] The observed increase in lipid content in melanomas is consistent with recent studies, which report that cancer cells present dysregulated lipid metabolism and intensified de novo lipogenesis.[32,33,34,35] Innocenzii *et al.*, show that there is an overexpression of fatty acid synthase in melanoma compared to the dermal and junctional melanocytic nevi examined as control group.[36] In another study, Sumantran *et al*. report that melanomas have upregulated genes that lead to an increase in fatty acid synthesis, metabolism of specific lipid second messengers and ganglioside synthesis.[37] Kwan *et al.* suggest from their study that adipocytes might be an exogenous supply of palmitic acid that promotes melanoma cell growth.[38] Other studies using HWVN Raman spectroscopy to differentiate different types of tumors or pre-tumor states (dysplasia) from their respective normal tissue, like breast cancer, cervical tissue cancer and liver cancer have reported similar findings, with tumor tissue showing higher intensities in the CH band, attributed to stretching vibrations of lipids, than normal tissue.[39-42]

In this study PCA-LDA classification was used to investigate the discriminatory power of the CH region of HWVN Raman spectra in discriminating melanoma from all the other lesion classes included in this analysis. For this analysis, the histopathological classes represented by less than five lesions have been excluded (combined melanocytic lesion, Spitz nevus, lentigo simplex, blue nevus and junctional melanocytic nevus) because the low number of cases in each class could introduce undesired variability into the analysis. This resulted in PCA-LDA based on a final set of 71 lesions (24 melanomas, 10 dysplastic/atypical melanocytic nevi, [23] compound melanocytic nevi and 14 dermal melanocytic nevi). The discriminating parameter used as input for LDA was a Boolean: melanoma or not-melanoma. Due to the small size of the database, only a leave-one sample-out cross validation was used. Figure 4 shows the Receiver-Operator Characteristic (ROC) curve generated from different discriminating threshold levels, showing the performance of the created LDA model for melanoma detection. Because we performed this experiment in a specialized pigmented lesion clinic, it follows that our study contained only benign pigmented lesions and melanoma that were difficult to distinguish even by trained dermatologists. The positive predictive value of the clinical diagnosis in the pigmented lesions clinic was 25%; i.e. only 37 out of 149 excised lesions was a melanoma. Our preliminary classification model correctly

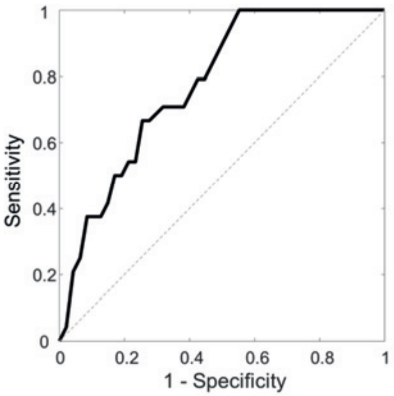

Figure 4. ROC curve of discrimination of melanoma using the PCA-LDA classification model with leave-one sample-out cross validation method. The area under the ROC curve is 0.77.

classified all melanoma with a specificity of 45%. This suggests that *in vivo* application of Raman spectroscopy, prior to lesion excision, might lead to a threefold reduction of the ratio of unnecessary excisions to melanoma excisions from 3:1 to 1:1. These results bode well for the development of an objective Raman spectroscopy instrument for objective melanoma diagnosis.

This is an encouraging result towards an application to help general practitioners and non-experienced dermatologists to discriminate melanoma from suspicious lesions and reduce unnecessary surgical excisions of benign melanocytic lesions. We are exploring the possibilities to transfer this technology to *in vivo* clinical application. Various approaches are conceivable to use this method *in vivo* such as a flexible fiber-optic probe for easy access of various parts of the body.

Conclusion

In this study we used a novel in-house built HWVN Raman spectrometer to obtain high quality Raman spectra of pigmented skin lesions suspected of melanoma. From the Raman spectra, we were able to identify the main spectral differences between melanoma and benign melanocytic lesions as increased contribution from symmetric CH_2 stretching vibrations of lipids in melanoma, when compared to the other lesions analyzed.

The obtained results demonstrate the potential of Raman spectroscopy as an objective clinical tool to help distinguishing melanoma from benign melanocytic lesions, which are often clinically misdiagnosed as melanoma, based on the spectroscopic information in the CH-stretching band.

Acknowledgements

This project is funded by the IOP Photonic Devices managed by the Netherlands Enterprise Agency, Ministry of the Economic Affairs from The Netherlands (grant no. IPD12004).

References

1. R. L. Barnhill, M. C. Mihm, G. Elgart, in *Skin Cancer*; Ed. K. Nouri, McGraw-Hill: China, 2007,140-166.
2. de Vries, E.; Bray, F.; Coebergh, J. W.; Ruiter, D. J.; Elder, D. E.; Thompson, J. F.; Barnill, R. L.; van Muijen, G. N. P.; Scolyer, R. A.; LeBoit, P. E. in *World Health Organization Classification of Tumors. Pathology and Genetics of Skin Tumors*; Eds. P. E. LeBoit, G. Burg, D. Weedon, A. Sarasain; IARC Press: France, 2006, 52-61.
3. B. Bandarchi, L. Ma, R. Navab, A. Seth, G. Rasty, *Dermatol Res Pract*., 2010, 2010, Article ID 583748 DOI:10.1155/2010/583748.
4. Skvara, H.; Teban, L.; Fiebiger, M.; Binder, M.; Kittler, H. *Arch Dermatol*., 2005, 141, 2, 155-160.
5. Binder. M.; Schwarz, M.; Winkler, A.; Steiner, A.; Kaider, A.; Wolff, K.; Pehamberger, H. *Arch Dermatol*., 1995, 131, 286-291.
6. Binder, M.; Puespoeck-Schwarz, M.; Steiner, A.; Kittler, H.; Muellner, M.; Wolff, K.; Pehamberger H. *J Am Acad Dermatol*., 1997, 36, 197-202.
7. van der Rhee, J. I.; Bergman, W.; Kukutsch, N. A., *Br J Dermatol*., 2010, 162, 563-567.
8. Kittler, H.; Pehamberger, H.; Wolff, K.; Binder, M., *Lancet Oncol*., 2002, 3, 159-165.
9. Morton, C. A.; Mackie, R. M. Br J Dermatol. 1998, 138, 283-287.
10. Grin, C. M.; Kopf, A. W.; Welkovich, B.; Bart, R. S.; Levenstein, M. J., *Arch Dermatol*., 1990, 126, 763-766.
11. Carli, P.; Mannone, F.; De Giorgi, V.; Nardini, P.; Chiarugi, A.; Giannoti, B., *Melanoma Res*., 2003, 2, 179-182.
12. Chen S. C.; Bravata, D. M.; Weil, E.; Olkin I., *Arch Dermatol*., 2001, 137, 1627-1634.
13. van der Rhee, J. I.; Bergman, W.; Kukutsch, N. A. Acta Derm Venereol. 2011, 91, 428-431.
14. Stevenson, A. D.; Mickan, S.; Mallett, S.; Ayya, M., *Dermatol Pract Concept*., 2013; 3, 19-27.
15. Åberg, P.; Birgersson, U.; Elsner, P.; Mohr, P.; Ollmar, *S. Exp Dermatol*., 2011, 20, 648-652.
16. Curiel-Lewandrowski, C.; Williams, C. M.; Swindells, K. J.; Tahan, S. R.; Astner, S.; Frankenthaler, R. A.; González, *S. Arch Dermatol*., 2004, 140, 1127-1132.
17. Monheit. G.; Cognetta, A. B.; Ferris, L.; Rabinovitz, H.; Gross, K.; Martini, M.; Grichnik, J. M.; Mihm, M.; Prieto, V. G.; Googe, P.; King, R.; Toledano, A.; Kabelev, N.; Wojton, M.; Gutkowicz-Krusin, D., *Arch Dermatol.,* 2011, 147, 188-194.
18. Westerhoff, K.; McCarthy, W. H.; Menzies, S. W., *Br J Dermatol*., 2000, 143, 1016-1020.
19. Leupold, D.; Scholz, M.; Stankovic, G.; Reda, J.; Buder, S.; Eichhorn, R.; Wessler, G.; Stücker, M.; Hoffmann, K.; Bauer, J; Garbe, C., *Pigment Cell Melanoma Res*., 2011, 24, 438-445.
20. Matthews, T. E.; Piletic, I. R.; Selim, M. A.; Simpson, M. J.; Warren, W. S., *Sci Transl Med*., 2011, DOI: 10.1126/scitranslmed.3001604.
21. Nijssen, A.; Maquelin, K.; Santos, L. F.; Caspers, P. J.; Bakker Schut, T. C.; den Hollander, J. C.; Neumann, M. H.; Puppels, G. J., *J Biomed Opt*., 2007, DOI: 10.1117/1.2750287.
22. Koljenović, S.; Bakker Schut, T. C.; Wolthuis, R.; de Jong, B.; Santos, L.; Caspers, P. J.; Kros, J. M.; Puppels, G. J., *J Biomed Opt*. 2005, 3, 1-11.
23. Santos, I.P.; Caspers, P.J.; Bakker Schut, T. C.; van Doorn, R.; Koljenović, S.; Puppels, G. J., *J Raman Spectrosc*., 2015, 46, 652–660.
24. Martens, H.; Stark, E. J , *Pharm Biomed Anal*., 1991, 9, 625-635.
25. Surmacki, J.; Musial, J.; Kordek, R.; Abramczyk, H., *Mol Cancer,* 2013, DOI:10.1186/1476-4598-12-48.
26. Brozek-Pluska, B.; Jablonska-Gajewicz, J.; Kordek, R.; Abramczyk, H., *J Med Chem.,* 2011, 54, 3386-3392.
27. Czamara, K.; Majzner, K.; Pacia, M. Z.; Kochan, K.; Kaczor, A.; Baranska, M. , *J Raman Spectrosc*., 2015, 46, 4-20.
28. Flach, C. R. in *Emerging Raman Applications and Techniques in Biomedical and Pharmaceutical Fields*; Ed. Matousek, P.; Morris, M., 2010, Springer - Verlag: Berlin Heidelgerg, 365-384.
29. Nyquist, R. A. *Interpreting Infrared, Raman, and Nuclear Magnetic Resonanse Spectra*; 2001, Academic Press: San Diego.
30. Howell, N. K.; Arteaga, G.; Nakai, S.; Li-

Chan, E. C., *J Agric Food Chem.*, 1999, 47, 924-933.

31. Gniadecka, M.; Philipsen, P. A.; Sigurdsson, S.; Wessel, S.; Nielsen, O. F.; Christensen, D. H.; Hercogova, J.; Rossen, K.; Thomsen, H. K.; Gniadecki, R.; Hansen, L. K.; Wulf, H. C., *J Invest Dermatol.,* 2004, 122, 443-449.
32. Currie, E.; Schulze, A.; Zechner, R.; Walther, T. C.; Farese, R. V., *Cell Metab.*, 2013, 18, 153-161.
33. Menendez, J. A.; Lupu, R., *Nat Rev Cancer.,* 2007, 7, 763-777.
34. Zhang, F. , *World J Biol Chem*., 2012, 3, 167.
35. Baenke, F.; Peck, B.; Miess, H.; Schulze, A., *Dis Model Mech*. 2013, 6, 1353-1363.
36. Innocenzi, D.; Alò, P.L.; Balzani, A.; Sebastiani, V.; Silipo, V.; La Torre, G.; Ricciardi, G.; Bosman, C.; Calvieri, S., *J Cutan Pathol.*, 2003, 30, 23-28.
37. Sumantran, V. N.; Mishra, P.; Sudhakar, N., *Indian Journal Biochem Biophys.,* 2015, 52, 125-131.
38. Kwan, H. Y.; Fu, X.; Liu, B.; Chao, X.; Chan, C. L.; Cao, H.; Su, T.; Tse, A. K.; Fong, W. F., Yu, Z. L., *J Biol Chem*., 2014, 289, 30525-30537.
39. Teh, S. K.; Zheng, W.; Ho, K. Y.; Teh, M.; Yeoh, K. G.; Huang Z. J Biomed Opt. 2008, 13, 3, DOI:10.1117/1.2939406.
40. Tania, M.; Khan, M. A.; Song, Y. , *Curr Oncol*., 2010, 17, 6-11.
41. Nieva, C.; Marro, M.; Santana-Codina, N.; Rao, S.; Petrov, D.; Sierra, A., *PLoS One*., 2012, DOI: 10.1371/journal.pone.0046456.
42. Tolstik, T.; Marquardt, C.; Matthäus, C.; Bergner, N.; Bielecki, C.; Krafft, C.; Stallmach, A.; Popp, J., *Analyst.,* 2014, 139, 6036-6043.

CHAPTER 5

Improving diagnosis of early stage cutaneous melanoma based on Raman spectroscopy

Inês P. Santos, Remco van Doorn, Peter J. Caspers, Tom C. Bakker Schut,

Elisa M. Barroso, Tamar Nijsten, Vincent Noordhoek Hegt,

Senada Koljenović and Gerwin J. Puppels

Submitted with modifications

Abstract

Clinical diagnosis of early melanoma is crucial to disease-free survival. When diagnosed early (Breslow-thickness less than 0.8 mm) melanoma can be cured by surgical excision, with a 5-year survival rate of > 97%. However, the clinical diagnosis of thin melanoma is subjective and can be exceedingly difficult, leading to missed diagnosis, or unnecessary excision of benign pigmented skin lesions.

It has been reported that among general practitioners, the sensitivity of diagnosing melanoma varies between 70-88% and among dermatologists between 82-100%. The number of benign pigmented lesions excised to diagnose one melanoma varies between 6-9 for dermatologists and between 20-30 for general practitioners. Obviously, an objective technique is needed to improve the diagnosis of early melanoma. In this study, we use Raman spectroscopy to assess freshly-excised melanocytic skin lesions that were clinically suspicious for melanoma.

We have developed a method to improve diagnosis of (thin) melanoma. A diagnostic model was developed based on high-wavenumber Raman spectra, obtained at multiple locations within freshly excised cutaneous melanocytic lesions. Measurements were performed on 174 lesions, clinically suspicious for melanoma, in a highly specialized out-patient clinic. The diagnostic model was validated on an independent data set of 96 lesions.

Approximately 60% of the melanomas included in this study were melanomas *in situ*. The invasive melanomas had an average Breslow thickness of 0.89 mm. The diagnostic model correctly classified all melanomas with a specificity of 43.8%. The diagnostic model for melanoma showed in this study a potential improvement of the number needed to treat from 6.0 to 2.7, at a sensitivity of 100%.

We demonstrate that, based on Raman spectroscopy, an accurate diagnosis of melanoma with Breslow thickness <0.8 mm can be made. This work signifies an important step towards objective accurate diagnosis of melanoma.

Introduction

Melanoma is a malignant tumor arising from melanocytes, the pigment-producing cells of the skin. It is the most aggressive and fatal form of skin malignancy. Its incidence has been steadily increasing in the last decades, with more than 232 000 new cases estimated worldwide in 2012.[1]

Melanoma must be diagnosed at an early stage. One of the most important prognostic factors of melanoma is the vertical depth of growth (Breslow thickness). In a primary lesion, the Breslow thickness is significantly correlated with metastatic propensity. Lesions that have a Breslow thickness less than 0.8 mm can be treated surgically with a high cure rate (5-year survival rate of > 97%).[2] In advanced stages, the 5-year survival rate can drop to 32%.[2]

The clinical diagnosis of melanoma is based on analysis of morphological criteria and is therefore, subjective and difficult. It is based on visual inspection of the lesion, aided by dermoscopy, by a dermatologist or a general practitioner. When a lesion is clinically suspected of melanoma, a diagnostic excision is indicated.

It has been reported that among general practitioners, the sensitivity of diagnosing melanoma varies between 70-88% and among dermatologists between 82-100%.[3] However, the number needed to treat (NNT, the number of benign pigmented lesions excised to detect one melanoma), varies between 6.3-8.7 by dermatologists,[4,5] and between 20-30 for general practitioners.[4-12] The NNT can be even higher in a population of patients < 30 years (NNT = 75) [6-10,12] or in high-risk populations (NNT = 34, *e.g.* multiple dysplastic nevi or familial melanoma)[13].

These numbers imply that melanomas can be clinically missed, with the risk of missing the opportunity to cure the patient, while many unnecessary excisions of benign lesions take place. An objective and easy-to-use technique that will support and improve the diagnosis of thin melanoma is needed to complement the still limited diagnostic toolbox in current clinical practice.

The reported efforts to develop techniques to improve the clinical diagnosis of melanoma are promising. Nevertheless, detecting early-stage melanomas is still a challenge. Various methods have been investigated to diagnose melanoma, most of which rely on the detection of morphological differences between benign and malignant pigmented skin lesions.[14] Examples of such methods are reflectance confocal microscopy,[15-17] confocal microscopy,[18,19] multispectral imaging,[20,21] automated dermoscopy image analysis[22] and electrical impedance spectroscopy.[23-25]

The implementation of these non-invasive diagnostic technologies is currently still low but is expected to increase gradually.[14-26] Several studies show improvement in diagnostic accuracy when combining one or more of these morphology-based methods with dermoscopy, even though most of these techniques are operator dependent and subject to interpretation.[15,16] Using confocal microscopy in an *in vivo* setting, Monheit *et al.* reported a sensitivity of 98.4% (detecting 125 out of 127 melanomas from which 44% were *in situ*) and a specificity of 9.9% with an independent validation set.[27] A recent pilot study conducted by Delpueyo *et al.* on multispectral imaging based on LEDs showed a sensitivity of 87.2% and specificity of 54.5% with an independent validation set.[21] Using reflectance confocal microscopy in clinically suspicious lesions in an *in vivo* setting, Alarcon *et al* reported a sensitivity of 97.8% and a specificity of 92.4% (264 lesions suspected of which 92 were confirmed melanomas).[15] The authors stated that 6 melanomas *in situ* were missed. The presented results are promising for reflectance confocal microscopy as an adjunct technique for melanoma diagnosis. The limitation of reflectance confocal microscopy is the dependence on the experience of the operator (sensitivity 91.0% *vs* 84.8% and specificity 80.0% *vs*. 77.9% for experienced vs recent users, respectively).[28] In a multicenter study, 1300 lesions were analyzed by electrical impedance spectroscopy for melanoma discrimination from benign lesions on suspected lesions: the observed sensitivity was 99.4% (161 out of 162 melanomas, with 1 melanoma *in situ* missed), and the specificity was 35.5% for benign melanocytic lesions excluding dysplastic nevi or 23.9% including them.[24] In another multicenter study, 2416 lesions were analyzed by electrical impedance spectroscopy for melanoma detection. Sensitivity of 96.6% and a specificity of 34.4% were reported.[29] From the 9 missed melanomas, 7 were *in situ*, other two had a Breslow thickness of 0.4 mm and 0.6 mm.

Compared to the morphology, biochemical tissue characteristics are more specific. Research in proteomics and genomics has shown that melanoma undergoes genomic alterations, such as deregulation of the MAPK signaling pathway and that melanoma have different gene expression from benign melanocytic lesions.[30-34] Raman spectroscopy is an optical non-destructive technique that goes beyond morphology analysis and characterizes the tissue at a molecular level. Raman spectra can be used as a highly specific tissue fingerprint, on the basis of which tissues can be classified. This objective technique does not require any labeling, reagents, or preparation of the tissue to be analyzed, which facilitates translation to the clinic. It has been amply demonstrated that Raman spectra can be used to distinguish cancer from healthy tissue, including pigmented skin lesions.[35-41]

Lui *et al.* developed a classification model to distinguish benign pigmented lesions from melanoma, using a large Raman measurement volume (200 µm core diameter single fiber that illuminates a 3.5 mm diameter skin area.[40] In this study, the clinical diagnoses were established by dermatologists and dermoscopy was not used. Only 28% of the clinically benign lesions were histopathologically confirmed.[40] The authors included *in vivo* Raman measurements acquired in 44 melanomas and 81 pigmented skin lesions. The validation of the model was not performed on an independent data set instead, leave-one-out cross-validation was used. The authors reported sensitivity of 99% and specificity of 15%. This system, Aura®-system (Verisante, Canada) for skin cancer detection was commercialized. In a more recent study, the same authors increased the number of lesions (only 9 melanomas were added) in the same clinical setting and performed an independent validation. The model discriminates between all skin cancers and pre-cancers (including melanomas, basal cell carcinomas, squamous cell carcinomas and actinic keratosis) from their benign counterparts.[42] In this study, the presented sensitivity was 99% and the specificity was 24%. In 2014, Lim *et al.* combined diffuse optical spectroscopy, laser-induced fluorescence spectroscopy and Raman spectroscopy to distinguish melanoma from non-melanoma pigmented lesions. The measurements were performed *in vivo*. They used a limited number of cases (12 melanoma versus 17 pigmented benign lesions). Based on non-independent, leave-one-out cross-validation, a sensitivity of 100% and specificity of 100% was found.[41] The authors did not clarify whether dermatologists used dermoscopy nor whether the pigmented benign lesions were melanocytic and clinically suspected for melanoma.[41]

Our group has previously demonstrated the feasibility to acquire high-quality Raman spectra of pigmented tissue samples in the short-wave infrared (SWIR) region.[43] The study was performed in a tertiary referral center for high-risk patients (familial melanoma, previous melanoma). All lesions suspicious for melanoma after evaluation by specialized dermatologists aided by dermoscopy were surgically excised. All lesions were evaluated by two expert pathologists. In that study, we measured 124 freshly excised melanocytic lesions. Some of them (n = 42) were histopathologically heterogeneous, i.e., did not have an even distribution of histological components throughout the lesion, leading to the possible sampling of non-melanocytic tissue (*e.g.* collagen or skin appendages). Because for heterogeneous lesions no accurate point-to-point correlation between the locations of the Raman measurements on the lesion and individual histological components could be made, these were not used for the development of a classification model. Therefore, the model was limited to histopathologically homogeneous lesions, which resulted in a specificity of 45% and a sensitivity of 100%.[39] We have confirmed that there is spectroscopic information in the 2820–3040 cm^{-1} region (assigned to CH_2 $-CH_3$ stretching vibrations), which can be used to discriminate melanoma from benign melanocytic lesions. The results showed that the most distinctive spectral feature between melanoma and benign melanocytic lesions is attributed to a higher lipid–protein ratio in melanoma.[39]

Next to heterogeneous aspect of melanocytic lesions, the thickness of the *stratum corneum* can also influence the representativeness of Raman measurements. Some lesions present a thick layer of keratinized layer on top, whereas others show a relatively thin *stratum corneum* (~10-20 µm), depending on the anatomical location of the lesion. This variance can influence the effective depth at which the tissue is sampled, and which could result in missing representative regions of the lesion, i.e. underlying melanocytic proliferation. Likewise, in benign lesions that do not present malignant melanocytes with the epidermis or papillary dermis, the Raman signal will have a significant contribution from collagen type I as the major extracellular matrix protein (reaching approximately 80–85% of the dry weight of the dermis).[44,45]

After our first study,[39] representative Raman sampling in heterogeneous melanocytic lesions remained a challenge. In this paper, we have developed a Raman spectroscopy method to distinguish melanoma from clinically suspicious benign melanocytic lesions irrespective of their histopathological heterogeneity. The fundamental requirement of the diagnostic model was to not miss any melanoma (100% sensitivity). In order to use representative Raman signals, we developed a filtering method to eliminate non-informative spectral contributions of keratin and collagen. The diagnostic model was validated on an independent data set.

Materials and Methods

1) Sample handling. This study was approved by the Medical Ethics Committee of the Leiden University Medical Center (LUMC) (C13.06). After clinical assessment performed by a dermatologist, pigmented skin lesions clinically suspicious for melanoma were excised and submitted for histopathological diagnosis in the dermatology outpatient clinic of the LUMC. These excisions were performed according to the national melanoma guideline and standard protocol of the LUMC department of dermatology. Immediately after surgery, the specimens were prepared for Raman spectroscopy measurements. They were rinsed with NaCl solution (0.9%), wiped with a gauze soaked in ethanol (70%, to remove residual ink from pen marker), gently flattened between two fused silica windows and inserted into a custom-made sample cartridge for Raman measurements, as illustrated in Figure 1. For detailed description, see our previous study.[39]

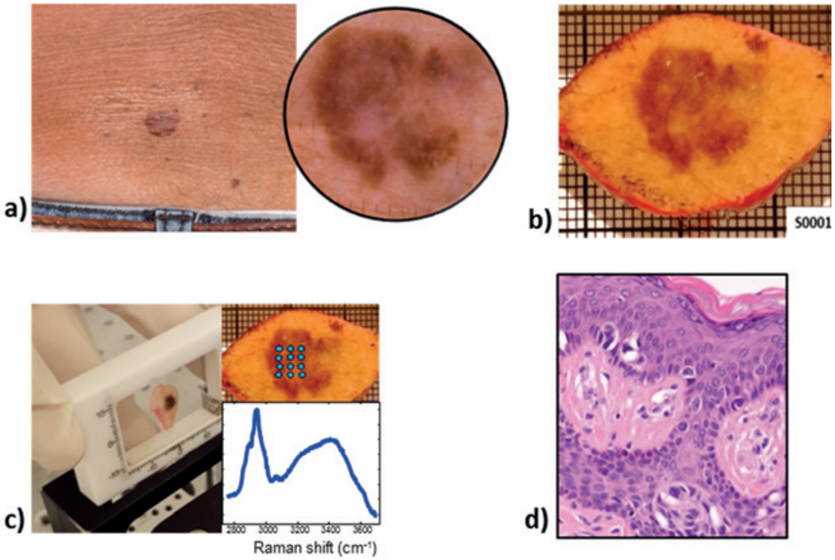

Figure 1. Sample handling. **a)** Clinical diagnosis was aided by dermoscopy (insert); **b)** Lesions suspicious for melanoma were excised; **c)** Specimen is inserted in the cartridge and multiple points were measured within the lesion (insert); **d)** Routine histopathological evaluation (image from H&E slide).

2) Raman spectroscopy measurements. Raman measurements were performed on freshly excised skin specimens, using a SWIR multichannel Raman instrument, which records in the spectral range 2780 to 3750 cm^{-1}. This instrument was constructed in-house and has been described previously.[43] The light source was a diode laser with a wavelength of 976 nm (IPS, Monmouth Junction, NJ, USA). The light was focused on the skin lesion to a spot with a diameter of ~6 µm. Per lesion, an average of 14 (range 9-19) point measurements were performed in the pigmented region of the excised lesion. Each point measurement had an integration time of 30 s. After the Raman spectroscopy measurements, the skin samples were emerged in a 4% formaldehyde solution and sent to pathology for the routine diagnostic procedure.

2.1. Calibration. All Raman spectra were corrected for the wavelength-dependent detection efficiency of the instrument, using an SRM2246 intensity standard (National Institute of Standards and Technology, Gaithersburg, MD), as explained elsewhere.[43] The absolute wavenumber axis was calibrated using the spectral lines of a neon–argon lamp and the Raman spectrum of cyclohexane. The Raman background that originates from the optics was subtracted from all spectra. Data were filtered by 5th order spline filter to remove fixed pattern noise.[39]

2.2. Reference spectra. As reference, Raman spectra were measured from collagen type I (Sigma-Aldrich, C7774 - CAS Number 9007-34-5). For the keratin Raman spectra were measured *in vivo* from the thick *stratum corneum* on the sole of the foot of a healthy volunteer.

Moreover, a set of reference spectra from tissue with low fluorescence background and high variance of Raman signal was created from the spectra of skin lesions used in this study, as follows. For each spectrum, the ratio between peak content and background content was calculated using the spectral region: 2830 cm^{-1} - 3020 cm^{-1} (CH_3 stretching vibrations, which are abundantly present in all biological tissues). A first-order polynomial baseline was fitted through the spectral points at 2830 cm^{-1} and 3020 cm^{-1}. Peak content was calculated as the integrated area above this baseline. Background was calculated as the integrated area below the baseline. The spectra with the highest 40% peak to background ratio values were selected and divided into 20 clusters using hierarchical cluster analysis. Only clusters that consisted of more than 5 spectra were selected, and the spectral average per cluster was calculated. The resulting 17 cluster average spectra were considered as an HWVN tissue reference spectral library.

3) Pre-processing of Raman spectra. All Raman spectra were pre-processed in the way described below. The software used for all computations in this study was Matlab R2015b (Mathworks Inc., Natick, MA).

3.1. Tissue background subtraction. A method described by Barroso *et al.* based on multiple regression fitting (MRF), was used for background correction.[46] MRF is an unsupervised method that corrects fluorescence spectra independently of the shape and intensity of the Raman signal. Briefly, a set of background-free library spectra and a 2nd order polynomial were fitted to the data using a non-negative least squares method. As the library spectra describe all Raman variance present in the data with minimal background signal, the fitted polynomial is a good approximation of the fluorescence background present in the data. The approximated backgrounds were subtracted from the respective spectra.

3.2. Correction for variations in the water signal. A similar procedure was performed to remove the influence of the water signal in the CH band. A reference spectrum of water was fitted to the data. The coefficient that better approximated the water reference spectrum for each one of the spectra measured was obtained. The water signal multiplied by the corresponding coefficient was subtracted from the correspondent data spectra.

3.3. Scaling. All the spectra were scaled to the average of all individual spectra using an extended multiplicative signal correction (EMSC) with a zero-order polynomial background[47] and cropped to the spectral range (2800–3050 cm^{-1}), which corresponds to the CH-stretching band region.

3.4. Detect spectrally heterogeneous samples. The spectral variance within each lesion was calculated (in the complete range 2800–3050 cm^{-1}). The spectra variance per lesion was then added in the spectral direction, to have a total spectral variance per sample. The variance of each sample was normalized with respect to the maximum variance. The lesions that present a high variance (in the top 10% of the ranked values) were considered spectrally heterogeneous and were added to the heterogeneous lesions group.

3.5. Signal orthogonalization for keratin and collagen. A Raman spectrum obtained from a melanocytic lesion can include contributions from several skin constituents, *e.g.* collagen from dermis and keratin from *stratum corneum*. These contributions are not informative for the discrimination of melanoma and benign melanocytic lesions, which do not originate from the *stratum corneum* or from the dermis. A method described by Maquelin *et al.* [48] was used to estimate the Raman signal variance in the spectra from keratin or from collagen. The method is based on a mathematical projection of the lesion Raman spectrum on the Raman signal of keratin or collagen. The results yield the Raman signal that cannot be distinguished from keratin or collagen. Subsequent subtraction of this projection from the spectrum results in the desired non-keratin or non-collagen related Raman lesion spectra (i.e. the vector component of the spectrum that is orthogonal to keratin or collagen).

In a first step, Raman spectra were orthogonalized with keratin. After projection and subsequent subtraction, the total integrated intensity (absolute area) of the orthogonalized signal was calculated. Given the fact that the spectra that have a low AUC cannot be distinguished from the spectra of keratin, it was assumed that the measurement was performed in a region with a thick overlying *stratum corneum*. Spectra of which the integrated value was below a certain threshold (i.e. high presence of keratin) were discarded. These Raman spectra were dominated by keratin and considered not suitable for classification. Orthogonalized spectra on keratin that presented an integrated area lower than 68% (i.e. high presence of keratin) were labelled as "*Not predicted*".

In a second step, the Raman spectra were orthogonalized with collagen. Lesion spectra that presented a low integrated value after projection and subsequent subtraction (i.e. spectra with high contribution of collagen) were considered to come from a benign lesion and removed from the data set for model creation. Orthogonalized spectra on collagen that presented an integrated area lower than 56% (i.e. high presence of collagen) were immediately classified as benign.

3.6. Outlier detection using PCA. A PCA model was used to identify outliers. The first 5 principal components, representing 99.9% of the variance in the data set, were used in the model. Outliers were detected by projecting the spectra on the model. The spectra that could not be explained by the model (i.e. the variance of the residual was larger than 1%) were marked as outliers.

4) Histopathological evaluation and exclusion criteria. After Raman measurements, histopathological samples were prepared as part of routine procedure and were evaluated by two expert pathologists dedicated to this study. The final histopathological diagnosis, upon agreement, was used as the gold-standard reference for correlation with the Raman measurement. All pigmented skin lesions clinically suspected of melanoma and surgically excised for diagnostic purpose were eligible for this study. Non-melanocytic lesions confirmed by histopathology were excluded. Benign melanocytic nevi classes of which less than 5 lesions were present in our data set, were excluded.

5) Histopathological classification used in this study. For the purpose of this study, the samples were divided into two groups based on histopathology: (1) homogeneous melanocytic lesions and (2) heterogeneous melanocytic lesions (Figure 2). Heterogeneous lesions were defined as those that did not have an even distribution of histological components throughout the melanocytic lesion in the most representative H&E slide. *E.g.* an uneven distribution of melanocytic nests surrounded by variable amount of collagen or other non-melanocytic tissue was considered heterogeneous. Also, lesions with a *stratum corneum* thickness of more than 300 µm, or lesions located at a depth of > 300 µm, were included in the heterogeneous group. Moreover, descriptive details were provided, as the thickness of the lesion, depth of the lesion location in the epidermis/dermis and thickness of *stratum corneum*.

6) Diagnostic model creation

6.1. Creation of training sets for the diagnostic model. From the homogeneous lesions, a subset was randomly selected, referred to as *Homogenous lesions set 1* (Figure 3). This set was used to create the PCA-LDA model (see below). Also, from the heterogeneous lesions a subset was randomly selected, referred to as *Heterogeneous lesions set 1*. This set was used to define the parameters for the diagnostic model. All histopathologically proven dysplastic nevi were excluded from model creation.

6.2. PCA-LDA model. A linear discriminant analysis (LDA) model was developed to distinguish melanoma from benign melanocytic lesions. The PCA-LDA model was created based on averaged spectra of *Homogeneous lesions set 1*. Principal component analysis (PCA) was performed to reduce the dimensionality of the data prior to LDA modelling. The scores of the spectra on the first 3 principal components were used as input parameter for the model. The discriminating parameter used as input for the PCA-LDA was a Boolean: "*melanoma*" or "*not-melanoma*".

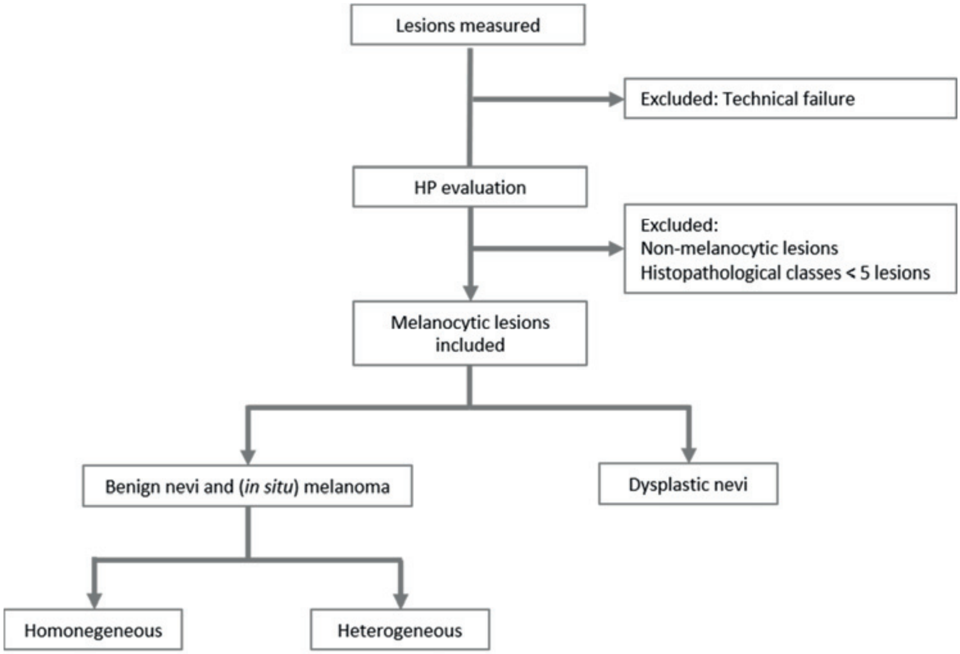

Figure 2. Flowchart of histopathological classification.

6.3 Parameters for the diagnostic model. The PCA-LDA model was applied to each individual point measurement of *Heterogeneous lesions set 1*. The model yields a probability for each individual point for being melanoma. These probabilities were used to establish the parameters of the diagnostic model. A lesion is classified as melanoma: (1) if 2 or more individual point measurements within a lesion have a PCA-LDA score higher than 0.35 and/or (2) at least 1 individual point measurement has a PCA-LDA score greater than 0.8. Otherwise, the lesion is classified as benign.

7) Diagnostic model validation on independent data. The diagnostic model was validated on an independent data set. The independent validation set was comprised of remaining homogeneous and heterogeneous lesions, referred as *Homogeneous lesions set 2* and *Heterogeneous lesions set 2* (Figure 3). The outcome of the model was a Boolean, "*melanoma*" or "*not-melanoma*". Specificity was defined as the fraction of correctly predicted negatives (not-melanoma) from the total number of benign melanocytic lesions. Sensitivity was calculated as the fraction of correctly predicted positives (melanoma) from the total number of melanomas.

8) Separate test on dysplastic nevi

Because there is no agreement whether dysplastic nevi must be considered benign, dysplastic were not included either in the diagnostic model or in the independent validation set. The diagnostic model was separately tested on the dysplastic nevi.

Results

In total, 222 freshly excised pigmented skin lesions clinically suspected of melanoma were measured. From those, a total of 48 were excluded: 17 for technical reasons, 28 non-melanocytic lesions (basal cell carcinoma, seborrheic wart, lichenoid keratosis, dermatofibroma, hemangioma, scar) and histopathological classes that contained less than 5 lesions (Spitz nevi, n=2 and combined melanocytic nevus, n = 1).

The characteristics of the remaining 174 lesions are summarized in Table 1. Of the 37 melanomas, 22 were *in situ* (59.4%) and 15 had an average Breslow thickness of 0.89 mm (range 0.2-3.0 mm).

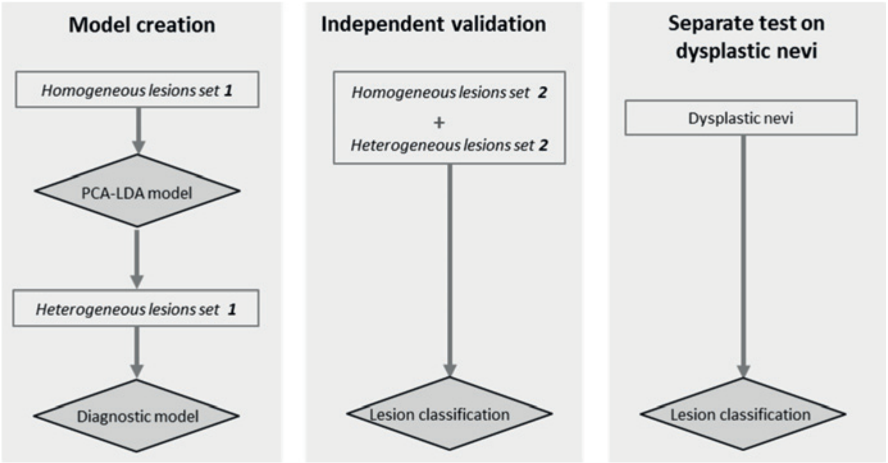

Figure 3. Lesions used for diagnostic model creation (left), lesions used for the independent validation (middle) and dysplastic nevi on which diagnostic model was separately applied (right).

Table 1. Summary of the lesions included.

Histopathological diagnosis	Average age (y, range)	Sex	Anatomical Location	Number of lesions	Average Breslow thickness (mm, range))
Melanoma					
in situ	58.5 (41 – 82)	10 female 12 male	Head and neck	2	
			Upper limb	5	
			Trunk	7	
			Lower limb	8	
invasive	52.9 (29 – 73)	10 female 5 male	Head and neck	2	0.89 (0.20-3.00)
			Upper limb	1	
			Trunk	4	
			Lower limb	8	
Dermal nevi	43.0 (16 – 68)	14 female 13 male	Head and neck	1	
			Upper limb	2	
			Trunk	14	
			Lower limb	11	
Compound nevi	46.6 (15 - 75)	25 female 18 male	Head and neck	-	
			Upper limb	4	
			Trunk	26	
			Lower limb	12	
			Unspecified	1	
Junctional nevi	51.5 (25 - 82)	10 female 6 male	Head and neck	1	
			Upper limb	2	
			Trunk	11	
			Lower limb	2	
Blue nevi	45.8 (19 - 87)	3 female 2 male	Head and neck	1	
			Upper limb	-	
			Trunk	4	
			Lower limb	-	
Dysplastic nevi	47.9 (23 - 77)	29 female 17 male	Head and neck	1	
			Upper limb	4	
			Trunk	34	
			Lower limb	6	
			Unspecified	1	

Diagnostic model creation. A total of 78 lesions were used for model creation (*Homogeneous lesions set 1 and Heterogeneous lesions set 1*). First, the Raman spectra of the *Homogeneous lesions set 1* (55 lesions) were used to create the PCA-LDA model. The Raman spectra of the *Heterogeneous lesions set 1* (23 lesions) were used to define the parameters for the diagnostic model. The histopathological diagnosis of the lesions included in the diagnostic model set are shown in Table 2. Figure 4 shows the PCA-LDA model discriminant for melanoma *versus* benign melanocytic lesions.

Table 2. Histopathological diagnosis of lesions included in the diagnostic model set and in the independent validation set.

Histopathological diagnosis		***Number of lesions per set***		
		Diagnostic model set	**Independent validation set**	**Total**
(*in situ*) Melanoma		20	17	37
Benign melanocytic nevi	Dermal	20	7	27
	Compound	27	16	43
	Junctional	9	7	16
	Blue	2	3	5
Total		**78**	**50**	**128**

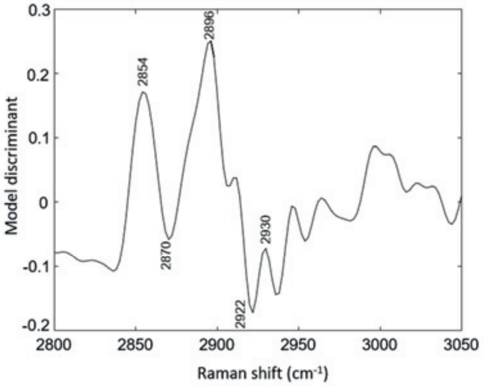

Figure 4. PCA-LDA model discriminant for melanoma *versus* benign nevi. The PCA-LDA model discriminant is a spectral representation of the discriminating differences between groups. The peaks at 2854 cm^{-1} (assigned to the symmetric CH_2 stretching vibrations of lipids) and 2896 cm^{-1} (assigned to asymmetric CH_2 stretching vibrations of lipids) show lipid features which are more pronounced in melanoma than in benign nevi.

Diagnostic model validation on independent data. *Homogeneous lesions set 2* (21 lesions) *and Heterogeneous lesions set 2* (29 lesions) were used for the independent validation of the diagnostic model. Table 2 shows the histopathological diagnosis of the lesions included in the independent validation set, comprising 17 melanomas (10 *in situ* and 7 thin melanomas with an average Breslow thickness of 0.42 mm, range 0.2-0.8 mm). Table 3 shows the contingency table of the diagnostic model validation. A specificity of 43.8% at 100% sensitivity was obtained, specificity defined as the fraction of correctly predicted negatives (not melanoma) from the total number of benign nevi in the independent validation set.

Table 3. Contingency table of the diagnostic model validation.

		Independent validation outcome		
		Benign nevi	Melanoma	Not predicted (high keratin)
Histopathological diagnosis	Benign nevi	**14**	18	1
	Melanoma	0	**16**	1

Eighteen benign melanocytic nevi were classified as melanoma, of which 7 were compound nevi, 5 junctional nevi, 4 dermal nevi and 2 blue nevi. None of the melanomas was misclassified.

Two lesions were identified by the keratin filter, both with thick *stratum corneum* (1 melanoma *in situ* and 1 compound nevus, shown in Figure 5). The measurements obtained in these lesions were identified and labeled as "*Not predicted*".

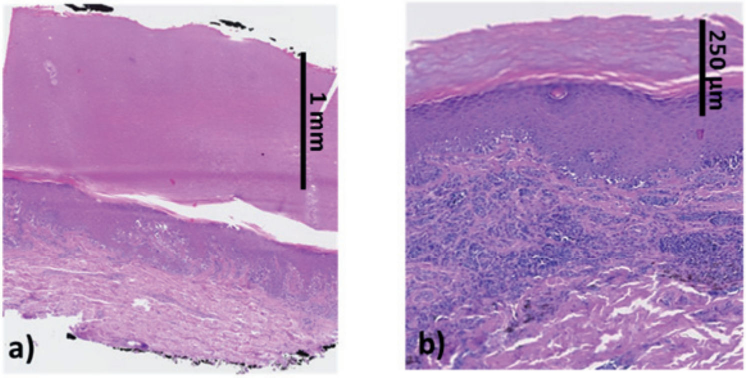

Figure 5. H&E stained thin tissue sections; **a)** melanoma *in situ* with a thick *stratum corneum* (1.2 mm); **b)** combined melanocytic nevus with a thick *stratum corneum* (200 µm). *N.B.*: the Raman spectra of these lesions showed high similarity with keratin and were labeled "*Not predicted*" by the diagnostic model.

Separate test on dysplastic nevi. The diagnostic model was separately tested on the dysplastic nevi. From the total 46 dysplastic nevi, 73.9% were classified as melanoma (Table 4).

Table 4. Outcome of the diagnostic model applied on the set of dysplastic nevi.

		Test outcome for dysplastic nevi		
		Benign nevi	Melanoma	Not predicted (high keratin)
Histopathological diagnosis	Dysplastic nevi	12	34	0

Discussion

Melanomas with a Breslow thickness of less than 0.8 mm are curable by surgical excision. In this study, a diagnostic model for melanoma based on Raman spectroscopy was developed and validated on an independent test set. All the included lesions had been excised because they were clinically suspicious for melanoma. The study was conducted on a specific patient population at high risk of developing melanoma. These patients frequently visit the specialized pigmented lesions clinic.

In our previous study we showed that homogeneous melanocytic lesions (*i.e.* with an even distribution of histological components throughout the melanocytic lesion) could be distinguished from melanoma with a high diagnostic power of almost 80% using Raman spectroscopy.[39] However, a substantial portion of melanocytic lesions is heterogeneous (*i.e.* without an even distribution of histological components throughout the melanocytic lesion). Clinical application requires that both homogeneous and heterogeneous melanocytic lesions can be classified. Therefore, in the current study, we included heterogeneous lesions in the development of the diagnostic model.

We divided the samples into two groups based on histopathology (homogeneous and heterogeneous) and created a PCA-LDA model using only homogeneous lesions. This ensured that the PCA-LDA model was based on an optimal match between Raman measurements and the reference histopathological diagnosis.

The PCA-LDA model discriminant visualizes discriminative spectral information between melanoma and benign nevi. A higher lipid content in melanoma is the strongest discriminative factor (Figure 4). The diagnostic model in this study was developed to distinguish melanoma from benign melanocytic lesions suspicious for melanoma.

Dysplastic nevi are melanocytic lesions that present histologically architectural disorder and cytological atypia.[50,51] Because there is no international consensus about whether dysplastic nevi must be considered benign[49,51-60,64], dysplastic nevi were not included in the diagnostic model. However, in clinical practice a significant portion of the lesions suspicious for melanoma are dysplastic nevi. Although the dysplastic nevi were not included in the development of the diagnostic model, we have applied the diagnostic model on these lesions as well.

This is the first Raman study addressing thin melanomas. The diagnostic model was optimized for highest possible specificity at a sensitivity of 100%. Nine to nineteen individual point measurements were obtained per lesion. A lesion was classified as melanoma if 2 or more individual point measurements had a PCA-LDA score higher than 0.35, or if at least 1 individual point measurement had a PCA-LDA score greater than 0.8. These criteria reflect a melanoma diagnosis based on either a single point measurement with high probability of melanoma or multiple point measurements with moderate probability. A limitation of this study is the lack of accurate correlation between the individual Raman point measurements and histopathology. We are currently developing a method for reliable and reproducible matching between the origin of individual Raman spectra and histological structures. It is expected that, when applying this method, the accuracy of the diagnostic model that we have developed will be further improved.

In this study, the NNT by dermatologists was 6.0 (222 excised lesions suspicious for melanoma, and 37 histopathologically confirmed melanomas). Twenty percent of the excised lesions suspicious for melanoma were dysplastic nevi. To calculate the NNT based on Raman diagnosis, 13 randomly selected dysplastic nevi were added to the validation set, so that this set also comprised 20% of dysplastic nevi. If the Raman instrument were used as an add-on to diagnose the dermatologist-selected lesions, the estimated NNT would be 2.7 (43 lesions tested positive by Raman spectroscopy and a total 16 histopathologically confirmed melanoma. There are indications that dysplastic nevi are associated with an increased risk of developing melanoma,[49, 61-63] which is suggestively supported by our results shown in Table 4.

In this study, we demonstrate that, based on Raman spectroscopy, an accurate diagnosis of melanoma with Breslow thickness <0.8 mm can be made. This work signifies an important step towards objective accurate diagnosis of melanoma.

References

1. Estimated Cancer Incidence, Mortality and Prevalence Worldwide in 2012," 2012. [Online]. Available: http://globocan.iarc.fr. [Accessed: 22-Mar-2017].
2. J. E. Gershenwald, R. A. Scolyer, K. R. Hess, V. K. Sondak, G. V. Long, M. I. Ross, A. J. Lazar, M. B. Faries, J. M. Kirkwood, G. A. McArthur, L. E. Haydu, A. M. M. Eggermont, K. T. Flaherty, C. M. Balch, and J. F. Thompson, *CA. Cancer J. Clin.*, 2017, 67, 6.
3. S. C. Chen, D. M. Bravata, E. Weil, and I. Olkin, *Arch. Dermatol.*, 2001, 137, 12, 1627–1634.
4. S. Sidhu, O. Bodger, N. Williams, and D. L. Roberts, *Clin. Exp. Dermatol.*, 2012, 37, 1, 6–9.
5. L. Kofler, M. Egger, and H. Kofler, *Clin. Dermatology*, 2014, 2, 2, 73–76.
6. R. Marks and a P. Dorevitch, *J. Am. Acad. Dermatol.*, 1994, 721–726.
7. J. K. Robinson and B. J. Nickoloff, *Arch. Dermatol.*, 2004, 140, 1, 49–56.
8. J. P. Banky, J. W. Kelly, D. R. English, J. M. Yeatman, and J. P. Dowling, *Arch. Dermatol.*, 2005, 141, 8, 998–1006.
9. N. Nathansohn, A. Orenstein, H. Trau, A. Liran, and J. Schachter, *Isr. Med. Assoc. J.*, 2007, 9, 10, 708–712.
10. C. Hansen, D. Wilkinson, M. Hansen, and G. Argenziano, *J. Am. Acad. Dermatol.*, 2009, 61, 4, 599–604.
11. P. Carli, F. Mannone, V. De Giorgi, P. Nardini, A. Chiarugi, and B. Giannotti, *Melanoma Res.*, 2003, 13, 2, 179–82.
12. G. Argenziano, L. Cerroni, I. Zalaudek, *et al*, *J. Am. Acad. Dermatol.*, 2012, 67, 1, 54–60.
13. N. Nathansohn, A. Orenstein, H. Trau, A. Liran, J. Schachter, *Isr Med Assoc J* , 2007, 9, 708-712
14. J. March, M. Hand, and D. Grossman, *J. Am. Acad. Dermatol.*, 2015, 72, 6, 929–941.
15. I. Alarcon, C. Carrera, J. Palou, L. Alos, J. Malvehy, and S. Puig, *Br. J. Dermatol.*, 2014, 170, 4, 802–808.
16. P. Guitera, S. W. Menzies, G. Argenziano, C. Longo, A. Losi, M. Drummond, R. A. Scolyer, and G. Pellacani, *Br. J. Dermatol.*, 2016, 175, 6, 1311–1319.
17. A. D. Stevenson, S. Mickan, S. Mallett, and M. Ayya, *Dermatol. Pract. Concept.*, 2013, 3, 4, 19–27.
18. C. Curiel-lewandrowski, C. M. Williams, K. J. Swindells, S. R. Tahan, S. Astner, R. A. Frankenthaler, and S. Gonza, *Arch Dermatol*, 2004, 140, 9, 2–7.
19. P. Guitera, S. W. Menzies, C. Longo, A. M. Cesinaro, R. A. Scolyer, and G. Pellacani, *J. Invest. Dermatol.*, 2012, 132, 10, 2386–2394.
20. R. R. Winkelmann, J. Yoo, N. Tucker, R. White, and D. S. Rigel, *J. Clin. Aesthet. Dermatol.*, 2014, 7, 12, 16–18.
21. X. Delpueyo, M. Vilaseca, S. Royo, M. Ares, L. Rey-Barroso, F. Sanabria, S. Puig, J. Malvehy, G. Pellacani, F. Noguero, G. Solomita, and T. Bosch, *J. Biomed. Opt.*, 2017, 22, 7, 79801.
22. L. Yu, H. Chen, Q. Dou, J. Qin, and P. A. Heng, *IEEE Trans. Med. Imaging*, 2017, 36, 4, 994–1004.
23. L. Rocha, S. W. Menzies, S. Lo, M. Avramidis, R. Khoury, L. Jackett, and P. Guitera, *Br. J. Dermatol.*, 2017, 12, 10, 3218–3221.
24. P. Mohr, U. Birgersson, C. Berking, C. Henderson, U. Trefzer, L. Kemeny, C. Sunderkötter, T. Dirschka, R. Motley, M. Frohm-Nilsson, U. Reinhold, C. Loquai, R. Braun, F. Nyberg, and J. Paoli, *Ski. Res. Technol.*, 2013, 19, 2, 75–83.
25. R. P. Braun, J. Mangana, S. Goldinger, L. French, R. Dummer, and A. A. Marghoob, *Dermatol. Clin.*, 2017, 35, 4, 489–493.
26. R. R. Winkelmann and D. S. Rigel, *J. Am. Acad. Dermatol.*, 2015, 73, 6, 1056–1059.
27. G. Monheit, A. B. Cognetta, L. Ferris, H. Rabinovitz, K. Gross, M. Martini, J. M. Grichnik, M. Mihm, V. G. Prieto, P. Googe, R. King, A. Toledano, N. Kabelev, M. Wojton, and D. Gutkowicz-Krusin, *Arch. Dermatol.*, 2011, 147, 2, 188–94.
28. F. Farnetani, A. Scope, R. P. Braun, S. Gonzalez, P. Guitera, J. Malvehy, M. Manfredini, A. A. Marghoob, E. Moscarella, M. Oliviero, S. Puig, H. S. Rabinovitz, I. Stanganelli, C. Longo, C. Malagoli, M. Vinceti, and G. Pellacani, *JAMA Dermatology*, 2015, 151, 10, 1075.
29. J. Malvehy, A. Hauschild, C. Curiel-Lewandrowski, P. Mohr, R. Hofmann-Wellenhof, R. Motley, C. Berking, D.

Grossman, J. Paoli, C. Loquai, J. Olah, U. Reinhold, H. Wenger, T. Dirschka, S. Davis, C. Henderson, H. Rabinovitz, J. Welzel, D. Schadendorf, and U. Birgersson, *Br. J. Dermatol.*, 2014, 171, 5, 1099–1107.

30. G. S. Inamdar, S. R. V. Madhunapantula, and G. P. Robertson, *Biochem. Pharmacol.*, 2010, 80, 5, 624–637.
31. D. Sengupta and A. J Tackett, *J. Proteomics Bioinform.*, 2016, 4, 9, 1–7.
32. J. A. Carlson, J. S. Ross, A. Slominski, G. Linette, J. Mysliborski, J. Hill, and M. Mihm, *J. Am. Acad. Dermatol.*, 2005, 52, 5, 743–775.
33. R. Akbani, K. C. Akdemir, B. A. Aksoy, *et al.*, *Cell*, 2015, 161, 7, 1681–1696.
34. G. Botti, L. Marra, A. Anniciello, G. Scognamiglio, V. Gigantino, and M. Cantile, *Int. J. Clin. Exp. Pathol.*, 2015, 8, 9, 9742–9751.
35. E. M. Barroso, R. W. H. Smits, C. G. F. Van Lanschot, P. J. Caspers, I. Ten Hove, H. Mast, A. Sewnaik, J. A. Hardillo, C. A. Meeuwis, R. Verdijk, V. N. Hegt, R. J. Baatenburg De Jong, E. B. Wolvius, T. C. Bakker Schut, S. Koljenović, and G. J. Puppels, *Cancer Res.*, 2016 76, 20, 5945-5953.
36. E. M. Barroso, R. W. H. Smits, T. C. B. Schut, I. Ten Hove, J. A. Hardillo, E. B. Wolvius, R. J. Baatenburg De Jong, S. Koljenović, and G. J. Puppels, *Anal. Chem.*, 2015, 87, 4, 2419–2426.
37. S. Koljenovic, T. C. Bakker Schut, R. Wolthuis, B. de Jong, L. Santos, P. J. Caspers, J. M. Kros, and G. P. Puppels, *J. Biomed. Opt.*, 2005, 3, 10, 1–11.
38. A. Nijssen, K. Maquelin, L. F. Santos, P. J. Caspers, T. C. Bakker Schut, J. C. Den Hollander, M. H. A. Neumann, and G. P. Puppels, *J. Biomed. Opt.*, 2007, 12, 3.
39. I. P. Santos, P. J. Caspers, T. C. Bakker Schut, R. van Doorn, V. Noordhoek Hegt, S. Koljenović, and G. J. Puppels, *Anal. Chem.*, 2016, 88, 15, 7683–7688.
40. H. Lui, J. Zhao, D. McLean, and H. Zeng, *Cancer Res.*,2012, 72, 10, 2491–2500.
41. L. Lim, B. Nichols, M. R. Migden, N. Rajaram, J. S. Reichenberg, M. K. Markey, M. I. Ross, and J. W. Tunnell, *J. Biomed. Opt.*, 2014, 19, 11, 117003.
42. J. Zhao, H. Lui, S. Kalia, and H. Zeng, *Anal. Bioanal. Chem.*, 2015, 407, 27, 8373–8379.
43. I. P. Santos, P. J. Caspers, T. Bakker Schut, R. van Doorn, S. Koljenović, and G. J. Puppels, *J. Raman Spectrosc.*, 2015, 46, 7l, 652–660.
44. J. A. McGrath and J. Uitto, in *Rook's Textbook of Dermatology*, 8th ed., ed.T. Burns, S. Breathnach, N. Cox, and C. Griffiths, 2010, Wiley-Blackwell, 3.1-3.53.
45. T. T. Nguyen, C. Gobinet, J. Feru, S. B. -Pasco, M. Manfait, and O. Piot, *Spectrosc. An Int. J.*, 2012, 27, 5–6, 421–427.
46. E. Barroso, T. Bakker Schut, P. J. Caspers, I. P. Santos, E. Wolvius, S. Koljenović, and G. J. Puppels, *J. Raman Spectrosc.*, 2018, 1-12.
47. H. Martens and E. Stark, *J. Pharm. Biomed. Anal.*, 1991, 9, 8, 625–635.
48. K. Maquelin, L. P. Choo-Smith, T. van Vreeswijk, H. P. Endtz, B. Smith, R. Bennett, H. A. Bruining, and G. J. Puppels, *Anal.Chem.*, 2000, 72, 1, 12–19.
49. A. Shain, B. Bastian, *Nature Reviews Cancer*, 2016, 16, 6, 345-358
50. A. M. Goldstein and M. A. Tucker, *Cancer Epidemiol. Biomarkers Prev.*, 2013, 22, 4, 528–532.
51. K. Duffy and D. Grossman, *J. Am. Acad. Dermatol.*, 2012, 67, 1, 1–27.
52. M. Arumi-Uria, N. S. McNutt, and B. Finnerty, *Mod. Pathol.*, 2003, 16, 1, 764–771.
53. N. Wall, B. De'Ambrosis, J. Muir, *Australasian Journal of Dermatology*, 2017, 58, 304-307
54. K. Engeln, K. Peters, J. Ho, J. Jedrych, D. Winger, L. Korb Ferris, T. Patton, *J Am Acad Dermatol*, 2017, 76,2, 244-249
55. P. Sapra, C. Rosen, S. Siddha, C. Lynde, *Journal of Cutaneous Medicine and Surgery*, 2015, 19, 5, 457-463
56. J.M. Naeyaert, L. Brochez, *N Eng J Med*, 2003, 349, 23, 2233-2240
57. R. Winkelmann, D. S. Rigel, *J Am Acad Dermatol*, 2015, 73, 6 1058-1059
58. C. Kim, S. Swetter, C. Curiel-Lewandrowski, J. M. Crichnik, D. Grossman, A. C. Halpern, J. M. Kirkwood, S. A. Leachman, A. A. Marghoob, M. E. Ming, K. Nelson, E. Veledar, S. Venna, S. Chen, JAMA Dermatol, 2015, 151, 2, 212-218.
59. K.C. Lee, S. Peacock, M.A. Winstock, G. A. Zhao, S. R. Knezevich, D. E. Elder, R. L. Barnhill, M. W. Piepkorn, L. M. Reisch, P. A. Carney, T. Onega, J. P. Lott, J. G. Elmore, *J Am Acad Dermatol*, 2016, 76, 1, 121-128
60. L. X. Tong, P. A. Wu, C. C. Kim, *J Am Acad Dermatol*, 2016, 74, 2, 389-391

61. J. A. Newton Bishop, “Lentigos, Melanocytic Naevi and Melanoma,” in *Rook’s Textbook of Dermatology*, 8th ed., T. Burns, S. Breathnach, N. Cox, and C. Griffiths, Eds. Wiley-Blackwell, 2010, 54.1-54.57

62. D. J. Santa Cruz, “Tumors of the skin,” in *Diagnostic Histopathology of Tumors*, 3th ed., C. D. M. Fletcher, Ed. Churchill Livingstone - Elsevier, 2007, 1423–1526

63. E. de Vries, F. Bray, J. W. Coebergh, L. Cerroni, D. J. Ruiter, D. E. Elder, J. F. Thompson, G. N. P. van Muijen, R. A. Scolyer, and P. E. LeBoit, “Malignant Melanoma: Introduction,” in *World Health Organization Classification of Tumors. Pathology and Genetics of Skin Tumors.*, Eds. P. E. LeBoit, G. Burg, D. Weedon, and A. Sarasain, IARC Press, 2006, 52–61

64. J. G. Elmore, R. L. Barnhill, D. E. Elder, G. M. Longton, M. S. Pepe, L. M. Reisch, P. A. Carney, L. J. Titus, H. D. Nelson, T. Onega, A. N. A. Tosteson, M. A. Weinstock, S. R. Knezevich, and M. W. Piepkorn, *BMJ*, 2017, 357.

CHAPTER 6

Raman spectroscopy for in vivo cancer detection and cancer surgery guidance: translation to the clinics

Inês P. Santos[†], Elisa M. Barroso[†], Tom C. Bakker Schut, Cornelia G. F. van Lanschot, Da-Hye Choi, Martine F. van der Kamp, Roeland W. H. Smits, Remco van Doorn, Rob M. Verdijk, Vincent Noordhoek Hegt, Jan H. von der Thüsen, Carolien H. M. van Deurzen, Linetta B. Koppert, Arno van Leenders, Patricia C. Ewing-Graham, Lena C. van Doorn, Clemens M. F. Dirven, Martijn B. Busstra, Jose Hardillo, Aniel Sewnaik, Ivo ten Hove, Hetty Mast, Dominiek A. Monserez, Cees Meeuwis, Robert J. Baatenburg de Jong, Tamar Nijsten, Eppo B. Wolvius, Peter J. Caspers, Gerwin J. Puppels[†] and Senada Koljenović[†],

Analyst, **2017**; 142 (17): 3025-3047.

[†] *These authors contributed equally to this work.*

Abstract

Oncological applications of Raman spectroscopy have been contemplated, pursued, and developed at academic level for at least 25 years. Published studies aim to detect pre-malignant lesions, detect cancer in less invasive stages, reduce the number of unnecessary biopsies and guide surgery towards the complete removal of the tumor with adequate tumor resection margins. This review summarizes actual clinical needs in oncology that can be addressed by spontaneous Raman spectroscopy and it provides an overview over the results that have been published between 2007 and 2017. An analysis is made of the current status of translation of these results into clinical practice. Despite many promising results, most of the applications addressed in scientific studies are still far from clinical adoption and commercialization. The main hurdles are identified, which need to be overcome to ensure that in the near future we will see the first Raman spectroscopy-based solutions being used in routine oncologic diagnostic and surgical procedures.

General introduction

In 2012 the World Health Organization (WHO) reported 14.1 million new cancer cases, 8.2 million cancer deaths and 32.6 million people living with cancer (within 5 years of diagnosis). These numbers are increasing, which motivates development of cancer treatment possibilities and technology for early detection of (pre-) malignancies.[1] The high mortality rate of cancer can be reduced by early and accurate diagnosis, and by adequate surgical treatment.[2] The reference standard for cancer diagnosis is histopathologic assessment of biopsies or diagnostic excisions of suspicious tissue. After biopsy/excision the tissue specimen is fixed, micro-sectioned and routinely stained with hematoxylin and eosin (H&E). The pathologist makes a diagnosis based on microscopic examination of the H&E stained section. Because only small portions of the lesional tissue are biopsied or excised for histopathological examination, there is the risk of sampling error and the pathology report remains a subjective assessment (with its inter and intra operator variability).[3] Studies have demonstrated that most tumor types develop through pre-malignant stages.[4,5] Therefore, the treatment of pre-malignant tissue can prevent the further development of cancer. Because the distinction between early-stage malignant, pre-malignant and benign tumors can be difficult to make, repeated biopsies/excisions are often taken. For sampling of tissue, literature reports positive predictive values as low as 22% for prostate cancer diagnosis,[6] 1.4% for breast cancer,[7] 18.5% in lung cancer screenings,[8] and 7–23% for melanoma diagnosis.[9] Despite the risk of these unnecessary biopsies/excisions, a substantial number of early stage tumors are still missed, which increases the risk of progression to a metastatic stage.

Introduction – early diagnosis/guided biopsy

A technique that helps to achieve representative biopsies and that would enable accurate and early *in vivo* diagnosis is needed. This tool should detect lesions in pre-malignant/early stages and assess large tissue areas in real-time to decrease sampling errors. Several techniques have been tested for biopsy guidance, such as optical coherence tomography (OCT), white light reflectance (WLR), auto-fluorescence and Raman spectroscopy.[10–14] OCT and WLR rely on the visualization of changes in tissue structure. These techniques provide little or no information about the molecular tissue composition and, therefore, generally have a low specificity.[10,12] Auto-fluorescence imaging is an optical technique that detects natural fluorescence emitted by fluorophores present in the tissues (*e.g.* flavins, collagen or hemoglobin), after excitation by a short-wavelength light source.

This emission can be captured in real-time, for example during endoscopy, and can be used for lesion detection or characterization.[13,14] Auto-fluorescence imaging has shown to improve the sensitivity of detection of early cancer, like epithelial neoplasia in esophagus and colon (sensitivities are 90% and 99%, respectively).[14] It also improves the diagnostic sensitivity (from 67% to 89%) for pre-malignant stages of lung cancer (*e.g.*, dysplasia and carcinoma *in situ*). It also improves the diagnostic sensitivity compared to white-light endoscopic imaging (from 67% to 89%) for pre-malignant stages of lung cancer. However, the specificity of this technique is low; a specificity of 64% for diagnosing pre-malignant stages of lung cancer, a specificity of 81% for detecting high-grade dysplasia and early cancer in Barrett's esophagus and a specificity of 35% for detection of pre-malignant colon polyps were reported.[14–16] Optical vibrational spectroscopic techniques, such as Raman spectroscopy, can provide high molecular specificity. The gradual changes from healthy tissue to tumor are reflected by their Raman spectra.[2,17–19] Raman spectroscopy is a technique for characterizing biological tissue *in vivo*, *ex vivo* or *in vitro* and for non-invasive detection of the molecular differences between tumor and healthy tissue. It does not require any labelling, reagents or other preparation of the tissue, which facilitates translation to the clinic. With the use of optical fibers many anatomical locations can be assessed *in vivo*.[20] Raman spectroscopy-based biopsy guidance can reduce the number of false positive biopsies and increase the accuracy of cancer diagnosis, with reported overall sensitivities and specificities between 73%–100% and 66%–100%, respectively.[18,21]

Introduction – guided surgery

After diagnosis the primary treatment for solid tumors is often surgery. The objective of surgical treatment is resection of all malignant tissue with adequate resection margins while preserving important healthy structures. Achieving adequate surgical margins is important for disease control and survival. Residual tumor after surgery is associated with poor survival and the need for additional surgery, adjuvant chemotherapy, radiation therapy, or a combination of these.[22–25] A number of studies have shown that the 5-year survival decreases significantly when tumor is not completely removed.[22–25] Intraoperative guidance tools can help to achieve adequate surgery. However, there are no widely used intraoperative guidance tools available yet. Current surgical resection techniques are based on subjective methods, such as palpation and visual inspection, to judge the border between normal and cancerous tissue. In order to support the intraoperative assessment of resection margins, frozen sections can be used.[26–28] A small piece of suspicious tissue is usually sampled from the wound bed (i.e. wound-driven assessment) by the surgeon. A microscopic evaluation of the frozen section is performed by the pathologist, directing operative management.[28] It has been reported that the frozen section procedure increases the rate of adequate resections and thereby decreases local recurrence and improves the survival rate.[29] Even though this procedure is successful for intraoperative assessment of the resection margins, it has its limitations: (1) it is time consuming, extending the duration of surgery and anesthesia;[30] (2) it is likely prone to sampling errors because only a small fraction of the resection margin can be investigated, and (3) it can introduce histologic disruption caused by rapid freezing, which makes the analysis more difficult.[31] Rosenthal *et al.* reported that at most 5% to 10% of the wound bed can be sampled and assessed with frozen section.[32] These limitations can lead to false negative results.[23,27,33–35] Consequently, there is much room for improvement in performing intraoperative assessment of the resection margins. In order to guide oncological surgery, techniques like intraoperative real-time MRI, intraoperative ultrasound, intraoperative OCT, fluorescence and Raman spectroscopy have been investigated in operating room environments. Real-time intraoperative MRI has been tested during surgical resection of brain cancer (i.e. glioma). Several studies have demonstrated that this modality can be used for surgery guidance and improves the extent of the tumor resection without increasing neurological deficits. This also has a positive impact on survival.[36–42] Some drawbacks of intraoperative MRI include: (1) operative defects that can affect the MRI image and decrease its accuracy;[43] (2) interpretation of the image by the surgeon and his capability to correlate the location of the lesion to the brain anatomy;[17,43] (3) significant surgical disruptions that prolong the operation time; (4) it requires a considerable investment to implement MRI-capable operating rooms; and (5) there is a need for contrast agents.[43] Intraoperative ultrasound has been used to localize the tumor, guide the resection especially among highly vascular tumors (*e.g.* breast), using probes that enhance contrast.[43,44] However, it is less sensitive for tumor margins and has shown lower resolution and accuracy compared to intraoperative MRI. Besides, its accuracy is affected by previous surgery, as almost any imaging modality.[43,45] A portable label-free optical coherent tomography (OCT) imaging system has been tested intraoperatively to assess breast resection margins and lymph nodes *ex vivo*.[46] The study showed promising results for real-time microscopic image guide breast cancer surgery. Structural-based imaging techniques (like OCT and intraoperative MRI) show promising results. Unfortunately, they lack chemical disease-specific information, which is essential for adequate tumor removal. Fluorescence imaging is another technique that has been applied to assess surgical resection margins. The technique requires administration of fluorescence agents and is based on the detection of fluorescently labelled structures during surgery. Various studies have reported that complete resection was achieved in a significantly higher percentage when fluorescence imaging was used, as compared to only regular white light.[47–50] The major disadvantages of fluorescence imaging are: (1) the need for fluorescence agents, and (2) the need to switch off the room lighting to maximize the detection of the weak fluorescence.[46] In addition, translational problems have been identified, related to the need of consistent manufacturing, to costs related with toxicology studies, and to the strict procedures for submission of a new investigational drug.[51] An interesting alternative would be a label-free imaging method, which avoids the risks associated with dye/drug reactions and the challenges associated with specific tumor targeting and non-specific binding Raman spectroscopy has also been implemented to guide oncological surgery. Several studies have demonstrated that this technique can be used for surgical guidance. For example, in brain cancer surgery, an intraoperative Raman system that measures directly brain tissue in the patient, has proven to distinguish dense and low-density cancer infiltration from benign brain tissue with a sensitivity of 93% and a specificity of 91%.[52] In another study, a real-time Raman intraoperative system was used during breast cancer surgery for assessment of freshly resected specimens. This study has demonstrated that Raman spectroscopy could discriminate cancerous tissue from normal breast tissue with a sensitivity of 83% and a specificity of 93%.[53] Implementing Raman spectroscopy in the clinical setting can have important benefits: (1) it can enable representative sampling for correct pathological diagnosis (biopsy guidance);(2) it can accurately assist in defining adequate resection margins during surgery; (3) it can reduce the sampling problem, during intraoperative assessment; (4) it can introduce a more objective assessment and (5) it can reduce the need for adjuvant therapies.[20] In the last years, several review articles reported the advances of Raman spectroscopy with the ultimate goal the clinical application for cancer diagnosis in different anatomical locations.[17,18,20,21,54–57] In these reviews the latest developments of technology adaptations for Raman cancer diagnostic applications are described. The latest clinical outcomes of Raman spectroscopy on (early) cancer detection at different sites in vitro, *ex vivo* and *in vivo* have been also reported. However, specifically the translation of Raman spectroscopic developments into oncological applications has not been addressed extensively before. The scope of this article is to provide an analysis of the translation of R&D results, obtained in oncological applications of Raman spectroscopy, into clinical practice. We discuss problems that still need to be solved in order to bring the technique successfully to the end-users in the hospital setting. The importance of defining the clinical needs and requirements, for different applications, is also explored in this review. We have limited our review to spontaneous Raman spectroscopy applications on *ex vivo* and/or *in vivo* human tissue samples. We refer to the other recent review articles for biomedical applications of non-linear Raman spectroscopy, such as coherent and surface-enhanced Raman scattering.[55,58,59]

Methods

Literature search. A search was carried out using the Web of Science™ library. Web of Science™ comprises the following databases: Web of Science™ Core Collection, KCI-Korean Journal Database, MEDLINE, Russian Science Citation Index and SciELO Citation INdex. For research articles the included period was from 2006 to 2017. For review articles the included period was from 2011 to 2017. The date of the final search was on 16th of January 2017. The search filter comprehended a combination of the keyword “Raman” with two of the following keywords: "tumo(u)r", "patient", "biopsy", "carcinoma", "assessment", "intraoperative", "cancer", "guidance", "surgery", "human", "diagnostics" and "translation". These keywords were searched as a topic in the article. Articles that had at least three of the topic words were considered for inclusion. Commentaries and opinion articles were excluded. Furthermore, studies on non-human samples and performed *in vitro* were not selected. Studies that used non-linear Raman spectroscopy were excluded. Cytological screening methods based on Raman spectroscopy are also being developed,[60,61] however to limit the scope we have chosen not to include such studies in this review. Articles that were not written in English were also discarded.

Definition of the clinical need. The clinical needs (clinical problems and their relevance) that could be solved by Raman spectroscopy applications were defined per cancer type as reported by the studies selected in this review. Furthermore, the information on clinical needs from current (inter)national guidelines and clinical articles (PubMed) were included. For clinical articles the included the period from 1990 to 2017 was regarded. Moreover, opinion from pathologists and surgeons was obtained based on personal interviews.
During the interviews clinical needs for another types of cancer than those addressed in the included studies were identified and discussed.

Raman spectroscopy applications. All the eligible Raman application studies were included, regardless the cancer type addressed. The included studies were divided considering two major oncological applications of Raman spectroscopy: (A) biopsy guidance/early diagnosis and (B) surgery guidance.

Progress of the companies. To address the progress of the companies that are developing/ have developed commercial Raman spectroscopy oncological applications towards implementation in the clinics, we have contacted leading companies in Raman spectroscopy (Tokyo Instruments Inc., Princeton Instruments Inc., Verisante Inc., ODS Medical Inc., Endofotonics Pte. Ltd., RiverD International B.V., EmVision LLC, Invenio Imaging Inc., Artphotonics GmbH., Carl Zeiss GmbH., Kaiser Optical systems Inc., Lambda solutions Inc., Horiba Jobin-Yvon Inc., B&W Tek Inc., Snowy Range instruments Inc., Wasatch Photonics Inc., Witec GmbH., Avantes B.V., Photonetc Inc. and Renishaw Plc.) to collect information. A questionnaire was sent to the companies with the following questions: 1) "Are you actively developing or collaborating in the development of oncological Raman *in vivo* and/or *ex vivo* tools for the clinics?"; 2) "Can you indicate what is the application?"; 3) "Do you have any scientific publication or can you share with us more information about the subject?"; 4) "When do you think that it will be available in the market? What is the prognosis?", and 5) "About the translation to the clinics, what hurdles have you encountered?".

Technology readiness level (TRL) classification of the studies. In order to provide an overview of the current status of the technology towards clinical translation we classified all the included studies based on the Technology Readiness Level (TRL).

The TRL is an index used to measure the maturity and usability of an evolving technology.[62] There are 10 levels (TRL 0 to TRL 9): at TRL 0 there is just an idea, but the concept is not yet proven or not yet tested; TRL 1 is related to basic research, when the principles are observed and postulated, but not experimentally proven; TRL 2 is associated with technology development, when the concept and application have been formulated; TRL 3 consists of applied research/ proof of concept, when the first laboratory tests are completed; at TRL 4 a small scale prototype has been realized, which is still working in a laboratory environment; at TRL 5 the prototype has been tested in intended environment; at TRL 6 the prototype system has been tested in the intended environment close to the expected performance; at TRL 7 use of the system has been demonstrated in an operational environment at a pre-commercial scale; TRL 8 is characterized by the first version of a commercial system, when manufacturing issues are solved; finally, at TRL 9, the technology is available for end users.

We have grouped the TRL levels of the Raman applications into 4 main categories: (A) the proof of concept has been tested in the laboratory (TLR 0-3), (B) first hardware and software have been developed, including the algorithms for detection of (pre-)malignant lesions, and experiments have been performed close to the intended environment (TLR 4), (C) the developed hardware and software were tested with an independent dataset in the intended environment and preferably at different centers (TLR 5-7), and (D) the first of a kind commercial system(s) are/will be available soon for end users (TLR 8-9).

Results

Clinical need and Raman applications

Definition of the clinical need. Prior to the development of technological tools aiming to improve diagnosis and/or treatment of cancer, it is important to define the actual clinical needs, because various clinical problems have different needs and solutions.

Currently, two main oncological clinical needs, which could be fulfilled by Raman spectroscopy, have been identified: (A) diagnostic tools for biopsy guidance for early diagnosis of (pre-)malignant, and (B) tools for surgery guidance, which can be used for intra-operative assessment of resection margins to achieve adequate tumor resection.

In this section we review several clinical problems in the process of diagnosis and surgical treatment of cancer.

Raman spectroscopy has been explored for oncological applications in numerous studies, employing various types of measurement systems, and targeting various types of cancers. This section also provides a review of the use of Raman spectroscopy *ex vivo* and *in vivo* for early diagnosis, biopsy guidance and surgery guidance of different types of cancer.

Based on the search terms, 42 research papers on oncological applications of Raman spectroscopy were included. From those, 36 studies regarded early diagnosis and biopsy guidance applications and 6 studies regarded surgery guidance applications.

Breast Cancer

Clinical need: The second leading cause of cancer-related deaths in women worldwide is breast cancer with an incidence rate of more than 1,670,000 and a mortality rate of 522,000.[1] Presently, screening mammography is used to identify breast lesions. When suspicious lesions are found histopathological diagnosis is the next step, based on fine-needle aspiration cytology (FNAC) and/or histological biopsy [63]. High sensitivity for FNAC (82-99.7%) and for biopsy (90.1-93%) is reported.[64–68]

The treatment of choice for ductal carcinoma *in situ* (DCIS) and early stage invasive cancer is breast conserving surgery. The surgery aims to preserve as much healthy tissue as possible while achieving negative resection margins.[69] This procedure is performed in 58-70% of the patients.[70,71] As a standard of treatment, patients receive adjuvant radiotherapy after surgery. In the Netherlands, resection margins are considered adequate when 'no tumor touches ink'.[72] Concerning pure DCIS resection margins of 2 mm are considered adequate. It is proven that patients with more than focal tumor positive resection margins have higher risk of developing recurrent disease.[73,74] When final histopathology shows a more than focal positive margin (concerning pure DCIS) an additional resection is performed. Re-resection rates varying between 7%-73% have been reported by different institutes.[73] Therefore, an intra-operative guidance with an objective and rapid tool is needed to achieve high adequate resection rates.

Raman applications for early diagnosis/biopsy guidance**:** Saha *et al.* developed a Raman spectroscopic tool for detecting microcalcifications, as an adverse sign, in breast tissue. An *ex vivo* study was conducted and Raman spectra were acquired in fresh stereotactic breast needle biopsies from 33 patients using a portable compact clinical multi-fiber Raman spectroscopy probe system. This first study resulted in a positive predictive value of 97% for detecting microcalcifications, demonstrating potential of Raman spectroscopy as real-time feedback tool for radiologists and to reduce unnecessary biopsies.[75]

Raman applications for surgery guidance: Barman *et al.* looked at the utility of Raman spectroscopy as a guidance tool for mastectomy procedures. Spectra were acquired *ex vivo* on freshly excised specimen from a total of 33 patients. The Raman instrument was a portable clinical fiber probe system. A classification algorithm was developed to differentiate breast cancer from healthy tissue. The reported sensitivity was 62.5% with a specificity of 100%. The accuracy obtained for differentiation between normal, fibrocystic change, fibroadenoma, and breast cancer was 82.2%.[76]

Skin Cancer

Clinical Need: The clinical diagnosis of skin cancer is conventionally based on visual inspection of morphologic characteristics of the lesions, usually supported by a dermoscope. This manner of diagnosing cancer is subjective and largely depends on the experience of the clinician.

Keratinocytic cancers: Keratinocytic cancers, such as the basal cell carcinoma (BCC) and squamous cell carcinoma (SCC), are two of the most common cancers in fair-skinned populations.[77] Only in the United Stated of America, about 3 million people are diagnosed with keratinocytic cancers per year. Although keratinocytic cancers are associated with low mortality rates both, BCC and SCC, can destruct surrounding tissue, recur and/or metastasize.[78]

SCC can be locally aggressive, difficult to treat and it is associated with a 0.5% - 5% risk of metastasis. An effective management can be challenging in cases of patients with multiple lesions, or patients that in the past were diagnosed with keratinocytic cancers, demonstrating the need for early diagnosis.[79]

Standard type of treatment for keratinocytic cancers is complete removal of the lesion by (1) standard surgical excision or (2) Mohs micrographic surgery (MMS). In standard surgical excision, resection margins are examined by the pathologist after the procedure. In low risk BCC a tumor free resection margin of 3 mm is recommended, and in high risk BCC a margin of 5 mm is advised.[78,80]

In MMS, complete resection margins are examined by the specifically trained dermatologist and/or pathologist during the procedure, aiming to spare healthy tissue while removing completely the cancer cells. MMS leads to fewer recurrences; however, this procedure is labor-intensive and time consuming.[81]

Therefore, a tool that could quickly detect the cancer cells at the resection margins, could guide the excision towards an adequate surgical margin and accelerate the surgical procedure.[21,82]

Melanoma: Melanoma is the most commonly fatal form of skin cancer with a worldwide incidence of 232,130 and mortality rate as high as 55,488.[1] Melanoma is preferably diagnosed at an early stage because of its metastatic disease. The vertical depth of growth in a primary melanoma, the Breslow thickness, is significantly correlated with metastatic propensity and thus prognosis. Melanoma with < 1mm thickness can be treated surgically with a high cure rate without reducing life expectancy (5-year survival is approximately 97%).[83,84] Once the melanoma is diagnosed at an invasive stage, the survival rate decreases enormously to approximately 40% for melanomas with a Breslow thickness >4mm.[83,85] Patients with thick melanomas and signs of distant metastasis are submitted to surgery and/or immunotherapy, which places a high burden on the patient's quality of life. Moreover, the effect of current treatments on patient survival is very limited.

Even with the use of a dermoscope by an experienced clinician, the sensitivity in diagnosing melanoma is between only 68% and 96% and it is very much depending on the clinician's experience. [9,86,87] Despite the large number of excised benign pigmented lesions (false positive suspicious lesions), 30% of early stage melanomas is still missed at the first clinical presentation and thereby present a risk to progress to a metastatic stage.[88] Because of the severe consequences when a melanoma is missed, many suspicious pigmented skin lesions are surgically removed. The clinical positive predictive values are as low as 7% to 23% for melanoma diagnosis by dermatologists in a specialized pigmented lesion clinic [9,89]. Therefore, a rapid, objective, real-time tool for clinical diagnosis could reduce the number of unnecessary excisions and, at the same time, guarantee early detection of melanoma.

Raman applications for early diagnosis/biopsy guidance: Investigations of Raman spectroscopy for skin cancer focus primarily on (early) detection of skin cancer and discrimination of benign from malignant and pre-malignant skin tumors.[2,18,79,90–95]

In 2008, Raman experiments were performed *in vivo* by Zhao *et al.* on 289 patients using a single fiber Raman probe; Raman spectra were measured from 9 different types of lesions, including BCC and SCC. The authors report a sensitivity of 91% and a specificity of 75% in differentiating malignant lesions from benign lesions. Malignant melanoma could be distinguished from pigmented benign lesions with reported sensitivity of 97% and specificity of 78%.[96]

In the same year, Lieber *et al.* used a portable Raman system with handheld probe for non-melanoma skin cancer diagnosis.[97] Lieber *et al.* performed an *in vivo* study on 19 patients. Using the same handheld probe, Lieber *et al.* report classification of the BCC, SCC, inflamed scar tissues and normal tissues with sensitivity of 100% and specificity of 91%. The reported overall classification accuracy was 95%.[98]

In 2012, Lui *et al.* measured 518 *in vivo* skin lesions from 453 patients. Malignant and pre-malignant lesions could be separated from benign skin lesions using a single fiber Raman probe with a reported sensitivity of 90% and a specificity of 64%. Benign pigmented lesions could be distinguished from melanoma with reported sensitivity of 90% and specificity of 68%. Melanomas could be separated from seborrheic keratosis with a reported sensitivity of 90% and specificity of 68%.[90] The specificities were 15%, 17% and 25% for a sensitivity of 99%, when three distinct discrimination tasks were investigated: melanoma *vs* pigmented benign lesions, all cancers *vs* benign lesions and melanoma *vs* seborrheic keratosis, respectively.

In 2012, Silveira *et al* reported an *in vivo* study using a Raman fiber probe in which they demonstrated differentiation of BCC from normal skin with an accuracy of 85%.[99]

Lim *et al.* determined the diagnostic capability of a multimodal spectral diagnosis for *in vivo* non-invasive disease diagnosis of melanoma and non-melanoma skin cancers. Measurements were performed with a custom-built clinical system that combines three fiber optic-based optical spectroscopy modalities: diffuse optical spectroscopy, laser-induced fluorescence spectroscopy, and Raman spectroscopy. Raman, fluorescence and reflectance spectra were acquired from 137 lesions in 76 patients. From the measured set, the number of lesions considered for the study were 100 (12 melanomas, 19 BCC, 38 SCC, 14 actinic keratosis and 17 non-melanoma pigmented lesions). When combining the three modalities, they reported a sensitivity of 100% and specificity of 100% for classifying melanoma *vs* non-melanoma pigmented lesions. BCC and SCC *vs* actinic keratosis were classified with a sensitivity of 95% and specificity of 71% also when combining the three modalities.[100]

In 2015, using a multi-fiber Raman probe, Schleusener *et al.* performed *in vivo* measurements on 104 subjects with lesions clinically suspected of being skin cancer (36 melanomas, 39 BCC and 29 SCC). Additionally, 67 measurements on benign pigmented nevi from 33 subjects were also included. Sensitivity and specificity for discriminating histopathologically confirmed melanoma from lesions clinically suspected of being melanoma (not histopathologically confirmed) were 52% and 67%, respectively. For discriminating histopathologically confirmed BCC from lesions clinically suspected of being BCC (not histopathologically confirmed) the sensitivity was 54% and specificity was 48%. The results for discriminating histopathologically confirmed SCC from lesions clinically suspected of being SCC (not histopathologically confirmed) were sensitivity of 52% and specificity of 27%. Discriminating histopathologically confirmed malignant lesions from lesions clinically suspected of being skin cancer, but not histopathologically confirmed, was not successful.[93]

Zhao *et al.*, in 2015, performed an independent clinical test on a total of 645 lesions from 409 patients. The sensitivity and specificity for discriminating skin cancers and precancers (including melanoma, BCC, SCC, and actinic keratoses) from benign skin disorders were 99% and 24%, respectively. This study provided an independent confirmation of *in vivo* skin cancer diagnosis by Raman spectroscopy.[92]

Santos *et al.* measured 82 freshly excised melanocytic lesions suspected of melanoma.[89] The measurements were performed using an in-house built Raman micro spectrometer optimized for measurements on pigmented skin lesions.[101] All 24 melanomas were correctly identified with a specificity of 45%. The authors indicated that Raman spectroscopy might lead to a 3-fold reduction of the ratio of unnecessary skin excisions and that their results should encourage the use of Raman spectroscopy *in vivo* systems by general practitioners and non-experienced dermatologists to discriminate melanoma from suspicious lesions and reduce unnecessary skin excisions.[89]

In 2017, Bratchenko *et al.* tested a combination of Raman spectroscopy with auto-fluorescence for melanoma and BCC diagnosis. They performed *ex vivo* measurements on 39 melanomas, 40 BCC's and respective healthy skin within the excised samples. The authors show that the combination of Raman spectroscopy with auto-fluorescence has an accuracy of 97.3% in discriminating BCC's from melanoma, whereas the determined accuracy for each modality separately is 79%.[102]

<u>Raman applications for surgery guidance:</u> Kong *et al.* combined auto-fluorescence with Raman spectroscopy for intraoperative detection of BCC in skin. This approach was developed to reduce the measuring time of whole tissue sections during the Mohs surgery procedure. First, the auto-

fluorescence images, which were taken at excitation wavelengths of 377 nm and 292 nm (corresponding to collagen and tryptophan excitation) were segmented. In this way, the normal dermis, which is dominated by collagen, was discarded and only the suspicious segments were sampled by Raman spectroscopy. Based on this approach, Kong *et al.*, demonstrated that BCC could be automatically detected with a sensitivity of 95% and a specificity of 94%.[94]

Lung Cancer

Clinical need: Lung cancer is one of the leading causes of cancer-related deaths in the world, with an incidence of 1 824 701 and mortality rate of 1,589,925. Reasons for the high mortality rate are the fact that patients tend to be diagnosed at an advanced stage and a lack of effective treatments. Part of the diagnostic process is white light bronchoscopy (whether or not combined with auto-fluorescence) combined with tissue biopsy for definitive pathology. A problem with this technique is that it suffers from either low sensitivity or specificity [102] and it is mainly accessible for centrally located lesions. Morever, the representativeness and quality of the transbronchial and endobronchial biopsies is difficult to assess during the procedure.[104]

Cytologic evaluation also plays an important role in the initial evaluation and diagnosis of patients with lung cancer, especially in the evaluation of suspicious lymph nodes.[105] Sampling errors and numerous mimics are the main pitfalls of the technique.[105] An objective optical tool that could be adapted to bronchoscopy or incorporated in a biopsy needle would be beneficial for biopsy guidance and early diagnosis of lung cancer.

In early stage disease, surgical management is the treatment of choice. Several studies showed better 5-year survival rate for lobectomy (complete removal of the pulmonary lobe where the tumor is situated) than for sublobar resection, where less than an entire pulmonary lobe is removed.[106–108] The sublobar resection procedure has been adopted in a number of centers. This procedure has been used for diagnosis and is considered sufficient for early stage disease and for non-cancerous lesions. Technical limitations that preclude negative surgical margins are a more challenging issue for sublobar resection than conventional lobectomy.[108] Ideally, complete tumor resection with resection margins of ≥ 2 cm by sublobar resection would be favorable, maintaining lung volume and function[108] while reducing the risk of local recurrence. Intraoperative frozen section has traditionally been the sole modality for achieving negative resection margins. However, in some cases, frozen sections are not representative enough to predict the final pathology. Thus, the histopathological evaluation of the frozen section is difficult, especially between non-invasive stage of the disease and minimally invasive stage.[109] The difficulty to predict the predominant pattern based on frozen section has been reported to be due mostly to sampling errors.[110] Moreover, the intraoperative assessment of margins is challenging owing to an underestimation of the margin distance in lung tissue. If the tumor is peripheral, it is easier to guarantee a large resection margin. However, when the tumor is centrally located it is more challenging to assure that adequate resection margins are achieved. Improvement of intraoperative assessment of resection margins is essential to amend sublobar surgery and reduce the local recurrence rate.

Raman applications for early diagnosis/biopsy guidance: The first study that demonstrated the technical feasibility of measuring *in vivo* lung lesions using Raman spectroscopy was conducted in 2008 by Short *et al*.[111] A multi-fiber Raman probe was implemented to complement white light and auto-fluorescence bronchoscopy for *in vivo* detection of lung cancer. Preliminary research on 26 patients demonstrated that the combination of Raman spectroscopy with white light bronchoscopy and auto-fluorescence bronchoscopy can improve the diagnostic specificity of lung cancer (reducing the number of unnecessary biopsies). With these combined technologies, the sensitivity and specificity achieved were above 90% for detection of lung cancer and high-grade dysplasia lesions. The authors stated that the use of Raman spectroscopy has potential for substantially reducing the number of false-positive biopsies associated with white light bronchoscopy and auto-fluorescence bronchoscopy.[112]

Recently, the same group used the bronchoscopic Raman spectroscopy *in vivo* in 80 patients (280 samples), using signal acquisition times of 1s. The detection of high grade dysplasia and malignant lung lesions resulted in a reported sensitivity of 90% at a specificity of 65%.[113]

Esophageal Cancer

Clinical need: Esophageal cancer has an incidence rate of 455 784 and mortality rate of 400 169.[114] There are two main types of esophageal cancer: squamous cell carcinoma and adenocarcinoma. Diagnosis is established with endoscopic guided biopsy. Esophageal adenocarcinoma develops in sequential stages of change in the mucosa. Firstly, there is a change from a normal squamous epithelium to a columnar cell epithelium (i.e. intestinal metaplasia), known as "Barrett's esophagus". The "Barrett's esophagus" is considered a pre-malignant stage because it is associated with 100 times higher risk of developing esophageal cancer.[115] Endoscopic identification of this pre-cancerous stage may enable early, minimally invasive therapeutic intervention (i.e. endomucosal resection). The greater the number of biopsies taken from the border of the lesion (at least six), the higher the diagnostic accuracy.[116,117] However, the increase in the number of biopsies performed may cause an increased risk of complications, such as gastrointestinal bleeding. Furthermore, still 11.3% of upper gastrointestinal tract cancers are missed with this technique.[118] Therefore, an objective, real-time tool for biopsy guidance could reduce the number of unnecessary biopsies and improve the diagnostic accuracy.

Surgical resection is the treatment of choice in early staged esophageal cancer. The optimal extent of esophageal resections is still controversial, but completeness of surgical resection is an important determinant for a better outcome. There are recommendations for clearance of tumor from proximal and distal margins, but this may vary depending upon the type of tumor. [119,120] The presence of tumor at a distance ≤1 mm of the circumferential resection appears to be a significant cause of local tumor recurrence and decreased survival.[121,122] An intraoperative assessment of the resection margins of esophageal excisions is essential to reduce the local recurrence rate and increase the survival rate.

<u>Raman applications for early diagnosis/biopsy guidance:</u> Teh *et al.* studied 21 dysplastic gastric lesions and 44 normal samples from 44 patients using *in vivo* multi-fiber Raman probe system. A sensitivity of 95% and specificity of 91%, between dysplastic and healthy stomach tissue was found.[123]

Bergholt *et al.* measured 924 Raman spectra *in vivo* from normal tissue and 111 from benign ulcers from 71 patients with an endoscopic multi-fiber Raman probe system. Malignant ulcers were correctly classified with a sensitivity of 82.1% and a specificity of 95.3%.[124]

An endoscopic multi-fiber Raman probe system for *in vivo* and on-line diagnosis of gastric cancer was developed by the group of Huang.[125] Using this system, they obtained a total of 2748 *in vivo* gastric tissue spectra from 305 patients: 2465 diagnosed as normal and 283 as cancer. The reported diagnostic accuracy for gastric cancer was 85.6% (sensitivity of 80.5% and specificity of 86.2%). Gastric cancer detection algorithms were further applied on 10 patients undergoing gastroscopy (Figure 1). The authors report a predictive accuracy of 80.0% (sensitivity of 90.0% and specificity of 73.3%).[125]

In 2014, Bergholt *et al.* performed an *in vivo* study for diagnosis of gastric dysplasia in Barrett's esophagus. A total of 450 patients underwent endoscopy in the upper gastrointestinal tract, Raman measurements were performed, biopsies were taken and submitted for histopathological evaluation. High grade dysplasia in Barrett's esophagus, non-dysplastic Barrett's esophagus and normal columnar lined epithelium could be discriminated with a reported sensitivity of 87% and a specificity of 84.7%.[126]

Wang *et al.* demonstrated that, using the *in vivo* endoscopic multi-fiber Raman probe system and acquisition times of 0.1-0.5s esophageal squamous cell carcinoma can be detected with sensitivity of 97% and specificity of 97%, based on the results from 48 patients.[127]

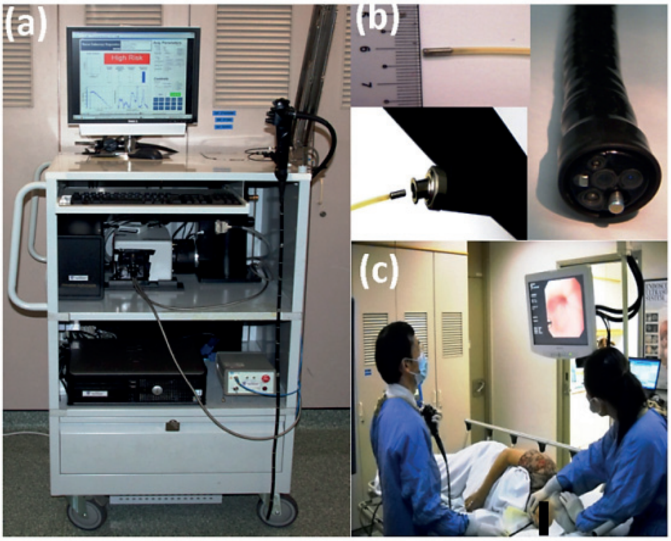

Figure 1. a) Photograph of Raman endoscopy system in clinic; **b)** insertion of the 1.8 mm Raman endoscopic probe into the working channel of an endoscope during gastroscopy; and **c)** routine Raman endoscopy procedure in clinic [123]. From Duraipandian *et al.* [123]. Reprinted with permission from SPIE.

Ishigaki *et al.* used a micro Raman probe system to examine *ex vivo* early-stage (stages 0 and I) esophageal cancer samples from 15 patients. They demonstrated a sensitivity of 81% and a specificity of 94% using leave-one-out cross validation.[128]

Using a Raman endoscopic multi-fiber probe during routine endoscopy examination, Lin *et al.* demonstrated *in vivo* that simultaneous use of the fingerprint and high-wavenumber part of the Raman spectrum can improve early diagnosis of gastric pre-cancers (sensitivity of 93% and specificity of 94%) in an independent dataset. A total of 48 patients were included. From this dataset, 80% of the spectra were used for training and 20% for testing. Using exclusively either the fingerprint or the high-wavenumber part, the area under the ROC curve was 0.972 and 0.928, respectively. When combining fingerprint and HWVN, the area under the ROC curve was 0.995.[129]

Head and Neck Cancer

Clinical need: Head and neck cancer includes cancer of the oral cavity, nasopharynx, oropharynx, hypopharynx, and the larynx. It has an incidence rate of 686 328 and a mortality rate of 375 665.[114] The most frequent type of cancer in head and neck region is the oral cavity squamous cell carcinoma (OCSCC). When a patient is suspected for a tumor in the head and neck region, all subsites will be examined with a flexible fiber optic endoscope. Examination under anesthesia is performed and biopsies are taken for tissue diagnosis.

Surgery is the mainstay of treatment, with adequate resection margins. Acceptable remaining function and physical appearance are the main goals. Inadequate resection margins influence negatively local control and prognosis.[130,131] In head and neck cancer, clear resection margins of >5mm are decisive for disease control and survival.[132,133] Achieving adequate resection margins is challenging. The lack of reliable intraoperative guidance and the proximity of tumors to vital structures are common causes of inadequate tumor resection. Recent studies show poor surgical success rates with inadequate tumor resection in oral cavity cancer surgery from 30% up to 85%.[23,33,134] Intraoperative assessment by means of frozen-section is the standard procedure. However, it can only be used for soft tissue and not for bone. Additionally, only a very small percentage of the resection margins can be investigated by this procedure and the selection of suspicious tissue depends on the surgeon's and/ or the pathologist's experience. These confounding factors also result in a high recurrence of oral cancer.[21,135] The two primary clinical needs are early diagnosis of OCSCC and intraoperative assessment of the complete resection margins, not only for soft tissue but also when bone is involved.

<u>Raman applications for early diagnosis/biopsy guidance:</u> In 2014, Krishna *et al*. created an *in vivo* multi-fiber Raman probe system and measured a total of 28 healthy volunteers and 171 patients with oral lesions. Spectra were annotated, based on histology or by clinical assessment, as oral squamous cell carcinoma (OSCC), oral submucosa fibrosis (OSMF), oral leukoplakia (OLK) and normal mucosa. Each group (OSCC, OSMF, OLK and normal) was correctly classified, when applying the developed diagnostic algorithm, in 89%, 85%, 82% and 85% of the cases, respectively.[136]

In 2015, Guze *et al.* conducted an *in vivo* pilot study with a Raman probe and measured oral diseases from 18 patients. Benign and malignant oral lesions were classified correctly with sensitivity of 100% and specificity of 77% using a multi-fiber Raman probe. Although, a larger study group was preferable, the results indicate that Raman spectroscopy is a promising diagnostic tool.[137]

<u>Raman applications for surgery guidance:</u> In 2015, the feasibility of identifying oral cancer tumor based on water concentration was demonstrated *ex vivo*, using high-wavenumber Raman spectra obtained from freshly excised resection specimens from oral cavity.[135]

Barroso *et al.* investigated how the water concentration changes across the border between tumor and the healthy surrounding tissue on *ex vivo* specimens from patients that underwent surgery for oral cavity squamous cell carcinoma. Measurements were performed on 20 patients using a confocal Raman microscope system. The results revealed consistent changes in the water concentration across the tumor border. Over distances of 4 to 6 mm across the tumor border, water concentrations changed from 76% ±8% in the tumor to 54%±24% in the healthy surrounding tissue.[138]

Brain cancer

Clinical need: The estimated incidence of brain cancer in the developed world is 7.1/100 000 with a high mortality of 5.3/100 000.[1] Neuroradiology is usually sufficient as the initial diagnostic modality for brain cancer. In some cases, stereotactic biopsy is needed to decide for primary resection versus chemo- radiation. For accurate histopathological diagnosis multiple tissue samples are obtained.[139] Brain biopsy may be complicated by sampling error and cerebral hemorrhage. [140,141] Therefore a rapid and objective tool is needed for optimal biopsy guidance to provide one representative brain tumor tissue sample, thus minimizing the risk of cerebral hemorrhage.

Treatment of choice for most primary brain cancer is surgery [17]. In low-grade gliomas the extent of tumor tissue resection is associated with improved patient outcome.[141–143] Three-dimensional stereotactic navigation, 5-ALA-fluorescence and intraoperative magnetic resonance imaging (MRI) are currently used to achieve optimal surgical results.[141,144] Unfortunately, distinguishing cancer from healthy tissue during surgery still is a challenge.[140,145] Generally, postoperative MRI demonstrates residual tumor in 69.6% of the cases.[145] The accuracy of navigation is influenced by the intent to preserve vital brain structures, inter-observer disagreement on the tumor transformation zone, and brain edema.[146] In the current practice, adoption of navigation techniques is limited owing to high costs and hampered by low evidence of survival benefit.[147] An optical, intra-operative tool to guide the surgeon towards tumor tissue in stereotactic biopsy and to identify adequate resections while preserving function brain structures with resection may improve patient outcome.

Raman applications for surgery guidance: Jermyn *et al.* in Montreal have developed a Raman system with a hand-held probe for intraoperative use during brain tumor resection. In an *in vivo* study, spectra were obtained from 17 patients with 0.2s acquisition time (Figure 2). Patients with grade 2 to 4 gliomas were included (66 normal spectra and 92 cancer spectra). They reported a sensitivity of 93% and a specificity of 91% in distinguishing normal brain tissue from dense cancer and normal brain invaded by cancer cells.[148]

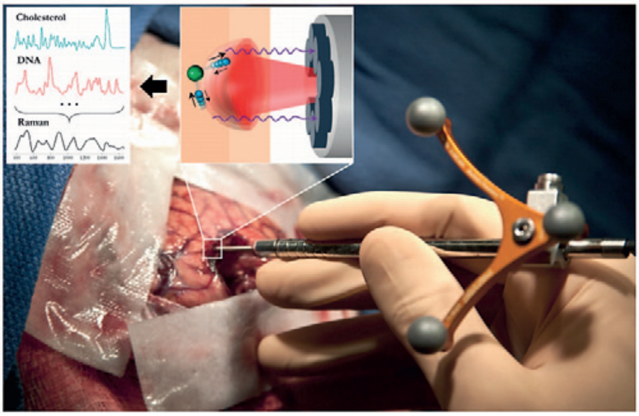

Figure 2. The handheld contact fiber-optic probe for Raman spectroscopy. The probe (Emvision, LLC) was used to interrogate brain tissue during surgery. A schematic diagram illustrated the excitation of different molecular species, such as cholesterol and DNA, to produce Raman spectra of cancer versus normal brain tissue [52]. From Jermyn *et al.*[52]. Reprinted with permission from the authors and AAAS.

Colorectal Cancer

Clinical need: Colorectal cancer (CRC) has an incidence rate of 1 360 602 and mortality rate of almost 700 000.[1] CRC is diagnosed after onset of symptoms or through screening by colonoscopy.[149] Screening detects early-stage malignancies or premalignant polyps (adenomas) and improves prognosis for the patient.[149] Colonoscopy miss rates are 2-6% for CRC and 20-26% for adenomas.[150,151] Additionally, many polyps with minimal malignant potential are removed without benefit to the patient.[149,152]

Despite its contribution to the effectiveness of colonoscopy, polypectomy is associated with increased risk of major complications (perforation, hemorrhage).[153] An objective biopsy guidance tool is therefore of clinical importance to reduce these limitations.

Surgery is the only curative modality for localized colon cancer. Proximal and distal resection margins should be at least 5 cm from the tumor.[154] Satisfyingly, positive margins in colon cancer resections are rare.[155] The most important indicator of outcome following resection of colon cancer is the tumor pathologic stage.[156]

Raman applications for early diagnosis/biopsy guidance: In 2008, Widjaja *et al.* measured 105 colon specimens *ex vivo* with an in-house built Raman probe [155]. From the 105 colon specimens 41 were normal, 18 were hyperplastic polyps and 46 were adenocarcinomas. In this study, the diagnostic accuracy was 98%.[157]

Short *et al.* conducted a study using Raman spectroscopy on *ex vivo* colon tissue from 18 patients, measuring both the fingerprint and high-wavenumber spectral regions. The results indicated that, using the high-wavenumber region, the non-malignant and the malignant groups could be classified correctly with a specificity of 89%. The authors referred that high-wavenumber region could be used *in vivo* to improve the identification of neoplastic lesions.[158]

Bergholt *et al.* tested the same approach *in vivo* (combined fingerprint and high-wavenumber spectral regions) on adenomatous polyps measured from 50 patients using an endoscopic multi-fiber Raman probe. Adenomatous polyps were separated from hyperplastic polyps with a sensitivity of 91% and specificity of 83%. The authors demonstrated that the analysis based on the combination of fingerprint and high-wavenumber spectral regions is superior to considering either region alone.[12]

Cervical cancer

Clinical need: Cervical cancer has a worldwide yearly incidence of 528 000 women and mortality of 266 000.[1] In recent years incidence and mortality rates have decreased because of the emergence of screening.[159] The primary method of screening is by cervical cytology with the Papanicolaou test (PAP). This has a high specificity (95–98%) but a low sensitivity (<50%).[160] This sensitivity of screening is increased by testing for Human Papilloma Virus (HPV) in the cervical swab.[161] Final diagnosis of cervical cancer is based on histopathology. For this colposcopy guided biopsy is recommended, with a sensitivity of 92% and specificity of 67%.[73] In low resource settings visual inspection of the cervix with biopsies is used with a specificity and sensitivity of 88-92% and 10-84%.[162,163] Treatment of cervical cancer is based on stage. Small tumors will be treated by surgery, and higher stages with chemotherapy. It is not to be expected that Raman spectroscopy has any value in the diagnostic or treatment of cervical cancer since the diagnostic accuracy of colposcopy guided biopsies will not be improved and precision treatment is not applicable for cervical cancer.

Raman applications for early diagnosis/biopsy guidance: Mo *et al*. measured Raman spectra from 46 patients *in vivo* with high-wavenumber Raman spectroscopy, to investigate cervical pre-cancer diagnosis. The Raman instrument used a ball-lens fiber-optic Raman probe. Cervical dysplasia could be distinguished from normal tissue with a reported sensitivity of 94% and specificity of 98%.[164]

Kanter *et al.* performed a clinical study on a total of 43 patients that underwent colposcopy-guided biopsy to investigate dysplasia. Using a portable Raman system with a fiber-optic probe, spectra were acquired of low grade squamous intraepithelial lesions, high grade squamous intraepithelial

lesions, metaplastic lesions and normal tissue. The classification accuracy for discriminating diseased from normal tissue was 88%, the sensitivity was 86% and the specificity was 97%.[165] The same group reported, in 2011, a sensitivity of 70% and a specificity of 83% for cervical pre-cancer diagnosis. In this study a total of 29 patients were included. Measurement were done *in vivo* using fiber-optic Raman probe with a ball-lens.[166] To improve diagnostic accuracy, Duraipandian *et al.* combined high-wavenumber and fingerprint Raman spectroscopy for cervical and pre-neoplasia detection. The obtained sensitivity and specificity were 85% and 81.7%, respectively.[167]
Rubina *et al.* performed *ex vivo* Raman measurements on 49 abnormal cervical specimens and 45 negative control cytology samples using a fiber-optic Raman microprobe system. Abnormal lesions were classified correctly in 84.5% of the cases. The authors suggested that presence of blood in abnormal specimens was a major cause of discrimination.[168,169]

Vulvar cancer

Clinical need: Vulvar cancer has an incidence of 1,300 women and mortality of 450 women per year.[170] This malignancy has a high curability in early-stage disease, but a poor prognosis for advanced-stage disease and recurrent disease. Diagnosis is based on histopathology of a biopsy of the vulva at the peripheral edge of the lesion,[171] whereby underlying stroma is included and possible necrotic tissue avoided.[172] *In vivo* diagnosis and biopsy guidance can be of great value for accurate diagnosis. Surgery is the main choice of treatment. In recent years surgical management has changed, were large radical and disfiguring resections make place for conservative surgery.[172] Resection margins of ≥8 mm are considered clear margins. Resection margins less than 8 mm result in local recurrence rates of 23-50%.[173,174] Surgical management of vulvar carcinoma aims to achieve a fine balance between adequate resection margins and preservation of sexual and urinary function.[172,175] An intra-operative tool for surgery guidance is therefore needed.

Raman applications for early diagnosis/biopsy guidance: During the literature search we have noticed that Raman applications have not been greatly developed for vulvar cancer. The most recent study, was developed by Frost *et al*.[176] They have evaluated the diagnostic performance of Raman Spectroscopy for differentiating a pre-malignant vulvar lesion (*lichen sclerosus*, LS) from other inflammatory vulvar conditions in fresh vulvar biopsies from 27 women. Biopsies resulted in circular discs o skin 3-4 mm in diameter (full thickness of the epidermis with underlying dermal tissue). Spectra were measured with a Raman micro-spectrometer (modified Renishaw system 1000 dispersion), which was coupled to a diode laser of 830 nm excitation wavelength and had a spot size of 15x17 µm. A classification model was created using principal components and multivariate linear discriminant analysis. Leave one sample out cross validation was used to validate the model. The model was able to correctly differentiate LS from other inflammatory vulvar conditions with a sensitivity of 91% and specificity of 80%. The authors suggested that the study demonstrates that Raman spectroscopy has potential for *in vivo* non-invasive diagnosis of vulvar skin conditions and when applied in the clinical setting may reduce the need for invasive tissue biopsy.[177]

Bladder Cancer

Clinical need: The global incidence rate for bladder cancer is 430 000 and mortality is 165 000.[1] The standard for diagnosis is cystoscopy, with biopsies of suspicious lesions, and transurethral resection (TUR) to confirm the diagnosis.[178] Unfortunately, small papillary bladder tumors and flat urothelial tumors can easily be overlooked.[179] This contributes to increased residual rates and a recurrence rate of 50% within 18 months. TUR is (also) the standard of treatment for small (Ta) bladder tumors. Incomplete resection results in a second operation and/or increased recurrence rate, resulting in poor long-term prognosis.[180–183] Thereby, high risk tumors grow fast with a mortality rate of 50%, despite treatment. Also, bladder cancers have the tendency to recur frequently, leading to re-operations, loss of function and worse patient outcome. Urinary markers are emerging but not able to outperform cystoscopy. These findings suggest that *in vivo* biopsy, biopsy guidance and surgery guidance is needed for early detection, accurate diagnosis and adequate resections, to improve patient outcome.

Raman applications for early diagnosis/biopsy guidance: The first *in vivo* Raman probe that was used in bladder was an Emvision® probe with a filtered six-around-one fiber configuration. The excitation wavelength was 785 nm. The probe used had a large measurement volume (~1 cm^3) and did not have any lenses. As a result, the probe collected Raman spectra not only from the upper urothelium surface of the bladder (where transitional cell carcinoma has its origin) but also from deeper layers. During the procedure of transurethral resection of bladder tumors (TURBT), spectra were collected from suspicious and non-suspicious locations (collection times of 1 to 5 s). Bladder cancer could be distinguished from normal bladder with a reported sensitivity of 85% and a specificity of 79%. Even though the results show the possibility of discerning normal from malignant bladder tissue using Raman spectroscopy, the authors suggest that using a Raman probe that collects shallower signal from the urothelium surface of the bladder would be ideal for early diagnosis. Also, the combination of auto-fluorescence with Raman spectroscopy could potentially improve the diagnostic capability, by using the sensitive auto-fluorescence modality to indicate suspicious regions for “optical biopsy” by the highly specific Raman spectroscopy modality.[184,185]

In 2012, a confocal Raman probe was designed by Barman *et al.* and it was used *ex vivo* for bladder cancer diagnosis in 14 patients. The confocal probe had depth of field of approximately 280 µm. The result of the confocal system had a significantly higher specificity with respect to large-volume Raman spectral data, with a sensitivity that was comparable to the large-volume Raman system.[60,177]

Prostate cancer

Clinical need: Prostate cancer is among the most common cancers in men worldwide, with an incidence of 1 094 916 and mortality rate of 307 481.[1] The diagnosis of prostate cancer is often made through transrectal ultrasound guided prostatic biopsy.[186] Ten to twelve core biopsies are recommended, with > 12 biopsies not being significantly more conclusive.[187,188] While the majority of prostate cancer patients is treated by radical prostatectomy or radiation therapy, an increasing number of men is actively surveyed for their disease without immediate treatment. In a significant number of men, radical prostatectomy is complicated by urinary and/ or erectile dysfunctions, which is related to eradication of the neurovascular bundles (NVB) localized in the dorsolateral peri-prostatic fat tissue. Operative removal of the prostate leaving the NBV intact can reduce post-operative complications. Decision-making on nerve-sparing surgery can be optimized by intra-operative assessment of the prostatic surgical margins. In practice, the urologist can only remove the prostate initially leaving the NVB *in situ*. In case intra-operative assessment of the prostatic surgical margin is negative, the NVB will remain intact; in case, the margin is positive the urologist can remove the NVB at a second term. Although intra-operative frozen-section assessment is able to increase nerve-sparing surgery from 81% to 97%, it is labor-intensive requiring an optimized work-flow for the fast throughput of a large number of frozen sections [189]. Intra-operative assessment of surgical margins using Raman spectroscopy might be a good alternative for extensive pathologic frozen sections and could be implemented at large scale in operation theatres or departments of pathology.

Raman spectroscopy applications: Spontaneous Raman spectroscopy has not been explored yet *in vivo* and/or *ex vivo* using human prostate cancer material. Raman-based studies were developed in the last years *in vitro*, using cell cultures and, more recently, *ex vivo* using peripheral nerves of rats.[177,190,191]

Instrumentation

When developing instrumentation for *in vivo* and *ex vivo* applications, the main technical problems are: speed of measurement, adaptation in clinical workflow, interference of background from tissue auto-fluorescence and high instrumentation costs.

In the last years we consider that the major technological advances in Raman spectroscopic systems for clinical applications have been in: (1) detector technology, (2) fiber-optic probe design, (3) combination with other techniques, and (4) new laser opportunities for low-cost systems.

(1) InGaAs detectors for short-wave infrared Raman spectroscopy

Until now the detection of Raman signals in the short-wave infrared (SWIR) region (>1100 nm) was constrained by limitations of the state-of-the-art detector technology for visible to NIR excitation (CCDs). An alternative in this spectral range is the Indium-Gallium-Arsenide (InGaAs) detector, which enables detection at wavelengths well above 1100 nm. Several companies have recently moved towards the SWIR range, and have introduced InGaAs-based Raman devices (*e.g.* Andor™, Anton Paar™, Horiba™, B&W Tek™). Xenics™ introduced an InGaAs camera that has a read-out noise at comparable levels as a CCD detector, and that consequently can achieve shot-noise limited Raman spectra in clinically acceptable integration times.[101] This development in detector technology enabled the use of longer excitation wavelengths for clinical applications on tissues with would otherwise suffer from strong laser-induced fluorescence of fluorophore-containing tissues. Santos *et al.* could measure melanocytic skin lesions without overwhelming tissue auto-fluorescence interference using a SWIR Raman system, with NIR 967 nm laser and an extreme low-noise InGaAs detector (Figure 3).[89]

Also Patil *et al*. and Pence *et al*. have reported dispersive Raman spectroscopy of tissues with strong auto-fluorescence (liver and kidney human tissues) using 1064 nm excitation in combination with an InGaAs detector array.[192,193] Laser-induced tissue fluorescence was significantly reduced compared to excitation with lasers in the visible wavelength range.

(2) Fiber-optic probes

Fiber probes for early diagnosis: Fiber-optic probes have enabled the use of Raman spectroscopy for *in vivo* clinical applications. The integration of Raman spectroscopy with other diagnostic techniques has been a major step in the development towards improved efficiency in biopsy guidance and early cancer diagnosis. Fiber probes that could be inserted into endoscopic

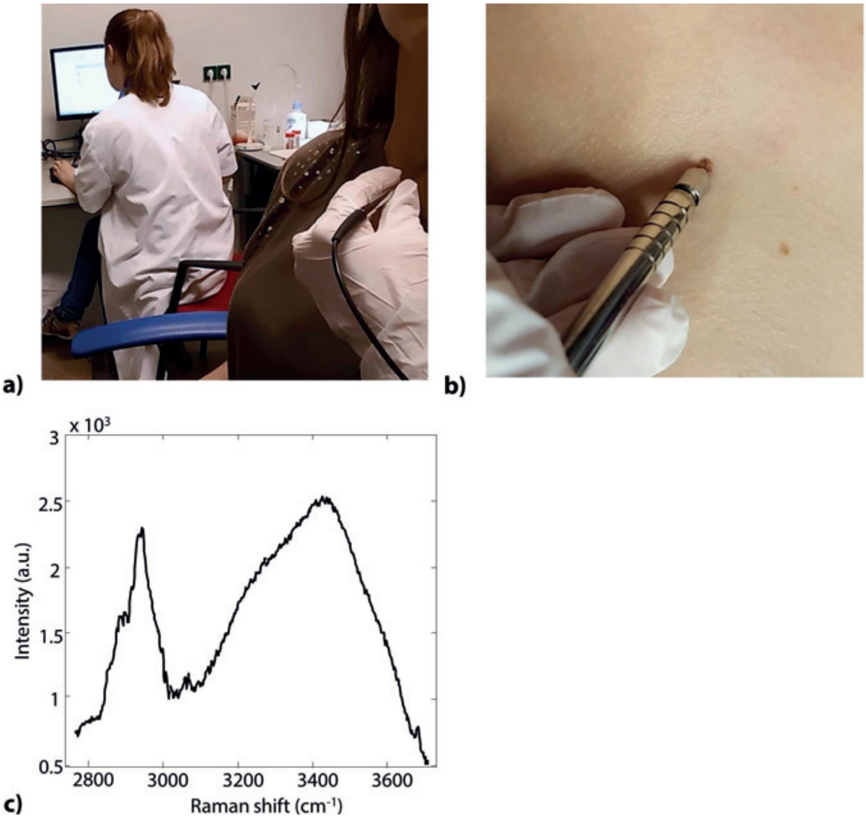

Figure 3. Implementation of SWIR Raman system in the dermatology outpatient clinic of Leiden University Medical Center for *in vivo* measurements. **a)** Photograph of a pigmented skin lesion. **b)** This was measured using a 976 nm laser excitation, the SWIR Raman instrument and a single fiber probe. The corresponding Raman spectrum measured *in vivo* is shown in **c)**. Exposure time: 30.

channels enabled *in vivo* measurements in hollow organs or surface assessment of solid organs: oral cavity,[136,137] lung,[111,113] upper gastroinstestinal tract,[123–127,129] colorectal,[12,158] bladder,[185] and cervical cancers.[164–167,194] Also, handheld fiber-based systems have been used for *in vivo* assessment of skin cancer,[88,90,91,94–96] and of brain cancers.[148,195]

In the last years numerous Raman probe designs have been developed, optimized and tested for clinical purposes. There has been an increased effort to tailor Raman probes to clinical needs and constraints defined by the specific clinical targets, specific pathophysiology of diseases, and specific anatomies of the region of interest (*e.g.* accessibility of the tissue, sample size, sampling depth).

Stevens *et al.* and Wang *et al.* have reviewed Raman fiber-optic probe designs and construction concerns, considering different oncological applications and respective clinical needs.[18,196]

Depth-selective fiber-optic Raman probes have been investigated for use in epithelial tissue associated with dysplasia.[197] Wang *et al.* developed a confocal fiber-optic Raman probe coupled with a ball lens to enhance *in vivo* Raman measurements from gastric pre-malignant epithelial tissue during endoscopy.[197,198] With a beveled fiber-optic probe coupled with a ball lens, the authors could limit their collection depth to 300 µm. Since gastric dysplasia initially evolves in the epithelial tissue layer (~300 µm), it is especially relevant for selective interrogation of the gastric epithelium.

Further work from the same group, featured a fully automated real-time Raman spectral diagnostics framework integrated with a multimodal image-guided Raman technique that enabled real-time *in vivo* cancer detection at routine endoscopy procedure, as shown in Figure 1.[199] The same fingerprint/high-wavenumber fiber-optic Raman endoscopic system was developed further by Bergholt *et al.* for routine clinical colonoscopy diagnosis, making use of a foot pedal control switch and an auditory feedback to the gastroenterologist.[199]

Using a similar probe in a hand-held confocal design, Duraipandian *et al.* measured *in vivo* fingerprint and HWVN Raman spectra during colposcopy.[167]

Agenant *et al.* used a novel clinical Raman probe for sampling superficial tissue to improve *in vivo* diagnosis of (superficial) urothelial carcinoma. This probe had a measurement depth of 0-200µm, which corresponds to the average urothelium depth. The probe is comprehended by 7 collection fibers, 1 excitation fiber and two component front lens.[200]

Fiber-optic probes for guided surgery

In the field of brain cancer, Jermyn *et al.* preformed *in vivo* Raman measurements during human brain cancer surgery for real-time identification of invasive cancer, using a handheld contact Raman spectroscopy probe.[52,195] Each measurement covered a 0.5mm diameter tissue area with a depth sampling up to ~1 mm in 0.2s. During the tumor resection, Raman signals were measured in the surgical cavity. The probe is comprehended by filters that were placed directly at the tip of the optical fibers. The spectra acquired with the handheld Raman probe (Figure 2) do indicate that there are still some challenges in developing probes and methods for correcting for spectral distortions mainly caused by the filter characteristics of the probes and subtraction of fluorescence signal backgrounds.[201]

A Raman system comprehended by a single fiber needle probe is currently being tested *ex vivo* by Head and neck surgeons and pathologists from Erasmus University Medical Center Rotterdam, The

Netherlands. This probe aims intraoperative inspection of the entire resection margin of specimens from patients that underwent surgery for oral cavity SCC (Figure 4).

(3) Combined Raman systems for guided surgery

In the field of dermatology, Kong *et al.* developed a scanning device that combines auto-fluorescence imaging and Raman spectroscopy to guide Mohs micrographic surgery (MMS) in the excision/treatment of high-risk skin basal cell carcinoma.[94] Although MMS provides the highest cure rates, it is a time-consuming technique (1 - 3 hours) needing highly trained personnel.

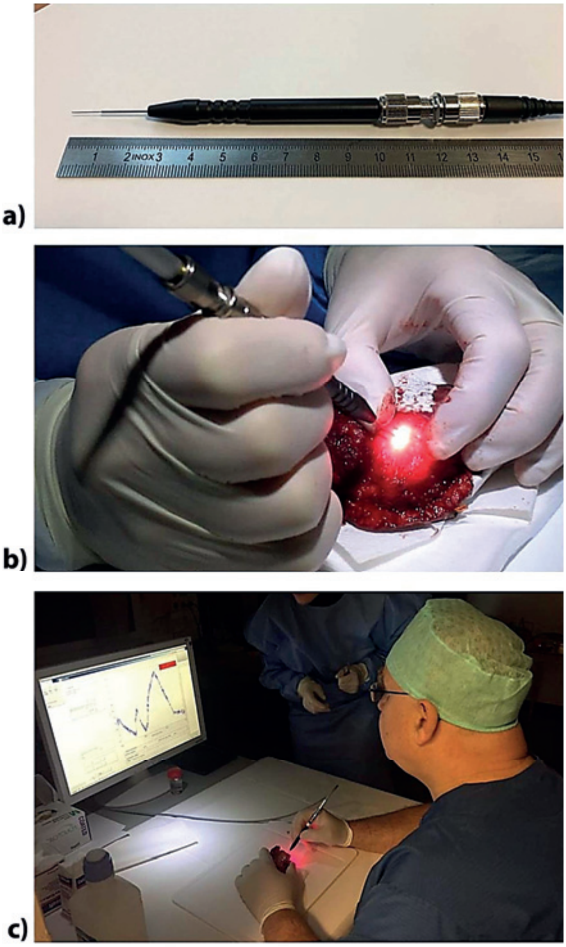

Figure 4. Single fiber needle probe for intraoperative assessment of the oral cavity SCC resection margins, developed by Artphotonics GmbH in collaboration with RiverD International B. V. and Erasmus University Medical Center, Rotterdam. a) Close up of the single fiber needle probe. b-c) Testing the single fiber needle probe for inspection of the freshly excised oral cavity specimens.

With the purpose of reducing the duration of scanning large areas of tissue, tissue auto-fluorescence imaging is used to determine the main spatial histological features of the sample, and this information is used to select and prioritize the sampling points for Raman spectroscopy (Figure 5).[94,202]

(4) New lasers

Recent developments in vertical-external-cavity surface-emitting laser (VECSEL) technology have brought their characteristics in the realm of Raman spectroscopy, with special interest for low-cost hand-held devices.[203] VECSELs are semiconductor lasers based on a vertical-cavity surface-emitting (VCSEL) geometry.

These types of lasers achieve a combination of high continuous-wave (CW) output power, due to a large gain area, and a low- divergence near-diffraction-limited beam, due to the transverse mode control of the extended cavity. The advantages of VECSELs over edge-emitting semiconductor lasers are circular output beam, easy array fabrication, small size, and low cost at mass production.[56,203–205]

Transferability

The Raman applications described above demonstrate potential of Raman spectroscopy to affect

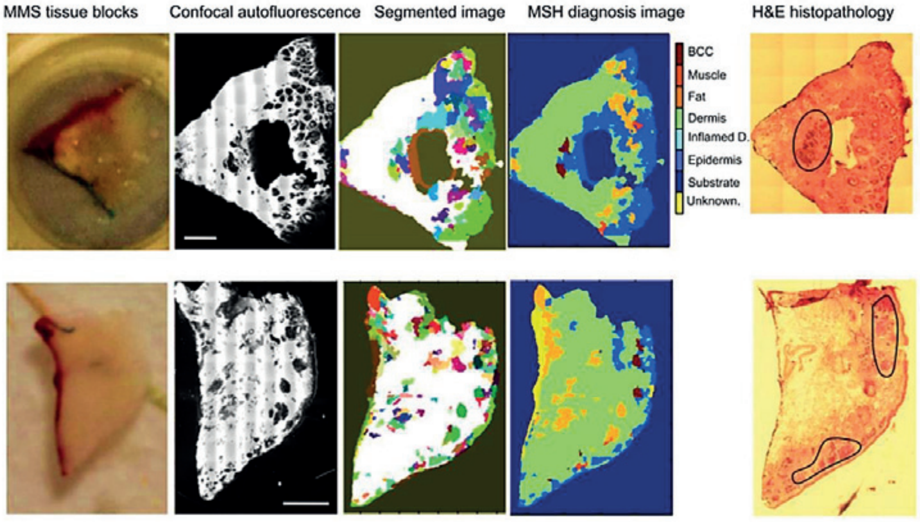

Figure 5. Multimodal spectral histopathological diagnosis of BCC in unsectioned tissue blocks as received from surgery. H&E histopathology images for adjacent sections are included for comparison (Scale bars: 2 mm).[94] Reprinted with permission from the authors and PNAS.

patient care. The major requirements for translation of a Raman equipment into clinical practice are: (1) well defined clinical need, (2) patient benefit proven and/or cost benefit, (3) equipment changes clinical practice, (4) demonstrated safety, reproducibility, robustness, and reliability (*e.g.* large clinical trials) and (5) regulatory approval.

First, it is important to verify beforehand that the developed Raman application addresses an actual clinical need and that the application can provide results of clinical relevance. This does not mean that the Raman instrument needs to give perfect results, as long as it can bring about measurable and cost effective improvements in patient care. Moreover, it is required that the instrument is introduced in the clinical workflow and is used/tested by clinicians.

Second, it is essential to demonstrate the safety, reproducibility, robustness, and reliability of the developed application in large clinical trials, to the end-users. And finally, receive approval from regulatory agencies.

Many of these aspects are now increasingly being addressed, which is a good sign of progress in the field towards clinical translation. However, for this translation continued effort is needed by searching for close collaboration and input from the medical community.

Additionally, to gain the confidence of clinicians to the potential value of Raman-based applications, it is essential to expose the results of Raman technologies over or in line with existing medical devices.[2,206] This should be done in large cohorts' studies based on patient outcomes and in direct comparison with the current gold standards.

Multidisciplinary networks are now being developed, such as the International Society for Clinical Spectroscopy (ClirSpec), European Photonics Industry Consortium (EPIC) and Raman4Clinics, which target especially these translational aspects. ClirSpec is a society, comprehended by spectroscopists and clinicians, that facilitates and promotes the translation of spectroscopy into the clinical environment, for the general benefit of patients (clirspec.org). Raman4Clinics is a platform for scientific communication, exchange, collaboration and for new research activities, combining the partners' expertise in technology, component, system and methodology development and medical application (www.raman4clinics.eu). EPIC is a network that promotes awareness of opportunities for the European photonic industry in healthcare (www.epic-assoc.com).

To provide an overview of the current status of the technology towards clinical translation, we classified all reviewed R&D results, based on the TRL. Figure 6 (2008-2017) shows the result from the technology readiness classification of the different Raman studies mentioned in the Raman applications section. From this figure, it is immediately clear that the majority of the developed applications appears to get stuck in category B (TRL 4).

These studies presented results of algorithms for (pre-)malignant tissue detection with data either collected *in vivo* or *ex vivo* with prototype Raman systems. However, validation of algorithms with an independent large dataset has not been proven yet. Some of the systems used in the analyzed studies are already further towards actual clinical use, and were classified as C, such as Zhao *et al*., Wang *et al*., Kong *et al*., and Duraipandian *et al*.[92,94,125,127]

Development of commercial instruments for oncological applications

We realized that most of the studies do not report a fully commercial product (ready to be used in the clinic). We therefore contacted the companies that are collaborating directly with the research groups presented in the Raman applications section. We also investigated the progress/potential interest of the companies which are developing or have developed commercial Raman spectroscopic systems for oncological applications.

We received information from the following leading companies in Raman spectroscopy: Avantes B.V., B&W Tek, EmVision LLC, Invenio B.V., Horiba Jobin-Yvon Inc. (HORIBA Scientific), ODS Medical Inc., Renishaw, RiverD International B.V., Verisante Technology Inc., and WITec B.V.. Based on the information received we have created a future perspective of clinical translation, which is presented in Figure 6 (2017-2021).

Progress reported by companies: B&W Tek has developed a Raman spectroscopic system, for the identification and qualification of cytostatics (*in-vitro*). B&W Tek is a company that provides instruments looking for R&D partners.

Invenio Imaging Inc. is developing a stimulated Raman scattering microscope for histological examination of fresh tissue. The most recent publication was in Nature Biomedical Engineering, early 2017.[207] The perspective of the company is to have the equipment ready to be commercialized later this year.

EmVision LLC does not manufacture or develop clinical systems, but the company is active in selling components, such as fiber-optic probes, to companies that are pursuing clinical systems.

HORIBA Scientific is an active member of Raman4Clinics European project and provides research and analytical Raman instruments for all kind of applications, including oncology.

ODS Medical Inc. is developing an *in vivo* Raman tool for surgical brain tumor resection.[148,208–211] The company predicts that the system will be commercialized within approximately 3 years (in 2020) following approval by regulatory bodies, including FDA.

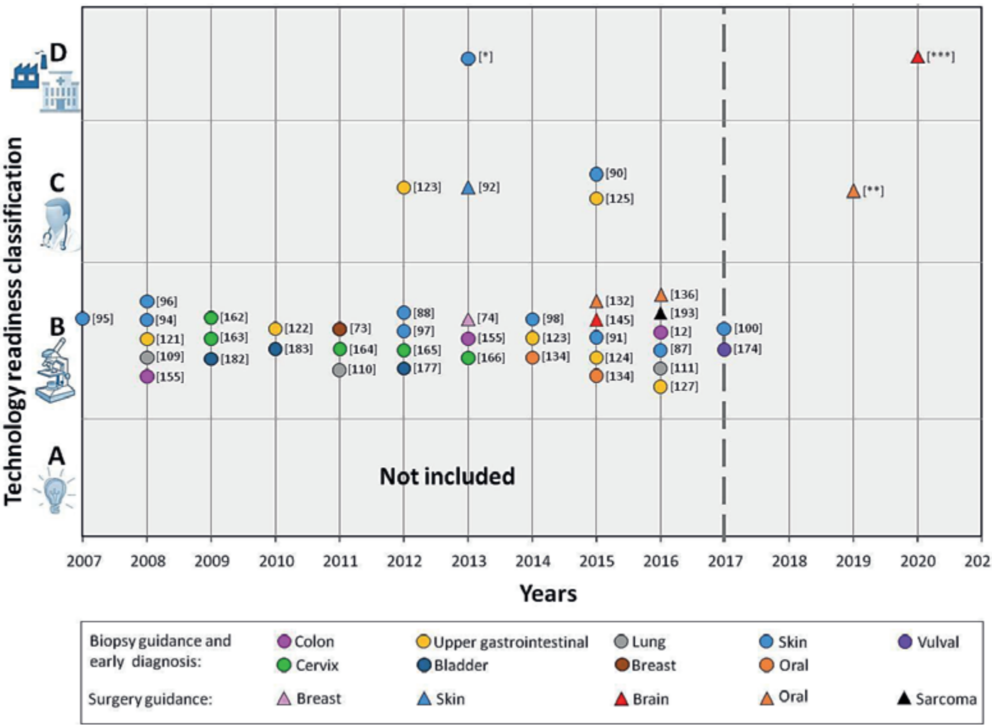

Figure 6. Illustration of the result from the technology readiness classification of the different Raman studies, mentioned in the Raman applications section. Verisante Technology Inc. is commercializing a device (Verisante Aura) for skin cancer detection [*]. In the graph is also plotted the prognosis (2017-2021) of further development/commercialization given by the companies RiverD International B.V. [**] and ODS Medical Inc. [***].

Renishaw has been actively developing a Raman system for *ex vivo* analysis of tissue cells and bio fluids for clinical use. The company is upgrading fiber-optic probe designs for clinical use during oncological surgery. This company has an *ex vivo* Raman spectroscopy platform (InVia series, Renishaw, Gloucestershire, U.K.) for a number of life-science and clinical applications including tissue pathology, neurobiology, stem cell research. Renishaw is currently developing a fast tissue imaging platform, which is based on the RA802 Pharmaceutical Analyser, for measuring uneven tissue surfaces with a minimum of sample preparation.[212–214] The new fast tissue imaging platform should be available in the summer of 2017.

RiverD International B.V. collaborates with the University of Nottingham in the development of an auto-fluorescence/Raman system for Mohs' micrographic surgery of basal cell carcinoma. Two prototype systems are currently being tested at the University of Nottingham, in UK, and at Erasmus University Medical Center Rotterdam, in the Netherlands. The systems are based on the concept described by the Nottingham group.[94] RiverD International B.V. is developing a Raman tool for surgical guidance of Head and neck tumor resection, which they predict to be ready for clinical trials in 2019. Currently, an *ex vivo* fiber-optic probe system is being developed for intraoperative inspection of resection margins of excised tissue. The company is also collaborating in an R&D project that aims to the development of a Raman spectroscopic device for use by dermatologists and general practitioners for objective assessment of pigmented skin lesions clinically suspected of melanoma.[89,101]

Verisante Technology Inc. is developing *in vivo* Raman technology for clinical oncology applications focused on: (1) *in vivo* non-invasive detection of skin cancers including melanoma and non-melanoma skin cancers; (2) endoscopy detection of cancers of internal organs such as lung cancers and gastro-intestinal cancers.[88,111,113,215–217] Currently, Verisante Technology Inc. is commercializing a skin cancer detection device (Verisante Aura, Figure 7) in Canada, Europe and Australia. Aura systems are being in use in several clinics in Canada. In figure 6, Verisante Aura is identified by [*].

WITec B.V. develops and commercializes confocal Raman microscope systems. The company is not actively involved in development of applications in the clinical oncology field. However, various users of the confocal Raman microscopes have applied their instruments in oncology-relevant research.[218–221]

Hurdles in translation reported by companies: Some of the companies have indicated what hurdles they have encountered when translating Raman systems into the clinics. One important issue can be assuring that high-quality data can be acquired consistently and robustly under intraoperative conditions, with minimal disruption of the surgical workflow.[210] It is also important to ensure that real-time high-accuracy tissue classification is provided to surgeons in an intuitive way and by simple metrics (user-friendliness).

Figure 7. Verisante Aura system for skin detection. Courtesy of Verisante Technology, Inc.

Another referred problem is to find funding/investors that can help to bring the product into the market. The fact that Raman spectroscopy is still a relatively unknown technique for most clinicians, was yet another hurdle mentioned. This can be partially explained by the fact that from all the scientific studies reviewed in this article only approximately 30% were published in medical oriented journals. Another explanation for Raman spectroscopy to be relatively unknown might be also partly due to this technique not being widely incorporated in the curriculum of clinicians or clinical researchers. To resolve this, more effort should be done towards publication of clinical Raman studies in medical oriented journals. Additionally, current academic leaders in the medical field, who have knowledge of clinical spectroscopy, should encourage the introduction of this subject in medical school curriculums alongside other medical imaging and diagnostic topics.

Discussion

In the last decade a strong effort has been made towards clinical implementation of Raman spectroscopy as an adjunct technique for early diagnosis, biopsy guidance and oncologic surgery guidance. The most recent studies aim to: (1) detect pre-malignant lesions,[113,125,126,136,164,222] which is one of the most effective ways to reduce the number of cancer cases, (2) detect cancer in less-invasive stages,[101,113,125,157,157] (3) reduce the number of unnecessary biopsies,[91,96,112,113] and (4) guide surgery towards complete removal of the tumor with adequate tumor resection margins, which reduces the need for post-operative treatment, decreases the aggressiveness of the post-operative treatment and increases patient survival [76,94,138,148,206].This means that Raman spectroscopy is used to detect (pre-)malignant lesions for guidance of clinical procedures. A next step would be to use Raman spectroscopy in diagnosis of (pre-)malignant lesions; *i.e.* differentiating between different types of cancer and grading (pre-)malignant lesions (*e.g.* differentiating high-grade from low-grade dysplasia).[12,111,126,127,136]

Raman spectroscopy may address all the clinical needs mentioned, because, in fact, all show the same fundamental problem: lack of pre- and intraoperative methods with sufficient or clinically relevant sensitivity and specificity. Raman spectroscopy is an objective technique that can add biochemical information, can be performed *in vivo* and can be used in real-time. Raman spectroscopy may, not only, address the need for rapid and objective intraoperative margin assessment, which is essential for surgical oncology. Raman spectroscopy could also help pathologists and surgeons to assure adequate resection margins intraoperatively.[2,20,21,82,148] Consequently, the use of this technique may help to improve the surgical outcome of the patients and to decrease the need for adjuvant therapy.

Additionally, Raman spectroscopy can also give an objective and reliable decision about malignancy and early malignant stages.[2,20,21,82,223] This technique could help medical professionals in assessing with a clinically relevant specificity and sensitivity the location for most representative biopsies.[2,21,223]

Many of the *in vivo* and *ex vivo* trials that aim for detection of malignant tissue have achieved sensitivities varying between 77% and 100% and specificities varying between 45% and 100%.

Studies that aimed for detection of pre-malignant lesions presented generally lower specificities (ranging between 63% and 97.8%) and sensitivities (ranging between 70% and 93.5%). Although these numbers are not perfect they demonstrate that Raman spectroscopy can help improving the current clinical practice.

In the past, a disadvantage of Raman spectroscopy was the low measurement speed. One way to overcome this is to complement Raman spectroscopy with other techniques, such as auto-fluorescence imaging. For instance, Kong *et al.* and McGregor *et al.* [94,113,224] have used auto-fluorescence imaging to quickly scan large areas of tissue for selection of the measurement locations for Raman spectroscopy, thereby reducing the time spent on redundant or non-relevant Raman measurements.[94,202]

From the work published in the recent years, we consider that the most notable advances in instrumentation of Raman spectroscopy include: (1) advances in the detector technology, (2) *in vivo* miniature fiber-optic probes to be used as an adjunct device to conventional endoscopes for biopsy targeting or for surgery guidance, (3) combined fluorescence microscopy and Raman spectroscopy systems for guided surgery, and (4) new lasers for low-cost Raman devices.

The number of scientific groups that are working towards implementation of Raman spectroscopy devices in clinical procedures is remarkable. Most of the studies (89%) still take place at the same technology readiness level (TRL-4, or class B). In these studies, algorithms have been developed for detection of (pre-)malignant tissue based on *in vivo* or *ex vivo* measurements, under conditions that approach the intended clinical environment. Validation of these algorithms based on large independent datasets obtained in the actual clinical workflow still needs to happen.

We have observed that approximately 30% of the reviewed studies were published in medical journals. In order to raise awareness and increase acceptance of Raman technologies among clinicians and clinical researchers results of Raman cancer diagnostic studies should be presented at medical conferences and published in medical journals. Better communication between clinicians and spectroscopists will facilitate understanding of the clinical requirements and challenges. The gap between technology developers and clinicians is narrowing due to the contribution of multidisciplinary networks like ClirSpec, Raman4Clinics (EU COST Action BM1401) and EPIC. These networks also actively pursue standardization of sample preparation, measurements, data analysis protocols, which will help to form a basis for transferability and thereby accelerate the developments discussed in this review. The networks can also have an important role in presenting Raman spectroscopy as a technology that can complement and facilitate the work of the clinicians and improve patient outcome.

In summary, based on the expectation given by the companies, we believe that within 5 years Raman-based oncological products will advance into routine clinical settings.

Acknowledgements

The authors would like to thank the Martin Isabelle, Jeremy Brites, Fran Adar, Daniel Barchewitz, Edwin Weusthof, Jan Toporski, Frédéric Leblond, Eric Marple, Jay Trautman,Viacheslav Artyushenko, Katsuo Morita, Ioan Notingher, Huang Zhiwei, Haishan Zeng, and Mads Bergholt for their input and valuable comments received in the preparation of this review.

Financial support is gratefully acknowledged from the Dutch Cancer Society: EMCR2017-8027, Innovative Research Programme – Photonics Devices (Netherlands Ministry of Economic Affairs): IPD12004, FNO (Fonds Nuts Ohra), Maurits en Anna de Kock Stichting, and ATOS Medical.

References

1. World Health Organization, GLOBOCAN 2012: Estimated Cancer Incidence, Mortality and Prevalence Worldwide in 2012, http://globocan.iarc.fr, (accessed 22 March 2017).
2. M. Çulha, *Bioanalysis*, 2015, 7, 2813–2824.
3. P. Mendoza, M. Lacambra, P.-H. Tan and G. M. Tse, *Patholog. Res. Int.,* 2011, 2011, 1–8.
4. D. Quail and J. Joyce, *Nat. Med.*, 2013, 19, 1423–1437.
5. S. R. Menakuru, N. J. Brown, C. A. Staton and M. W. R. Reed, *Br. J. Cancer*, 2008, 99, 1961–1966.
6. L. P. Bokhorst, X. Zhu, M. Bul, C. H. Bangma, F. H. Schröder and M. J. Roobol, *BJU Int*., 2012, 110, 1654–1660.
7. M. Rominger, C. Wisgickl and N. Timmesfeld, *RoFo*, 2012, 184, 1144–1152.
8. A. McWilliams, M. C. Tammemagi, J. R. Mayo, H. Roberts, G. Liu, K. Soghrati, K. Yasufuku, S. Martel, F. Laberge, M. Gingras, S. Atkar-Khattra, C. D. Berg, K. Evans, R. Finley, J. Yee, J. English, P. Nasute, J. Goffin, S. Puksa, L. Stewart, S. Tsai, M. R. Johnston, D. Manos, G. Nicholas, G. D. Goss, J. M. Seely, K. Amjadi, A. Tremblay, P. Burrowes, P. MacEachern, R. Bhatia, M.-S. Tsao and S. Lam, *N. Engl. J. Med*., 2013, 369, 910–9.
9. P. Carli, F. Mannone, V. De Giorgi, P. Nardini, A. Chiarugi and B. Giannoti, *Melanoma Res*, 2003, 2, 179–182.
10. W.-C. Kuo, J. Kim, N. D. Shemonski, E. J. Chaney, D. R. Spillman and S. A. Boppart, *Biomed. Opt. Express*, 2012, 3, 1149–61.
11. L. P. Hariri, M. Mino-Kenudson, M. B. Applegate, E. J. Mark, G. J. Tearney, M. Lanuti, C. L. Channick, A. Chee and M. J. Suter, Chest, 2013, 144, 1261–1268.
12. M. S. Bergholt, K. Lin, J. Wang, W. Zheng, H. Xu, Q. Huang, J. L. Ren, K. Y. Ho, M. Teh, S. Srivastava, B. Wong, K. G. Yeoh and Z. Huang, *J. Biophotonics*, 2016, 9, 333–342.
13. D. Shin, N. Vigneswaran, A. Gillenwater and R. Richards-Kortum, *Future Oncol.,* 2010, 6, 1143–54.
14. L. M. Wong Kee Song, S. Banerjee, D. Desilets, D. L. Diehl, F. A. Farraye, V. Kaul, S. R. Kethu, R. S. Kwon, P. Mamula, M. C. Pedrosa, S. A. Rodriguez and W. M. Tierney, *Gastrointest. Endosc.*, 2011, 73, 647–650.
15. Y. Wang, Q. Wang, J. Feng and Q. Wu, *Patient Prefer. Adherence*, 2013, 7, 621–631.
16. A. Nijssen, S. Koljenović, T. C. Bakker Schut, P. J. Caspers and G. J. Puppels, *J. Biophotonics*, 2009, 2, 29–36.
17. B. Broadbent, J. Tseng, R. Kast, T. Noh, M. Brusatori, S. N. Kalkanis and G. W. Auner, *J. Neurooncol.*, 2016, 130, 1–9.
18. W. Wang, J. Zhao, M. Short and H. Zeng, *J. Biophotonics*, 2015, 8, 527–545.
19. X. Li, Y. Wang, X. Zhang, D. Wang and J. Lin, *Conf. Proc. IEEE Eng. Med. Biol. Soc.*, 2005, 2, 1453–6.
20. C. Kallaway, L. M. Almond, H. Barr, J. Wood, J. Hutchings, C. Kendall and N. Stone, *Photodiagnosis Photodyn. Ther.*, 2013, 10, 207–219.
21. H. McGregor, W. Wang, M. Short and H. Zeng, *Adv. Heal. Care Technol*., 2016, 2, 13.
22. A. Binahmed, R. W. Nason and A. A. Abdoh, *Oral Oncol*., 2007, 43, 780–784.
23. R. W. H. Smits, S. Koljenović, J. A. Hardillo, I. ten Hove, C. A. Meeuwis, A. Sewnaik, E. A. C. Dronkers, T. C. Bakker Schut, T. P. M. Langeveld, J. Molenaar, V. N. Hegt, G. J. Puppels and R. J. Baatenburg de Jong, *Head Neck*, 2016, 38, E2197–E2203.
24. J. K. Dillon, C. B. Brown, T. M. McDonald, D. C. Ludwig, P. J. Clark, B. G. Leroux and N. D. Futran, *J. Oral Maxillofac. Surg*., 2015, 73, 1182–1188.
25. Y. Neuzillet, M. Soulie, S. Larre, M. Roupret, G. Defortescu, T. Murez, G. Pignot, A. Descazeaud, J. J. Patard, P. Bigot, L. Salomon, P. Colin, J. Rigaud, C. Bastide, X. Durand, A. Valeri, F. Kleinclauss, F. Bruyere and C. Pfister, *BJU Int*., 2013, 111, 1253–1260.
26. S. Gokavarapu, L. M. C. Rao, M. Mahajan, N. Parvataneni, K. V. V. N. Raju and R. Chander, Br. *J. Oral Maxillofac. Surg*., 2015, 53, 875–879.
27. M. D. Williams, *Curr. Oncol. Rep*., 2016, 18, 54.
28. J. R. Miedema and H. V Hunt, *J. Gastrointestin. Liver Dis*., 2010, 19, 181–5.
29. T. P. Olson, J. Harter, A. Muñoz, D. M. Mahvi and T. Breslin, *Ann. Surg. Oncol*., 2007, 14, 2953–2960.

30. R. Emmadi and E. L. Wiley, *Int. J. Surg. Oncol*., 2012, 2012, 1–9.
31. H. E. Trejo Bittar, P. Incharoen, A. D. Althouse and S. Dacic, *Mod. Pathol*., 2015, 28, 1058–63.
32. E. L. Rosenthal, J. M. Warram, K. I. Bland and K. R. Zinn, *Ann. Surg*., 2015, 261, 46–55.
33. M. A. Varvares, S. Poti, B. Kenyon, K. Christopher and R. J. Walker, *Laryngoscope,* 2015, 125, 2298–2307.
34. N. D. Magee, J. R. Beattie, C. Carland, R. Davis, K. McManus, I. Bradbury, D. A. Fennell, P. W. Hamilton, M. Ennis, J. J. McGarvey and J. S. Elborn, *J. Biomed. Opt*., 2010, 15, 026015(1-8).
35. E. R. McIntosh, S. Harada, J. Drwiega, M. S. Brandwein-Gensler and J. Gordetsky, *Ann. Diagn. Pathol*., 2015, 19, 326–329.
36. C. Senft, A. Bink, K. Franz, H. Vatter, T. Gasser and V. Seifert, *Lancet Oncol*., 2011, 12, 997–1003.
37. C. Senft, B. Schoenes, T. Gasser, J. Platz, A. Bink, K. Franz and V. Seifert, *J. Neurosurg. Anesthesiol*., 2011, 23, 241–6.
38. J. M. Wong, J. R. Panchmatia, J. E. Ziewacz, A. M. Bader, I. F. Dunn, E. R. Laws and A. a Gawande, *Neurosurg. Focus*, 2012, 33, E16.
39. J.-S. Wu, Y. Mao, L.-F. Zhou, W.-J. Tang, J. Hu, Y.-Y. Song, X.-N. Hong and G.-H. Du, *Neurosusrgery*, 2007, 61, 935–949.
40. E. B. Claus, A. Horlacher, L. Hsu, R. B. Schwartz, D. Dello-Iacono, F. Talos, F. A. Jolesz and P. M. Black, *Cancer*, 2005, 103, 1227–1233.
41. D. Kuhnt, A. Becker, O. Ganslandt, M. Bauer, M. Buchfelder and C. Nimsky, *Neuro. Oncol*., 2011, 13, 1339–1348.
42. P. L. Kubben, K. J. ter Meulen, O. E. M. G. Schijns, M. P. ter Laak-Poort, J. J. van Overbeeke and H. van Santbrink, Lancet Oncol., 2011, 12, 1062–1070.
43. J. D. Visgauss, W. C. Eward and B. E. Brigman, *Orthop. Clin. North Am*., 2016, 47, 253–264.
44. F. Prada, A. Perin, A. Martegani, L. Aiani, L. Solbiati, M. Lamperti, C. Casali, F. Legnani, L. Mattei, A. Saladino, M. Saini and F. Dimeco, *Neurosurgery*, 2014, 74, 542–552.
45. T. Selbekk, A. S. Jakola, O. Solheim, T. F. Johansen, F. Lindseth, I. Reinertsen and G. Unsgård, Acta Neurochir. (Wien)., 2013, 155, 973–980.
46. S. J. Erickson-Bhatt, R. M. Nolan, N. D. Shemonski, S. G. Adie, J. Putney, D. Darga, D. T. McCormick, A. J. Cittadine, A. M. Zysk, M. Marjanovic, E. J. Chaney, G. L. Monroy, F. A. South, K. A. Cradock, Z. G. Liu, M. Sundaram, P. S. Ray and S. A. Boppart, *Cancer Res*., 2015, 75, 3706–3712.
47. W. Stummer, U. Pichlmeier, T. Meinel, O. D. Wiestler, F. Zanella and H. J. Reulen, *Lancet Oncol*., 2006, 7, 392–401.
48. G. Widhalm, B. Kiesel, A. Woehrer, T. Traub-Weidinger, M. Preusser, C. Marosi, D. Prayer, J. A. Hainfellner, E. Knosp and S. Wolfsberger, *PLoS One,* DOI:10.1371/journal.pone.0076988.
49. W. Stummer, J.-C. Tonn, H. M. Mehdorn, U. Nestler, K. Franz, C. Goetz, A. Bink and U. Pichlmeier, *J. Neurosurg*., 2011, 114, 613–623.
50. D. W. Roberts, P. A. Valdés, B. T. Harris, D. Ph, K. M. Fontaine, A. Hartov, X. Fan, S. Ji, D. Sc, S. S. Lollis, B. W. Pogue, F. Leblond and D. Tor, *J. Neuroserg*., 2011, 114, 595–603.
51. E. D. Agdeppa and M. E. Spilker, *AAPS J*., 2009, 11, 286–299.
52. M. Jermyn, K. Mok, J. Mercier, J. Desroches, J. Pichette, K. Saint-Arnaud, L. Bernstein, M.-C. Guiot, K. Petrecca and F. Leblond, *Sci. Transl. Med*., 2015, 7, 274ra19-274ra19.
53. A. S. Haka, Z. Volynskaya, J. a Gardecki, J. Nazemi, R. Shenk, N. Wang, R. R. Dasari, M. Fitzmaurice and M. S. Feld, *J. Biomed. Opt*., 2009, 14, 54023.
54. N. Kourkoumelis, I. Balatsoukas, V. Moulia, A. Elka, G. Gaitanis and I. D. Bassukas, *Int. J. Mol. Sci*., 2015, 16, 14554–14570.
55. L. A. Austin, S. Osseiran and C. L. Evans, *Analyst,* 2016, 141, 476–503.
56. I. Pence and A. Mahadevan-Jansen, *Chem. Soc. Rev*., 2016, 45, 1958–1979.
57. D. W. Shipp, F. Sinjab and I. Notingher, *Adv. Opt.Photonics*, 2017, 9, 315–428..
58. C. Krafft, I. W. Schie, T. Meyer, M. Schmitt and J. Popp, *Chem. Soc. Rev*., 2016, 45, 1819–1849.
59. C. H. Camp Jr and M. T. Cicerone, *Nat. Photonics*, 2015, 9, 295–305.
60. L. T. Kerr, T. M. Lynn, I. M. Cullen, P. J. Daly, N. Shah, S. O'Dea, A. Malkin and B. M. Hennelly, *Anal. Methods*, 2016, 8, 4991–5000.
61. M. Isabelle, N. Stone, H. Barr, M. Vipond, N. Shepherd and K. Rogers, *Spectroscopy*, 2008, 22, 97–104.
62. European Commission, *Horizon 2020; Work programme 2014-2015*, 2014.
63. J. M. Johnson, R. R. Dalton, S. M. Wester,

J. Landercasper and P. J. Lambert, *Arch Surg*, 1999, 134, 712–716.

64. M. Wang, X. He, Y. Chang, G. Sun and L. Thabane, *The Breast*, 2017, 31, 157–166.
65. W. Sun, a Li, F. Abreo, E. Turbat-Herrera and W. D. Grafton, *Diagn. Cytopathol.*, 2001, 24, 421–5.
66. B. Lieske, D. Ravichandran and D. Wright, *Br. J. Cancer*, 2006, 95, 62–66.
67. Y.-H. Yu, W. Wei, J.-L. Liu, *et al.*, *BMC Cancer*, 2012, 12, 41.
68. M. Kazi, Suhani, R. Parshad, V. Seenu, S. Mathur and K. P. Haresh, *World J. Surg.*, 2017, 41, 1528–1533.
69. M. C. van Maaren, L. de Munck, J. J. Jobsen, P. Poortmans, G. H. de Bock, S. Siesling and L. J. A. Strobbe, *Breast Cancer Res. Treat.*, 2016, 160, 511–521.
70. A. A. Onitilo, J. M. Engel, R. V. Stankowski and S. A. R. Doi, *Clin. Med. Res.*, 2015, 13, 65–73.
71. S. Agarwal, L. Pappas, L. Neumayer, K. Kokeny and J. Agarwal, *JAMA Surg.*, 2014, 149, 267.
72. I. O. Ellis, P. Carder, S. Hales, A. H. S. Lee, S. E. Pinder, E. Rakha, T. Stephenson, S. Al-Sam, R. Deb, A. Hanby, R. Liebmann, E. Provenzano, D. Rowlands, C. A. Wells, N. Anderson, A. Girling, M. Ibrahim, E. Mallon and C. Quinn, *Pathology reporting of breast disease in surgical excision specimens incorporating the dataset for histological reporting of breast cancer*, 2016.
73. E. L. Vos, S. Siesling, M. H. A. Baaijens, C. Verhoef, A. Jager, A. C. Voogd and L. B. Koppert, *Breast Cancer Res. Treat.*, 2007, DOI:10.1007/s10549-017-4232-6.
74. L. Jacobs, *Ann. Surg. Oncol.*, 2008, 15, 1271–1272.
75. A. Saha, I. Barman, N. C. Dingari, S. McGee, Z. Volynskaya, L. H. Galindo, W. Liu, D. Plecha, N. Klein, R. R. Dasari and M. Fitzmaurice, *Biomed. Opt. Express*, 2011, 2, 2792.
76. I. Barman, N. C. Dingari, A. Saha, S. McGee, L. H. Galindo, W. Liu, D. Plecha, N. Klein, R. R. Dasari and M. Fitzmaurice, Cancer Res., 2013, 73, 3206–3215.
77. A. Lomas, J. Leonardi-Bee and F. Bath-Hextall, *Br. J. Dermatol.*, 2012, 166, 1069–1080.
78. K. G. Lewis and M. A. Weinstock, *Arch Dermatol*, 2004, 140, 837–842.
79. E. Drakaki, T. Vergou, C. Dessinioti, A. J. Stratigos, C. Salavastru and C. Antoniou, *J. Biomed. Opt.*, 2013, 18, 61221.
80. Basaalcercarcinoom - Klinische marges BCC, https://richtlijnendatabase.nl/richtlijn/basaalcelcarcinoom/conventionele_chirurgische_excisie_bcc/klinische_marges_bcc.html, (accessed 25 April 2017).
81. E. van Loo, K. Mosterd, G. A. M. Krekels, M. H. Roozeboom, J. U. Ostertag, C. D. Dirksen, P. M. Steijlen, H. A. M. Neumann, P. J. Nelemans and N. W. J. Kelleners-Smeets, *Eur. J. Cancer*, 2014, 50, 3011–3020.
82. M. Jermyn, J. Desroches, K. Aubertin, K. St-arnaud, J. Madore, E. De Montigny, M. Guiot, D. Trudel, C. Brian, K. Petrecca and F. Leblond, *Phys. Med. Biol.*, 2016, 61, R370–R400.
83. R. Siegel, J. Ma, Z. Zou and A. Jemal, CA. *Cancer J. Clin.*, 2014, 64, 9–29.
84. C. M. Balch, J. E. Gershenwald, S. J. Soong, J. F. Thompson, M. B. Atkins, D. R. Byrd, A. C. Buzaid, A. J. Cochran, D. G. Coit, S. Ding, A. M. Eggermont, K. T. Flaherty, P. A. Gimotty, J. M. Kirkwood, K. M. McMasters, M. C. Mihm, D. L. Morton, M. I. Ross, A. J. Sober and V. K. Sondak, *J. Clin. Oncol.*, 2009, 27, 6199–6206.
85. P. V. Dickson and J. E. Gershenwald, *Surg. Oncol. Clin. N. Am.*, 2011, 20, 1–17.
86. H. Kittler, H. Pehamberger, K. Wolff and M. Binder, *Lancet Oncol.,* 2002, 3, 159–65.
87. C. A. Morton and R. M. Mackie, *Br. J. Dermatol.*, 1998, 138, 283–7.
88. J. I. van der Rhee, W. Bergman and N. a Kukutsch, *Acta Derm. Venereol.*, 2011, 91, 428–31.
89. I. P. Santos, P. J. Caspers, T. C. Bakker Schut, R. van Doorn, V. Noordhoek Hegt, S. Koljenović and G. J. Puppels, *Anal. Chem.*, 2016, 88, 7683–7688.
90. H. Lui, J. Zhao, D. McLean and H. Zeng, *Cancer Res.*, 2012, 72, 2491–2500.
91. C. Lieber, S. K. Majumder, D. Billheimer, D. L. Ellis and A. Mahadevan-Jansen, *J. Biomed. Opt.*, 2008, 13, 24013.
92. J. Zhao, H. Lui, S. Kalia and H. Zeng, Anal. *Bioanal. Chem.*, 2015, 407, 8373–8379.
93. J. Schleusener, P. Gluszczynska, C. Reble, I. Gersonde, J. Helfmann, J. W. Fluhr, J. Lademann, J. Röwert-Huber, A. Patzelt and M. C. Meinke, *Exp. Dermatol.*, 2015, 24, 767–772.
94. K. Kong, C. J. Rowlands, S. Varma, W. Perkins, I. H. Leach, A. a Koloydenko, H. C. Williams and I. Notingher, *Proc. Natl. Acad. Sci. U. S. A.*, 2013, 110, 15189–94.

95. K. Eberhardt, C. Stiebing, C. Matthäus, M. Schmitt and J. Popp, *Expert Rev. Mol. Diagn*., 2015, 15, 773–87.
96. J. Zhao, H. Lui, D. I. McLean and H. Zeng, Conf. Proc. *IEEE Eng. Med. Biol. Soc*., 2008, 2008, 3107–3109.
97. C. Lieber and A. Mahadevan-Jansen, *Opt. Express*, 2007, 15, 11874–11882.
98. C. A. Lieber, S. K. Majumder, D. L. Ellis, D. D. Billheimer and A. Mahadevan-Jansen, *Lasers Surg Med*, 2008, 40, 461–467.
99. L. Silveira, Jr., F. L. Silveira, B. Bodanese, M. T. T. Pacheco and R. a. Zângaro, *Proc. SPIE*, 2012, 8207, 82070X–1–7.
100. L. Lim, B. Nichols, M. R. Migden, N. Rajaram, J. S. Reichenberg, M. K. Markey, M. I. Ross and J. W. Tunnell, *J. Biomed. Opt*., 2014, 19, 117003.
101. I. P. Santos, P. J. Caspers, T. Bakker Schut, R. van Doorn, S. Koljenović and G. J. Puppels, *J. Raman Spectrosc*., 2015, 652–660.
102. I. A. Bratchenko, D. N. Artemyev, O. O. Myakinin, Y. A. Khristoforova, A. A. Moryatov, S. V. Kozlov and V. P. Zakharov, *J. Biomed. Opt*., 2017, 22, 27005.
103. J. Sun, D. H. Garfield, B. Lam, J. Yan, A. Gu, J. Shen and B. Han, *J Thorac Oncol*., 2011, 6, 1336–1344.
104. P. Jain, S. Hadique and A. C. Mehta, in *Interventional Bronchoscopy*, Humana Press, Totowa, NJ, 2013, vol. 100, pp. 15–44.
105. M. O. Idowu and C. N. Powers, *Int. J. Clin. Exp. Pathol*., 2010, 3, 367–385.
106. R. J. Ginsberg and L. V. Rubinstein, *Ann. Thorac. Surg*., 1995, 60, 615–623.
107. R. J. Landreneau, D. J. Sugarbaker, M. J. Mack, S. R. Hazelrigg, J. D. Luketich, L. Fetterman, M. J. Liptay, S. Bartley, T. M. Boley, R. J. Keenan, P. F. Ferson, R. J. Weyant, K. S. Naunheim, J. B. Mark, J. R. Benfield, R. Cohen and A. N. Thomas, *J. Thorac. Cardiovasc. Surg*., 1997, 113, 691–700.
108. J. D. Blasberg, H. I. Pass and J. S. Donington, *J Thorac Oncol*., 2010, 5, 1583–1593.
109. S. Liu, R. Wang, Y. Zhang, Y. Li, C. Cheng, Y. Pan, J. Xiang, Y. Zhang, H. Chen and Y. Sun, *J. Clin. Oncol*., 2016, 34, 307–313.
110. Y.-C. Yeh, J. Nitadori, K. Kadota, A. Yoshizawa, N. Rekhtman, A. L. Moreira, C. S. Sima, V. W. Rusch, P. S. Adusumilli and W. D. Travis, *Histopathology*, 2015, 66, 922–938.
111. M. A. Short, S. Lam, A. McWilliams, J. Zhao, H. Lui and H. Zeng, *Opt. Lett*., 2008, 33, 711–3.
112. M. A. Short, S. Lam, A. M. McWilliams, D. N. Ionescu and H. Zeng, *J. Thorac. Oncol*., 2011, 6, 1206–1214.
113. H. C. McGregor, M. A. Short, A. McWilliams, T. Shaipanich, D. N. Ionescu, J. Zhao, W. Wang, G. Chen, S. Lam and H. Zeng, *J. Biophotonics*, 2016, 13, n/a-n/a.
114. J. Ferlay, I. Soerjomataram, R. Dikshit, S. Eser, C. Mathers, M. Rebelo, D. M. Parkin, D. Forman and F. Bray, *Int. J. Cancer*, 2015, 136, E359–E386.
115. J. Rees, P. Lao-Sirieix, A. Wong and R. Fitzgerald, *Cochrane Database Syst. Rev*., 2011, 2010–2012.
116. N. Lal, D. K. Bhasin, a K. Malik, N. M. Gupta, K. Singh and S. K. Mehta, *Gut*, 1992, 33, 724–6.
117. Y. Choi, H. S. Choi, W. K. Jeon, B. I. Kim, D. Il Park, Y. K. Cho, H. J. Kim, J. H. Park and C. Il Sohn, *J. Korean Med. Sci*., 2012, 27, 36–39.
118. S. Menon and N. Trudgill, *Endosc. Int. Open*, 2014, 2, E46–E50.
119. S. Tsutsui, H. Kuwano, M. Watanabe, M. Kitamura and K. Sugimachi, *Ann. Surg*., 1995, 222, 193–202.
120. A. G. Casson, S. J. Darnton, S. Subramanian and L. Hiller, *Ann. Thorac. Surg*., 2000, 69, 205–209.
121. P. M. Sagar, D. Johnston, M. J. McMahon, M. F. Dixon and P. Quirke, *Br. J. Surg*., 1993, 80, 1386–1388.
122. S. P. Dexter, H. Sue-Ling, M. J. McMahon, P. Quirke, N. Mapstone and I. G. Martin, *Gut*, 2001, 48, 667–670.
123. S. K. Teh, W. Zheng, K. Y. Ho, M. Teh, K. G. Yeoh and Z. Huang, Br. J. Cancer, 2008, 98, 457–65.
124. M. S. Bergholt, W. Zheng, K. Lin, K. Y. Ho, M. Teh, K. G. Yeoh, J. B. Y. So and Z. Huang, *Analyst*, 2010, 135, 3162–3168.
125. S. Duraipandian, M. S. Bergholt, W. Zheng, K. Y. Ho, M. Teh, K. G. Yeoh, J. B. Y. So, A. Shabbir and Z. Huang, *J. Biomed. Opt*., 2012, 17, 81418.
126. M. S. Bergholt, W. Zheng, K. Y. Ho, K. G. Yeoh, M. Teh, J. B. Y. So and Z. Huang, *Proc. SPIE*, 2014, 8939, 89390M.
127. K. Lin, J. Wang, M. Sylvest Bergholt, W. Zheng, H. Xu, J. Ren, K. Yu Ho, M. Teh, K. Guan Yeoh and Z. Huang, in *Proc. of SPIE*, eds. M. J. Suter, S. Lam, M. Brenner, G. J. Tearney and T. D. Wang, Nature Publishing Group, 2015, vol. 9304, p. 93040V.
128. M. Ishigaki, Y. Maeda, A. Taketani, B. B.

Andriana, R. Ishihara, K. Wongravee, Y. Ozaki and H. Sato, *Analyst*, 2015, 141, 1027–33.

129. J. Wang, K. Lin, W. Zheng, K. Yu Ho, M. Teh, K. Guan Yeoh and Z. Huang, *Sci. Rep*., 2015, 5, 12957.
130. P. J. Slootweg, G. J. Hordijk, Y. Schade, R. J. J. Van Es and R. Koole, *Oral Oncol*., 2002, 38, 500–503.
131. N. Al-Rajhi, Y. Khafaga, J. El-Husseiny, M. Saleem, W. Mourad, A. Al-Otieschan and A. Al-Amro, *Oral Oncol*., 2000, 36, 508–514.
132. T. Helliwell and J. Woolgar, *Dataset for histopathology reporting of mucosal malignancies of the nasal cavities and paranasal sinuses*, 2013.
133. T. Helliwell and J. Woolgar, *Dataset for histopathology reporting of mucosal malignancies of the larynx*, 2013.
134. J. Hoffmannová, R. Foltán, M. Vlk, M. Šipoš, E. Horká, G. Pavlíková, R. Kufa, O. Bulík and J. Šedý, *Int. J. Oral Maxillofac. Surg*., 2010, 39, 561–567.
135. E. M. Barroso, R. W. H. Smits, T. C. B. Schut, I. Ten Hove, J. A. Hardillo, E. B. Wolvius, R. J. Baatenburg De Jong, S. Koljenović and G. J. Puppels, *Anal. Chem*., 2015, 87, 2419–2426.
136. H. Krishna, S. K. Majumder, P. Chaturvedi, M. Sidramesh and P. K. Gupta, *J. Biophotonics*, 2014, 7, 690–702.
137. K. Guze, H. C. Pawluk, M. Short, H. Zeng, J. Lorch, C. Norris and S. Sonis, *Head Neck*, 2015, 37, 511–517.
138. E. M. Barroso, R. W. H. Smits, C. G. F. Van Lanschot, P. J. Caspers, I. Ten Hove, H. Mast, A. Sewnaik, J. Hardillo, C. Meeuwis, R. Verdijk, V. N. Hegt, R. J. Baatenburg De Jong, E. B. Wolvius, T. C. Bakker Schut, S. Koljenović and G. J. Puppels, *Cancer Res*., 2016, 76, 5945–5953.
139. E. T. Wong and J. K. Wu, Clinical presentation and diagnosis of brain tumors, https://www.uptodate.com/contents/clinical-presentation-and-diagnosis-of-brain-tumors?source=search_result&search=brain cancer&selectedTitle=1~150#H22, (accessed 12 May 2017).
140. T. Hollon, S. Lewis, C. W. Freudiger, X. Sunney Xie and D. A. Orringer, *Neurosurg. Focus*, 2016, 40, E9.
141. S. Koljenović, L.-P. Choo-Smith, T. C. Bakker Schut, J. M. Kros, H. J. van den Berge and G. J. Puppels, *Lab. Investig*., 2002, 82, 1265–1277.
142. N. F. Marko, R. J. Weil, J. L. Schroeder, F. F. Lang, D. Suki and R. E. Sawaya, *J. Clin. Oncol*., 2014, 32, 774–782.
143. N. Sanai, S. Chang and M. Berger, *J Neurosurg*, 2011, 115, 945–947.
144. F. K. Lu, D. Calligaris, O. I. Olubiyi, I. Norton, W. Yang, S. Santagata, X. S. Xie, A. J. Golby and N. Y. R. Agar, *Cancer Res*., 2016, 76, 3451–3462.
145. F. Albert, M. Forsting, K. Sartor, H. Adams and S. Kunze, *Neurosurgery*, 1994, 34, 45–61.
146. S. Ulmer, World J. Radiol., 2014, 6, 538–43.
147. M. Ji, S. Lewis, S. Camelo-Piragua, S. H. Ramkissoon, M. Snuderl, S. Venneti, A. Fisher-Hubbard, M. Garrard, D. Fu, A. C. Wang, J. A. Heth, C. O. Maher, N. Sanai, T. D. Johnson, C. W. Freudiger, O. Sagher, X. S. Xie and D. A. Orringer, *Sci. Transl. Med*., 2015, 7, 309ra163-309ra163.
148. M. Jermyn, K. Mok, J. Mercier, J. Desroches, J. Pichette, K. Saint-Arnaud, M.-C. Guiot, K. Petrecca and F. Leblond, in *Science Translational Medicine*, eds. R. R. Alfano and S. G. Demos, 2015, vol. 7, p. 93180D.
149. M. B. Wallace and R. Keisslich, *Gastroenterology*, 2010, 138, 2140–2150.
150. B. Bressler, L. F. Paszat, Z. Chen, D. M. Rothwell, C. Vinden and L. Rabeneck, *Gastroenterology*, 2007, 132, 96–102.
151. E. Quintero, C. Hassan, C. Senore and Y. Saito, *Gastroenterol. Res. Pract*., 2012, 2012, 846985.
152. A. Stallmach, C. Schmidt, A. Watson and R. Kiesslich, *J. Biophotonics*, 2011, 4, 482–489.
153. W. R. Kessler, T. F. Imperiale, R. W. Klein, R. C. Wielage and D. K. Rex, *Endoscopy*, 2011, 43, 683–691.
154. H. Nelson, N. Petrelli, A. Carlin and E. Al, *J Natl Cancer Inst*, 2001, 93, 591.
155. R. Amri, L. G. Bordeianou, P. Sylla and D. L. Berger, *JAMA Surg*., 2015, 150, 890–8.
156. J. B. O'Connell, M. a Maggard and C. Y. Ko, *J. Natl. Cancer Inst*., 2004, 96, 1420–1425.
157. E. Widjaja, W. Zheng and Z. Huang, *Int. J. Oncol*., 2008, 32, 653–662.
158. M. A. Short, I. T. Tai, D. Owen and H. Zeng, *Opt. Express*, 2013, 21, 5025–34.
159. L. Peirson, D. Fitzpatrick-Lewis, D. Ciliska and R. Warren, *Syst. Rev*., 2013, 2, 35.
160. K. Nanda, D. C. Mccrory, E. R. Myers, L. a Bastian, V. Hasselblad, J. D. Hickey and

D. B. Matchar, *Ann Intern Med*., 2000, 132, 810–819.

161. J. Cuzick, C. Clavel, K.-U. Petry, C. J. L. M. Meijer, H. Hoyer, S. Ratnam, A. Szarewski, P. Birembaut, S. Kulasingam, P. Sasieni and T. Iftner, *Int. J. Cancer*, 2006, 119, 1095–1101.

162. R. A. Mustafa, N. Santesso, R. Khatib, A. A. Mustafa, W. Wiercioch, R. Kehar, S. Gandhi, Y. Chen, A. Cheung, J. Hopkins, B. Ma, N. Lloyd, D. Wu, N. Broutet and H. J. Schünemann, *Int. J. Gynecol. Obstet*., 2016, 132, 259–265.

163. Z. Eftekhar, P. Rahimi-Moghaddam, F. Yarandi and R. Brojerdi, *Asian Pac. J. Cancer Prev*., 2005, 6, 69–71.

164. J. Mo, W. Zheng, J. J. H. Low, J. Ng, a Ilancheran and Z. Huang, *Anal. Chem*., 2009, 81, 8908–15.

165. E. M. Kanter, E. Vargis, S. Majumder, M. D. Keller, E. Woeste, G. G. Rao and A. Mahadevan-Jansen, *J. Biophotonics*, 2009, 2, 81–90.

166. S. Duraipandian, W. Zheng, J. Ng, J. J. H. Low, A. Ilancheran and Z. Huang, *Analyst*, 2011, 136, 4328.

167. S. Duraipandian, W. Zheng, J. Ng, J. J. H. Low, a. Ilancheran and Z. Huang, *Anal. Chem*., 2012, 84, 5913–5919.

168. I. R. M. Ramos, A. Malkin and F. M. Lyng, *Biomed Res. Int*., 2015, 2015, 1–9.

169. S. Rubina, M. Amita, D. Kedar K., R. Bharat and C. M. Krishna, *Vib. Spectrosc*., 2013, 68, 115–121.

170. Vulval cancer mortality statistics, http://www.cancerresearchuk.org/health-professional/cancer-statistics/statistics-by-cancer-type/vulval-cancer/mortality#heading-Zero, (accessed 4 April 2017).

171. R. Wessels, D. M. de Bruin, D. J. Faber, H. H. van Boven, A. D. Vincent, T. G. van Leeuwen, M. van Beurden and T. J. M. Ruers, *J. Biomed. Opt*., 2012, 17, 116022.

172. T. H. Dellinger, A. A. Hakim, S. J. Lee, M. T. Wakabayashi, R. J. Morgan and E. S. Han, *J. Natl. Compr. Cancer Network*, 2017, 15, 121–128.

173. J. M. Heaps, Y. S. Fu, F. J. Montz, N. F. Hacker and J. S. Berek, *Gynecol. Oncol*., 1990, 38, 309–314.

174. J. K. Chan, V. Sugiyama, H. Pham, M. Gu, J. Rutgers, K. Osann, M. K. Cheung, M. L. Berman and P. J. DiSaia, *Gynecol. Oncol*., 2007, 104, 636–641.

175. R. Wessels, M. van Beurden, D. M. de Bruin, D. J. Faber, A. D. Vincent, J. Sanders, T. G. van Leeuwen and T. J. M. Ruers, *Int. J. Gynecol. Cancer*, 2015, 25, 112–118.

176. J. Frost, L. Ludeman, K. Hillaby, R. Gornall, G. Lloyd, C. Kendall, A. C. Shore and N. Stone, *Analyst*, 2017, 142, 1200–1206.

177. T. Minamikawa, Y. Harada and T. Takamatsu, *Sci. Rep*., 2015, 5, 17165.

178. P. E. Clark, N. Agarwal, M. C. Biagioli, M. A. Eisenberger, R. E. Greenberg, H. W. Herr, B. A. Inman, D. A. Kuban, T. M. Kuzel, S. M. Lele, J. Michalski, L. C. Pagliaro, S. K. Pal, A. Patterson, E. R. Plimack, K. S. Pohar, M. P. Porter, J. P. Richie, W. J. Sexton, W. U. Shipley, E. J. Small, P. E. Spiess, D. L. Trump, G. Wile, T. G. Wilson, M. Dwyer, M. Ho and National Comprehensive Cancer Network (NCCN), *J. Natl. Compr. Cancer Netw*., 2013, 11, 446–75.

179. I. Barman, N. C. Dingari, G. P. Singh, R. Kumar, S. Lang and G. Nabi, *Anal. Bioanal. Chem*., 2012, 404, 3091–3099.

180. D. Jocham, H. Stepp and R. Waidelich, *Eur. Urol*., 2008, 53, 1138–1150.

181. L. M. Seltz and S. D. Herrell, Curr. *Opin. Urol*., 2016, 26, 259–263.

182. Z. A. Dotan, K. Kavanagh, O. Yossepowitch, M. Kaag, S. Olgac, M. Donat and H. W. Herr, *J. Urol*., 2007, 178, 2308–2313.

183. G. Novara, R. S. Svatek, P. I. Karakiewicz, E. Skinner, V. Ficarra, Y. Fradet, Y. Lotan, H. Isbarn, U. Capitanio, P. J. Bastian, W. Kassouf, H. M. Fritsche, J. I. Izawa, D. Tilki, C. P. Dinney, S. P. Lerner, M. Schoenberg, B. G. Volkmer, A. I. Sagalowsky and S. F. Shariat, *J. Urol*., 2010, 183, 2165–2170.

184. M. C. M. Grimbergen, C. F. P. van Swol, R. O. P. Draga, P. van Diest, R. M. Verdaasdonk, N. Stone and J. H. L. R. Bosch, in *Proc. SPIE*, eds. N. Kollias, B. Choi, H. Zeng, R. S. Malek, B. J. Wong, J. F. R. Ilgner, K. W. Gregory, G. J. Tearney, L. Marcu, H. Hirschberg and S. J. Madsen, 2009, vol. 7161, p. 716114.

185. R. O. P. Draga, M. C. M. Grimbergen, P. L. M. Vijverberg, C. F. P. Van Swol, T. G. N. Jonges, J. A. Kummer and J. L. H. Ruud Bosch, *Anal. Chem*., 2010, 82, 5993–5999.

186. E. Ruijter, C. Van De Kaa, G. Miller, D. Ruiter, F. Debruyne and J. Schalken, *Endocr. Rev*., 1999, 20, 22–45.

187. K. Eichler, S. Hempel, J. Wilby, L. Myers, L. M. Bachmann and J. Kleijnen, *J. Urol*., 2006, 175, 1605–1612.

188. N. Mottet, J. Bellmunt, M. Bolla, E. Briers,

M. G. Cumberbatch, M. De Santis, N. Fossati, T. Gross, A. M. Henry, S. Joniau, T. B. Lam, M. D. Mason, V. B. Matveev, P. C. Moldovan, R. C. N. van den Bergh, T. Van den Broeck, H. G. van der Poel, T. H. van der Kwast, O. Rouvière, I. G. Schoots, T. Wiegel and P. Cornford, *Eur. Urol.*, 2016, 71, 1–12.

189. T. Schlomm, P. Tennstedt, C. Huxhold, T. Steuber, G. Salomon, U. Michl, H. Heinzer, J. Hansen, L. Budäus, S. Steurer, C. Wittmer, S. Minner, A. Haese, G. Sauter, M. Graefen and H. Huland, *Eur. Urol.*, 2012, 62, 333–340.
190. M. Li, S. R. Banerjee, C. Zheng, M. G. Pomper and I. Barman, *Chem. Sci.*, 2016, 7, 6779–6785.
191. R. E. Kast, S. C. Tucker, K. Killian, M. Trexler, K. V. Honn and G. W. Auner, *Cancer Metastasis Rev.*, 2014, 33, 673–693.
192. C. A. Patil, I. J. Pence, C. A. Lieber and A. Mahadevan-Jansen, *Opt. Lett.*, 2014, 39, 303–306.
193. I. J. Pence, C. A. Patil, C. A. Lieber and A. Mahadevan-Jansen, *Biomed. Opt. Express*, 2015, 6, 2724–37.
194. S. Duraipandian, W. Zheng, J. Ng, J. J. H. Low, A. Ilancheran and Z. Huang, *J. Biomed. Opt.*, 2013, 18, 67007.
195. J. Desroches, M. Jermyn, K. Mok, C. Lemieux-Leduc, J. Mercier, K. St-Arnaud, K. Urmey, M.-C. Guiot, E. Marple, K. Petrecca and F. Leblond, *Biomed. Opt. Express*, 2015, 6, 2380–97.
196. O. Stevens, I. E. Iping Petterson, J. C. C. Day and N. Stone, *Chem. Soc. Rev.*, 2016, 45, 1919–1934.
197. J. Wang, M. S. Bergholt, W. Zheng and Z. Huang, *Opt. Lett.*, 2013, 38, 2321–3.
198. J. Wang, K. Lin, W. Zheng, K. Y. u Ho, M. Teh, K. G. uan Yeoh and Z. Huang, *Anal. Bioanal. Chem.*, 2015, 407, 8303–8310.
199. S. Duraipandian, M. S. Bergholt, W. Zheng, K. Y. Ho, M. Teh, K. G. Yeoh, J. B. Y. So, A. Shabbir and Z. Huang, *J. Biomed. Opt.*, 2012, 17, 81418.
200. M. Agenant, M. Grimbergen, R. Draga, E. Marple, R. Bosch and C. van Swol, *Biomed. Opt. Express*, 2014, 5, 1203–16.
201. G. J. Puppels, *Cancer Res.*, 2017, 77, 2775–2778.
202. S. Takamori, K. Kong, S. Varma, I. Leach, H. C. Williams and I. Notingher, *Biomed. Opt. Express*, 2015, 6, 98.
203. I. P. Santos, A. van der Lee, X. Gu, P. J. Caspers, T. C. Bakker Schut, R. van Doorn, V. Noordhoek Hegt, S. Koljenović and G. J. Puppels, *J. Raman Spectrosc.*, , DOI:10.1002/jrs.5124.
204. M. Kuznetsov, in *Semiconductor Disk Lasers. Physics and Technology*, ed. O. G. Okhotnikov, WILEY-VCH, Weinheim, 2010.
205. W. P. Pallmann, C. A. Zaugg, M. Mangold, V. J. Wittwer, H. Moench, S. Gronenborn, M. Miller, B. W. Tilma, T. Südmeyer and U. Keller, *Opt. Express*, 2012, 20, 24791.
206. J. Q. Nguyen, Z. S. Gowani, M. O'Connor, I. J. Pence, T. Q. Nguyen, G. E. Holt, H. S. Schwartz, J. L. Halpern and A. Mahadevan-Jansen, *Lasers Surg. Med.*, 2016, 48, 774–781.
207. D. A. Orringer, B. Pandian, Y. S. Niknafs, T. C. Hollon, J. Boyle, S. Lewis, M. Garrard, S. L. Hervey-Jumper, H. J. L. Garton, C. O. Maher, J. A. Heth, O. Sagher, D. A. Wilkinson, M. Snuderl, S. Venneti, S. H. Ramkissoon, K. A. McFadden, A. Fisher-Hubbard, A. P. Lieberman, T. D. Johnson, X. S. Xie, J. K. Trautman, C. W. Freudiger and S. Camelo-Piragua, *Nat. Biomed. Eng.*, 2017, 1, 27.
208. K. St-Arnaud, K. Aubertin, M. Strupler, M. Jermyn, K. Petrecca, D. Trudel and F. Leblond, *Opt. Lett.*, 2016, 41, 4692–4695.
209. M. Jermyn, J. Desroches, J. Mercier, K. Saint-Arnaud, M.-C. Guiot, F. Leblond and K. Petrecca, *Biomed. Opt. Express*, 2016, 7, 247–248.
210. J. Desroches, A. Laurence, M. Jermyn, M. Pinto, M.-A. Tremblay, K. Petrecca and F. Leblond, *Analyst,* 2017, 142, 1185–1191.
211. M. Jermyn, J. Desroches, J. Mercier, M.-A. Tremblay, K. St-Arnaud, M.-C. Guiot, K. Petrecca and F. Leblond, *J. Biomed. Opt.*, 2016, 21, 94002.
212. M. Isabelle, J. Dorney, A. Lewis, G. R. Lloyd, O. Old, N. Shepherd, M. Rodriguez-Justo, H. Barr, K. Lau, I. Bell, S. Ohrel, G. Thomas, N. Stone and C. Kendall, *Faraday Discuss.*, 2016, 187, 87–103.
213. R. Gaifulina, A. T. Maher, C. Kendall, J. Nelson, M. Rodriguez-Justo, K. Lau and G. M. Thomas, *Int. J. Exp. Pathol.*, 2016, 97, 337–350.
214. K. Lau, M. Isabelle, G. R. Lloyd, O. Old, N. Shepherd, I. M. Bell, J. Dorney, A. Lewis, R. Gaifulina, M. Rodriguez-Justo, C. Kendall, N. Stone, G. Thomas and D. Reece, in *Biomedical Vibrational*

Spectroscopy, eds. A. Mahadevan-Jansen and W. Petrich, 2016, vol. 9704, p. 97040B.

215. M. A. Short, W. Wang, I. T. Tai and H. Zeng, *J. Biophotonics*, 2016, 9, 44–48.
216. J. Zhao, H. Lui, D. I. McLean and H. Zeng, *Appl. Spectrosc*., 2007, 61, 1225–32.
217. J. Zhao, H. Lui, D. I. McLean and H. Zeng, *Skin Res. Technol*., 2008, 14, 484–92.
218. H. Abramczyk, B. Brozek-Pluska, J. Surmacki, J. Musial and R. Kordek, *Analyst*, 2014, 139, 5547–59.
219. L. Mavarani, D. Petersen, S. F. El-Mashtoly, A. Mosig, A. Tannapfel, C. Kötting and K. Gerwert, *Analyst*, 2013, 138, 4035–9.
220. T. Tolstik, C. Marquardt, C. Matthäus, N. Bergner, C. Bielecki, C. Krafft, A. Stallmach and J. Popp, *Analyst*, 2014, 139, 6036–43.
221. G. Lech, R. Słotwiński, M. I. Słodkowski and I. W. Krasnodębski, *World J. Gastroenterol*., 2016, 22, 1745–1755.
222. J. Wang, K. Lin, W. Zheng, K. Ho, M. Teh, K. Yeoh and Z. Huang, *Faraday Discuss*., 2015, 187, 377–392.
223. S. Devpura, K. N. Barton, S. L. Brown, O. Palyvoda, S. Kalkanis, V. M. Naik, F. Siddiqui, R. Naik and I. J. Chetty, *Med. Phys*., 2014, 41, 50901.
224. K. Kong, F. Zabar, E. Rakha, I. Ellis, A. Koloydenko and I. Notingher, *Phys. Med. Biol*., 2014, 59, 6141–6152.

CHAPTER 7

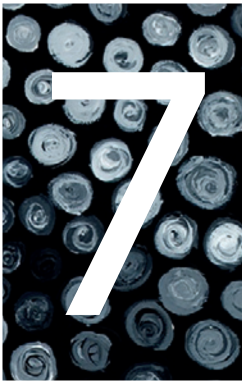

Single-fiber probe for in vivo Raman spectroscopy of pigmented skin lesions

Introduction

In the previous chapters of this thesis, an *in-house* developed focused-beam Raman spectroscopy setup was presented. The setup was used to measure Raman spectra of excised skin lesions. In order to add the option to perform *in vivo* Raman measurements, the setup was adapted to accept a fiber-optic probe extension that can be easily inserted in the existing optical path. This enables switching between the two measurement layouts without the necessity to re-align the optical paths. The fiber-optic probe layout enables *in vivo* measurements on the skin on different parts of the body of the patient, which was not possible with the original configuration.

A significant problem associated with fiber-optic probes is that the laser light generates a Raman signal in the fiber material (usually fused silica), which is reflected at the distal end of the probe and re-enters the probe together with the Raman signal generated in the tissue. Often the probe signal is more intense than the Raman signal of interest. Technically, this unwanted signal can be filtered out, but this requires the used of a separate emission fiber with an optical filter at the distal end that transmits the laser wavelength and blocks the Raman signal generated in the probe. One or more collection fibers are then required to deliver the Raman signal from the tissue to the spectrometer. This makes the fiber-probe configuration complicated and expensive. In the past, we have discovered that fused silica optical fibers show negligible Raman signal in the high-wavenumber (HWVN) Raman spectral range. This means that filtering and separation of excitation and signal collection fibers can be omitted, and simple and cheap fiber-optical probes with a single optical fiber for excitation and collection can be used.[1]

In order to detect melanoma in an early stage, the equipment must collect Raman signal from the epidermis and superficial dermis (first 200-300 µm from skin surface), which is the depth at which early-stage melanoma is located.

In this study, we have implemented the simplest probe design, a single, unfiltered optical fiber. The purpose of this study is to test the feasibility of the single-fiber probe for *in vivo* early melanoma diagnosis. We characterize the sampling depth of this single-fiber probe to test its suitability for early melanoma diagnosis. We also compare the signal quality of Raman spectra obtained with the fiber configuration to the Raman spectra acquired with the focused beam configuration.

Materials and Methods

1) Raman instrumentation and signal acquisition

Focused beam configuration for ex vivo measurements. The laser light is focused on the tissue by an achromatic lens (f=35 mm, NA 0.36). The Raman scattered light is collected by the same lens and projected onto the entrance slit of the spectrometer, which records the Raman spectra in the spectral range 2780 to 3750 cm^{-1}. This instrument is described in detail in chapter 2.

Single-fiber configuration for in vivo measurements. A single multimode fiber with a silica core and silica cladding (customized FG050LGA, Thorlabs Inc, Germany, NA 0.22, core diameter 50 µm, polypropylene inner tubing, threaded Kevlar reinforcement and black PVC outer tubing) was implemented in the SWIR multichannel Raman instrument. A removable adapter that can be easily inserted and removed from the optical path allows changing from the focused beam configuration to the fiber-probe configuration without realignment or changes to the existing optical path. A right-angle mirror (12.5 mm, Silver, Thorlabs Inc, Germany) was used to fold the 976 nm laser light (IPS, Monmouth Junction, NJ, USA) beam towards an achromatic lens (25mm FL, NIR II coated, Edmund Optics, Barrington NJ, USA), which focused the laser light on the fiber. The fiber was inserted in a stainless-steel fiber handle to facilitate cleaning and handling of the fiber (Figure 1). No filters or extra lenses were used at the distal end of the probe.

Calibration. Raman spectra were corrected for the wavelength-dependent detection efficiency of the setup using an SRM2246 intensity standard (National Institute of Standards and Technology, Gaithersburg, MD).[2] The absolute wavenumber axis was calibrated using the spectral lines of a neon–argon lamp and the Raman spectrum of cyclohexane.

2) Fiber-probe characterization

Sampling depth. To estimate the sampling depth, the fiber-optic probe was mounted in a one-axis (vertical) micrometer stage so that its tip was positioned on top of a fused silica glass plate. At the initial position, the fiber tip was placed in direct contact with the silica glass, with no space between the glass and the fiber. A few drops of 20% Intralipid® emulsion (Fresenius Kabi BV, Netherlands) were put on a fused silica glass plate, around the fiber probe (Figure 2a). Intralipid® 20% is a phospholipid micelles emulsion often used as skin phantom, to simulate the optical properties of the skin, including melanocytic nevi and melanoma.[3,4] The fiber probe was then translated upwards, moving away from fused the silica glass, in steps of 20 µm (Figure 2b). Measurements with an integration time of 30 s were done at each position from 0 to a 500 µm distance to the fused silica plate. The sampling depth was then estimated as the depth at which the integrated Raman signal between 2770 and 3710 cm^{-1} stopped increasing, *i.e.* the signal reached 95% of its maximum intensity (Figure 2c), indicating that the measurement depth is shorter than the distance between the fiber and the fused silica plate.

The integrated intensity over the 2770-3710 cm^{-1} range was used as a measure of the signal intensity. The signal intensity was plotted as a function of the distance between the fiber tip and the silica glass to determine the sampling depth. The same experiment was repeated using water (as a non-scattering medium), with a step size of 50 µm.

3) Raman skin measurements

In vivo Raman spectroscopy measurements. *In vivo* measurements were performed on volunteers with benign pigmented skin lesions and on patients with skin lesions clinically suspected of melanoma, before surgical excision. The skin was not pre-treated in any way. Room lights were turned off but a LED lamp without emission in the SWIR range was left turned on during the fiber measurements. The fiber probe was placed on the skin lesion and approximately 15 Raman measurements were performed in multiple locations within the lesion. At each point, an integration time of 30 s was used. The *in vivo* measurements were approved by the Medical Ethics Committee of the Leiden University Medical Center (P16.315). Informed consent was obtained from the patients prior to the procedure.

Ex vivo Raman spectroscopy measurements. Immediately after surgical excision, Raman measurements were performed as described elsewhere.[5] When using the focused beam configuration, the excised skin lesion was enclosed in a cartridge and inserted in the focus of the laser beam. The laser focus was a spot with a diameter of ~6 µm. For fiber-optic probe measurements, the probe was placed directly on the excised skin lesion and approximately 15 measurements were performed on different points within the pigmented region of the lesion. Each point measurement had an integration time of 30 s.

4) Tissue measurement spectral pre-processing

Signal-to-noise ratio of Raman spectra In this study, the signal-to-noise ratio (SNR) is defined as the ratio between the integrated signal in the CH band (2310–2350 cm^{-1}) and the square-root of the sum of the integrated signal and tissue background in the same range (2310–2350 cm^{-1}). The calculation of the signal-to-noise ratio was performed before background subtraction and before scaling.

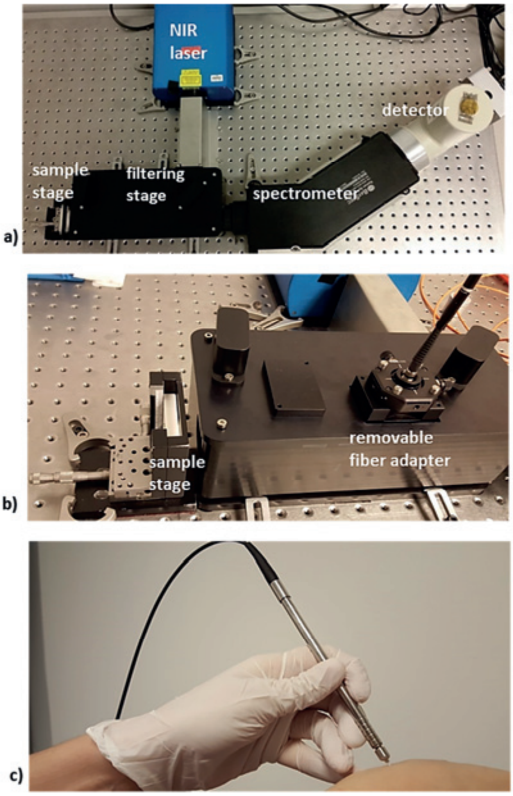

Figure 1. a) Picture of the SWIR Raman spectroscopy setup; **b)** The removable fiber adapter enables changing from the focused beam configuration to the fiber-probe configuration without realignment of the existing optical path; **c)** Picture of the single fiber-optic probe with an aluminum holder.

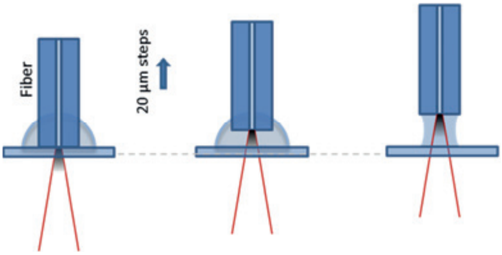

Figure 2. Graphical representation of the sampling depth measurement. **a**) In the initial position the fiber tip touches the silica glass. The grayed part in the cone of light indicates the cone of unknown length that the spectrometer is able to get signal from**; b)** the fiber probe was then translated upwards, moving away from fused the silica glass, in steps of 20 µm; **c)** The cone is fully inside the liquid, which is the point where the intensity of the Raman signal stops increasing.

Tissue luminescent background signal subtraction. The presence of luminescence background signal in the Raman spectra acquired from pigmented skin lesions is low due to the NIR (976 nm) excitation wavelength. A method described by Barroso *et al.* based on multiple regression fitting (MRF), was used for background correction. This method has been described in detail elsewhere.[6]

Correction for variations in the water signal. A scaling algorithm was used to remove the influence of the broad water OH signal on the CH band. A reference spectrum of water was fitted to the spectrum, and the coefficient that best scaled the water reference spectrum to the water signal in the measured spectrum was determined. The water signal multiplied by this coefficient was then subtracted from the measured spectrum (Figure 3).

Scaling. Each spectrum was scaled on the average of all spectra using an extended multiplicative signal correction (EMSC) with a zero-order polynomial background [7] after background subtraction. Spectra were cropped to the spectral range (2800–3050 cm^{-1}), which corresponds to the CH-stretching band region.

Results

Sampling depth of the fiber-optic probe. **Figure** Figure 4 shows the integrated intensity of the CH band and OH band in intralipid emulsion as a function of the distance between the fiber tip and the fused silica plate. The sampling depth was determined as the depth at which the signal intensity reached 95% of its maximum intensity, which was at 245 μm.

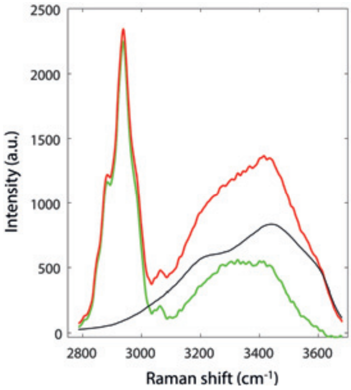

Figure 3. Example of correction for variation in water signal. The original spectrum is plotted in red. A reference spectrum of water was fitted to the spectrum, and the was determined. The water signal multiplied by the coefficient that best scaled the water reference spectrum to the water signal (plotted in black) is subtracted from the measured spectrum. The result of this subtraction (final spectrum) is plotted in green.

Figure 5 shows the integrated intensity of water as a function of the distance between the fiber tip and the fused silica plate. The sampling depth was determined as the depth at which the signal intensity showed reached 95% of its maximum intensity, which was at 570 μm.

SNR comparison of tissue spectra acquired with open-air focused beam configuration and with fiber probe. In this study, 55 excised pigmented lesions clinically suspected of melanoma were measured with the Raman spectroscopy instrument with the focused beam configuration. With the fiber probe configuration, 39 lesions were measured (21 excised lesions clinically suspected of

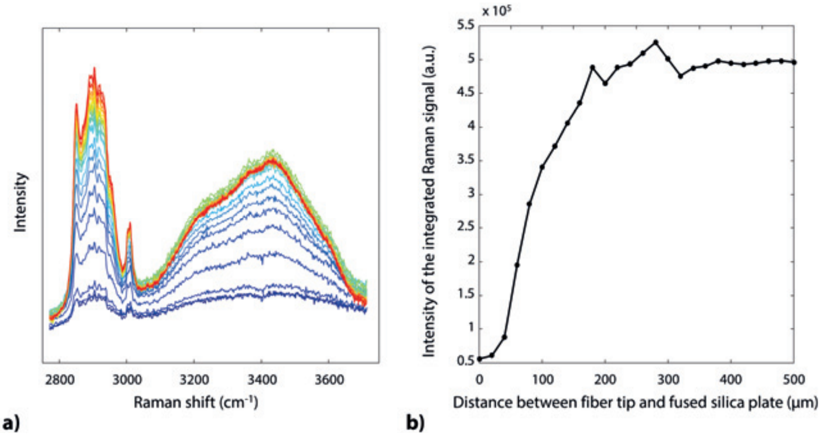

Figure 4. Sampling depth measurements of the fiber-optic probe in a 20% intralipid emulsion. **a)** Raman spectra measured at different distances between the fiber tip and the fused silica plate; **b)** Integrated intensity (2770-3710 cm^{-1}) of the Raman spectra depicted in (**a**) as a function of the distance between the fiber tip and the fused silica plate.

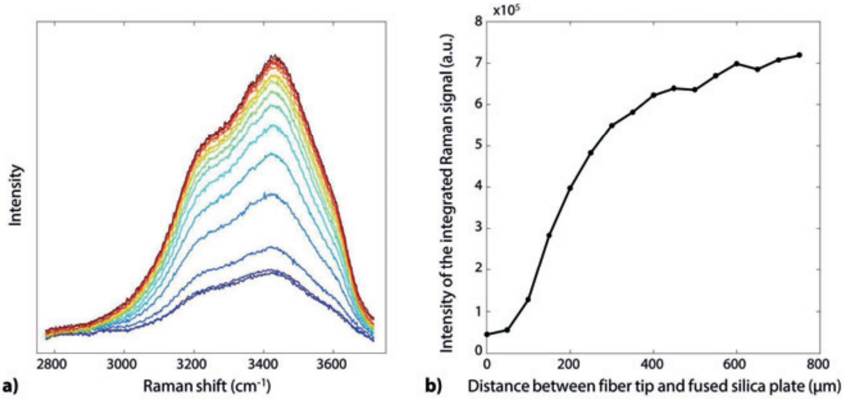

Figure 5. Sampling depth measurements of the fiber-optic probe in water. **a)** Raman spectra measured at different distances between the fiber tip and the fused silica plate; **b)** Integrated intensity (2770-3710 cm^{-1}) of the Raman spectra depicted in (**a**) as a function of the distance between the fiber tip and the fused silica plate.

melanoma and 18 benign lesions from volunteers). Figure 6 shows the distribution of the SNR values for spectra measured with both configurations. The average SNR of spectra measured with the focused beam configuration was 132.0 (SD 49.3) and the average SNR of spectra measured with the fiber probe was 136.7 (SD 36.4).

Example of *in vivo* Raman spectra of pigmented skin lesion. A typical example of Raman spectra of a pigmented skin lesion measured *in vivo* with the single-fiber probe is shown in Figure 7.

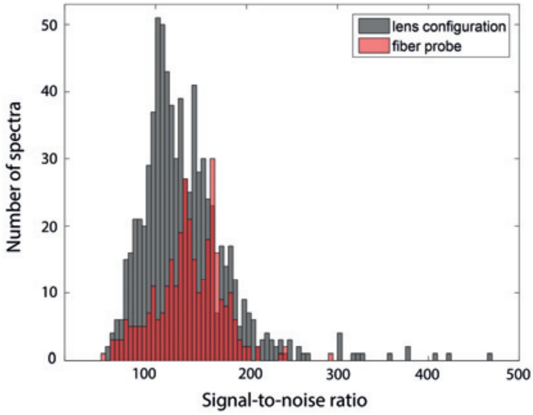

Figure 6. Distribution of SNR values of Raman spectra acquired with open-air focused beam (grey) configuration and acquired with the fiber probe (red).

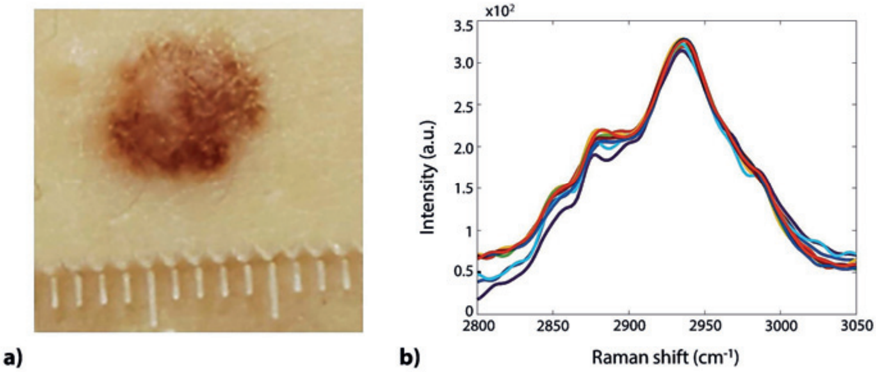

Figure 7. a) Pigmented skin lesion measured *in vivo* with the single-fiber probe; **b)** Raman spectra acquired using the single-fiber probe on the pigmented skin lesion depicted in a). Each spectrum had an integration time of 30 s.

Discussion

The objectives of this study were: (1) to characterize the sampling depth of the single-fiber probe for early melanoma diagnosis and (2) test the compatibility of signal quality and spectral variations of the Raman spectra obtained with the single-fiber probe on the *ex vivo* classification model created with Raman spectra obtained with the open-air focused beam configuration.

To measure the sampling depth of the single-fiber probe on the skin, a 20% intralipid emulsion was used as skin model. The sampling depth is influenced by light absorption and scattering in the tissue. Intralipid emulsions are often used to simulate the absorbing and scattering properties of skin.[8-11] From Figure 4, the integrated Raman signal of the intralipid emulsion stabilizes around 245 µm. The same experiment in water shows an integrated signal intensity stabilizing around 570 µm (Figure 5). The much smaller sampling depth observed in intralipid is most likely caused by the strong scattering properties of intralipid, which limits the acquisition of Raman signal to a more superficial depth. The optical properties of the intralipid® emulsion, resembles better the optical properties of the human skin than water does. Therefore we expect that the sampling depth in tissue is closer to 245 µm than to 570 µm. With respect to the envisioned application, this sampling depth of about 200 µm relevant because malignant melanocytes in early melanoma are also located in the upper 200-300 µm of the skin.

The SNR values for spectra measured with the focused-beam configuration and with the fiber configuration are largely comparable. More studies are missing to determine whether the *in vivo* Raman spectra acquired with the fiber-optic configuration can be predicted using the *ex vivo* classification model.

Conclusion

In this study, we show the feasibility to acquire high-quality Raman spectra from pigmented skin lesions using a single-fiber probe. We conclude that the fiber-probe collects Raman signal from the first 245 µm from the skin surface. This sampling depth is ideal for detection of malignant melanocytes in the epidermis as in early-stage melanoma. Finally, the quality of the spectra obtained using the single-fiber probe was comparable to the quality of the spectra obtained with the lens setup.

Future work

For the future, a multiple fiber probe with 7 fibers developed by RiverD and Avantes will be implemented in the Raman instrument (Figure 8). In this multi-fiber probe, all the fibers are used to transmit laser light and to collect Raman signal. This enables that an area of ~200 µm^2 is probed at the same time in 7 different spots. The orientation of the fibers is hexagonal (one in the center and six around) in one end (sample side) and a linear array in the other end (to connect to the entrance slit of the spectrometer). This will refine the multiple point measurements assessment, improving the Raman sampling of the lesions. In Chapter 5, it was presented a method that uses multiple point measurement analysis to improve diagnosis of thin melanomas. With the developed method, the diagnostic model correctly classified all melanomas with a specificity of 43.8%. This demonstrates that, based on Raman spectroscopy, an accurate diagnosis of thin melanomas can be made.

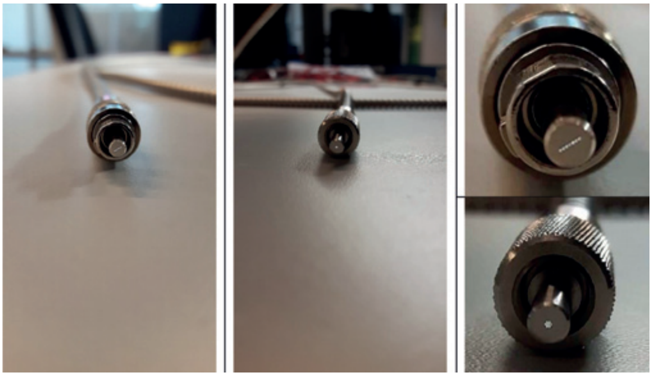

Figure 8. Multifiber probe.

References

1. L. F. Santos, R. Wolthuis, S. Koljenović, R. M. Almeida, and G. J. Puppels, *Anal. Chem.*, 2005, 77, 20, 6747–6752.
2. I. P. Santos, P. J. Caspers, T. Bakker Schut, R. van Doorn, S. Koljenović, and G. J. Puppels, *J. Raman Spectrosc.*,2015,46, 7l, 652–660.
3. A. M. Grant, K. Sry, R. Saager, F. Ayers, T. J. Pfefer, K. M. Kelly, S.-H. Tseng, and A. J. Durkin, *Proc. SPIE, Biomed. Appl. Light Scatt. III*, 2009, 7187,718702, 1–12.
4. T. J. Muldoon, S. A. Burgess, B. R. Chen, D. Ratner, and E. M. C. Hillman, *Biomed. Opt. Express*, 2012, 3, 7.
5. I. P. Santos, P. J. Caspers, T. C. Bakker Schut, R. van Doorn, V. Noordhoek Hegt, S. Koljenović, and G. J. Puppels, *Anal. Chem.*, 2016, 88, 15, 7683–7688.
6. E. Barroso, T. Bakker Schut, P. J. Caspers, I. P. Santos, E. Wolvius, S. Koljenović, and G. J. Puppels, *J. Raman Spectrosc.,* 2018, 1-11.
7. H. Martens and E. Stark, *J. Pharm. Biomed. Anal.*,1991, 9, 8, 625–635.
8. J. E. Smit, A. F. Grobler, and R. W. Sparrow, *Photochem. Photobiol.*, 2011, 87, 1, 64–71.
9. Y. S. Yamamoto, T. Itoh, H. Sato, and Y. Ozaki, *Vib. Spectrosc.*, 2014, 74, 132–136.
10. H. Ding, J. Q. Lu, K. M. Jacobs, and X.-H. Hu, *J. Opt. Soc. Am. A. Opt. Image Sci. Vis.*,2005, 22, 6, 1151–7.
11. P. Lai, X. Xu, and L. V Wang, *J. Biomed. Opt.*,2014, 19, 3, 35002.

CHAPTER 8

General discussion and prospects

This thesis presents Raman spectroscopy as a method to characterize the molecular composition of cutaneous melanocytic lesions with the purpose of improving the clinical diagnosis of melanoma, especially thin melanomas which can be cured by surgical excision.

Raman spectroscopy has two strong characteristics: (1) it provides discriminating information based on the molecular composition of the lesion and (2) it provides objective results, which are not influenced by the clinician's interpretation. In the last decade a strong effort has been made towards clinical implementation of Raman spectroscopy (described in Chapter 6) as an adjunct technique for early diagnosis, biopsy guidance and oncologic surgery guidance. The most recent studies aim to: (1) detect pre-malignant lesions,[1-6] which is one of the most effective ways to reduce the number of cancer cases, (2) detect cancer in less-invasive stages,[1,2,7-8] (3) reduce the number of unnecessary biopsies,[9-12] and (4) guide surgery towards complete removal of the tumor with adequate tumor resection margins, which reduces the need for post-operative treatment, decreases the aggressiveness of the post-operative treatment and increases patient survival.[13-17] However, until recent years, the application of Raman spectroscopy for the analysis of pigmented lesions was a major hurdle. When using visible or near-infrared laser excitation wavelengths the absorption of light by melanin pigment results in strong laser-induced tissue fluorescence. Because of this, it was difficult to obtain high-quality Raman spectra from pigmented tissues.

The work described in this thesis shows the development of a Raman instrument that enabled the assessment of melanocytic lesions and the development of a method to distinguish melanoma from benign melanocytic nevi. The obtained results reflect the potential of Raman spectroscopy as an adjunct tool for the clinical diagnosis of cutaneous melanocytic lesions. Although histology is considered the gold standard for the diagnosis of melanoma, a recent study demonstrated that the accuracy and reproducibility among pathologists is far from perfect. Therefore, the introduction of adjuvant techniques such as Raman spectroscopy should be evaluated in an *ex vivo* setting to assist pathologist in optimal diagnosis of melanocytic lesions, especially in dysplastic and thin (*in situ*) melanoma's.[18]

For now, the intended target-users for the Raman tool are dermatologists and general practitioners. In the same way that dermoscopy provides detailed morphological information that can be used by the clinician in the decision for diagnostic excision, Raman spectroscopy provides information on the biochemical composition of tissue. Therefore, a Raman tool can bring added value after visual inspection of the lesion (including dermoscopy), as an objective, second-level examination tool. This thesis is divided in two parts. In the first part (Chapters 2 and 3) technological advances and development of instrumentation required to obtain high-quality

Raman signals from pigmented skin lesions are described. The second part (Chapters 4 and 5) describes the implementation of the developed Raman instrument in the clinic, for *ex vivo* measurements on freshly excised skin lesions that were clinically suspicious for melanoma.

A **crucial step** was the shift of the excitation wavelength to the near-infrared (976 nm) and consequently, to detect the Raman signal in the short-wave infrared (1340-1540 cm^{-1}) (Chapter 2). This shift of excitation wavelength was necessary to obtain high-quality Raman spectra from pigmented biological samples in short integration times compatible with clinical applications, and has proven successful. In measurements on over 300 lesions, tissue auto-fluorescence did not pose a problem even in cases of high presence of melanin. Because tissue auto-fluorescence has been a major technological hurdle, this opens new possibilities for Raman spectroscopy of highly pigmented samples in oncological applications for skin and other types of tissues (*e.g*. liver, kidney, lung). In a wider perspective, also other fields could benefit from this technology, for example the food industry.

In the studies presented, we have limited the analysis of the Raman spectra to the CH stretching bands of the high-wavenumber spectral region (2800-3050 cm^{-1}). The main reason was to avoid spectral interference by absorption bands of water, which happens to overlap with the OH-band of water in the Raman spectra recorded by our instrument. This thesis demonstrates that the CH stretching bands used in the analysis contain spectral information to discriminate melanoma from benign melanocytic lesions. This offers possibilities for development of a much simplified Raman device, which detects only a small part of the high-wavenumber spectral range. A simplified Raman device would promote the implementation of this technique in clinical practice considerably because the current settings are too costly and the measurements too cumbersome.

Another important technological development presented in this thesis is the demonstration of the feasibility of a novel vertical-external-cavity surface-emitting laser (VECSEL) for Raman spectroscopy (Chapter 3). VECSELs offer interesting characteristics as low-cost laser sources: small size, narrow linewidth, high power stability, good power efficiency and a circular beam profile which facilitates focusing of the laser beam. Moreover, the wavelength of a VECSEL can be engineered over a broad range in the near-infrared, which gives flexibility for different requirements from specific applications. We implemented the VECSEL in the Raman instrument and showed, for the first time, Raman spectra of pigmented skin lesions in the SWIR region using a VECSEL as laser source. This demonstrated that the VECSEL fulfills the requirements of a laser source in a Raman application, which could eventually lead to the choice of VECSELs as the source of light in low-cost compact hand-held Raman devices in various applications.

The second part of this thesis (Chapters 4 and 5) demonstrates the application of the developed technology for measurements on pigmented skin lesions. The lesions clinically suspicious for melanoma were excised for diagnostic purpose and measured directly after excision. The prototype instrument was placed in a tertiary referral clinic for pigmented skin lesions at the Leiden University Medical Center (LUMC). **In a first application study** (Chapter 4), a total of 82 melanocytic lesions were included and the results from Raman spectroscopy were correlated with the histopathological diagnosis. For the purpose of this study, the samples were divided into histopathologically homogeneous and heterogeneous lesions. Heterogeneous lesions were defined as those that did not have an even distribution of histological components. In this study, only homogeneous lesions were included. Clear spectral differences were observed between melanoma and benign nevi. We discovered that melanoma had higher lipid content. The preliminary model resulted in a specificity of 45% at a sensitivity of 100% for melanoma, which was determined by leave-one sample-out cross-validation.

However, a clinical application requires that both homogeneous and heterogeneous melanocytic lesions can be classified. In the **next study** (Chapter 5), we included heterogeneous lesions in the development of the diagnostic model (Chapter 5). Decision strategies were explored to diagnose a lesion based on multiple measurements within the lesion. The results showed that the lipid content was the main spectral difference between melanoma and benign nevi, which is in agreement with the findings from Chapter 4. The diagnostic model was validated on an independent data set of 50 lesions. The validation set was comprised of 10 *in situ* melanomas and 7 with an average Breslow thickness of 0.42 mm. The results showed that all melanomas were detected (sensitivity of 100%) at a specificity of 43.8%. Because there is no international consensus about whether dysplastic nevi must be considered benign,[18-29] dysplastic nevi were not included in the diagnostic model, but were separately tested. From the total 46 dysplastic nevi, 73.9% were classified as melanoma.

Even though high-grade dysplastic nevi are associated to an increased melanoma risk, [19] there is debate about the management of this type of lesions, mainly due to lack of knowledge regarding dysplastic nevi epidemiology and evolution.[30] A statement signed by the members of the Pigmented Lesion Subcommittee of the Melanoma Prevention Working Group in the United States of America, recommends that: (1) pigmented lesions clinically and/or dermoscopically suspicious for melanoma should be surgically excised; (2) clinically atypical nevi stable in appearance should be followed-up; (3) histologically confirmed mild and moderate dysplastic nevi with clear margin do not need to be re-excised, whereas in the case of positive margins, a close follow-up is recommended. [30] The same management is followed by the majority of Canadian dermatologists.[31] A survey of Australian dermatologists reported that all dermatologists would re-excise an incompletely removed severely dysplastic nevus, even though their opinion was divided whether to treat such a lesion as a melanoma *in situ* or a mild dysplastic nevus.[32]

There are indications that dysplastic nevi are associated with an increased risk of developing melanoma,[19, 33-35] which is suggestively supported by the results shown in Chapter 5. We demonstrate that, based on Raman spectroscopy, an accurate diagnosis of melanoma with Breslow thickness <0.8 mm can be made. This work signifies an important step towards objective diagnosis of melanoma.

Prospects

The Raman instrument presented in this thesis was an experimental prototype. A necessary next step is the development of an *in vivo* Raman spectroscopic device which is compatible with the clinical workflow. This will require several technological developments, in particular with respect to the detector, *in vivo* miniature fiber-optic probes, and the lasers source.

One of the critical aspects that needs to be solved in the field of detector technology is to decrease the cost of short-wave infrared (SWIR) detectors. The InGaAs imaging camera implemented in the instrument described in this thesis was a high-end imaging camera which had not been developed for spectroscopic applications. The high-end device was necessary to provide sensitivity and extremely low-noise characteristics required to enable high-quality Raman spectra in the SWIR region. At the start of the RASKIN project this detector was the only one of a few in the market, with sufficient specifications to meet our requirements, in particular with such interesting noise characteristics. However, this camera was not designed for biomedical or even spectroscopic applications. The fact that it needed cooling with liquid nitrogen is one illustrative example of the differences between the intended use and the envisioned use, as described in this thesis. Also, the cost of this type of detector technology is out of reach for most biomedical applications. Currently, cheaper solutions in the detector technology for the SWIR region with better noise characteristics are appearing in the market.

The heterogeneity at a histopathological level of the melanocytic lesions presented initially as a major hurdle. An obvious limitation of this study is the lack of correlation between the location of the individual Raman measurements in the lesion with histopathology. We are currently developing a method for a reliable and reproducible correlation. It is expected that, when applying this method, the accuracy of the Raman tool for clinical diagnosis can be improved.

To ensure the transferability into a clinical application, it is important that the Raman measurement volume is representative of the entire lesion and that the diagnostic result from Raman spectroscopy correlates with the gold standard histopathological evaluation. For further improvement an interesting future development would be the combination of Raman spectroscopy with an image-based technique. In this way, the entire lesion could be quickly scanned by an image-based technique to identify the most suspicious regions, which would then guide the selection of locations for Raman measurements. This would help to reduce the time spent on Raman measurements on non-representative locations.

The experimental prototype and the diagnostic model were developed based on melanocytic skin lesions suspicious for melanoma. With this model, this instrument could be used in a specialized dermatology clinic. To optimize the diagnostic model for different settings the current model needs to be expanded to include more types of suspicious skin lesions, considering the multitude of skin lesions that dermatologists and general practitioners can possibly encounter. In order to create algorithms to distinguish melanoma from many different types of skin lesions, deep-learning algorithms would be preferable. Deep-learning algorithms for melanoma detection have been flourishing in the last years.[36-38] Artificial intelligence algorithms require huge amounts of data but are strong at extracting patterns. An interesting future possibility is the use of deep-learning algorithms to integrate Raman spectroscopic instruments with morphology-based techniques, in order to create powerful diagnostic models for melanoma.

In order to validate the current instrument, it is important to be able to collect *in vivo* Raman data of pigmented skin lesions in a large clinical study. After achieving sufficient evidence to introduce the modality into the clinical diagnostic decision process, commercial developments can be initiated.

Raman spectroscopy has proved to be a versatile and interesting technique with inherent advantageous characteristics that promote clinical applications. Raman spectroscopy has proven to be an answer to the need of an easy-to-use, real-time objective tool to improve the clinical diagnosis of melanocytic lesions. I believe that, in the near future, the implementation of Raman devices in the routine clinical diagnosis will become a reality.

References

1. H. C. McGregor, M. A. Short, A. McWilliams, T. Shaipanich, D. N. Ionescu, J. Zhao, W. Wang, G. Chen, S. Lam and H. Zeng, *J. Biophotonics*, 2017, 10, 1, 98-110.
2. S. Duraipandian, M. S. Bergholt, W. Zheng, K. Y. Ho, M. Teh, K. G. Yeoh, J. B. Y. So, A. Shabbir and Z. Huang, *J. Biomed. Opt*., 2012, 17, 81418.
3. M. S. Bergholt, W. Zheng, K. Y. Ho, K. G. Yeoh, M. Teh, J. B. Y. So and Z. Huang, *Proc. SPIE*, 2014, 8939, 89390M
4. H. Krishna, S. K. Majumder, P. Chaturvedi, M. Sidramesh and P. K. Gupta, *J. Biophotonics*, 2014, 7, 690–702.
5. J. Mo, W. Zheng, J. J. H. Low, J. Ng, A. Ilancheran and Z. Huang, *Anal. Chem*., 2009, 81, 8908–15.
6. J. Wang, K. Lin, W. Zheng, K. Ho, M. Teh, K. Yeoh and Z. Huang, *Faraday Discuss*., 2015, 187, 377–392.
7. I. P. Santos, P. J. Caspers, T. Bakker Schut, R. van Doorn, S. Koljenović and G. J. Puppels, *J. Raman Spectrosc*., 2015, 652–660.
8. E. Widjaja, W. Zheng and Z. Huang*, Int. J. Oncol*., 2008, 32, 653–662.
9. C. Lieber, S. K. Majumder, D. Billheimer, D. L. Ellis and A. Mahadevan-Jansen, *J. Biomed. Opt*., 2008, 13, 24013.
10. J. Zhao, H. Lui, D. I. McLean and H. Zeng, Conf. Proc. *IEEE Eng. Med. Biol. Soc*., 2008, 2008, 3107–3109.
11. M. A. Short, S. Lam, A. M. McWilliams, D. N. Ionescu and H. Zeng, *J. Thorac. Oncol*., 2011, 6, 1206–1214.
12. H. C. McGregor, M. A. Short, A. McWilliams, T. Shaipanich, D. N. Ionescu, J. Zhao, W. Wang, G. Chen, S. Lam and H. Zeng, *J. Biophotonics*, 2017, 10, 1, 98-110.
13. I. Barman, N. C. Dingari, A. Saha, S. McGee, L. H. Galindo, W. Liu, D. Plecha, N. Klein, R. R. Dasari and M. Fitzmaurice, Cancer Res., 2013, 73, 3206–3215.
14. K. Kong, C. J. Rowlands, S. Varma, W. Perkins, I. H. Leach, A. a Koloydenko, H. C. Williams and I. Notingher, *Proc. Natl. Acad. Sci. U. S. A*., 2013, 110, 15189–94.
15. E. M. Barroso, R. W. H. Smits, C. G. F. Van Lanschot, P. J. Caspers, I. Ten Hove, H. Mast, A. Sewnaik, J. Hardillo, C. Meeuwis, R. Verdijk, V. N. Hegt, R. J. Baatenburg De Jong, E. B. Wolvius, T. C. Bakker Schut, S. Koljenović and G. J. Puppels, *Cancer Res*., 2016, 76, 5945–5953.
16. M. Jermyn, K. Mok, J. Mercier, J. Desroches, J. Pichette, K. Saint-Arnaud, M.-C. Guiot, K. Petrecca and F. Leblond, in *Science Translational Medicine*, eds. R. R. Alfano and S. G. Demos, 2015, vol. 7, p. 93180D.
17. J. Q. Nguyen, Z. S. Gowani, M. O'Connor, I. J. Pence, T. Q. Nguyen, G. E. Holt, H. S. Schwartz, J. L. Halpern and A. Mahadevan-Jansen, *Lasers Surg. Med*., 2016, 48, 774–781.
18. J. G. Elmore, R. L. Barnhill, D. E. Elder, G. M. Longton, M. S. Pepe, L. M. Reisch, P. A. Carney, L. J. Titus, H. D. Nelson, T. Onega, A. N. A. Tosteson, M. A. Weinstock, S. R. Knezevich, and M. W. Piepkorn, *BMJ*, 2017, 357.
19. A. Shain, B. Bastian, Nature Reviews Cancer, 2016, 16, 6, 345-358.
20. K. Duffy and D. Grossman, *J. Am. Acad. Dermatol*., 2012, 67, 1, 1–27.
21. M. Arumi-Uria, N. S. McNutt, and B. Finnerty, *Mod. Pathol*., 2003, 16, 1, 764–771.
22. N. Wall, B. De'Ambrosis, J. Muir, *Australasian Journal of Dermatology*, 2017, 58, 304-307
23. K. Engeln, K. Peters, J. Ho, J. Jedrych, D. Winger, L. Korb Ferris, T. Patton, *J Am Acad Dermatol*, 2017, 76,2, 244-249
24. P. Sapra, C. Rosen, S. Siddha, C. Lynde, *Journal of Cutaneous Medicine and Surgery*, 2015, 19, 5, 457-463
25. J.M. Naeyaert, L. Brochez, *N Eng J Med*, 2003, 349, 23, 2233-2240
26. R. Winkelmann, D. S. Rigel, *J Am Acad Dermatol*, 2015, 73, 6 1058-1059
27. C. Kim, S. Swetter, C. Curiel-Lewandrowski, J. M. Crichnik, D. Grossman, A. C. Halpern, J. M. Kirkwood, S. A. Leachman, A. A. Marghoob, M. E. Ming, K. Nelson, E. Veledar, S. Venna, S. Chen, JAMA Dermatol, 2015, 151, 2, 212-218.
28. K.C. Lee, S. Peacock, M.A. Winstock, G. A. Zhao, S. R. Knezevich, D. E. Elder, R. L. Barnhill, M. W. Piepkorn, L. M. Reisch, P. A. Carney, T. Onega, J. P. Lott, J. G. Elmore, *J Am Acad Dermatol*, 2016, 76, 1, 121-128
29. L. X. Tong, P. A. Wu, C. C. Kim, *J Am Acad Dermatol*, 2016, 74, 2, 389-391

30. C. C. Kim, S. M. Swetter, C. Curiel-Lewandrowski, J. M. Grichnik, D. Grossman, A. C. Halpern, J. M. Kirkwood, S. A. Leachman, A. A. Marghoob, M. E. Ming, K. C. Nelson, E. Veledar, S. S. Venna, and S. C. Chen, *JAMA dermatology*, 2015, 151, 2, 212–218.
31. P. Sapra, C. Rosen, S. Siddha, C. Lynde, *Journal of Cutaneous Medicine and Surgery*, 2015, 19, 5, 457-463.
32. N. Wall, B. De'Ambrosis, J. Muir, *Australasian Journal of Dermatology*, 2017, 58, 304-307.
33. J. A. Newton Bishop, "Lentigos, Melanocytic Naevi and Melanoma," in *Rook's Textbook of Dermatology*, 8th ed., T. Burns, S. Breathnach, N. Cox, and C. Griffiths, Eds. Wiley-Blackwell, 2010, 54.1-54.57
34. D. J. Santa Cruz, "Tumors of the skin," in *Diagnostic Histopathology of Tumors*, 3th ed., C. D. M. Fletcher, Ed. Churchill Livingstone - Elsevier, 2007, 1423–1526
35. E. de Vries, F. Bray, J. W. Coebergh, L. Cerroni, D. J. Ruiter, D. E. Elder, J. F. Thompson, G. N. P. van Muijen, R. A. Scolyer, and P. E. LeBoit, "Malignant Melanoma: Introduction," in *World Health Organization Classification of Tumors. Pathology and Genetics of Skin Tumors.*, P. E. LeBoit, G. Burg, D. Weedon, and A. Sarasain, Eds. IARC Press, 2006, 52–61
36. A. Esteva, B. Kuprel, R. A. Novoa, J. Ko, S. M. Swetter, H. M. Blau, and S. Thrun, *Nature*, 2017, 542, 7639, 115–118.
37. X. Zhang, *Comput. Assist. Surg.*, 2017, 22(sup 1), 267–277.
38. Y. Li and L. Shen, *Sensors (Basel)*, 2018, 18, 2

CHAPTER 9

Summary

Nederlanse sammenvatting

Sumário

Summary

Cutaneous melanoma is the most aggressive and fatal form of skin malignancy. Its incidence has been steadily increasing in the last decades, with more than 232 000 new cases estimated worldwide in 2012.

The earliest possible clinical diagnosis of melanoma is of foremost importance for a good prognosis for the patient. When melanoma is diagnosed at an early stage it can be cured by surgical excision. When diagnosed at a later stage melanoma has a considerable risk of progression to lethal metastatic disease. The clinical examination and diagnosis of melanoma is based upon visual inspection and recognition of the morphologic characteristics. This method is subjective and open to the interpretation of the clinicians. The clinical differentiation between melanoma and benign melanocytic lesions can be challenging, even for experienced dermatologists. Because of the low clinical diagnostic accuracy for melanoma, an objective tool is needed to assist the clinical assessment of skin lesions that are suspected of melanoma. Improving the early diagnosis of melanoma constitutes therefore an important clinical objective.

Raman spectroscopy has shown to be a successful method to distinguish cancer from healthy tissue based on the analysis of the biochemical composition of tissues. However, until recent years, the application of Raman spectroscopy for the analysis of pigmented lesions was a major hurdle. When using visible or near-infrared laser excitation wavelengths, the absorption of light by melanin in pigmented skin lesions results in strong laser-induced tissue fluorescence. Because of this, it was difficult to obtain high-quality Raman spectra from pigmented tissues. The objective of the research described in this thesis was to develop a Raman spectroscopic instrument that enables the assessment of melanocytic skin lesions and to develop a method based on Raman spectroscopy as a non-invasive objective technique to improve the clinical diagnosis of melanoma.

Chapter 2 describes the development of a multi-channel short-wave infrared (SWIR) Raman instrument that enables the collection of Raman signal from pigmented tissue with low fluorescence background. In this study, we described the implementation of a novel low-noise InGaAs imaging camera as a detector for Raman spectroscopy. The results show that this instrument could obtain high-quality high-wavenumber (HWVN) Raman spectra with low fluorescence background of pigmented samples, which would not be possible with CCD-based instruments. The feasibility of using this detector for Raman spectroscopy was demonstrated by fast shot-noise limited measurements of pigmented biological samples.

In **Chapter 3** a study that investigates the feasibility of an alternative low-cost and small laser source developed within the RASKIN project in relation to the requirements set by this biomedical application is described. The vertical external-cavity surface-emitting laser (VECSEL) is characterized and implemented in the SWIR Raman spectroscopy instrument. VECSELs are an interesting alternative laser source for Raman spectroscopy. They offer a narrow linewidth, high power stability, good power efficiency and circular beam profile characteristics, and their wavelength can be engineered over a broad range in the near-infrared. In addition, they offer the potential of low-cost mass production, and they are small in size. For the first time, Raman spectra of pigmented skin lesions with a VECSEL in the SWIR region were demonstrated. The results show that the VECSEL fulfills the requirements of a laser source to be applied in Raman spectroscopy, opening the possibility of using VECSELs for low-cost compact hand-held Raman spectroscopy applications.

Chapter 4 describes how the developed instrument was employed to obtain Raman measurements of freshly excised skin lesions clinically suspected of melanoma in the clinic. The main objective was to explore whether there was spectroscopic information in the high-wavenumber range of the Raman spectra (2800–3050 cm^{-1}) to discriminate melanoma from benign melanocytic lesions and what would be the main spectral differences between melanoma and benign melanocytic lesions. Only histopathologically homogeneous lesions were included (82 lesions). The results showed that melanomas present increased lipid content compared to the benign lesions. In this study, a classification model was developed using PCA-LDA to investigate the discriminatory power of the CH region of HWVN Raman spectra. The model was optimized to discriminate melanoma from benign nevi, with a leave-one sample-out cross-validation. Our preliminary classification model correctly classified all melanomas (sensitivity of 100%) with a specificity of 45%.

Chapter 5 describes a development of a Raman spectroscopy method to distinguish melanoma from clinically suspicious benign melanocytic lesions, irrespective of their histopathologically heterogeneity. An important aspect of the study was that the diagnostic model was validated on an independent data set, with both histopathologically homogeneous and heterogeneous lesions. The independent validation set comprised 17 melanomas (10 *in situ* and 7 with an average Breslow thickness of 0.89 mm). The diagnostic model correctly classified all melanomas (sensitivity of 100%) at a specificity of 43.8%. The diagnostic model for melanoma showed in this study a potential improvement of the number needed to treat from 6.0 to 2.7, at a sensitivity of 100%. We demonstrate that, based on Raman spectroscopy, an accurate diagnosis of thin melanomas can be made. This work signifies an important step towards an objective accurate diagnosis of melanoma.

Chapter 6 provides an analysis of the status of translation of Raman spectroscopy oncological applications into the clinics. In this chapter we defined the clinical needs and requirements, for different cancer types, from the clinical point of view. The problems that need to be solved in order to bring the technique successfully to the end-users in the hospital setting are also discussed.

In **Chapter 7** the first steps towards the adaptation of the SWIR multi-channel Raman spectroscopy instrument for *in vivo* measurements are presented. The feasibility of the simplest possible probe design, which is a single-fiber probe, for melanoma diagnosis was tested. The sampling depth of the fiber-optic probe was characterized.

Finally, in **Chapter 8** a general conclusion is drawn from the work developed and described in this thesis, as well as a discussion about the prospects of the implementation of Raman spectroscopy to improve the clinical diagnosis of melanoma.

Nederlandse samenvatting

Het melanoom is de meest agressieve en dodelijke vorm van huidkanker. De incidentie is de afgelopen decennia geleidelijk toegenomen, met wereldwijd meer dan 232.000 nieuwe gevallen geschat in 2012. Wanneer het melanoom in een vroeg stadium wordt gediagnosticeerd, kan het curatief behandeld worden door middel van een chirurgische resectie. Als het melanoom in latere stadia gediagnosticeerd wordt, heeft het een grotere kans op metastatische ziekte met de dood tot gevolg. Klinisch onderzoek en de diagnose zijn gebaseerd op visuele inspectie en herkenning van de morfologische kenmerken. Deze methode is echter subjectief en is afhankelijk van de interpretatie van artsen. Daarom kan de klinische differentiatie tussen een melanoom en een goedaardige melanocytaire laesie uitdagend zijn, zelfs voor ervaren dermatologen. Vanwege de lage klinische diagnostische nauwkeurigheid van het melanoom is objectief hulpmiddel nodig om te assisteren bij de klinische beoordeling van voor melanoom verdachte huidlaesies is. Een belangrijk klinisch doel is dan ook het optimaliseren van de vroege diagnose van het melanoom.

Raman spectroscopie blijkt een succesvolle methode te zijn om kanker te onderscheiden van gezond weefsel op basis van de biochemische samenstelling van een weefsel. Echter, bij het toepassen van Raman spectroscopie bij de analyse van gepigmenteerde biologische weefsels, zoals melanocytaire huidlaesies, worden enkele problemen ondervonden. Bij gebruik van zichtbare of kortegolf-infrarode laserexcitatiegolflengten resulteert de absorptie van licht door melanine in gepigmenteerde huidlaesies in een sterke, door laser geïnduceerde, weefselfluorescentie. Dit sterke fluorescentiesignaal maskeert het zwakkere Raman signaal, waardoor het moeilijk, zo niet onmogelijk, is om kwalitatief goede Raman spectra uit gepigmenteerde weefsels te verkrijgen.

Het doel van het in dit proefschrift beschreven onderzoek was om een op Raman spectroscopie gebaseerd instrument te ontwikkelen, voor het beoordelen van melanocytaire huidlaesies. Tevens was het doel een methode te ontwikkelen op basis van een niet-invasieve, objectieve, op Raman gebaseerde techniek, de klinische diagnose van het melanoom te verbeteren.

Hoofdstuk 2 beschrijft het ontwikkelen van een meerkanaals kortegolf-infrarood (short-wave infrared, SWIR) Raman instrument, waarmee Raman signalen uit gepigmenteerde weefsels met een lage fluorescentie-achtergrond verzameld kunnen worden. In deze studie beschreven we de implementatie van een nieuwe geluidsarme InGaAs-beeldcamera die werd gebruikt als een spectroscopische detector. De resultaten tonen aan dat dit instrument hoogwaardige HWVN Raman spectra met een lage fluorescentie-achtergrond van gepigmenteerde weefsels kon verkrijgen, wat niet mogelijk zou zijn met op CCD gebaseerde instrumenten. De bruikbaarheid van deze detector voor Raman spectroscopie werd gedemonstreerd met snelle, door schrootruis gelimiteerde metingen, aan gepigmenteerde biologische weefsels.

In **hoofdstuk 3** wordt een studie beschreven dat onderzoek doet naar het gebruik van een alternatieve goedkope en kleine laserbron die ontwikkeld is binnen het RASKIN project op basis van de eisen die door de toepassing gesteld werden. De karakteristieken van een vertical external-cavity surface-emitting laser (VECSEL) zijn in kaart gebracht en vervolgens geïmplementeerd in het SWIR Raman spectroscopie-instrument. VECSEL's kunnen fungeren als een alternatieve laserbron in Raman spectroscopie. Ze bieden een smalle lijnbreedte, een hoge vermogens-stabiliteit, goede efficiëntie, ronde bundel profiel karakteristieken, en de golflengte kan in het kortegolf-infrarood spectrum over een breed bereik worden aangepast. Daarnaast zijn ze geschikt voor goedkope massaproductie, en zijn ze klein van formaat. Voor het eerste werd met een VECSEL Raman spectra van gepigmenteerde huidlaesies in het kortegolf-infrarood spectrum aangetoond. De resultaten van deze studie tonen aan dat de VECSEL voldoet aan de eisen van een laserbron die kan worden toegepast in Raman spectroscopie, waardoor er de mogelijkheid wordt gecreëerd om VECSEL's te gebruiken voor goedkope, compacte, draagbare Raman spectroscopische toepassingen.

In **Hoofdstuk 4** wordt omschreven hoe het reeds ontwikkelde instrument werd gebruikt om in de kliniek Raman metingen te verkrijgen van vers uitgesneden, op melanoom verdachte huidlaesies. Het voornaamste doel was om te onderzoeken of op basis van spectroscopische informatie in het HWN bereik van de Raman spectra (2800-3050 cm^{-1}), het melanoom onderscheiden kon worden van goedaardige melanocytaire laesies. Daarnaast wilden we de belangrijkste spectrale verschillen tussen een melanoom en goedaardige melanocytaire laesies weergeven. In deze studie werden alleen de histopathologisch homogene laesies geanalyseerd. Er werden in totaal 82 met chirurgie verkregen laesies gemeten. De resultaten toonden aan dat de lipiden concentratie in een melanoom hoger is in vergelijking met de lipiden concentratie in goedaardige laesies. In deze studie werd een classificatiemodel ontwikkeld met behulp van PCA-LDA om het discriminerend vermogen van de CH-regio in HWVN Raman spectra te onderzoeken. Het model werd geoptimaliseerd om melanoom te onderscheiden van alle andere laesies met een leave-one-sample-out-kruisvalidatie. Ons voorlopig classificatiemodel classificeerde alle melanomen correct (sensitiviteit van 100%) met een specificiteit van 45%.

Hoofdstuk 5 beschrijft de ontwikkeling van een nauwkeurige methode om een melanoom te onderscheiden van goedaardige melanocytaire laesies (die aanvankelijk klinisch verdacht werden voor melanoom). Een belangrijk aspect van deze studie is dat het classificatiemodel werd gevalideerd op een onafhankelijke dataset, met daarin zowel histopathologisch homogene als heterogene laesies.

De onafhankelijke validatie set bevatte 17 melanomen (10 in situ en 7 met een gemiddelde Breslow dikte van 0.89 mm). Alle melanomen werden correct geclassificeerd door het diagnostisch model (sensitiviteit 100%) met een specificiteit van 43.8%. Bij een sensitiviteit van 100% toonde het diagnostisch model een verbetering van het 'number needed to treat' van 6 naar 2.7%. Met deze studie hebben we aangetoond dat we op basis van Raman spectroscopie een accurate diagnose kunnen stellen van melanomen met een kleine Breslow dikte. Deze studie is dan ook een belangrijke stap in de ontwikkeling van het stellen van een accurate diagnose van het melanoom.

Hoofdstuk 6 biedt een analyse van de status van de translatie van Raman spectroscopie naar de kliniek. In dit hoofdstuk hebben we de klinische behoeften en vereisten voor verschillende kankertypen gedefinieerd vanuit klinisch oogpunt. De problemen die moeten worden opgelost om de techniek met succes naar de eindgebruikers in de ziekenhuisomgeving te vertalen, worden ook besproken in dit hoofdstuk.

In **hoofdstuk 7** worden de eerste aanpassing gepresenteerd die nodig zijn om het SWIR meerkanaals Raman spectroscopie instrument te gebruiken voor *in vivo* metingen. Tevens werd het meest eenvoudige ontwerp voor een probe (een single-fiber probe) voor melanoom diagnose getest. Ten slotte werd de meet-diepte van fiber-optische probe bepaald.

Tot slot wordt in **Hoofdstuk 8** de algemene conclusie van dit proefschrift omschreven en de discussie over de vooruitzichten voor de realisatie van Raman spectroscopie voor klinische diagnose van melanomen in de dermatologie uitgezet.

Sumário

Melanoma é o tipo de cancro cutâneo mais agressivo e letal. A sua incidência tem vindo a aumentar consistentemente nas últimas décadas, com mais de 232 000 novos casos a nível mundial em 2012.

O diagnóstico clínico de melanoma mais precocemente possível é da maior importância para um prognóstico favorável para o paciente. Quando o melanoma é diagnosticado numa fase inicial, a cura pode ser assegurada através de excisão cirúrgica. Contudo, se diagnosticado numa fase tardia há um risco considerável de progressão para uma fase metastática. O exame e o diagnóstico clínico de melanoma são baseados na avaliação visual da lesão e no reconhecimento das suas características morfológicas. Este é um método subjectivo e sujeito a interpretação por parte dos médicos. Desta forma, a diferenciação clínica entre melanoma e lesões melanocíticas benignas pode ser bastante difícil, mesmo para dermatologistas experientes. Devido à limitada precisão de diagnóstico clínico, existe necessidade de um equipamento objectivo que possa auxiliar a avaliação clinica de lesões suspeitas de melanoma. Um objectivo clínico importante é, portanto, melhorar o diagnóstico precoce de melanoma.

A espectroscopia de Raman tem demonstrado ser um método bem sucedido para discriminar tecidos cancerosos de tecidos saudáveis, através da análise da composição bioquímica dos mesmos. Contudo, existe um obstáculo à aplicação da espectroscopia de Raman na análise de amostras biológicas pigmentadas. Ao usar lasers com emissão de comprimento de onda na gama visível ou infravermelho próximo em lesões cutâneas pigmentadas, a absorção de luz pelo pigmento melanina origina uma forte auto-fluorescência no tecido. Essa fluorescência é intensa e dissimula o ténue sinal de Raman tornando difícil, senão impossível, obter espectros Raman de alta qualidade a partir de tecidos pigmentados.

O objetivo do trabalho descrito nesta tese foi desenvolver um instrumento de espectroscopia de Raman que permitisse a avaliação de lesões cutâneas melanocíticas e desenvolver um método baseado na espectroscopia de Raman como técnica objetiva e não-invasiva para melhorar o diagnóstico clínico de melanoma.

O **Capítulo 2** descreve o desenvolvimento de um equipamento de espectroscopia de Raman multicanal que opera na região de infravermelho e que permite a aquisição de sinal Raman a partir de tecidos pigmentados com baixo nível de fluorescência. Neste estudo, descrevemos a implementação de uma câmara de imagem InGaAs de baixo ruído como um detector para espectroscopia de Raman. Os resultados mostram que com este instrumento é possível adquirir

espectros de amostras pigmentadas com elevada qualidade e com um baixo nível de fluorescência, o que não seria possível com instrumentos com detectores CCD (charge-coupled devices). A viabilidade de utilizar este detector para espectroscopia de Raman foi demonstrada pela capacidade em adquirir sinais limitados apenas por ruído *shot* em amostras biológicas pigmentadas e num curto tempo de aquisição.

No **Capítulo 3** é descrito um estudo que investiga a viabilidade de uma alternativa fonte laser de baixo-custo e compacta desenvolvida no âmbito do projeto RASKIN tendo em conta os requisitos estabelecidos pela nossa aplicação biomédica. Um laser Vertical External-cavity Surface-emitting laser (VECSEL) foi caracterizado e implementado no instrumento de espectroscopia de Raman desenvolvido. Os VECSELs são uma fonte laser alternativa interessante para a espectroscopia de Raman. Eles oferecem uma largura espectral estreita, elevada estabilidade de potência, boa eficiência energética e características de perfil de feixe circular. O seu comprimento de onda pode ser seleccionado numa ampla faixa de comprimentos de onda na região do infravermelho. Além disso, eles oferecem o potencial de baixo custo quando produzidos em larga escala, e são de tamanho compacto. Foram demonstrados, pela primeira vez, espectros Raman de lesões de pele pigmentadas obtidos a partir de um VECSEL. Os resultados mostram que o VECSEL cumpre os requisitos de uma fonte laser a ser aplicada em espectroscopia de Raman, abrindo a possibilidade de implementar VECSELs em aplicações de espectroscopia de Raman portáveis e de baixo custo.

O **Capítulo 4** descreve como este instrumento de espectroscopia de Raman desenvolvido foi utilizado numa clínica dermatológica para obter medições Raman de lesões de pele recém excisadas, clinicamente suspeitas de melanoma. O principal objetivo foi explorar a existência de informação espectroscópica na gama high-wavenumber (HWVN) do sinal Raman (2800-3050 cm^{-1}) para discriminar melanoma de lesões melanocíticas benignas e quais seriam as principais diferenças espectrais. Apenas lesões homogéneas a nível histopatológico foram incluídas neste estudo (82 lesões). Os resultados mostraram que os melanomas apresentam uma maior contribuição de lípidos em comparação com as lesões benignas. Neste estudo, um modelo de classificação usando *principal component analysis- linear discriminant analysis* (PCA-LDA) foi desenvolvido para investigar o poder discriminatório da região CH da gama HWVN dos espectros Raman. O modelo foi optimizado para discriminar melanoma das lesões benignas incluídas na análise. O nosso modelo preliminar classificou correctamente todos os melanomas (sensibilidade de 100%) com uma especificidade de 45%, obtido através de uma validação cruzada *leave-one-sample-out*.

O **Capítulo 5** descreve o desenvolvimento de um método para a discriminação entre melanomas e lesões melanocíticas benignas clinicamente suspeitas, irrespectivamente da sua heterogeneidade a nível histopatológico. Um aspecto importante deste estudo é que o modelo de classificação foi validado num conjunto de dados independente, tanto com lesões homogéneas como heterogéneas a nível histopatológico. O conjunto de dados independente conteve 17 melanomas (10 *in situ* e 7 com uma espessura média de 0.89 mm). O modelo de diagnóstico classificou correctamente todos os melanomas (100% de sensibilidade) para uma especificidade de 43.8%. O modelo de diagnóstico mostrou uma potencial melhoria do número necessário para tratar de 6.0 para 2.7, com uma sensibilidade de 100%. Foi demonstrado que, através de espectroscopia de Raman, é possível realizar um diagnóstico preciso de melanomas em estágio inicial. Este trabalho representa um importante passo com vista a um diagnóstico objectivo e preciso de melanoma.

O **capítulo 6** fornece uma análise do estado da transferência de aplicações oncológicas baseadas em espectroscopia de Raman para a prática clínica. Neste capítulo, definimos as necessidades clínicas e os requisitos, para diferentes tipos de cancro, do ponto de vista clínico. Também são discutidos os problemas que precisam ser ultrapassados para levar a técnica com sucesso aos utilizadores finais em ambiente hospitalar.

No **Capítulo 7**, são apresentados os primeiros passos para a adaptação do instrumento de espectroscopia Raman SWIR para medições *in vivo*. Foi testada a viabilidade para o diagnóstico de melanoma de uma sonda de fibra óptica mais simples possível, uma sonda de fibra única. A profundidade de amostragem da sonda de fibra óptica foi caracterizada.

Finalmente, no **Capítulo 8**, é extraída uma conclusão geral do trabalho desenvolvido e descrito nesta tese, bem como uma discussão sobre as perspectivas futuras para a implementação da espectroscopia de Raman com vista a melhoria do diagnóstico clínico de melanoma.

CHAPTER 10

About the author

Biography

Inês Pereira dos Santos was born in Fundão, Portugal, on the 24th September 1982. In 2000, after graduating from high school, she moved to Coimbra to study for a Bachelor of Science in Nursing at the Nursing School of Coimbra. After she obtained the BSc degree in 2004, she started her full-time professional activity as registered nurse at the Hospital and University Center of Coimbra. She has always been very curious and she always enjoyed challenging herself. At the same time, she decided to pursue for a second degree, in Biomedical Engineering. She carried out the integrated master in Biomedical Engineering in the University of Coimbra from 2006 till 2012 and her job as registered nurse, between 2004 and 2013.

For her Master thesis in Biomedical Engineering she became a member of the group of Prof. dr. Carlos Correia under supervision of dr. João Cardoso, in the Instrumentation Center of the Physics department of the University of Coimbra. In 2012, after finishing her MSc degree, she decided to continue her postgraduate education abroad. From 2013 till 2018 she performed her PhD research at the department of dermatology of Erasmus University Medical Center in Rotterdam, the Netherlands, under supervision of Prof. dr. Tamar Nijsten, dr. Peter Caspers, and dr. Senada Koljenović and mentorship of dr. Gerwin Puppels and dr. Tom Bakker Schut. The results of the work perfomed in these 5 years are presented in this thesis.

List of Publications

Characterization and subtraction of luminescence background signals in high-wavenumber Raman spectra of human tissue
Elisa M. Barroso, Tom C. Bakker Schut, Peter J. Caspers, **Inês P. Santos**, Eppo B. Wolvius, Senada Koljenović, and Gerwin J. Puppels, *Journal of Raman Spectroscopy*, 2018, DOI: 10.1002/jrs.5338

Raman spectroscopy for in vivo cancer detection and cancer surgery guidance: translation to the clinics
Inês P. Santos†, Elisa M. Barroso†, Tom C. Bakker Schut, Cornelia G. F. van Lanschot, Da-Hye Choi, Martine F. van der Kamp, Roeland W. H. Smits, Remco van Doorn, Rob M. Verdijk, Vincent Noordhoek Hegt, Jan H. von der Thüsen, Carolien H. M. van Deurzen, Linetta B. Koppert, Arno van Leenders, Patricia C. Ewing-Graham, Lena C. van Doorn, Clemens M. F. Dirven, Martijn B. Busstra, Jose Hardillo, Aniel Sewnaik, Ivo ten Hove, Hetty Mast, Dominiek A. Monserez, Cees Meeuwis, Robert J. Baatenburg de Jong, Tamar Nijsten, Eppo B. Wolvius, Peter J. Caspers, Gerwin J. Puppels†, and Senada Koljenović†, *Analyst,* 2017; 142, 17, 3025-3047

Novel VECSEL for short-wave infrared Raman spectroscopy applications
Inês P. Santos, Alexander van der Lee, Xi Gu, Peter J. Caspers, Tom C. Bakker Schut, Remco van Doorn, Vincent Noordhoek Hegt, Senada Koljenović, Gerwin J. Puppels, *Journal of Raman Spectroscopy*, 2017, 48, 6, 872–877.

Raman spectroscopic characterization of melanoma and benign melanocytic lesions suspected of melanoma using high-wavenumber Raman spectroscopy
Inês P. Santos, Peter J. Caspers, Tom C. Bakker Schut, Remco van Doorn, Vincent Noordhoek Hegt, Senada Koljenović, and Gerwin J. Puppels, *Analytical Chemistry*, 2016, 88, 15, 7683-7688.

Implementation of a novel low-noise InGaAs detector enabling rapid near-infrared multichannel Raman spectroscopy of pigmented biological samples
Inês P. Santos, Peter J. Caspers, Tom Bakker Schut, Remco van Doorn, Senada Koljenović, and Gerwin J. Puppels, *Journal of Raman Spectroscopy,* 2015, 46,7, 652-660.

Improving clinical diagnosis of early stage cutaneous melanoma based on Raman spectroscopy

Inês P. Santos, Remco van Doorn, Peter J. Caspers, Tom C. Bakker Schut, Elisa M. Barroso, Tamar Nijsten, Vincent Noordhoek Hegt, Senada Koljenović† and Gerwin J. Puppels†

(Manuscript submitted)

† *These authors contributed equally to this work.*

PhD Portfolio

Summary of PhD training

Name of PhD student: Inês Pereira dos Santos
Erasmus MC Department: Department of Dermatology
PhD period: 2013-2018
Promotor(s): Prof. dr. T. Nijsten
Co-promotor(s): dr. P. Caspers
dr. S. Koljenović

Courses:

Writing successful grant proposals	2017
Workshop in Photoshop & Illustrator CS5	2015
Biomedical English writing and communication course	2014
Academic integrity course	2014
IOP Presentation skill course	2013

Seminars and research meetings:

Department research meetings	Oral presentations	2013-2017
Research group weekly meetings	Oral presentations	2013-2017
Seminar "Technologie in huidzorg" (invited speaker), Haagse Hogeschool, Den Haag	Oral presentation	2017
Dermatology seminar (Patienten Demonstratie meeting), LUMC, Leiden	Oral presentation	2015
Skintermezzo dermatology meeting, EMC, Rotterdam	Oral presentation	2015
Daniel Den Hoed Day, EMC, Rotterdam	Poster presentation	2013

National/International conferences with presentations:

NVED – Dutch Society experimental Dermatology Annual meeting, Lunteren, The Netherlands	Oral presentation	2016
SPEC 2016, Montreal, Canada	Poster presentation	2016
WIN-O, Ede, The Netherlands	Oral presentation	2016
IOP Photonic devices Symposium 2015, Amsterdam	Poster presentation	2015
SPEC 2014, Krakow, Poland	Poster presentation	2014
IOP Photonic devices Symposium 2014, Amsterdam	Oral presentation	2014
IOP Photonic devices Symposium 2013, Leiden	Poster presentation	2013

Supervision:

Supervision of Martijn Jansen, B.Sc. student in Applied Physics	2016

Lectures:

Medical students in Imaging minor course	Oral presentation	2016

Appendix

List of Abbreviations

AUC	area under the curve
ADU	analog-to-digital converter units
BCC	basal cell carcinoma
CCD	charge coupled device
CH	carbon-hydrogen
CRC	colorectal cancer
CSD	chronic sun damage
CW	continuous wave
DBR	distributed Bragg reflector
DCIS	ductal carcinoma *in situ*
DNA	deoxyribonucleic acid
EMSC	extended multiplicative signal correction
EPIC	European Photonics Industry Consortium
FDA	Food and Drug Administration
FN	false negatives
FNAC	fine-needle aspiration cytology
FP	false positives
FT	Fourier-transform
H&E	hematoxylin and eosin stain
HWVN	high-wavenumber
InGaAs	indium gallium arsenide
LDA	Linear discriminant analysis
LED	light-emitting diode
LUMC	Leiden University Medical Center
OH	oxygen-hydrogen
MAPK	mitogen-activated protein kinase
MMS	Mohs micrographic surgery
MRF	multiple regression fitting
MRI	magnetic resonance imaging
NA	numerical aperture
NaCl	sodium chloride
NH	nitrogen-hydrogen
NIR	near-infrared
NIST	National Institute of Standards and Technology
NNT	number needed to treat
NVB	neurovascular bundles
OCSCC	oral cavity squamous cell carcinoma
OCT	optical coherence tomography
OD	optical density
OLK	oral leukoplakia
OSCC	oral squamous cell carcinoma
OSMF	oral submucosa fibrosis
PAP	Papanicolau test
PCA	principal component analysis
QW	quantum well
R&D	research and development
ROC	receiver operator characteristic
RNA	ribonucleic acid
RR	resonance Raman
RS	Raman spectroscopy
RWI	read-while-integrate
SCC	squamous cell carcinoma

SD	standard deviation
SERS	surface enhanced Raman spectroscopy
SNR	signal-to-noise ratio
SRM	standard reference material
SSM	superficial spreading melanoma
SWIR	short-wave infrared
TEM	transverse electromagnetic
TP	true positives
TRL	technology readiness levels
TUR	transurethral resection
TURBT	transurethral resection of bladder tumors
UV	ultraviolet
VCSEL	vertical-cavity surface-emitting laser
VECSEL	vertical-external-cavity surface emitting laser
WHO	World Health Organization